

Discrete Dynamics in Nature and Society

Dynamical Modeling, Analysis, and Control of Information Diffusion over Social Networks

Lead Guest Editor: Chenquan Gan

Guest Editors: Qingyi Zhu, Wei Wang, and Jianxin Li





Dynamical Modeling, Analysis, and Control of Information Diffusion over Social Networks

Discrete Dynamics in Nature and Society

Dynamical Modeling, Analysis, and Control of Information Diffusion over Social Networks

Lead Guest Editor: Chenquan Gan

Guest Editors: Qingyi Zhu, Wei Wang, and Jianxin
Li



Copyright © 2021 Hindawi Limited. All rights reserved.

This is a special issue published in “Discrete Dynamics in Nature and Society.” All articles are open access articles distributed under the Creative Commons Attribution License, which permits unrestricted use, distribution, and reproduction in any medium, provided the original work is properly cited.

Editorial Board

Akbar Ali, Saudi Arabia
Douglas R. Anderson, USA
Viktor Avrutin, Germany
Stefan Balint, Romania
Kamel Barkaoui, France
Gian I. Bischi, Italy
Gabriele Bonanno, Italy
Florentino Borondo, Spain
Filippo Cacace, Italy
Jose Luis Calvo-Rolle, Spain
Pasquale Candito, Italy
Giulio E. Cantarella, Italy
Antonia Chinnì, Italy
Cengiz Çinar, Turkey
Carmen Coll, Spain
Giancarlo Consolo, Italy
Alicia Cordero, Spain
Ralf Cox, The Netherlands
Giuseppina D'Agù, Italy
Binxiang Dai, China
Manuel De la Sen, Spain
Beatrice Di Bella, Italy
Luisa Di Paola, Italy
Xiaohua Ding, China
Tien Van Do, Hungary
Marcio Eisencraft, Brazil
Elmetwally Elabbasy, Egypt
Hassan A. El-Morshedy, Egypt
Daniele Fournier-Prunaret, France
Genni Fragnelli, Italy
Ciprian G. Gal, USA
Marek Galewski, Poland
Caristi Giuseppe, Italy
Gisèle R Goldstein, USA
Vladimir Gontar, Israel
Chris Goodrich, USA
Pilar R. Gordo, Spain
Luca Guerrini, Italy
Juan L. G. Guirao, Spain
Antonio Iannizzotto, Italy
Giuseppe Izzo, Italy
Sarangapani Jagannathan, USA

Ya Jia, China
Emilio Jiménez Macías, Spain
Nikos I. Karachalios, Greece
Polinapiliñho F. Katina, USA
Eric R. Kaufmann, USA
Nickolai Kosmatov, USA
Victor S. Kozyakin, Russia
Mustafa R. S. Kulenovic, USA
Kousuke Kuto, Japan
Junqing Li, China
Li Li, China
Wei Li, China
Aihua Li, USA
Miguel Ángel López, Spain
Ricardo López-Ruiz, Spain
Rodica Luca, Romania
A. E. Matouk, Saudi Arabia
Akio Matsumoto, Japan
Rigoberto Medina, Chile
Driss Mehdi, France
Vicenç Méndez, Spain
Alfredo Morales, USA
Dorota Mozyrska, Poland
Yukihiko Nakata, Japan
Luca Pancioni, Italy
Garyfalos Papashinopoulos, Greece
Juan Pavón, Spain
Ewa Pawluszewicz, Poland
Alfred Peris, Spain
Adrian Petrusel, Romania
Andrew Pickering, Spain
Tiago Pinto, Spain
Chuanxi Qian, USA
Youssef N. Raffoul, USA
Maria Alessandra Ragusa, Italy
Aura Reggiani, Italy
Paolo Renna, Italy
Marko Robnik, Slovenia
Yuriy Rogovchenko, Norway
Silvia Romanelli, Italy
Christos J. Schinas, Greece
Daniel Sevcovic, Slovakia



Leonid Shaikhet, Israel
Seenith Sivasundaram, USA
Charalampos Skokos, South Africa
Benjamin Miranda Tabak, Brazil
Piergiulio Tempesta, Spain
Tetsuji Tokihiro, Japan
J. R. Torregrosa, Spain
Fabio Tramontana, Italy
Firdaus E. Udwadia, USA
Sundarapandian Vaidyanathan, India
Jose C. Valverde, Spain
Hector Vazquez-Leal, Mexico
Francisco R. Villatoro, Spain
Hubertus Von Bremen, USA
Junwei Wang, China
Rui Wang, China
Chun Wei, China
Zeshui Xu, China
Bo Yang, USA
Zhengqiu Zhang, China
Guang Zhang, China
Ying Zhang, USA
Haoran Zhang, Sweden
Lu Zhen, China
Yong Zhou, China
Zuonong Zhu, China




Contents

Dynamical Modeling, Analysis, and Control of Information Diffusion over Social Networks

Chenquan Gan , Qingyi Zhu , Wei Wang , and Jianxin Li 


Editorial (2 pages), Article ID 9815653, Volume 2021 (2021)

A Novel Method for Automatic Extrinsic Parameter Calibration of RGB-D Cameras

Qin Shi , Huansheng Song , and Shijie Sun 


Research Article (9 pages), Article ID 5251898, Volume 2021 (2021)

Information Spreading on Activity-Driven Temporal Networks with Two-Step Memory

Linfeng Zhong, Xiaoyu Xue, Yu Bai, Jin Huang, Qing Cheng, Longyang Huang, and Weijun Pan 



Research Article (7 pages), Article ID 4506012, Volume 2021 (2021)

Research on Wireless Sensor Network Security Location Based on Received Signal Strength Indicator Sybil Attack

Hongbin Wang and Liping Feng 

Research Article (9 pages), Article ID 1306084, Volume 2020 (2020)

A New Collaborative Filtering Recommendation Method Based on Transductive SVM and Active Learning

Xibin Wang , Zhenyu Dai, Hui Li , and Jianfeng Yang



Review Article (15 pages), Article ID 6480273, Volume 2020 (2020)

Modelling and Analysis of Propagation Behavior of Computer Viruses with Nonlinear Countermeasure Probability and Infected Removable Storage Media

Xulong Zhang  and Yong Li 


Research Article (7 pages), Article ID 8814319, Volume 2020 (2020)

Defending against Online Social Network Rumors through Optimal Control Approach

Da-Wen Huang , Lu-Xing Yang, Xiaofan Yang , Yuan Yan Tang, and Jichao Bi


Research Article (13 pages), Article ID 6263748, Volume 2020 (2020)

A Configurable Semantic-Based Transformation Method towards Conceptual Models

Tiexin Wang , Jingwen Cao, Chuanqi Tao, Zhibin Yang, Yi Wu, and Bohan Li


Research Article (14 pages), Article ID 6718087, Volume 2020 (2020)

The Influence of Network Structural Preference on Link Prediction

Yongcheng Wang, Yu Wang, Xinye Lin, and Wei Wang 


Research Article (9 pages), Article ID 6148273, Volume 2020 (2020)

Influence of Student Depression on the Spread of Public Opinion in University

Nie Min, Yang Lei, Luo Weimin, Guowu Yang, and Hu Xia 




Research Article (9 pages), Article ID 9378037, Volume 2020 (2020)

Weibo Rumor Recognition Based on Communication and Stacking Ensemble Learning

Yu Wu , Yan Zeng, Jie Yang, and Zhenni Zhao

Research Article (12 pages), Article ID 9352153, Volume 2020 (2020)

A Subjective Expressions Extracting Method for Social Opinion Mining

Mingyong Yin , Haizhou Wang , Xingshu Chen , Hong Yan, and Rui Tang
Research Article (10 pages), Article ID 2784826, Volume 2020 (2020)


Modeling a Rumor Propagation in Online Social Network: An Optimal Control Approach

Rachid Ghazzali , Amine El Bhih , Adil El Alami Laaroussi , and Mostafa Rachik
Research Article (12 pages), Article ID 6724815, Volume 2020 (2020)

C-SIW Rumor Propagation Model with Variable Propagation Rate and Perception Mechanism in Social Networks

Liqing Qiu , and Shuqi Liu 
Research Article (12 pages), Article ID 5712968, Volume 2020 (2020)



Impact of Immunization Strategies on the Dynamics of Social Contagions

Hao Peng, Wangxin Peng, Dandan Zhao , Zhaolong Hu, Jianmin Han, and Zhonglong Zheng
Research Article (9 pages), Article ID 5284348, Volume 2020 (2020)

Dynamical Modeling, Analysis, and Control of Information Diffusion over Social Networks: A Deep Learning-Based Recommendation Algorithm in Social Network

Kefei Cheng, Xiaoyong Guo , Xiaotong Cui, and Fengchi Shan 
Research Article (8 pages), Article ID 3273451, Volume 2020 (2020)

Modeling and Analysis of Dynamic Social Ties in D2D Collaborative Video Transmission

Qi Zhang, Zufan Zhang , Tian Zeng, and Xiaoke Li 
Research Article (7 pages), Article ID 1915840, Volume 2020 (2020)

Editorial

Dynamical Modeling, Analysis, and Control of Information Diffusion over Social Networks

Chenquan Gan ¹, Qingyi Zhu ², Wei Wang ³ and Jianxin Li ⁴

¹*School of Communication and Information Engineering, Chongqing University of Posts and Telecommunications, Chongqing 400065, China*

²*School of Cyber Security and Information Law, Chongqing University of Posts and Telecommunications, Chongqing 400065, China*

³*College of Computer Science, Sichuan University, Chengdu 610065, China*

⁴*School of Information Technology, Deakin University, Melbourne 3125, Australia*

Correspondence should be addressed to Chenquan Gan; gcq2010cqu@163.com

Received 13 October 2021; Accepted 13 October 2021; Published 21 October 2021

Copyright © 2021 Chenquan Gan et al. This is an open access article distributed under the Creative Commons Attribution License, which permits unrestricted use, distribution, and reproduction in any medium, provided the original work is properly cited.

Information diffusion is a complex and dynamic process that involves the topological factor of social networks and the geographical and psychological factors of individuals. It has a wide range of applications, including online marketing, recommendation systems, and prevention of malware and rumors' propagation. Although lots of dynamical models describing the behaviors of information diffusion have been proposed, it is still a challenging interdisciplinary task to explain and predict the dynamics of the diffusion process in complex networks.

This special issue provides both theoreticians and practitioners with a platform to disseminate their research on the modeling, analysis, and optimization of information diffusion over social networks. All manuscripts submitted to this special issue have been reviewed via the peer-reviewing process. Based on the reviewers' comments, 16 original research articles have been accepted for publication in this well-reputed journal.

Rumor spreading is very common in information diffusion and worth studying. D. W. Huang et al. and R. Ghazzali et al. explored rumor propagation in online social networks through the optimal control approach. L. Qiu and S. Liu proposed a corrector-ignorant-spreader-weakener (C-SIW) rumor propagation model that considers the impact of variable propagation rate and perception mechanism. Y. Wu et al. studied Weibo rumor recognition by combining with communication and stacking ensemble learning.

Network structure has an important impact on information dissemination and has always received great attention. L. Zhong et al. presented an information spreading model for an activity-driven temporal network. H. Wang and L. Feng considered the information security on wireless sensor networks. Y. Wang et al. focused on the influence of network structural preference perturbation through deletion on link prediction. Q. Zhang et al. analyzed the impact of social ties on video transmission in device-to-device (D2D) communications through a stochastic approach. H. Peng et al. investigated the effect of immunization strategies on social contagions through a non-Markovian threshold model. X. Zhang and Y. Li discussed the influence of countermeasure and removable storage media on the propagation behavior of computer viruses under the fully connected networks. N. Min et al. showed the impact of student depression on the spread of public opinion in the university through a social network.

Recommendation system is an important application of information dissemination, and there are many related methods worth studying in this regard. X. Wang et al. developed a personalized recommendation approach combining the semisupervised support vector machine and active learning for collaborative filtering recommendation applications. K. Cheng et al. designed a deep-learning-based recommendation algorithm to solve the problem of data sparsity in news recommendation for social networks. M. Yin et al. proposed a representation method that

combines different features with word vectors for social opinion mining. T. Wang et al. established a configurable semantic-based automatic conceptual model transformation methodology to improve the efficiency of the building process. Q. Shi et al. introduced a method that employs the depth map to perform extrinsic calibration automatically.

Conflicts of Interest

The editors declare that they have no conflicts of interest regarding the publication of this special issue.

Acknowledgments

The editors are very grateful to all of the authors for their outstanding contributions in this field and the reviewers for their valuable comments on the evaluation of the papers during the reviewing process.

*Chenquan Gan
Qingyi Zhu
Wei Wang
Jianxin Li*

Research Article

A Novel Method for Automatic Extrinsic Parameter Calibration of RGB-D Cameras

Qin Shi , Huansheng Song , and Shijie Sun 

School of Information Engineering, Chang'an University, Xi'an 710064, China

Correspondence should be addressed to Huansheng Song; hshsong@chd.edu.cn

Received 8 July 2020; Accepted 6 July 2021; Published 15 July 2021

Academic Editor: Manuel De la Sen

Copyright © 2021 Qin Shi et al. This is an open access article distributed under the Creative Commons Attribution License, which permits unrestricted use, distribution, and reproduction in any medium, provided the original work is properly cited.

Calibration of extrinsic parameters of the RGB-D camera can be applied in many fields, such as 3D scene reconstruction, robotics, and target detection. Many calibration methods employ a specific calibration object (i.e., a chessboard, cuboid, etc.) to calibrate the extrinsic parameters of the RGB-D color camera without using the depth map. As a result, it is difficult to simplify the calibration process, and the color sensor gets calibrated instead of the depth sensor. To this end, we propose a method that employs the depth map to perform extrinsic calibration automatically. In detail, the depth map is first transformed to a 3D point cloud in the camera coordinate system, and then the planes in the 3D point cloud are automatically detected using the Maximum Likelihood Estimation Sample Consensus (MLE-SAC) method. After that, according to the constraint relationship between the ground plane and the world coordinate system, all planes are traversed and screened until the ground plane is obtained. Finally, the extrinsic parameters are calculated using the spatial relationship between the ground plane and the camera coordinate system. The results show that the mean roll angle error of extrinsic parameter calibration was -1.14° . The mean pitch angle error was 4.57° , and the mean camera height error was 3.96 cm. The proposed method can accurately and automatically estimate the extrinsic parameters of a camera. Furthermore, after parallel optimization, it can achieve real-time performance for automatically estimating a robot's attitude.

1. Introduction

RGB-D cameras, such as Kinect [1–6], PrimeSense, and Asus Xtion Pro, are traditional RGB cameras with added infrared cameras. Figure 1 shows the structure of a Kinect camera. It can be seen that it includes a color camera, infrared camera, and an infrared illuminator. The color camera outputs a color image, the infrared camera outputs a depth image, and the infrared illuminator emits infrared light for the calculation of the depth image. With the emergence of low-cost RGB-D cameras such as Kinect, the camera and illuminator are increasingly used for tasks such as 3D scene reconstruction and navigation [8, 9], target recognition and tracking [10, 11], 3D measurement [12–15], and even social networks [16], for which the extrinsic parameters of the camera often must be calibrated.

For example, in target detection and recognition [11], the extrinsic parameters of the camera should be calibrated first,

and then pedestrians in the scene are tracked. If the extrinsic parameters of the camera can be obtained, the negative effects of perspective can be eliminated. In addition, the detection algorithm can be unified, and the recognition process can be simplified, thus accelerating recognition speed.

However, studies of the calibration of RGB-D cameras mainly focus on the extrinsic parameters of the color camera relative to the infrared camera [17, 18]. Calibrating the extrinsic parameters of an RGB-D camera is often similar to the calibration of the color camera, and the method of chessboard calibration is generally used to calibrate the color camera [19]. Munaro et al. [10] used a chessboard to calibrate the extrinsic parameters of multiple cameras and carried out pedestrian detection based on this. This calibration method did not make full use of the depth information provided by the RGB-D camera, and the calibration results were essentially the extrinsic parameters of the color

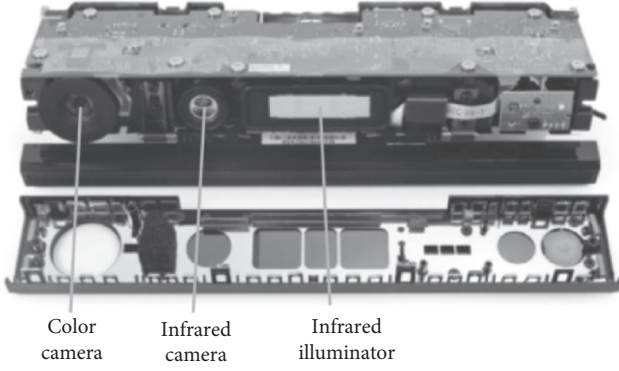


FIGURE 1: Sensor structure of the Kinect V2 [7].

camera. If it were directly used for 3D reconstruction of the depth map, then there would be a large error. Shibo and Qing [20] designed a calibration board for RGB-D infrared camera recognition, which had holes with regular intervals and calibrated the infrared camera by automatically identifying holes. The need to design special calibration objects increased the difficulty of calibration. Liao et al. [17] divided the calibration into three categories: calibration that required a calibrator, calibration that required human intervention, and fully automatic calibration. The proposed method belonged to the third category.

Liao et al. [17] divided the extrinsic parameter calibration methods for RGB-D cameras into three categories: (1) the first was to calibrate the extrinsic parameters of the color camera and then to use the extrinsic parameter $T_{C'}^D$ of the color camera and images collected by the infrared camera to obtain the extrinsic parameter T_D of the infrared camera through transformation $T_D = T_{C'}^D T_{C'}$. This method can directly use the color image calibration method, but it needs the extrinsic parameters of the color camera relative to the infrared camera and does not use the information provided by the depth map, so the process is complicated. (2) The second was to detect the features on the depth map provided by the infrared camera by designing a specific calibration object to obtain the extrinsic parameters of the camera based on the features (such as chessboard corners). (3) The third method used the depth map to calibrate the extrinsic parameters of the camera. The calibration was carried out by detecting the target on the depth map and using the relationship between the target and the world coordinate system. This method directly used the depth information, which greatly simplified the process and improved the efficiency of calibration. Our proposed method, which we will call the ground plane calibration method, is based on the automatic calibration of the extrinsic parameters of a ground plane detection camera and belongs to the third category. This method can directly calibrate the infrared camera of an RGB-D camera using its depth information.

2. Extrinsic Parameter Calibration

RGB-D cameras can be divided into color cameras and infrared cameras. For this study, the extrinsic parameters of an infrared camera were calibrated. Thus, extrinsic

parameter calibration refers to that of infrared cameras. The extrinsic parameter of the camera is

$$T_C^W = \begin{bmatrix} R_C^W & 0 \\ t_C^W & 1 \end{bmatrix}, \quad (1)$$

where $T_C^W \in \mathbb{R}^{4 \times 4}$ and $R_C^W \in \mathbb{R}^{3 \times 3}$ are the rotation matrices of the camera, $t_C^W \in \mathbb{R}^{1 \times 3}$ is the translation matrix of the camera, and $(\cdot)_C^W$ represents the transformation from the camera coordinate system to the world coordinate system.

Figure 2 shows the flowchart of extrinsic parameter calibration. After the establishment of a world coordinate system, the depth image is first obtained from the RGB-D camera. Then, the depth image is transformed to a 3D point cloud under the camera coordinate system using the internal parameters of the infrared camera. After that, the ground plane in the point cloud is solved by iteration. Subsequently, the extrinsic parameters of the camera are obtained by calculation.

2.1. Establishment of the Camera Coordinate System and World Coordinate System. The camera is in a 3D coordinate system, where the infrared camera is the origin, as shown in Figure 3. The infrared camera is the origin O_C of the camera coordinate system. The X_C axis is along the transverse direction of Kinect. The Z_C is perpendicular to Kinect and points in the shooting direction.

The world coordinates can generally be established at will. For facilitating the calculation of extrinsic parameters of the camera, as shown in Figure 4, the world coordinates should meet the following requirements.

- (1) The origin of the world coordinate system is the projection point of the origin of the camera coordinate system on the ground plane
- (2) The Y_W axis is the projection of the Z_C axis of the camera coordinate system on the ground
- (3) The Z_W axis is downwardly perpendicular to the ground plane
- (4) The coordinate system is a right-hand system

In this way, it is convenient to find the point group corresponding to camera coordinates and world coordinates and simplify the calibration process.

2.2. Calculation of Extrinsic Parameters of the Camera. The matrix of transformation from the camera coordinate system to the world coordinate system, that is, the extrinsic parameter T_C^W of the camera, is a 4×4 matrix with 12 unknown parameters, as shown in (1). First, the transformation matrix T_W^C from the world coordinate system to the camera coordinate system is calculated to obtain the extrinsic parameters of the camera:

$$T_C^W = T_W^C^{-1}. \quad (2)$$

A point in the camera coordinate system is $P_C^{(i)}$, and the corresponding point in the world coordinate system is $P_W^{(i)}$, as shown in Figure 5. Four special points are selected in the world coordinate system:

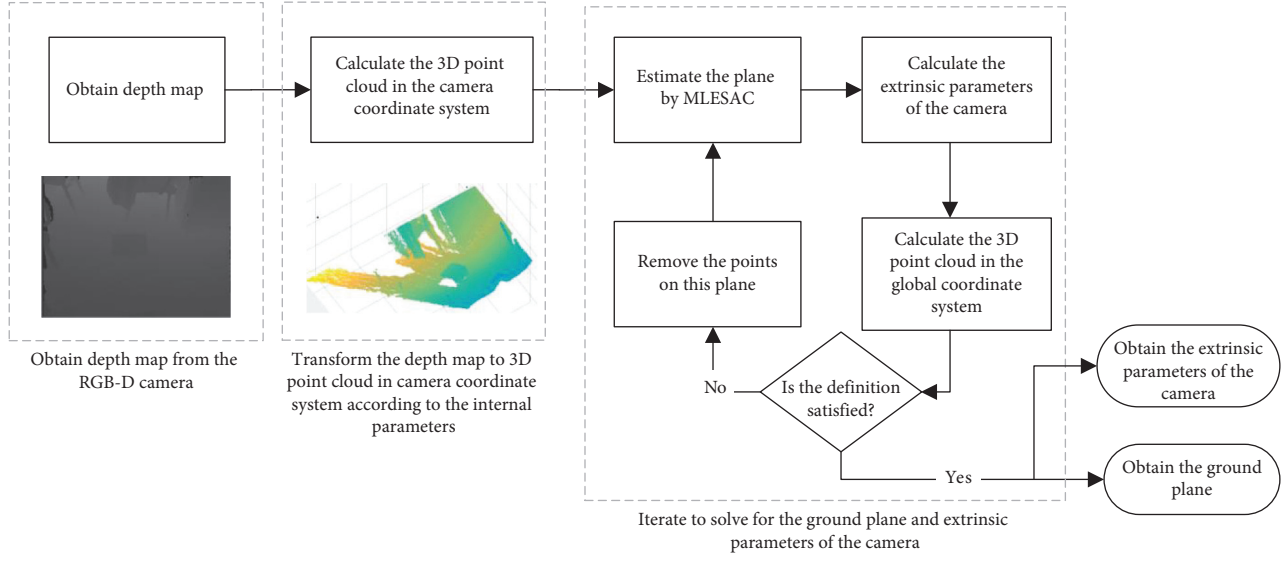


FIGURE 2: Process of extrinsic parameter calibration of the camera.



FIGURE 3: Camera coordinate.

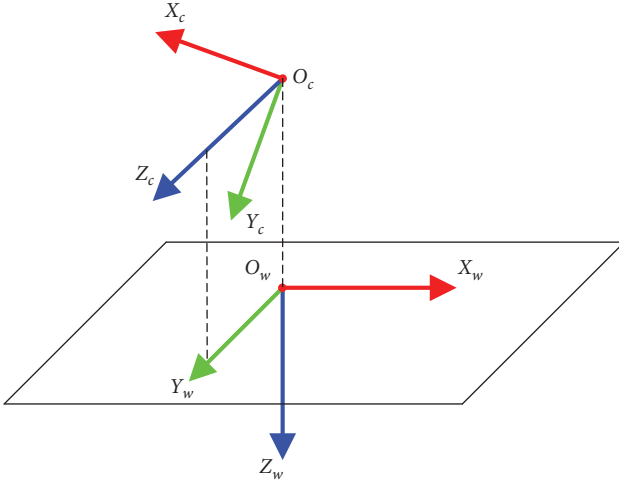


FIGURE 4: The position of world coordinate.

$$\begin{cases} P_w^{(0)} = [0 \ 0 \ 0], \\ P_w^{(1)} = [1 \ 0 \ 0], \\ P_w^{(2)} = [0 \ 1 \ 0], \\ P_w^{(3)} = [0 \ 0 \ 1]. \end{cases} \quad (3)$$

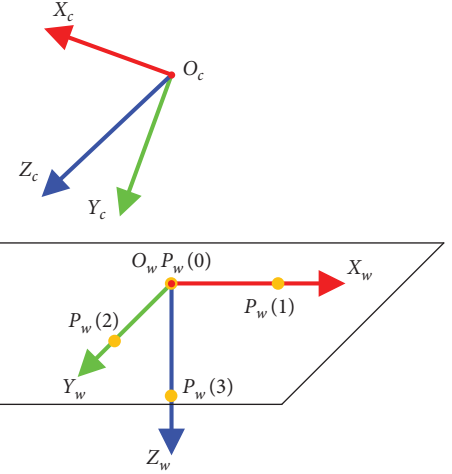


FIGURE 5: Selected points in world coordinate.

By calculating the corresponding points in the camera coordinate system, that is, $P_C^{(0)}, P_C^{(1)}, P_C^{(2)}$, and $P_C^{(3)}$, the value of ${}^C_W T$ can be obtained as

$${}^C_W T = \begin{bmatrix} \frac{(P_C^{(1)} - P_C^{(0)})^T}{\|(P_C^{(1)} - P_C^{(0)})\|_2} & \frac{(P_C^{(2)} - P_C^{(0)})^T}{\|(P_C^{(2)} - P_C^{(0)})\|_2} & \frac{(P_C^{(3)} - P_C^{(0)})^T}{\|(P_C^{(3)} - P_C^{(0)})\|_2} & 0 \\ \frac{P_C^{(0)}}{\|P_C^{(0)}\|_2} & & & 1 \end{bmatrix}. \quad (4)$$

It is known that the plane in the camera coordinate system is $ax + by + cz + d = 0$. Its normal vector perpendicular to the ground is $\vec{n}_C = [a \ b \ c]$ and $\|\vec{n}_C\|_2 = 1$. As the origin of the world coordinate system is the projection of the origin of the camera coordinate system on the plane, the

coordinates corresponding to the origin $P_W^{(0)}$ of the world coordinate in the camera coordinate system are

$$P_C^{(0)} = \frac{|d|}{\sqrt{a^2 + b^2 + c^2}} \vec{n}_C. \quad (5)$$

If point $P_W^{(3)} = [0 \ 0 \ 1]$ is on the Z axis of the world coordinate system and $O_C, P_C^{(0)}$, and $P_C^{(3)}$ are collinear, then

$$P_C^{(3)} = P_C^{(0)} + \vec{n}_C. \quad (6)$$

Because the Y_W axis is the projection of the Z_C axis on the plane,

$$P_C^{(2)} = P_C^{(0)} + \vec{n}_y, \quad (7)$$

where \vec{n}_y is the unit vector of $\overrightarrow{P_C^{(0)}P_C^{(2)}}$,

$$\vec{n}_y = \frac{\overrightarrow{P_{Z_c} - P_C^{(0)}}}{\left\| \overrightarrow{P_{Z_c} - P_C^{(0)}} \right\|_2}. \quad (8)$$

P_{Z_c} is the projection of point $[0 \ 0 \ 1]$ in the camera coordinate system to the plane. By solving (9), the projection point can be obtained as

$$\begin{cases} ax + by + cz + d = 0, \\ \frac{x - x_0}{a} = \frac{y - y_0}{b} = \frac{z - z_0}{c}, \end{cases} \quad (9)$$

where a, b, c , and d are the parameters of the plane equation and (x_0, y_0, z_0) is a random point on the plane.

After $P_C^{(0)}, P_C^{(2)}$, and $P_C^{(3)}$ are obtained, $P_C^{(1)}$ can be obtained by vector cross-multiplication as

$$P_C^{(1)} = \frac{\overrightarrow{P_C^{(2)} - P_C^{(0)}} \times \overrightarrow{P_C^{(3)} - P_C^{(0)}}}{\left\| \overrightarrow{P_C^{(2)} - P_C^{(0)}} \times \overrightarrow{P_C^{(3)} - P_C^{(0)}} \right\|_2}. \quad (10)$$

By solving (5)–(7) and (10), the coordinates of four points selected from the world coordinate system in the camera coordinate system are obtained. Then, the transformation matrix from the world coordinate point to the camera coordinate point is obtained by solving (4). Finally, the extrinsic parameter matrix of the infrared camera is obtained by solving (2).

3. Ground Plane Estimation

Toward facilitating plane detection, the depth map is first transformed to a 3D point cloud in the camera coordinate system using internal parameters. Then, the maximum likelihood estimation sample consensus (MLE-SAC) method [21] is used to extract the plane. The ergodic plane is iterated to obtain the extrinsic parameters. Next, the extrinsic parameters and point cloud are used to determine whether the plane is a ground plane, and we finally obtain the extrinsic parameters of the camera, as shown in Figure 6.

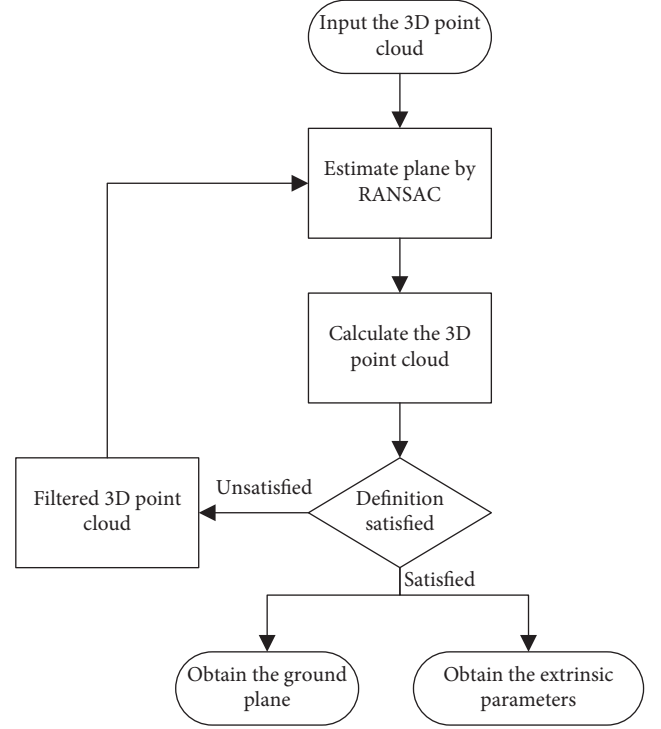


FIGURE 6: The process of ground plane estimation.

3.1. Transformation of Depth Map to 3D Point Cloud in the Camera Coordinate System. Consider the following:

$$\begin{cases} f_x = \frac{f}{d_x}, \\ f_y = \frac{f}{d_y}, \\ Z_C = d_p * s, \\ X_C = \frac{(u_I - c_x) \cdot Z_C}{f_x}, \\ Y_C = \frac{(v_I - c_y) \cdot Z_C}{f_y}. \end{cases} \quad (11)$$

Figure 7 shows the imaging model of the camera. The coordinate axes of the image plane are X_I and Y_I , respectively. The imaging point of point $P_C = (X_C, Y_C, Z_C)$ in the camera coordinate system on the image plane is $p_I = (u_I, v_I)$. The focal length of the camera is f . The coordinates of the intersection of the optical axis and the image plane are c_x and c_y . The length and width of the pixels are d_x and d_y , respectively. The value of the pixel is d_p . The proportion of Z coordinate values corresponding to the value of pixels in the camera coordinate system is s .

Then, (u, v, d_p) can be transformed to (X_C, Y_C, Z_C) , as shown in (11).

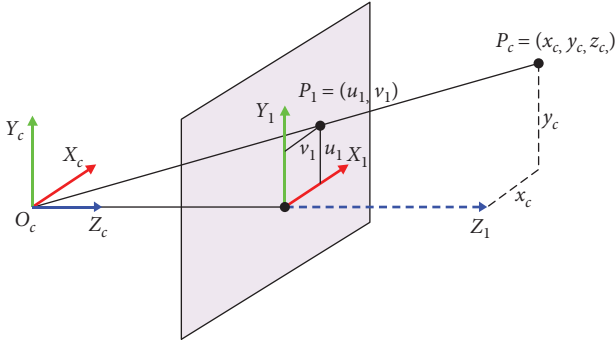


FIGURE 7: The model of the camera.

3.2. Ground Plane Estimation. Ground plane estimation is the basis of subsequent extrinsic parameter calculation of the camera. Its accuracy determines the accuracy of extrinsic camera parameters. In a scene, multiple planes will be fitted out. Then, whether the plane is a ground plane is determined according to the following conditions:

$$\begin{cases} \theta < \frac{\pi}{4}, \\ \text{median } P_{W_i}^Z > \min P_{C_0}^Z + \varepsilon, \end{cases} \quad (12)$$

where θ is the angle between the X_c axis of the camera and the plane; median is the operation of taking the median value; $P_{W_i}^Z$ is the set of interior point Z-values of the fitted plane model; $P_{C_0}^Z$ is the set of exterior point Z-values of the fitted plane model; and ε is the set tolerance value. Equation (12) represents two conditions: (1) the inclination angle of the camera relative to the plane does not exceed 45° and (2) after the exterior parameter is calculated according to the plane, the point cloud is transformed to the world coordinate system. The point set on the plane has the largest Z-value.

According to this definition, the planes were screened to calculate the qualified ground plane. The flowchart is shown in Figure 6.

First, the 3D point cloud in the camera coordinate system was input, and the plane was calculated using the MLESAC method. The set of interior points satisfying the plane was recorded. By using this plane and the method in Section 2.2, the extrinsic parameters of the camera were calculated. Combined with the internal parameters of the camera, the 3D point cloud in the camera coordinate system was transformed to the 3D point cloud in the world coordinate system, and it was judged whether the conditional equation (12) was met. If not, then the recorded set of interior points was removed from the point cloud, and fitting of the plane continued. Otherwise, the plane was the ground plane. No further operation was conducted, and the extrinsic parameters of the camera were output.

4. Experiment

4.1. Experiment Process. In this experiment, a PrimeSense camera was used to collect video data, and MATLAB was used for simulation to validate the proposed algorithm. To

facilitate the accuracy comparison, the chessboard calibration results of the color camera were used as the reference data. Because the matrix was not suitable for comparison, the extrinsic parameters were transformed to camera height (H), roll angle (θ), and pitch angle (ϕ). The calibration accuracy was measured by comparing the camera height, roll angle, and pitch angle. Following the world coordinates established in Section 2, the values can be obtained as

$$\begin{cases} H = Z_c, \\ \phi = \arccos(P_c^{(2)} \cdot P_w^{(2)}), \\ \theta = \arccos(P_c^{(0)} \cdot P_w^{(2)}), \end{cases} \quad (13)$$

where $P_c^{(2)}$ is the camera Z-axis in the world coordinate, $P_c^{(0)}$ is the camera X-axis in the world coordinate, and $P_w^{(2)}$ is the world Z-axis.

The experiment was carried out according to the following steps.

- (1) A PrimeSense camera was used to collect video data (each frame of the video had a clear chessboard), including color video and depth video.
- (2) N ($N > 20$) video frames were selected randomly from the color video as the input to the Zhang camera calibration method [19], and the internal camera parameters were estimated.
- (3) Each frame of the color video was traversed. The camera's extrinsic parameters were estimated using the internal parameters and the chessboard corner detected by the current frame, and the camera attitudes ($H_{\text{chessboard}}$, $\phi_{\text{chessboard}}$, and $\theta_{\text{chessboard}}$) of each frame of color video were obtained.
- (4) Each frame of depth video was traversed. The ground plane was detected using the proposed method, and the extrinsic parameters of the camera were estimated to obtain the camera attitudes (H_{plane} , ϕ_{plane} , and θ_{plane}) of each frame of depth video.

The camera height difference (ΔH), roll angle difference ($\Delta\theta$), and pitch angle difference ($\Delta\phi$) of each frame was calculated, using the following equations:

$$\begin{cases} \Delta H = H_{\text{chessboard}} - H_{\text{plane}}, \\ \Delta\phi = \phi_{\text{chessboard}} - \phi_{\text{plane}}, \\ \Delta\theta = \theta_{\text{chessboard}} - \theta_{\text{plane}}. \end{cases} \quad (14)$$

The video formats collected in Step 1 are shown in Table 1.

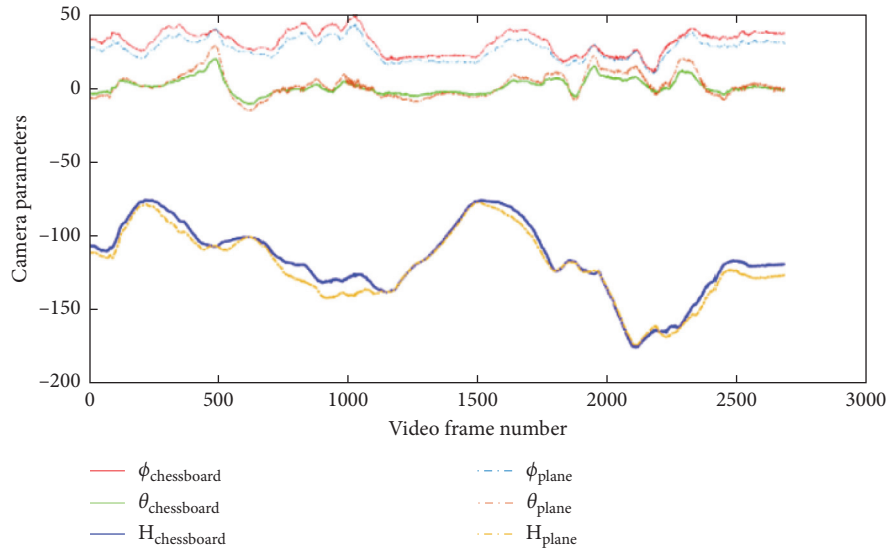
Each frame of the video contained a chessboard, as shown in Figure 8. In the experiment, the chessboard was used to estimate the camera's extrinsic parameters, which were taken as the reference data. Because different chessboards corresponded to different internal parameters when the camera's internal parameters were calculated using the Zhang calibration method [19], Steps 1 to 3 were executed 86 times. Each video frame could estimate 86 extrinsic parameters, with their medians as the reference data.

TABLE 1: Parameters of video.

	Color video	Depth video
Video size (pixel)	320 × 240	320 × 240
Frame rate (frame/s)	30	30
Duration (s)	89.4	89.4
Pixel byte (byte)	24	16
Video format	RGB24	Mono16



FIGURE 8: Color video frame comprising chessboard.

FIGURE 9: The result of the checkboard calibration method. The units of $\phi_{\text{chessboard}}$, $\theta_{\text{chessboard}}$, ϕ_{plane} , and θ_{plane} are degree, and the units of $H_{\text{chessboard}}$ and H_{plane} are centimeter.

The size of a chessboard was 7×9 , and both the length and width of each chessboard were 40 mm. The camera's extrinsic parameters, as obtained through chessboard calibration, are shown in Figure 8.

In Figure 9, $\theta_{\text{chessboard}}$, $\phi_{\text{chessboard}}$, and $H_{\text{chessboard}}$ are the medians of the camera pitch angle, roll angle, and height, respectively, as measured using the chessboard method and θ_{plane} , ϕ_{plane} , and H_{plane} are the medians of the camera pitch angle, roll angle, and height, respectively, as measured using the proposed method.

Figure 10 shows the experimental errors, and Table 2 shows the final measured results.

4.2. Error Analysis. Because there was no high-precision instrument to measure the extrinsic parameters of the camera in the experiment, these were measured using the chessboard calibration method and taken as the reference data to measure the accuracy of the proposed method. The factors affecting the accuracy of this experiment are as follows.

- (1) First is quantization error of corner detection. Because the video frame used was 240×320 pixels, the quantization error of corner detection was quite large when calculating the camera's internal and extrinsic parameters.

TABLE 2: Table of extrinsic parameters error of camera.

	Maximum	Minimum	Mean
θ	7.49	-0.75	4.47
ϕ	4.87	-9.62	-3.87
H	15.21	-1.15	3.96

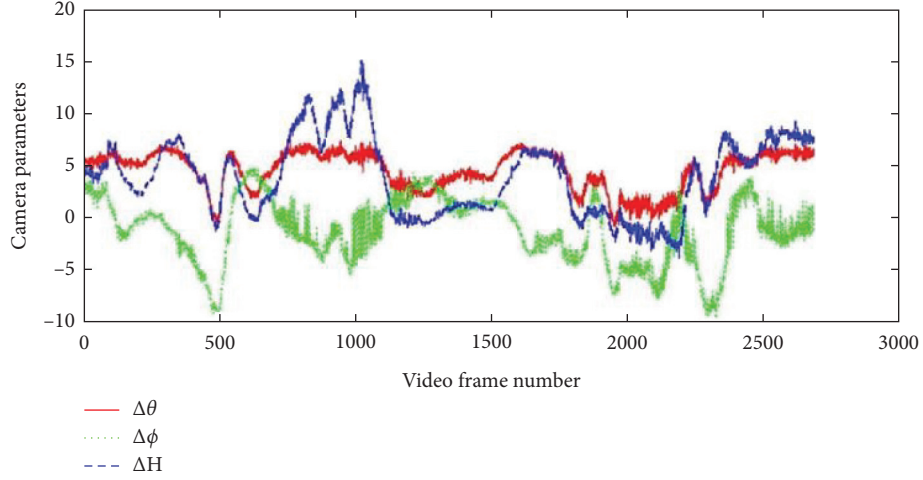


FIGURE 10: Test result. The camera height difference (ΔH), roll angle difference ($\Delta\theta$), and yaw angle difference ($\Delta\phi$) of each frame were calculated by (13). The units of $\Delta\theta$ and $\Delta\phi$ are degree, and the unit of ΔH is centimeter.

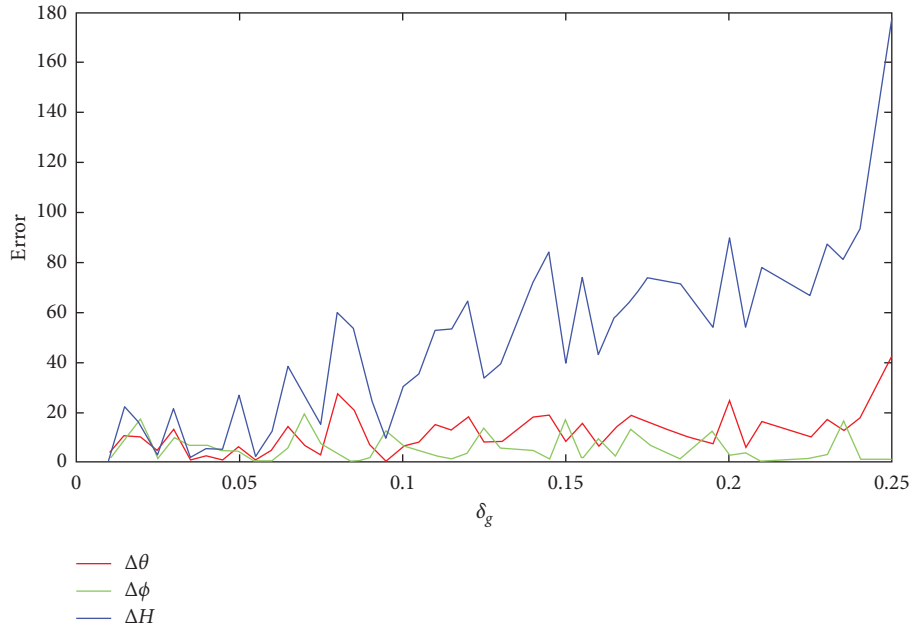


FIGURE 11: The effect of noise on the result. The error units of roll angle difference ($\Delta\theta$) and yaw angle difference ($\Delta\phi$) are degrees, and the error unit of camera height difference (ΔH) is centimeter.

- (2) The chessboard method and the proposed method were, respectively, used to measure the extrinsic parameters of the RGB-D camera's color sensor and infrared camera.
- (3) The noise of the RGB-D camera scanning scene data would affect the detection of the ground plane, thus affecting the accuracy of the camera's extrinsic parameters.

- (4) The parameters to stop MLESAC iteration in ground plane detection would also affect the results of this experiment.

4.3. Influence of Scene Noise on Ground Plane Detection. RGB-D cameras have many noise sources, such as temperature, incident angle and intensity of ambient light, and texture [22]. The MLESAC used in this study could deal with small amounts of noise, but not with scenes with too much noise or data loss.

- (1) Strong sunlight would cause too many ground plane noise points, resulting in inaccurate estimation of plane parameters and a slight influence on the camera height and roll angle.
- (2) If the reflectivity of the ground was too high (for example, a mirror was placed on the ground), the data of this area would be lost. If too much data were missing, then the ground plane could not be detected, and the extrinsic parameters of the camera could not be estimated.

To verify the influence of noise on camera attitude, Figure 11 shows the error change of camera attitude with the increase of Gaussian noise variance in the 929th frame. The mean value of Gaussian noise was 0, and the variance was δ_g . It can be seen that with the increase of noise variance, the height error increases, and the stability of pitch angle and roll angle decreases. In addition, when the variance is greater than 0.25, the plane cannot be correctly estimated.

5. Conclusion

During pedestrian detection based on RGB-D cameras, due to the impact of environmental vibration, an RGB-D camera will shift its original position, and the extrinsic parameters will change greatly, which will directly affect the detection accuracy. By using the automatic extrinsic parameter calibration method proposed in this study, the extrinsic parameters can be automatically corrected when there is no pedestrian, so as to solve the above problem.

The proposed method can be applied to the automatic adjustment of extrinsic parameters of 3D cameras (speckle, TOF, and binocular camera) and has high parallelism. After parallel implementation, it is instantaneous and can be used for the automatic calibration of extrinsic parameters of 3D cameras on mobile robots.

In this method, we extracted the plane from the 3D point cloud and used the position relationship between the plane and world coordinates to obtain a camera's extrinsic parameters, which were used to determine whether the current plane was a ground plane. If not, then the next plane would be used to calculate the extrinsic parameters until the ground plane was found, and the extrinsic parameters of the infrared camera were obtained. In this study, the conditions of the ground plane were given, which could guarantee the correctness of the established world coordinate system and creatively combine the plane detection with the extrinsic parameter estimation, so as to achieve the objective of

automatic extrinsic parameter calibration. This method does not require an additional calibration object, and it is aimed at the calibration of infrared cameras. The results are reliable.

The currently proposed method has the limitation that there needs to be a ground plane in the scene. If the ground plane cannot get detected, then the calibration cannot be carried out regularly. Two problems still must be solved: (1) to improve the accuracy of calibration and use targets such as pedestrians in scenes to carry out fine calibration and (2) to calibrate the extrinsic parameters of multiple cameras automatically according to the common area taken by multiple cameras. If no common area is taken by the two cameras, then a simple calibration object should be designed for automatic calibration to be carried out according to the geometric size of the calibration object.

The MATLAB resource code and the video data used to support the findings of this study are available from the corresponding author upon request.

Data Availability

Data are available on request to the corresponding author.

Conflicts of Interest

The authors declare that they have no conflicts of interest.

Acknowledgments

This work was supported in part by the Natural Science Foundation of China under Grant 61572083, in part by the Ministry of Education Joint Fund Project of China under Grant 6141A02022610, in part by the Fundamental Research Fund for the Central Universities of China under Grants 310824173601, 300102249304, and 300102248303, in part by the Fundamental Research Funds for the Central Universities Team Cultivation Project under Grant 300102248402, and in part by the Funds for Shaanxi Key R&D Program under Grant 2018ZDXMGY-047.

References

- [1] Microsoft. Kinect for X-Box 360[EB/OL]. 2017-01-01[2017-10-12], <https://support.xbox.com/en-US/browse/xbox-one/accessories/Kinect>.
- [2] Wikipedia. Kinect[EB/OL]. 2018-01-12 [2017-08-29], <https://en.wikipedia.org/wiki/Kinect>.
- [3] F. Barak, S. Alexander, M. Meir et al., "Depth mapping using projected patterns," US8493496B2[P], 2013.
- [4] R. A. El-laithy, J. Huang, and M. Yeh, "Study on the use of Microsoft Kinect for robotics applications," in *Proceedings of the 2012 IEEE/ION Position, Location and Navigation Symposium*, pp. 1280–1288, IEEE, Myrtle Beach, SC, USA, April 2012.
- [5] Z. Zhang, "Microsoft kinect sensor and its effect," *IEEE Multimedia*, vol. 19, no. 2, pp. 4–10, 2012.
- [6] J. Han, L. Shao, D. Xu, and J. Shotton, "Enhanced computer vision with microsoft kinect sensor: a review," *IEEE Transactions on Cybernetics*, vol. 43, no. 5, pp. 1318–1334, 2013.
- [7] P. Fankhauser, M. Bloesch, D. Rodriguez et al., "Kinect v2 for mobile robot navigation: evaluation and modeling," in

- Proceedings of International Conference on Advanced Robotics (ICAR)*, IEEE, Istanbul, Turkey, July 2015.
- [8] F. Endres, J. Hess, J. Sturm, D. Cremers, and W. Burgard, "3-D mapping with an RGB-D camera," *IEEE Transactions on Robotics*, vol. 30, no. 1, pp. 177–187, 2014.
 - [9] M. Labbé and F. Michaud, "Online global loop closure detection for large-scale multi-session graph-based SLAM," in *Proceedings of 2014 IEEE/RSJ International Conference on Intelligent Robots and Systems*, pp. 2661–2666, IEEE, Chicago, IL, USA, September 2014.
 - [10] M. Munaro, F. Basso, and E. Menegatti, "OpenPTrack: open source multi-camera calibration and people tracking for RGB-D camera networks," *Robotics and Autonomous Systems*, vol. 75, pp. 525–538, 2016.
 - [11] M. Munaro and E. Menegatti, "Fast RGB-D people tracking for service robots," *Autonomous Robots*, vol. 37, no. 3, pp. 227–242, 2014.
 - [12] E. Lachat, H. Macher, T. Landes, and P. Grussenmeyer, "Assessment and calibration of a RGB-D camera (Kinect v2 sensor) towards a potential use for close-range 3D modeling," *Remote Sensing*, vol. 7, no. 10, pp. 13070–13097, 2015.
 - [13] C. Chen, B. Yang, S. Song et al., "Calibrate multiple consumer RGB-D cameras for low-cost and efficient 3D indoor mapping," *Remote Sensing*, vol. 10, no. 2, 2018.
 - [14] J. Chow, D. Lichti, J. Hol, G. Bellusci, and H. Luinge, "IMU and multiple RGB-D camera fusion for assisting indoor stop-and-go 3D terrestrial laser scanning," *Robotics*, vol. 3, no. 3, pp. 247–280, 2014.
 - [15] D. R. dos Santos, M. A. Basso, K. Khoshelham, E. de Oliveira, N. L. Pavan, and G. Vosselman, "Mapping indoor spaces by adaptive coarse-to-fine registration of RGB-D data," *IEEE Geoscience and Remote Sensing Letters*, vol. 13, no. 2, pp. 262–266, 2016.
 - [16] J. Li, T. Cai, K. Deng, X. Wang, T. Sellis, and F. Xia, "Community-diversified influence maximization in social networks," *Information Systems*, vol. 92, Article ID 101522, 2020.
 - [17] Q. H. Liao, M. Liu, L. Tai et al., "Extrinsic calibration of 3D range finder and camera without auxiliary object or human intervention," 2017, <https://arxiv.org/abs/1703.04391>.
 - [18] F. Basso, E. Menegatti, and A. Pretto, "Robust intrinsic and extrinsic calibration of RGB-D cameras," 2017, <https://arxiv.org/abs/1701.05748>.
 - [19] Z. Zhang, "A flexible new technique for camera calibration," *IEEE Transactions on Pattern Analysis and Machine Intelligence*, vol. 22, no. 11, pp. 1330–1334, 2000.
 - [20] L. Shibo and Z. Qing, "A new approach to calibrate range image and color image from kinect," in *Proceedings of International Conference on Intelligent Human-Machine Systems and Cybernetics*, pp. 252–255, Washington, DC, USA, August 2012.
 - [21] P. H. S. Torr and A. Zisserman, "MLESAC: a new robust estimator with application to estimating image geometry," *Computer Vision and Image Understanding*, vol. 78, no. 1, pp. 138–156, 2000.
 - [22] A. Belhedi, A. Bartoli, S. Bourgeois, V. Gay-Bellile, K. Hamrouni, and P. Sayd, "Noise modelling in time-of-flight sensors with application to depth noise removal and uncertainty estimation in three-dimensional measurement," *IET Computer Vision*, vol. 9, no. 6, pp. 967–977, 2015.

Research Article

Information Spreading on Activity-Driven Temporal Networks with Two-Step Memory

Linfeng Zhong,¹ Xiaoyu Xue,² Yu Bai,¹ Jin Huang,¹ Qing Cheng,¹
Longyang Huang,¹ and Weijun Pan ¹

¹Civil Aviation Flight University of China, Guanghan 618307, China

²College of Cybersecurity, Sichuan University, Chengdu 610065, China

Correspondence should be addressed to Weijun Pan; wjpan@cafuc.edu.cn

Received 31 July 2020; Revised 16 August 2020; Accepted 13 November 2020; Published 16 January 2021

Academic Editor: Chenquan Gan

Copyright © 2021 Linfeng Zhong et al. This is an open access article distributed under the Creative Commons Attribution License, which permits unrestricted use, distribution, and reproduction in any medium, provided the original work is properly cited.

Information spreading dynamics on the temporal network is a hot topic in the field of network science. In this paper, we propose an information spreading model on an activity-driven temporal network, in which a node is accepting the information depends on the cumulatively received pieces of information in its recent two steps. With a generalized Markovian approach, we analyzed the information spreading size, and revealed that network temporality might suppress or promote the information spreading, which is determined by the information transmission probability. Besides, the system exists a critical mass, below which the information cannot globally outbreak, and above which the information outbreak size does not change with the initial seed size. Our theory can qualitatively well predict the numerical simulations.

1. Introduction

Information spreading on social networks is a hot topic in the fields of network science, computer science, and physics [1–9]. Research studies wish to know the evolutionary mechanisms and diffusion laws of the information, and further design some effective measure to control the information spreading. Using the massive real-data, researchers revealed many important evolution mechanisms, such as social reinforcement effect and memory effect [10–12]. To include those important evolution mechanisms into the information spreading dynamics, scholars proposed some successful models [13–18]. For instance, Watts [19] generalized the threshold model to complex networks, and revealed that the information spreading size first increases then decreases with the average degree of the network.

With these proposed mathematical models, the important question is how the network topologies affect the spreading dynamics. The studies in this topic can be divided into three aspects according to the complexity of the network. The first one is the effects of static networks. For static networks, research studies addressed the influences

of the degree distribution, weight distribution, and community on the information spreading [20–26]. An important conclusion is that a small fraction of nodes with large degrees makes the information outbreak with any values of information transmission probability [27, 28]. In reality, individuals can transmit the information through more than one communication channel. Therefore, using the multiplex networks describes the real-world network more accurately [29–32], which is the second aspect. Research studies revealed that the network multiplexity could suppress or promote the information spreading, which depends on the interaction between two networks [33–36]. The third aspect is that the effects of temporal network [37–42] on information spreading, since the nodes and connections do not always exist. Scholtes et al. [43] revealed that the spreading dynamics might speed up and slow down the information spreading on non-Markovian temporal networks. Wang et al. [44] proposed a heuristic method immunization strategy for information spreading on the temporal network.

To our best knowledge, when including the reinforcement and memory effect into the information spreading

model, the study about the effects of network temporality on information spreading dynamics is still lacking. To this end, we propose an information spreading model, in which a node is accepting the information when its cumulative received information in the recent two steps is more significant than a threshold in Section 2. With a generalized Markovian approach, we analyze the information spreading size in Section 3. Moreover, we perform extensive numerical simulations on activity-driven temporal networks in Section 4.

2. Model

In this section, we introduce the information spreading on temporal networks with two-step memory.

2.1. Activity-Driven Network. We first introduce the activity-driven temporal network $\mathcal{G} = (\mathcal{G}_1, \dots, \mathcal{G}_{t_{\max}})$ which is proposed by Perra et al. [45–47], where t_{\max} is the maximum time step. We set $t_{\max} = 100$ in this paper. The activity-driven network is build according to the following three steps for a given network size N . (i) For each node i , a potential activity x_i is assigned according to a given distribution $f(x)$. In this paper, we assume that $f(x)$ follows a power-law distribution. Specifically, $f(x) = \varrho x^{-\gamma_e}$, where γ_e is an exponent of potential activity distribution, and $\varrho = \sum_x x^{-\gamma_e}$, $\varepsilon \leq x < 1$. In numerical simulations, we set $\varepsilon = 0.001$. The larger the value of γ_e , the more homogeneous of potential activity, which induces the more homogeneous of degree distribution. (ii) At time step, we generate a temporal network \mathcal{G}_t . Each node i becomes active with probability $a_i = \eta x_i$, where η is a parameter. If node i becomes active, it will connect m nodes randomly. Otherwise, node i can only receive other connections. (iii) At the end of time step t , all edges are deleted. We repeated steps (i)–(iii) until $t = t_{\max}$. According to the above three steps, the average degree of network \mathcal{G}_t is $\langle k_t \rangle = 2m\eta\varepsilon((\gamma_e - 1)/(\gamma_e - 2))$. By adjusting the values of η , ε , and m , we can set the average degree of network \mathcal{G}_t .

2.2. Information Spreading Model. In this subsection, we introduce a novel information spreading model in which each node can remember the pieces of information it received in recent two steps. The information spreading dynamics is described by a generalized susceptible-infected-susceptible (SIS) model. A node in the susceptible state means that it had not accepted or believed the truth of the information but may accept it when its misgivings were eliminated. A node in the infected state means that it has accepted the information and is willing to share it with neighbors. To include the willingness to accept the information, we introduce an adoption threshold of θ ; the higher the value of θ , the less willing to accept the information. In what follows, we introduce how the information is spreading on activity-driven temporal networks.

Initially, we randomly select p fraction of nodes in the infected state, and the remaining $1 - p$ nodes in the susceptible state and every node do not obtain any pieces of

information, i.e., $m_i(t = 0) = 0$. At each time step t , every infected node i tries to transmit the information to its every susceptible neighbor on network \mathcal{G}_t , e.g., node j , with probability λ . If node j received the information, its received accumulated pieces of information become $m_j \leftarrow m_j + 1$. When node j received enough pieces of information from infected neighbors in recent steps, i.e., $m_j(t - 1) + m_j(t) \geq \theta$, node j becomes infected. Since every node can only remember the recent two-step memory about its accumulated, we here call our model as “two-step-memory” (TSM)-based information spreading. The infected node i recovers with probability γ and returns to a susceptible state. Note that when $t = t_{\max}$, the next time step is $t = 0$. The information spreading dynamics evolves until there are no nodes in the infected state, or the time step reaches $t_f = 1000$.

3. Theory

In this section, we propose a generalized discrete Markovian approach [44, 48–50] to steady the TSM-based information spreading dynamics on activity-driven temporal networks. In the theory, we assume that every node transmitting the information to susceptible is independent. As a result, the dynamical correlations among the state of neighbors are neglected.

The $p_i(t)$ is denoted as the probability that node i is in the infected state at time t , and $1 - p_i(t)$ is denoted as the probability of node i is in the susceptible state. For a susceptible node j , it becomes infected state at time t only when its received accumulated pieces of information in time steps t and $t - 1$ are larger than the threshold θ . $q_j^n(t)$ is denoted as the probability of the node j obtaining n pieces of information from infected neighbors at time t simultaneously on the network \mathcal{G}_t . To compute the value of $q_j^n(t)$, we should consider three aspects: (i) select n neighbors from the neighbor set ∂j of node j , and denote the subset as Θ . (ii) Every node in Θ transmits the information to node j with probability $\prod_{\ell \in \Theta} \lambda p_\ell(t)$. (iii) Each node in the set $\partial j / \Theta$ does not transmit the information to node j . Combining the above three aspects, we obtain the expression of $q_j^n(t)$ as

$$q_j^n(t) = \sum_{\Theta \subseteq \partial j, |\Theta|=n} \prod_{\ell \in \Theta} \lambda p_\ell(t) \prod_{h \in \partial j / \Theta} (1 - \lambda p_h(t)), \quad (1)$$

where $|\Theta|$ represents the number of elements in set Θ . Once we know the expression of $p_i(t)$, we obtain the value of $q_j^n(t)$.

To compute the value of $p_i(t)$, we should consider two aspects. On the one hand, node i is in the infected state at time $t - 1$ but does not recover at time t . The probability of this event is $p_i(t - 1)(1 - \gamma)$. On the other hand, node i is in the susceptible state at time $t - 1$, and we obtained more than θ pieces of information at time steps $t - 1$ and t with probability:

$$\Gamma_i(t) = (1 - p_i(t - 1)) \left(1 - \sum_{n=0}^{\theta-1} Q_i^n(t) \right), \quad (2)$$

where $Q_i^n(t)$ represents that node i received at most $\theta - 1$ pieces of information from neighbors at time $t - 1$ and t . The expression of $Q_i^n(t)$ is

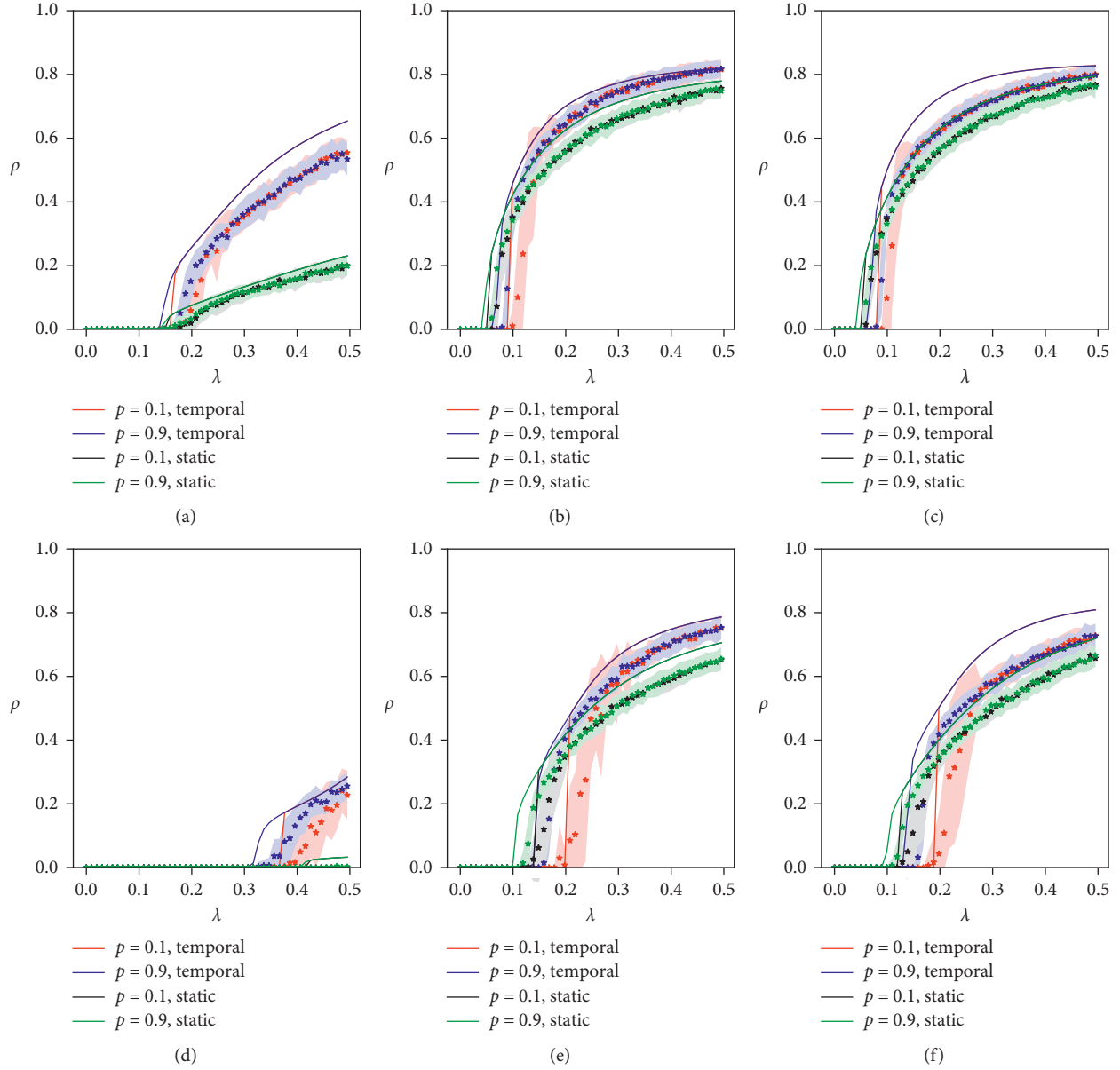


FIGURE 1: Information spreading on activity-driven networks and the corresponding static networks. The information spreading size ρ in the steady-state versus the information transmission probability λ with potential distribution exponent: (a) $\gamma_e = 2.1$, (b) $\gamma_e = 3.0$, and (c) $\gamma_e = 3.5$ with adoption threshold $\theta = 2$. ρ is a function of λ with (d) $\gamma_e = 2.1$, (e) $\gamma_e = 3.0$, and (f) $\gamma_e = 3.5$ with $\theta = 3$. Other parameters are set to be $m = 50$, $\gamma = 0.2$, $\langle k_i \rangle = 10$, and $N = 200$. The lines are theoretical predictions according to equations (1)–(5), and symbols are average values of numerical predictions. The shadow represents the standard deviations of numerical simulations. In each subfigure, the lines and symbols in the same color have the same parameter.

$$Q_i^n(t) = \sum_{m=0}^n q_i^m(t-1) q_i^{n-m}(t). \quad (3)$$

Considering the above two aspects, we obtain the evolution of $p_i(t)$ as

$$p_i(t) = p_i(t-1)(1-\gamma) + (1-p_i(t-1)) \left(1 - \sum_{n=0}^{\theta-1} Q_i^n(t) \right). \quad (4)$$

Averaging all values of $p_i(t)$, we obtain the probability that a node is randomly selected in the infected state at time t as

$$\rho(t) = \frac{1}{N} \sum_{i=1}^N p_i(t). \quad (5)$$

In the steady-state, the fraction of nodes in the infected state can be denoted as ρ for simplicity.

According to equation (4), the nonlinearity of the system makes us hardly obtain an analytical threshold. Therefore, we locate the threshold of the system by using the following method: observing the peak of $\Delta\rho$, which defines as

$$\Delta\rho = |\rho_{\lambda+\delta\lambda} - \rho_{\lambda}|, \quad (6)$$

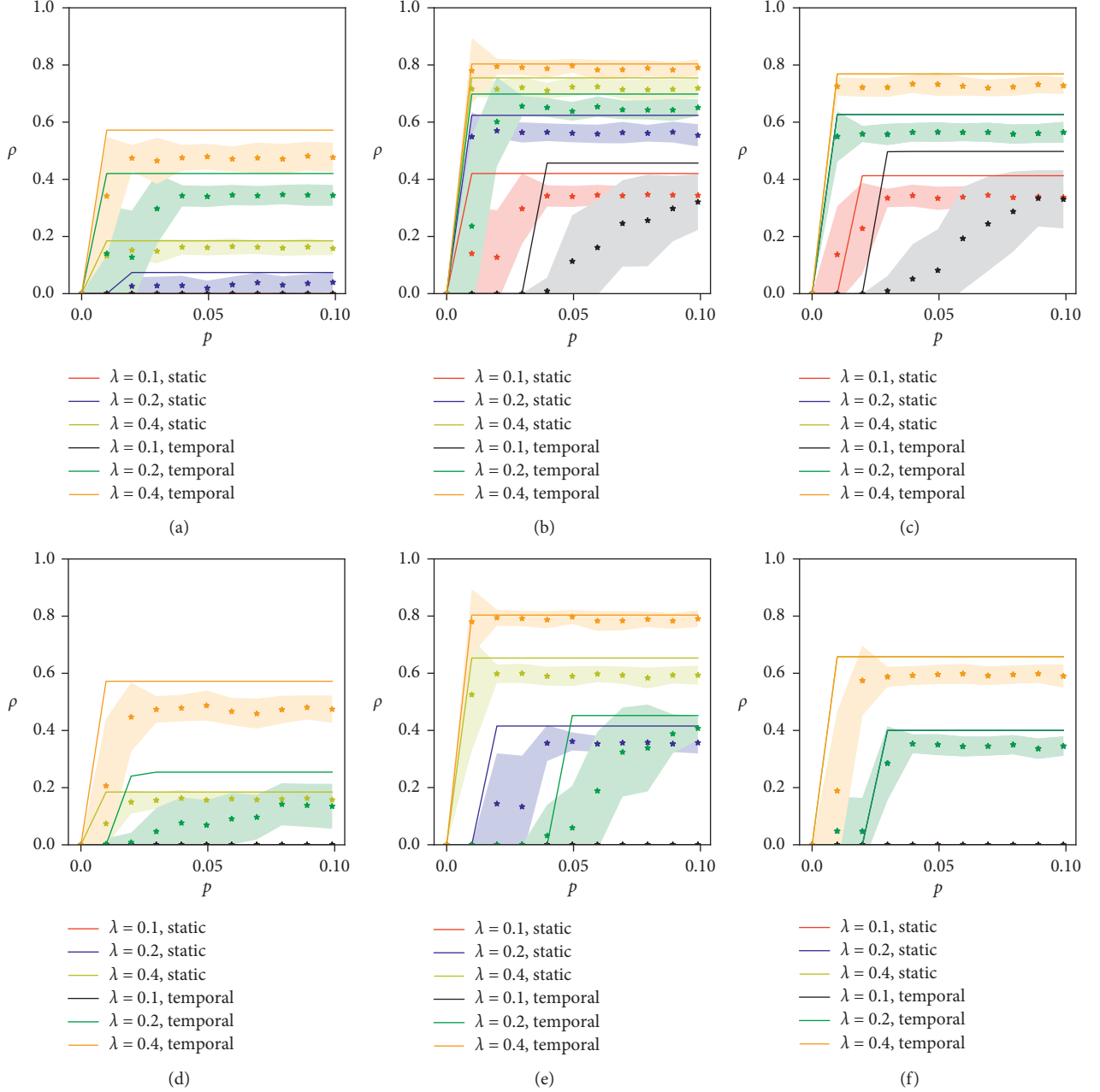


FIGURE 2: Information spreading on activity-driven networks and the corresponding static networks. The information spreading size ρ versus initial seed size p with potential distribution exponent (a) $\gamma_e = 2.1$, (b) $\gamma_e = 3.0$, and (c) $\gamma_e = 3.5$ with adoption threshold $\theta = 2$. ρ versus p with (d) $\gamma_e = 2.1$, (e) $\gamma_e = 3.0$, and (f) $\gamma_e = 3.5$ with $\theta = 3$. Other parameters are set to be $m = 50$, $\gamma = 0.2$, $\langle k_t \rangle = 10$, and $N = 200$. The lines are theoretical predictions, and symbols are average values of numerical predictions. The shadow represents the standard deviations of numerical simulations. In each subfigure, the lines and symbols in the same color have the same parameter.

where ρ_λ is the information outbreak size with information transmission probability λ , and $\delta\lambda$ is a small increment of λ . At the threshold point, $\Delta\rho$ reaches its maximum value [51].

The above theoretical derivation is for the information spreading dynamics on temporal networks. When studying the spreading dynamics on static networks, we only need to set $\mathcal{G}_t = \mathcal{G}_{t'}$ for $t \neq t'$.

4. Results

In this section, we will perform extensive numerical simulations on the activity-driven temporal networks and their corresponding static networks. To build the static network, we only need to generate network \mathcal{G}_1 and set the remaining temporal network equal to network \mathcal{G}_1 . All numerical simulation results presented in this paper are averaged over 500 times.

In Figure 1, we first investigate the information spreading size ρ on both temporal and static networks for a given average degree $\langle k_t \rangle = 10$. We focus on the following three aspects. (i) How the temporal network affects the information spreading? We reveal two distinct results. For small values of λ , the temporal network structure suppresses the information spreading since the network connectivity is small than that in its corresponding static networks. However, when λ is very large, the temporal network structure promoting the information spreading since a node in a temporal network can connect more distinct nodes. We note that the results are not affected by the initial seed size of p and γ_e . (ii) The phase transition of the system is the second point we will discuss. We find that the system always exhibits a hysteresis loop. Specifically, the spreading size ρ depends on the initial seed size p between the invasion threshold λ_{inv} and persistence threshold λ_{pre} [52]. The two threshold points can be located by using equation (6). (iii) The third point we investigate in Figure 1 is how γ_e affects ρ . We find that ρ increases with γ_e on both temporal and static networks. That is to say, the more homogeneous the degree distribution of the network, the less robust of the network for information spreading. The theoretical predictions agree well with the numerical simulation results. The differences between the theoretical and numerical predictions are induced by the strong dynamical correlations among the states among neighbors.

We further investigate the effects of initial seed size p on the information spreading dynamics in Figure 2. For any values of θ and λ , there is a finite value of critical mass p_c , below which the information cannot outbreak globally and above which the information outbreak size does not change with p . For the effects of network temporality, there have two situations. When $\theta = 2$, the network temporality suppresses the information spreading for small values of λ , e.g., $\lambda = 0.2$. However, when $\theta = 3$, the network temporality always promotes the information spreading regardless of the value of λ . Our suggested theory can qualitatively describe the above phenomena.

5. Conclusions

In this paper, we study the information spreading dynamics on activity-driven temporal networks. To study the effects of network temporality on information spreading, we first proposed an information spreading model, which assumes that a node accepting the information depends on the cumulatively received pieces of information from neighbors in the recent two steps. Then, we developed a generalized Markovian approach to describe the information spreading dynamics, and gave the expression of the information outbreak size. By performing extensive numerical simulations, we found that network temporality may suppress and promote the spreading of information. Specifically, the network temporality suppresses the information spreading for small values of information transmission probability, while promoting the information spreading for large values of information transmission probability. Finally, we found that the system has a critical mass. When the initial seed size

is smaller than the critical mass, the information cannot outbreak globally. When the initial size is larger than the critical mass, the information spreading size does not change with the initial seed size values. Our presented results help us understand the effects of network temporality on information spreading dynamics. And the results can also help us analyze the traffic of the complex dynamic aviation network.

Data Availability

The datasets used in the present study are available from the first author upon reasonable request (googlezlf@163.com).

Conflicts of Interest

The authors declare that they have no conflicts of interest.

Acknowledgments

This work was supported by the National Natural Science Foundation of China (grant no. U1733203), the Safety Foundation of CAAC (no. AQ20200019), and the Foundation of CAFUC (no. J2020-084).

References

- [1] C. Castellano, S. Fortunato, and V. Loreto, "Statistical physics of social dynamics," *Reviews of Modern Physics*, vol. 81, no. 2, p. 591, 2009.
- [2] S. Boccaletti, G. Bianconi, R. Criado et al., "The structure and dynamics of multilayer networks," *Physics Reports*, vol. 544, no. 1, pp. 1–122, 2014.
- [3] Z.-K. Zhang, C. Liu, X.-X. Zhan, X. Lu, C.-X. Zhang, and Y.-C. Zhang, "Dynamics of information diffusion and its applications on complex networks," *Physics Reports*, vol. 651, pp. 1–34, 2016.
- [4] M. Kitsak, L. K. Gallos, S. Havlin et al., "Identification of influential spreaders in complex networks," *Nature Physics*, vol. 6, no. 11, pp. 888–893, 2010.
- [5] W. Wang, Q.-H. Liu, J. Liang, Y. Hu, and T. Zhou, "Co-evolution spreading in complex networks," *Physics Reports*, vol. 820, pp. 1–51, 2019.
- [6] Y. Yi, Z. Zhang, L. T. Yang, C. Gan, X. Deng, and L. Yi, "Reemergence modeling of intelligent information diffusion in heterogeneous social networks: the dynamics pers," *IEEE Transactions on Network Science and Engineering*, vol. 99, p. 1, 2020.
- [7] J. Wang and J. Wang, "Cross-correlation complexity and synchronization of the financial time series on potts dynamics," *Physica A: Statistical Mechanics and Its Applications*, vol. 541, Article ID 123286, 2020.
- [8] J. Wang and J. Wang, "Measuring the correlation complexity between return series by multiscale complex analysis on potts dynamics," *Nonlinear Dynamics*, vol. 89, no. 4, pp. 2703–2721, 2017.
- [9] J. Wang, J. Wang, and H. E. Stanley, "Multiscale multifractal DCCA and complexity behaviors of return intervals for potts price model," *Physica A: Statistical Mechanics and Its Applications*, vol. 492, pp. 889–902, 2018.
- [10] H. P. Young, "The dynamics of social innovation," *Proceedings of the National Academy of Sciences*, vol. 108, no. 4, pp. 21285–21291, 2011.

- [11] D. Centola, "The spread of behavior in an online social network experiment," *Science*, vol. 329, no. 5996, pp. 1194–1197, 2010.
- [12] D. Centola, "Physician networks and the complex contagion of clinical treatment," *JAMA Network Open*, vol. 3, no. 1, Article ID e1918585, 2020.
- [13] D. Centola, *How Behavior Spreads: The Science of Complex Contagions*, Vol. 3, Princeton University Press, Princeton, NJ, USA, 2018.
- [14] D. Guilbeault, J. Becker, and D. Centola, "Complex contagions: a decade in review," in *Complex Spreading Phenomena in Social Systems*, Springer, Berlin, Germany, 2018.
- [15] D. Centola, "The social origins of networks and diffusion," *American Journal of Sociology*, vol. 120, no. 5, pp. 1295–1338, 2015.
- [16] M. Zheng, L. L. ü, M. Zhao et al., "Spreading in online social networks: the role of social reinforcement," *Physical Review E*, vol. 88, no. 1, p. 12818, 2013.
- [17] L. Lü, D.-B. Chen, and T. Zhou, "The small world yields the most effective information spreading," *New Journal of Physics*, vol. 13, no. 12, Article ID 123005, 2011.
- [18] W. Wang, M. Tang, H.-F. Zhang, and Y.-C. Lai, "Dynamics of social contagions with memory of nonredundant information," *Physical Review E*, vol. 92, no. 1, p. 12820, 2015.
- [19] D. J. Watts, "A simple model of global cascades on random networks," *Proceedings of the National Academy of Sciences*, vol. 99, no. 9, pp. 5766–5771, 2002.
- [20] M. Del Vicario, A. Bessi, F. Zollo et al., "The spreading of misinformation online," *Proceedings of the National Academy of Sciences*, vol. 113, no. 3, pp. 554–559, 2016.
- [21] G. Miritello, E. Moro, and R. Lara, "Dynamical strength of social ties in information spreading," *Physical Review E*, vol. 83, no. 4, p. 45102, 2011.
- [22] Y. Sun, C. Liu, C.-X. Zhang, and Z.-K. Zhang, "Epidemic spreading on weighted complex networks," *Physics Letters A*, vol. 378, no. 7–8, pp. 635–640, 2014.
- [23] Y. Feng, L. Ding, Y.-H. Huang, and L. Zhang, "Epidemic spreading on weighted networks with adaptive topology based on infective information," *Physica A: Statistical Mechanics and Its Applications*, vol. 463, pp. 493–502, 2016.
- [24] X. Chu, J. Guan, Z. Zhang, and S. Zhou, "Epidemic spreading in weighted scale-free networks with community structure," *Journal of Statistical Mechanics: Theory and Experiment*, vol. 2009, no. 7, Article ID P07043, 2009.
- [25] L.-F. Zhong, J.-G. Liu, and M.-S. Shang, "Iterative resource allocation based on propagation feature of node for identifying the influential nodes," *Physics Letters A*, vol. 379, no. 38, pp. 2272–2276, 2015.
- [26] L.-F. Zhong, Q.-H. Liu, W. Wang, and S.-M. Cai, "Comprehensive influence of local and global characteristics on identifying the influential nodes," *Physica A: Statistical Mechanics and Its Applications*, vol. 511, pp. 78–84, 2018.
- [27] R. Pastor-Satorras and A. Vespignani, "Epidemic spreading in scale-free networks," *Physical Review Letters*, vol. 86, no. 14, p. 3200, 2001.
- [28] R. Pastor-Satorras and A. Vespignani, "Epidemic dynamics and endemic states in complex networks," *Physical Review E*, vol. 63, no. 6, p. 66117, 2001.
- [29] M. Kivelä, A. Arenas, M. Barthélemy, J. P. Gleeson, Y. Moreno, and M. A. Porter, "Multilayer networks," *Journal of Complex Networks*, vol. 2, no. 3, pp. 203–271, 2014.
- [30] P. J. Mucha, T. Richardson, K. Macon, M. A. Porter, and J.-P. Onnela, "Community structure in time-dependent, multiscale, and multiplex networks," *Science*, vol. 328, no. 5980, pp. 876–878, 2010.
- [31] J. Gómez-Gardenes, I. Reinares, A. Arenas, and L. M. Floría, "Evolution of cooperation in multiplex networks," *Scientific Reports*, vol. 2, p. 620, 2012.
- [32] J. Y. Kim and K.-I. Goh, "Coevolution and correlated multiplexity in multiplex networks," *Physical Review Letters*, vol. 111, no. 5, p. 58702, 2013.
- [33] K.-M. Lee, C. D. Brummitt, and K.-I. Goh, "Threshold cascades with response heterogeneity in multiplex networks," *Physical Review E*, vol. 90, no. 6, p. 62816, 2014.
- [34] C. D. Brummitt, K.-M. Lee, and K.-I. Goh, "Multiplexity-facilitated cascades in networks," *Physical Review E*, vol. 85, no. 4, p. 45102, 2012.
- [35] Z. Li, F. Yan, and Y. Jiang, "Cross-layers cascade in multiplex networks," *Autonomous Agents and Multi-Agent Systems*, vol. 29, no. 6, pp. 1186–1215, 2015.
- [36] Q. Guo, X. Jiang, Y. Lei, M. Li, Y. Ma, and Z. Zheng, "Two-stage effects of awareness cascade on epidemic spreading in multiplex networks," *Physical Review E*, vol. 91, no. 1, p. 12822, 2015.
- [37] P. Holme, "Modern temporal network theory: a colloquium," *The European Physical Journal B*, vol. 88, no. 9, p. 234, 2015.
- [38] N. Masuda and P. Holme, *Temporal Network Epidemiology*, Springer, Berlin, Germany, 2017.
- [39] P. Holme and J. Saramäki, "Temporal networks," *Physics Reports*, vol. 519, no. 3, pp. 97–125, 2012.
- [40] S. Lee, L. E. Rocha, F. Liljeros, and P. Holme, "Exploiting temporal network structures of human interaction to effectively immunize populations," *PloS One*, vol. 7, no. 5, Article ID e36439, 2012.
- [41] J. Tang, M. Musolesi, C. Mascolo, and V. Latora, "Temporal distance metrics for social network analysis," in *Proceedings of the 2nd ACM Workshop on Online Social Networks*, pp. 31–36, Barcelona, Spain, August 2009.
- [42] N. Masuda and P. Holme, "Predicting and controlling infectious disease epidemics using temporal networks," *F1000prime Reports*, vol. 5, no. 6, 2013.
- [43] I. Scholtes, N. Wider, R. Pfitzner, A. Garas, C. J. Tessone, and F. Schweitzer, "Causality-driven slow-down and speed-up of diffusion in non-markovian temporal networks," *Nature Communications*, vol. 5, no. 1, pp. 1–9, 2014.
- [44] W. Wang, Y. Ma, T. Wu, Y. Dai, X. Chen, and L. A. Braunstein, "Containing misinformation spreading in temporal social networks," *Chaos: An Interdisciplinary Journal of Nonlinear Science*, vol. 29, no. 12, Article ID 123131, 2019.
- [45] N. Perra, B. Gonçalves, R. Pastor-Satorras, and A. Vespignani, "Activity driven modeling of time varying networks," *Scientific Reports*, vol. 2, p. 469, 2012.
- [46] M. Karsai, N. Perra, and A. Vespignani, "Time varying networks and the weakness of strong ties," *Scientific Reports*, vol. 4, p. 4001, 2014.
- [47] N. Perra, A. Baronchelli, D. Mocanu, B. Gonçalves, R. Pastor-Satorras, and A. Vespignani, "Random walks and search in time-varying networks," *Physical Review Letters*, vol. 109, no. 23, Article ID 238701, 2012.
- [48] S. Gómez, A. Arenas, J. Borge-Holthoefer, S. Meloni, and Y. Moreno, "Discrete-time Markov chain approach to contact-based disease spreading in complex networks," *EPL (Europhysics Letters)*, vol. 89, no. 3, p. 38009, 2010.
- [49] L. Pan, W. Wang, S. Cai, and T. Zhou, "Optimal interlayer structure for promoting spreading of the susceptible-infected-

- susceptible model in two-layer networks,” *Physical Review E*, vol. 100, no. 2, p. 22316, 2019.
- [50] E. Valdano, L. Ferreri, C. Poletto, and V. Colizza, “Analytical computation of the epidemic threshold on temporal networks,” *Physical Review X*, vol. 5, no. 2, p. 21005, 2015.
- [51] X. Chen, W. Wang, S. Cai, H. E. Stanley, and L. A. Braunstein, “Optimal resource diffusion for suppressing disease spreading in multiplex networks,” *Journal of Statistical Mechanics: Theory and Experiment*, vol. 2018, no. 5, p. 53501, 2018.
- [52] H. Yang, M. Tang, and T. Gross, “Large epidemic thresholds emerge in heterogeneous networks of heterogeneous nodes,” *Scientific Reports*, vol. 5, p. 13122, 2015.

Research Article

Research on Wireless Sensor Network Security Location Based on Received Signal Strength Indicator Sybil Attack

Hongbin Wang and Liping Feng 

Department of Computer Science, Xinzhou Teachers University, Xinzhou, Shanxi 034000, China

Correspondence should be addressed to Liping Feng; fenglp@yeah.net

Received 28 July 2020; Revised 26 September 2020; Accepted 28 October 2020; Published 12 November 2020

Academic Editor: Qingyi Zhu

Copyright © 2020 Hongbin Wang and Liping Feng. This is an open access article distributed under the Creative Commons Attribution License, which permits unrestricted use, distribution, and reproduction in any medium, provided the original work is properly cited.

This paper studies the security location mechanism of the sensor network node under the attack of Sybil and analyzes the safe attacks which are possibly accepted and safe requirement in the location system. Since RSSI (Received Signal Strength Indicator) possesses the energy transmission function, different transmission energy will cause it to produce different RSSI readings. Furthermore, this kind of method cannot increase the burden on Wireless Sensor Network (WSN). It conducts an analysis between two receiving nodes, compares RSSI ratios to tackle the problem of time inconsistency of RSSI, and sets a threshold to detect Sybil by the emulation results. Research shows that the ratio value of different receiving nodes by using RSSI can resolve time difference because of the RSSI or unreliability which results from the asymmetry of transmission ratio. The thesis makes a comparison that the number of receiving nodes has an influence on attack effect. Utilizing the RSSI ratio values can exactly detect the Sybil attack. Emulation findings demonstrate that the detection method put forward by the thesis owns better security.

1. Introduction

Wireless Sensor Network (WSN) is composed of a great number of sensor nodes by means of wireless communicational technology and self-organization mode. It has a wide applicable prospect in the civilian aspect and the military aspect, but at present, the researches about WSN still have a lot of questions to solve, such as routing protocol, location technology, and network security. Location technology is one of the significant technologies of WSN. WSN establishes spatial relationship depending on the node's position to report the monitored incident. In addition, the node's position, which can help routing and other network functions, is also an essential basis. However, the location of the network node is easy to be attacked by enemies, because WSN is mainly used under the hostile and unguarded environment. The fragility depends on the importance of the security issue in the process of location.

This paper studies the security location mechanism of sensor network node under the attack of RSSI Sybil; RSSI

(Received Signal Strength Indicator) ranging technology is known for its low energy consumption, low cost, and easy to implement and has been widely used. But in the face of complex security environment, to resist attacks has become a key issue of applying the RSSI ranging technology to WSN.

2. Basic Principle of RSSI

RSSI calculates the loss of signal in the propagation process using the known signal strength at the receiving node according to the received signal strength and then transforms the propagation loss into the distance using the theoretical or empirical signal propagation model.

First, the basic principle of RSSI was introduced. The relationship between the transmitted power and the received power of radio signal can be expressed as formula (1), where P_R was the received power of radio signal, P_T was the transmitted power of radio signal, r was the distance between receiving unit and transmitting unit, n was the propagation factor, and its value depended on the environment of radio signal propagation.

$$P_R = \frac{P_T}{r^n}. \quad (1)$$

Formula (2) can be obtained by taking the logarithm on both sides of formula (1):

$$10 \lg r = 10 \lg \frac{P_T}{P_R}. \quad (2)$$

If the transmitted power of the node was known, formula (3) can be obtained by substituting the transmitted power into formula (2):

$$10 \lg P_R = A - 10 \lg r. \quad (3)$$

$10 \lg P_R$, the left part of formula (3), was the expression of converting the received signal power to dBm, which can be expressed directly as formula (4), where A can be regarded as the received signal power when the signal was transmitted 1 m:

$$P_R (\text{dBm}) = A - 10 \lg r. \quad (4)$$

By formula (4), it can be seen that the value of constants A and n determined the relationship between the received signal strength and signal transmission distance, and the influence of the two constants on the signal transmission distance was analyzed. First, assume that n remained unchanged. When the A changed, then the signal propagation factor n was a constant, and the relationship between the RSSI and propagation distance was obtained under different initial transmitted signal power, showing that the radio signal attenuation was very serious in the near distance propagation process and not serious in the long-distance propagation process. When the transmitted signal power increased, the propagation distance increased was approximated for the ratio of the signal power increase to the slope of the curve in the gentle phase.

When A remained unchanged, the relationship between the RSSI and propagation distance was obtained under different n . The smaller the value of n , the smaller the radio signal attenuation in the propagation process, and the farther the propagation distance of the radio signal. Increasing the transmitted signal power can increase the propagation distance. The propagation factor depended mainly on the attenuation, multipath effect, and interference reflection of the radio signal in the air. The smaller the interference, the smaller the propagation factor n , the farther the propagation distance of radio signal, the closer the propagation curve of the radio signal to the theoretical curve, and the more accurate the RSSI ranging [1].

Due to the limitation of the condition, no field measurement experiment was conducted in this paper. In the literature [2], a wireless sensor node made of CC2420 was used to measure the relationship between the RSSI and propagation distance, and a series of measurement experiments were conducted only in the open area, where the RSSI was received signal strength indication, which was represented by an 8-bit signed complement and stored in the RSSI_VAL memory of CC2420.

According to a large number of experimental measurements, the relationship between the RSSI and propagation distance was very complicated, which was related to the existence of obstacles, the distance between the node and the ground, and the antenna angle. When the transmitting node and the receiving node were not less than 2 m from the ground, the influence of antenna angle on the relationship between the RSSI and propagation distance was very small, and the error caused by the antenna angle was also very small. Therefore, when the transmitting node and the receiving node were placed about 2 m away from the ground, the RSSI mean and distance data were measured as in Table 1 [3].

After fitting, formula (5) of calculating the distance using the RSSI value was obtained:

$$d = 0.0023 \times \text{RSSI}^2 + (-0.4345) \times \text{RSSI} - 4.1458, \quad (5)$$

where the unit of d was m and the unit of RSSI was dBm.

Figure 1 shows that there was a certain error between the fitting curve and the actual distance, which was affected by many factors, such as climate and obstacles. Thus, the traditional and classical attenuation model of radio signal propagation was as

$$\text{RSSI}(d) = \text{RSSI}(d_0) - 10 \lg \left(\frac{d}{d_0} \right) + \zeta_\sigma, \quad (6)$$

where $\text{RSSI}(d)$ was the RSSI intensity value received from the place d meter from the transmitter, unit: dBm; $\text{RSSI}(d_0)$ was the RSSI intensity value received from the unknown node d_0 meter from the transmitter, unit: dBm; d was the distance between the transmitter and the receiver; d_0 was the reference distance, unit: m; λ was the path attenuation index, which was closely related to the surrounding environment and obstacles; ζ_σ was the standard deviation, which was the normal random variable of σ depending on the specific multipath environment, unit: dBm.

The RSSI ranging was a ranging method to judge the location of the target node using the appropriate radio propagation model by measuring the intensity of the radio frequency signal received by CC2420. The key to this method was to estimate the distance between the unknown node and multiple beacon nodes with the measured attenuation degree of radio frequency signal. Finally, the location of the unknown node was estimated with the measured distance value.

Formula (7) was obtained by formula (6):

$$d = 10 \frac{\text{RSSI}(d_0) - \text{RSSI}(d) + \zeta_\sigma}{10\lambda} \times d_0. \quad (7)$$

Formula (7) was the classical computation relation between the distance d and RSSI, where λ and ξ_σ were closely related to the external environment.

Table 2 showed the range of values of λ and ξ_σ in different environment.

There are many mathematical models for calculating the attenuation of radio waves, but there is no explicit mathematical model between the path attenuation and distance.

TABLE 1: RSSI average value and distance data.

Distance (m)	20	30	50	80	100
RSSI average value (dBm)	-10.897	-16.771	-19.378	-23.921	-24.509

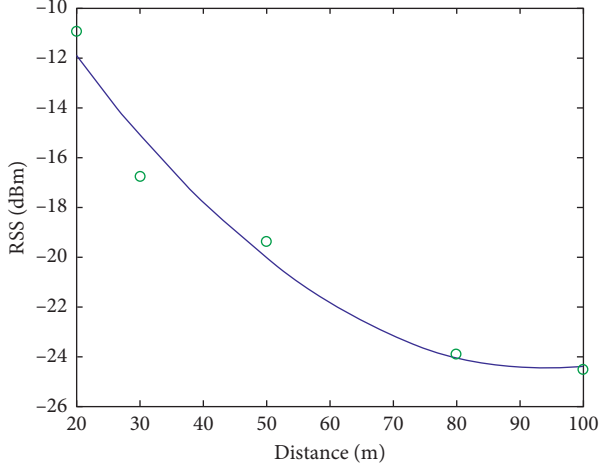


FIGURE 1: Echoism between RSSI and distance.

TABLE 2: The values of λ and ξ_σ in different condition.

Environmental conditions	Path attenuation index λ	Deviation ξ_σ
Playground	$2.7 < \lambda < 3.4$	$1.55 < \xi_\sigma < 4.12$
Corridor	$1.9 < \lambda < 2.2$	$1.37 < \xi_\sigma < 3.32$
Laboratory	$1.4 < \lambda < 2.2$	$2.39 < \xi_\sigma < 3.46$
Alley	$2.1 < \lambda < 3.0$	$2.19 < \xi_\sigma < 4.47$
Patio	$2.8 < \lambda < 3.8$	$1.00 < \xi_\sigma < 3.03$
Balcony	$1.4 < \lambda < 2.4$	$2.00 < \xi_\sigma < 4.00$
Road	$3.3 < \lambda < 3.7$	$2.97 < \xi_\sigma < 4.27$
Grassland	$4.6 < \lambda < 5.1$	$1.67 < \xi_\sigma < 2.23$

There are pure empirical models based on various measurements and semiempirical models for theoretical analysis based on physical parameter measurements. The best applicability of a particular model depends on whether it can simulate the actual working environment of a wireless system; thus, the method of mathematical model calibration for propagation attenuation was proposed. When using this method, the RSSI means of specific distances were obtained by collecting the measured data and used to correct the propagation model in the region to obtain the attenuation characteristics of the signal in the region in the propagation process. Therefore, the results predicted by the model were more close to the results in the actual field environment, which thus effectively improve the node localization accuracy.

The RSSI-based localization algorithm calculated the distance between unknown node and beacon node using the received value of the measured signal by formula (7). The acquisition of RSSI intensity value can be implemented

either by unknown node or by beacon node. The method was called self-localization if the acquisition of RSSI intensity value was implemented by unknown node, and telemetric localization by beacon nodes. In the self-localization mode, the target node can measure the distance between itself and multiple beacon node in WSN and then calculate the location relative to the beacon node. By contrast, in the telemetric localization mode, the RSSI intensity value of unknown node was measured by the beacon node to determine the location of unknown node. For the self-localization mode, the RF transmitted power of each beacon node was the same. For the telemetric localization mode, the WSN must have both the function of power measurement to determine the RF transmitted power of each unknown node and the ability of data transmission [4].

As shown in Figure 2, suppose (x_i, y_i) was the location coordinate of the i th beacon node in WSN; (x, y) was the location coordinate of the unknown node; RSSI_{i-t} was the RSSI value of the i th beacon node received by the unknown node at t ; and the distance between the unknown node and the i th beacon node was obtained by formula (7); thus, formula (8) was established:

$$\Gamma(x, y) = \sum_{i=1}^n W_i \left[\sqrt{(x - x_i)^2 + (y - y_i)^2} - d_{i-t} \right]^2, \quad (8)$$

where n was the total number of beacon nodes in WSN.

At this point, the localization problem was transformed into the problem of finding the minimum value of the function of two variables in mathematics, where W_i was the weighting factor. From the geometric point of view, in the coordinate system, the distance between the unknown node (x, y) and the i th beacon node (x_i, y_i) met the following geometric relation:

$$d_{i-t} = \sqrt{(x - x_i)^2 + (y - y_i)^2}. \quad (9)$$

Suppose the RSSI decay was the same in the communication between the unknown node and its adjacent beacon node; then formula (10) can be obtained from formula (9):

$$AX = B, \quad (10)$$

where

$$A = \begin{bmatrix} 2(x_1 - x_n) & 2(y_1 - y_n) \\ \vdots & \vdots \\ 2(x_{n-1} - x_n) & 2(y_{n-1} - y_n) \end{bmatrix}, \quad B = \begin{bmatrix} x_1^2 - x_n^2 + y_1^2 - y_n^2 + d_n^2 - d_1^2 \\ \vdots \\ x_{n-1}^2 - x_n^2 + y_{n-1}^2 - y_n^2 + d_n^2 - d_{n-1}^2 \end{bmatrix}, \quad (11)$$

$$X = \begin{bmatrix} x \\ y \end{bmatrix}.$$

Thus, the coordinate of unknown node can be expressed by the least square method:

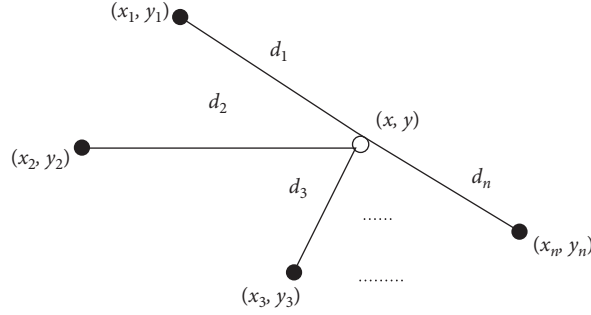


FIGURE 2: Classic RSSI position location.

$$\hat{X} = (A^T W A)^{-1} A^T W B, \quad (12)$$

where W was symmetric positive definite matrix (simple diagonal positive definite matrix), and selecting the appropriate weighting matrix can effectively improve the location accuracy.

$$\text{When } W = \begin{bmatrix} 1, 0, \dots, 0 \\ 0, 1, \dots, 0 \\ \dots \dots \dots \\ 0, \dots, 1, 0 \\ 0, \dots, 0, 1 \end{bmatrix}, \text{ formula (12) was trilateration}$$

method.

3. Application Advantages of RSSI

The RSSI is an important method to solve the problem of node localization. Its main application advantages are as follows:

- (1) Convenient application: The RSSI is the received signal strength from the other side in mutual communication and often can be extracted directly from the hardware in normal communication between wireless sensor nodes without requiring additional devices, which is of great significance to reduce the network cost and complexity.
- (2) Symmetry: The RSSI value is often symmetric, so the RSSI value between two nodes can be completed only by sending and receiving a message packet, which is of great significance to reduce the complexity of localization algorithm and the application scene which is not very demanding for location accuracy.
- (3) Distance monotonicity: The distance value between the RSSI value and node is monotonic and becomes smaller with the increase of distance. Therefore, the RSSI can meet the requirements of ranging and ranging-free localization algorithms.

4. Detection Method of Sybil Attacks

The solution to Sybil attacks based on RSSI will not increase the burden of WSN. When a message was received, the receiver will contact the RSSI with the sender ID. Later, when another message containing the same RSSI but with different sender ID was received, the receiver will assume it

as a Sybil attack. However, this method was not feasible due to the difference in receiving time of RSSI [5, 6]. In addition, the energy of WSN transmitter can be easily changed, so one Sybil node can send messages with different IDs and transmission energies in order to deceive the receiving node. With the function of energy transmission, sending messages with different transmission energies will result in different RSSI readings.

In this paper, a method of solving the Sybil attacks in WSN based on RSSI was studied. This method had good robustness and simple structure and can be easily implemented in sensors. According to the existing data, this method is the best way to solve the Sybil attacks in WSN.

It was verified by experiment that although the RSSI was unreliable and had time differences and nonequivalent transmission ratios [5], these problems can be easily solved by using the RSSI ratios of multiple receiving nodes that were introduced in the literature [7]. The problem of time differences in RSSI ratios was studied with a variable RSSI receiver by experiment, and the standard deviation was very small. Then the reliable intervals of these time differences were given by the experiments of different distances. To simplify the problem, there was no need to calculate the location of the sender so as to avoid the calculation of distance attenuation, thus reducing the calculation requirements of the system.

The literature [8–11] studied the localization algorithm based on the distance between nodes obtained by RSSI ranging. In WSN, theoretically, the spatial location of an unknown node can be determined by the trilateration method through the RSSI information of four anchor nodes. Thus, the location of all sensors can be found. Suppose that the i th node received the radio signal from the O th node; thus, the RSSI was

$$R_i = \frac{P_0 \cdot K}{d_i^\alpha}, \quad (13)$$

where R_i was RSSI, P_0 was the transmitted signal energy, K was constant, d_i was the Euclidean distance, and α was the rate of change between distance and energy. Suppose the j th node received the radio signal from the O th node; thus, R_j had the same calculation conclusion similar to formula (13).

Thus, the RSSI ratios of the i th node and the j th node were obtained:

$$\frac{R_i}{R_j} = \frac{(P_o \cdot K/d_i^\alpha)}{(P_o \cdot K/d_j^\alpha)} = \left(\frac{d_i}{d_j}\right)^\alpha. \quad (14)$$

Formula (15) can be obtained by solving the following i th, j th, k th, and l th receiving nodes by the location coordinate (x, y) of node:

$$\begin{aligned} & (x - x_i)^2 + (y - y_i)^2 \\ &= \left(\frac{R_i}{R_j}\right)^{1/\alpha} \left((x - x_j)^2 + (y - y_j)^2\right) \\ &= \left(\frac{R_i}{R_k}\right)^{1/\alpha} \left((x - x_k)^2 + (y - y_k)^2\right) \\ &= \left(\frac{R_i}{R_l}\right)^{1/\alpha} \left((x - x_l)^2 + (y - y_l)^2\right), \end{aligned} \quad (15)$$

where (x_i, y_i) was the location coordinate of the i th node and the location coordinate of other nodes was similar.

When a message was received, four detection nodes calculated the location of the sender by formula (15) and contacted the location of the sender with the message containing the sender ID. Later, when another message containing different sender ID was received, the receiver will assume it as a Sybil attack as the calculation structure of location coordinate of the sender was the same as earlier.

However, the amount of calculation of the location of each node by formula (15) was very huge. In fact, it was not necessary to detect the Sybil nodes through this calculation. The location of all x, y and x_i, y_i remained consistent; thus, the Sybil attacks can be detected by comparing the RSSI ratio of the received message. Suppose the IDs of four detection nodes were D_1, D_2, D_3 , and D_4 , respectively, and the forged IDs of one Sybil node were S_1 and S_2 . The topology is shown in Figure 3.

At t_1 , the Sybil node broadcast a message and forged its ID as S_1 . The four neighbor nodes received the energy ratio and S_1 from the Sybil node, transmitted the message containing their own ID, and received the RSSI from the Sybil node to the normal node. Note that R_i^k was RSSI value (when the transmitting node K received the signal of the i th node). Thus, D_1 calculated the ratio for each node:

$$\begin{aligned} & \frac{R_{D_1}^{S_1}}{R_{D_2}^{S_1}}, \\ & \frac{R_{D_1}^{S_1}}{R_{D_3}^{S_1}}, \\ & \frac{R_{D_1}^{S_1}}{R_{D_4}^{S_1}}. \end{aligned} \quad (16)$$

And these ratios were stored.

Similarly, at t_2 , the Sybil node broadcast a message again and forged its ID as S_2 . The four neighbor nodes received the energy ratio from the Sybil node and reported it to D_1 . Thus, D_1 calculated each other's ratio:

$$\begin{aligned} & \frac{R_{D_1}^{S_2}}{R_{D_2}^{S_2}}, \\ & \frac{R_{D_1}^{S_2}}{R_{D_3}^{S_2}}, \\ & \frac{R_{D_1}^{S_2}}{R_{D_4}^{S_2}}. \end{aligned} \quad (17)$$

At this point, D_1 can detect the Sybil nodes according to the ratios at t_1 and t_2 . D_1 can conclude that if the gap between the values of two messages was close to zero, then there was a Sybil attack in this region. The received energy ratio was the same, so the location was the same. Normally, the messages broadcast by the node came from multiple IDs, but when there was a Sybil attack, the messages broadcast by the node came from the same ID. The following formula was used to calculate:

$$\begin{aligned} & \left(\frac{R_{D_1}^{S_1}}{R_{D_2}^{S_1}} = \frac{R_{D_1}^{S_2}}{R_{D_2}^{S_2}}\right), \\ & \left(\frac{R_{D_1}^{S_1}}{R_{D_3}^{S_1}} = \frac{R_{D_1}^{S_2}}{R_{D_3}^{S_2}}\right), \\ & \left(\frac{R_{D_1}^{S_1}}{R_{D_4}^{S_1}} = \frac{R_{D_1}^{S_2}}{R_{D_4}^{S_2}}\right). \end{aligned} \quad (18)$$

If formula (18) was valid, a Sybil attack was detected.

5. Experimental Simulation Analysis

Ideally, if the transmitting node and receiving node are kept in place, the RSSI will remain the same. Even under these conditions, the RSSI still fluctuates in the actual situation. Therefore, in this paper, the amount of the fluctuation was determined by experiment to further study the difference in the RSSI and explore how to solve this problem.

First, a node with constant energy (0 dbm) was used to transmit the message "nihao." Another node was used as a receiving node to automatically capture the RSSI values through the program TOS_Msg->strength in TinyOS and to transmit them to the PC through the RSC-232 serial port. The transmitting node transmitted this message 2,000 times. The distance between the transmitting node and the receiving node was set as 30 cm and changed to 1 m to repeat the experiment, as shown in Figure 4.

The mean and standard deviation σ of the data in Figure 4(a) were 54.55 and 14.32, respectively, and the mean and standard deviation σ of the data in Figure 4(b) were 133.26 and 12.38, respectively, suggesting RSSI

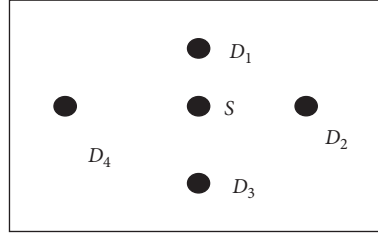


FIGURE 3: Topology model.

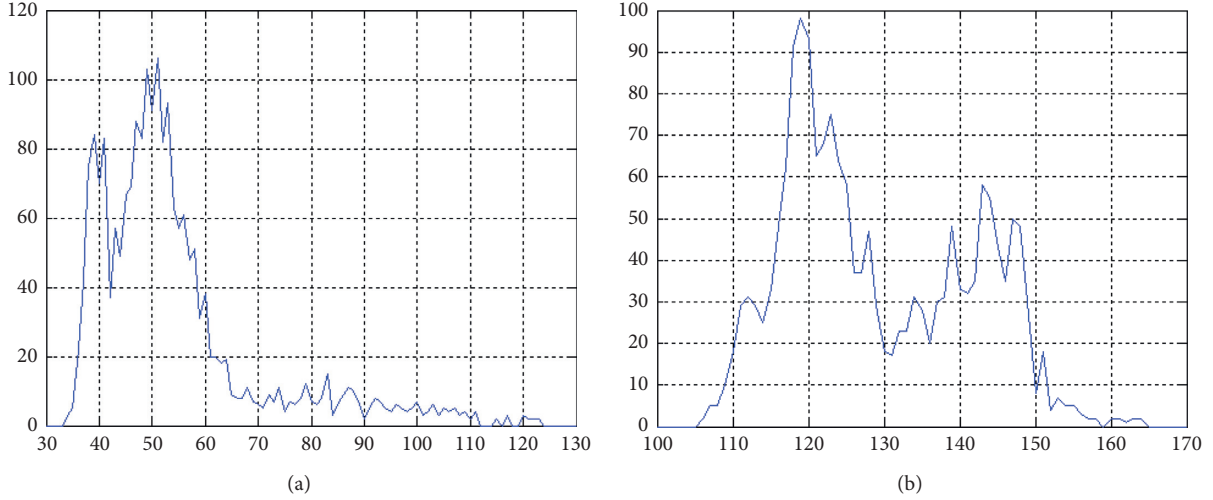


FIGURE 4: Comparison of RSSI difference. (a) The distance is 30 cm (X: RSSI value; Y: frequency of occurrence). (b) The distance is 1 m (X: RSSI value; Y: frequency of occurrence).

inconsistency. The correlation between the RSSI values was very small, making it unsuitable for detecting the Sybil attacks.

Then, two receiving nodes were used to analyze and compare their RSSI ratios to solve the problem of RSSI time inconsistency. It should be noted that the RSSI ratios also needed to solve the problem that the transmitting nodes had different transmission energies. In this experiment, the transmitting node broadcast a message 2,000 times with random and different transmission energies each time. The two receiving nodes recorded the RSSI values and transmit them to the base station to connect to the PC. The distance between the transmitting node and the receiving node was changed to 1 m to repeat the experiment twice.

The base station calculated the RSSI ratios of the two receiving nodes at t_1 and t_2 , respectively, and then calculated and recorded the difference between the two RSSI ratios, as shown in Figure 5.

The mean and standard deviation σ of the data in Figure 5(a) were 0 and 0.068, respectively, and the mean and standard deviation σ of the data in Figure 5(b) were 0 and 0.098, respectively, suggesting RSSI inconsistency. The difference in the RSSI ratio at point 0 controlled other data changes. The -0.2 and 0.2 in Figure 5(a) appeared only once in 2000 times (accounting for 0.5% of the total times), and the same applied to the -0.35 and 0.425 in Figure 5(b).

Therefore, a threshold $k * \sigma$ was set to determine the Sybil node. If $K > 3$, the Sybil attacks can be stably detected by the following formula according to the algorithm given earlier. If s_1 and s_2 were different but had the same location, the Sybil attacks can be inferred by judging whether the difference in the RSSI ratios of two events was within the threshold $k * \sigma$.

$$\begin{aligned} \left(\frac{R_{D_1}^{S_1}}{R_{D_2}^{S_1}} - \frac{R_{D_1}^{S_2}}{R_{D_2}^{S_2}} \right) &< \sigma, \\ \left(\frac{R_{D_1}^{S_1}}{R_{D_3}^{S_1}} - \frac{R_{D_1}^{S_2}}{R_{D_3}^{S_2}} \right) &< \sigma, \\ \left(\frac{R_{D_1}^{S_1}}{R_{D_4}^{S_1}} - \frac{R_{D_1}^{S_2}}{R_{D_4}^{S_2}} \right) &< \sigma. \end{aligned} \quad (19)$$

If the standard deviation deviated from the Gaussian distribution by about 70%, the threshold σ meant that the detected rate of the Sybil node was 70%. To reach 99.9%, the threshold was set as 5σ .

To estimate the influence of distance on the threshold σ , the second step experiment was repeated by increasing the distance between the transmitter and the receiver. The

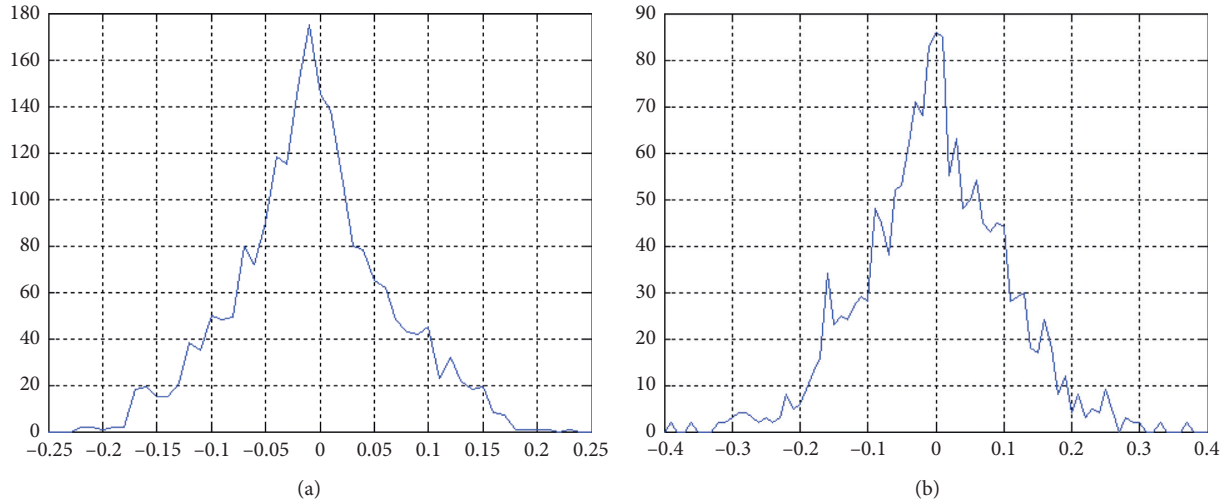


FIGURE 5: Comparison of RSSI difference. (a) The RSSI ratio at t_1 (X: RSSI value; Y: frequency of occurrence). (b) The RSSI ratio at t_2 (X: RSSI value; Y: frequency of occurrence).

second step experiment was performed 100 times at each distance, and the range of changing the distance was 1 m to 10 m, and the step length was 1 m.

As shown in Figure 6, the data 1 was median value, the data 2 was mean, the data 3 was standard deviation distribution, and the σ deviation will not exceed 0.15. Thus, the conclusion was drawn that if σ was set as 0.15, the Sybil node can be protected from attack when the threshold was set as 0.75.

Based on the Sybil attack protocol, the detection effect of RSSI was detected through different experimental steps. In the first step, four receiving nodes were used. In the second step, two receiving nodes were used. In the last step, as a control experiment, the Sybil nodes were limited by the transmission energy of changing nodes to evaluate the integrity and accuracy of the detection technology.

In the first step, four detection nodes were used to detect the Sybil attacks. First, the integrity of the detection technology was evaluated by experiment. The node distribution topology is shown in Figure 7(a). There was one Sybil node and four receiving nodes in WSN. When the Sybil node broadcast a message, the four detection nodes will record the RSSI value and ID according to the message, and D_2 , D_3 , and D_4 will transmit the data to D_1 . When the Sybil node broadcast a message with different IDs and transmission energies, the four detection nodes will record the RSSI value and ID according to the new message and then transmit the data to D_1 again. D_1 detected the Sybil attacks in WSN by formula (18).

The threshold was set as $5 * \sigma$. According to the previous analysis, the threshold was set as 0.75. To avoid message conflict in the experiment, the transmission time of each message was controlled with a timer. In the experiment, the Sybil node broadcast a message once every 30 seconds, and the receiving nodes transmitted the data to D_1 three seconds after detecting the Sybil node.

The distance between the receiving nodes and the Sybil node was changed to repeat the above experiment 100 times.

Transmitting the message at a 30-second interval meant that the topology was changed every one minute. Even in this case, D_1 can detect the Sybil attacks.

To detect the accuracy, the topology was changed, as shown in Figure 7(b). Here, the Sybil nodes in WSN were ignored, and two normal nodes were deployed to use only their own ID to broadcast messages. For the purpose of energy efficiency, some protocols required nodes to transmit messages with different transmission energies. The transmission energy will inevitably change when the energy of battery reduced and the environment changed, so the two normal nodes broadcast messages with different transmission energies. It should be noted that when the receiving nodes analyzed by the RSSI ratio, the change of transmission energy will not affect the correctness of evaluation of the Sybil nodes by the normal nodes. In each operation, the normal nodes' mutual locations were changed.

In the 100 times of experiments, D_1 did not report any Sybil attack. Even when the two normal nodes were only a few centimeters away, D_1 did not detect any Sybil node in WSN. Thus, the conclusion was drawn that four detection nodes can be used to detect the Sybil attacks based on RSSI.

In the second step, two detection nodes were used to detect the Sybil attacks. First, the integrity of the detection technology was evaluated by experiment the same as the first step. The node distribution topology is shown in Figure 8(a). There were two receiving nodes and one Sybil node. The distance between the receiving nodes and the Sybil node was changed to repeat the experiment 100 times the same as above. Because there were only two receiving nodes, only one comparison by formula (18) was required.

A conclusion similar to the first step was drawn that D_1 can detect the Sybil attacks in WSN.

To study whether the detection nodes can identify the Sybil attacks or normal events, the topology shown in Figure 8(b) was adopted. There were two monitors and two normal nodes in the topology, and each normal node had different IDs and transmission energies. The experimental

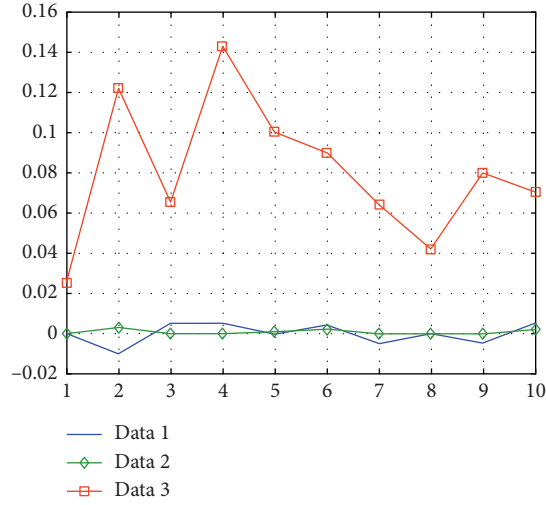


FIGURE 6: Distribution of median, mean value, and standard deviation (X: distance (m)).

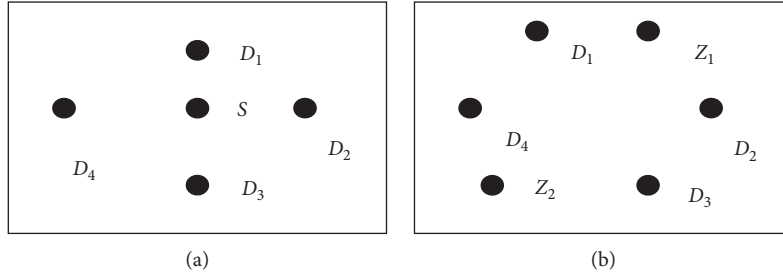


FIGURE 7: Four nodes detect Sybil attacking topology model. (a) 4 detection nodes and 1 Sybil node topology; (b) 4 detection nodes and 2 normal node topologies.

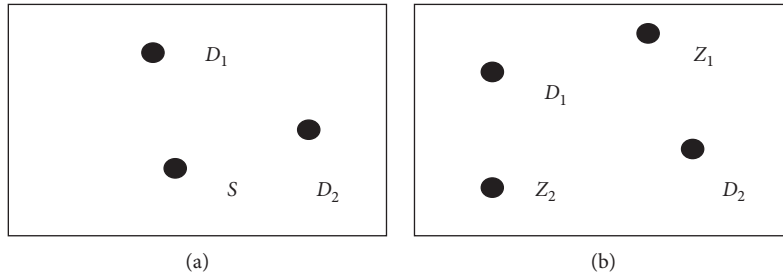


FIGURE 8: Two nodes detect Sybil attacking topology model. (a) 2 detection nodes and 1 Sybil node topology; (b) 2 detection nodes and 1 normal node topologies.

steps were the same as above, but only one comparison was required. The locations of the normal nodes were changed to repeat the experiment 100 times. During the 100 times of experiments, D_1 did not accurately detect the Sybil attack three times; that is, the error rate was lower than 5% when there were only two receiving nodes.

It should be noted that the Sybil attacks can be detected with only one transmission when there were two receiving nodes. Therefore, the energy consumption will be very small, but the error rate will increase. However, the integrity was more important than accuracy for the Sybil attacks; that is, the consequence of failing to detect the Sybil nodes was

much more serious than low accuracy. Based on this evaluation, it was suggested that the detection of Sybil attacks based on RSSI used two detection nodes rather than four detection nodes.

6. Conclusion

In this paper, first, the basic principle and typical algorithm of RSSI were introduced. Then, a detection method of Sybil attacks based on RSSI was proposed, the formulas of the basic principle were derived, and a simulation experiment of the algorithm was conducted. From the experiment results,

the appropriate threshold was found. The simulation results showed that the detection method can effectively resist the Sybil attacks. Finally, the effects of the number of receiving nodes on the detection effect of Sybil attacks were compared, and the Sybil attacks can be accurately detected by using the RSSI ratios of two receiving nodes. The method will be simulated in a larger and more complex environment so as to further study the stability and security of the work in the future.

Data Availability

The values of the initial experimental distance and the coordinate value are set by authors, and the remaining parameters are empirical data.

Conflicts of Interest

The authors declare that there are no conflicts of interest regarding the publication of this paper.

Acknowledgments

This work was supported by Cultivate Scientific Research Excellence Programs of Higher Education Institutions in Shanxi (2020KJ025); Research Project Supported by Shanxi Scholarship Council of China (2020-139); Xinzhou Teachers University Academic Leader Project.

References

- [1] W. E. I. Dapeng, *Research on Node Location Algorithm in Wireless Sensor Networks*, Taiyuan University of Technology, Shanxi, China, 2015.
- [2] Z. Haoling, S. Shou, and W. Xia, "Dynamic distance estimation algorithm based on RSSI and LQI," *Electronic Measurement Technology*, vol. 30, no. 2, pp. 142–144, 2017.
- [3] Y. Sun, "Review of wireless sensor networks," *Journal of Communication*, vol. 25, no. 4, pp. 114–124, 2019.
- [4] Y. Liu, *Design and Implementation of Wireless Sensor Network Positioning System*, Northwestern Polytechnical University, Xian, China, 2017.
- [5] D. Kotz, C. Newport, R. S. Gray, J. Liu, Y. Yuan, and C. Elliott, "Experimental evaluation of wireless simulation assumptions," in *Proceedings of the 7th ACM International Symposium on Modeling, Analysis and Simulation of Wireless and Mobile Systems (MSWiM'04)*, Venice, Italy, 2014.
- [6] G. Zhou, T. He, S. Krishnamurthy, and J. A. Stankovic, "Impact of radio irregularity on wireless sensor networks," in *Proceedings of the 2nd International Conference on Mobile Systems, Applications, and services (MobiSys' 04)*, Boston, MA, USA, 2018.
- [7] S. Zhong, L. Li, Y. G. Liu, and Y. R. Yang, "Privacy-preserving location based services for mobile users in wireless networks," Technical Report YALEU/DCS/TR-1297, Yale Computer Science, July 2014.
- [8] D. Niculescu and B. Nath, "Ad2Hoc positioning systems (APS)," in *Proceedings of the 2001 IEEE Global Telecommunications Conference (IEEE GLOBECOM 01)*, San Antonio, TX, USA, 2011.
- [9] D. Niculescu and B. Nath, "DV based positioning in ad hoc networks," *Journal of Telecommunication Systems*, no. 22, pp. 267–280, 2013.
- [10] Y. Feng and S. Haoshan, "An intelligent location algorithm for wireless sensor networks based on ranging," *Chinese Journal of Sensors and Actuators*, vol. 21, no. 1, pp. 135–140, 2018.
- [11] M. M. Patil, U. Shaha, U. B. Desai et al., "Localization in wireless sensor networks using three masters," in *Proceedings of the Personal Wireless Communications (ICPWC)*, New Delhi, India, 2015.

Review Article

A New Collaborative Filtering Recommendation Method Based on Transductive SVM and Active Learning

Xibin Wang ^{1,2}, Zhenyu Dai,³ Hui Li ³ and Jianfeng Yang¹

¹School of Data Science, Guizhou Institute of Technology, Guiyang 550003, Guizhou, China

²Special Key Laboratory of Artificial Intelligence and Intelligent Control of Guizhou Province, Guiyang 550003, Guizhou, China

³College of Computer Science & Technology, Guizhou University, Guiyang 550025, Guizhou, China

Correspondence should be addressed to Hui Li; cse.huili@gzu.edu.cn

Received 4 August 2020; Revised 21 September 2020; Accepted 15 October 2020; Published 2 November 2020

Academic Editor: Qingyi Zhu

Copyright © 2020 Xibin Wang et al. This is an open access article distributed under the Creative Commons Attribution License, which permits unrestricted use, distribution, and reproduction in any medium, provided the original work is properly cited.

In the collaborative filtering (CF) recommendation applications, the sparsity of user rating data, the effectiveness of cold start, the strategy of item information neglect, and user profiles construction are critical to both the efficiency and effectiveness of the recommendation algorithm. In order to solve the above problems, a personalized recommendation approach combining semisupervised support vector machine and active learning (AL) is proposed in this paper, which combines the benefits of both TSVM (Transductive Support Vector Machine) and AL. Firstly, a “maximum-minimum segmentation” of version space-based AL strategy is developed to choose the most informative unlabeled samples for human annotation; it aims to choose the least data which is enough to train a high-quality model. And then, an AL-based semisupervised TSVM algorithm is proposed to make full use of the distribution characteristics of unlabeled samples by adding a manifold regularization into objective function, which is helpful to make the proposed algorithm to overcome the traditional drawbacks of TSVM. Furthermore, during the procedure of recommendation model construction, not only user behavior information and item information, but also demographic information is utilized. Due to the benefits of the above design, the quality of unlabeled sample annotation can be improved; meanwhile, both the data sparsity and cold start problems are alleviated. Finally, the effectiveness of the proposed algorithm is verified based on UCI datasets, and then it is applied to personalized recommendation. The experimental results show the superiority of the proposed method in both effectiveness and efficiency.

1. Introduction

With the rapid development of the Internet applications and e-commerce, how to quickly and accurately recommend items (including goods, news, services) to different users that they are interested in has become a critical focus and many researchers have been devoted to this area. The personalized recommendation system is an effective method to solve this problem. It actively mines the users' preferences and pushes personalized items to target users.

Currently, the widely used recommendation methods [1] include collaborative filtering (CF), content-based, knowledge-based, and association rules-based recommendation. Among them, the most successful approach is the recommendation based on CF techniques, which can be divided

into two categories: memory-based and model-based methods. The memory-based CF is to filter and recommend items that users are interested in by calculating similarity measures of user preferences. It mainly uses user behavior information to make recommendations. The model-based CF is based on user preference information samples, training a recommendation model, and then calculating and generating recommendation results based on real-time user preferences.

However, the CF algorithm has the following problems:

- (1) *Data Sparsity and Cold Start Problems* [2]. For the memory-based CF algorithm, it is mainly based on the “user-item” rating matrix. When the matrix is very sparse, the performance of finding the nearest

neighbor will decrease significantly. Additionally, it is hard to draw any inferences for users or items, about which it has not yet gathered sufficient information; the so-called cold start problem will occur. In this case, it is more difficult to find data related to the new elements. For the model-based CF, in most implementations, users' historical preferences are stored in sparse matrices, and there are some obvious problems in the calculation of the sparse matrix, including the possibility that a few users' wrong preferences may have a great impact on the accuracy of the recommendation.

- (2) *Item and User Information May Be Discarded in Modeling.* The memory-based CF algorithm mainly makes use of the user's behavior information for recommendation, ignoring the information of items and users, which is of great help to improve the accuracy of recommendation.
- (3) *Data Quality Problem.* In model-based CF, the accuracy of recommendation may heavily rely on the number and quality of users' historical preference data.
- (4) *Scalability Issues.* With the advent of the era of big data, the rapid growth of users and items poses severe challenges to the scalability of the traditional CF algorithm.

In order to solve the data sparsity problem, many researchers try to use a small number of labeled data and machine learning methods such as classification, clustering, and dimension reduction to enhance the dataset. However, these methods have a common problem: when there are few labeled samples used in model construction, the prediction accuracy often is not high enough. In fact, in the real-world application scenarios, it can be found that most of the samples have no label information, and only very few samples are with labels, often resulting in high sparseness of the dataset, and even a "cold start" problem, which is quite unfavorable for discovering users' potential preferences. Additionally, the manual annotation method has the problems of high cost and is time-consuming [3]. Thus, how to combine the limited labeled samples and a large number of unlabeled samples to build a "user-item" association relationship model to predict users' interest preference for personalized recommendation has become an urgent issue.

Semisupervised learning (SSL) and active learning (AL) can effectively solve the problem of building a high-performance model with only a small amount of labeled data. SSL refers to labeling and utilizing unlabeled data according to some information that can be learned by oneself. On the contrary, AL is interactively exploring the unknown information of unlabeled data according to certain strategies and labeling them with domain knowledge. In this procedure, a small number of labeled "user-item" association data and a large number of unlabeled data are used to construct a model-based personalized recommendation; meanwhile, the ability to discover users' potential preferences is improved.

Based on the aforementioned idea, a semisupervised SVM recommendation algorithm based on AL is proposed in this paper, which uses the minimum principle of feasible domain segmentation in AL strategies to query the most informative samples for labeling. Furthermore, to make better use of the distribution characteristics of unlabeled data during the training process, a graph-based manifold regularization term was introduced into the objective function. Simultaneously, to further utilize the users' label data, valuable review information is mined and added to the feature vector to extract the users' potential preferences.

The main contributions of this paper include the following:

- (1) A method combining SSL and AL is proposed to solve the problem of recommendation quality degradation caused by the scarcity of labeled data in real scenarios. This method is very suitable for application scenarios where the data in the recommendation system is extremely sparse and the data filling quality cannot be guaranteed. Because AL strategy attaches great importance to the quality of data, only a small number of high-quality items are chosen.
- (2) An AL strategy is proposed in this paper to identify those unlabeled samples that cause the largest reduction of version space for labeling. Meanwhile, the batch sampling mode can be also used in the sample labeling process to obtain better training efficiency.
- (3) This paper combines item and user information as the features of the prediction model. And in order to achieve a better performance of the annotation, the users' preference/behavior information (label information) is used as an important index for querying and labeling unlabeled samples to guide the labeling process.
- (4) AL selectively interacts with users and asks for information such as item ratings, which can supplement those aspects of interest with sparse data, helping the interest model to be comprehensive, and achieve a better performance of the recommendation system.

2. Related Work

Traditional collaborative filtering algorithms are mainly divided into three categories: user-based collaborative filtering (UserCF), item-based collaborative filtering (ItemCF) [4], and hybrid collaborative filtering algorithms based on both [5, 6]. In recent years, many researchers have focused on solving data sparsity, cold start problem, neglecting item and user information (demographic information), and scalability problems of collaborative filtering. For the first four problems, the following strategies are frequently utilized:

- (1) Employ machine learning algorithm to predict unrated data, such as naive Bayesian [7], support vector machine (SVM) [8], neural networks [9], topic model [10], and deep learning collaborative filtering

algorithms [11]. These strategies usually employ classification algorithm to fill data; the performance of them largely depends on the quality and quantity of the training samples. However, in most real application scenarios, there are only a few labeled samples; thus, the prediction accuracy often tends to be not satisfactory. Therefore, some researchers proposed personalized recommendation method based on active learning to achieve high score prediction. In [12], a user-centered method is developed, and a model based on the interaction between conversation and collaborative filtering is proposed. By using this model, users can provide relevant information such as ratings under specific motivation; thus, the users can clearly know the benefits of what they are doing; meanwhile, their probability of active ratings is increased. In [13], matrix decomposition was incorporated into the tree structure, employed to accelerate the tree construction and predict the ratings of tree nodes. Since the item with the highest predicted rating may be the user's favorite item, the idea in [14] is to predict the rating of unlabeled items with the highest predicted ratings. Reference [15] proposes a binary prediction method, which changes the nonnull value in the "user-item" rating matrix to 1 and the null value to 0, then predicts the position marked as 0 in the converted matrix, and judges the probability that the user knows the item according to the predicted value. It maximized the possibility of users' actively rating. Reference [16] proposes a novel multi-label active learning approach for web service tag recommendation, which can identify a small number of most informative web services to be tagged by domain experts. Furthermore, it minimized the domain expert efforts by learning and leveraging the correlations among tags to improve the active learning process. Reference [17] proposes leveraging the idea of pool-based active learning to realize a scalable service classification approach. Instead of manually labeling a large number of services to construct a complete training set, the approach starts with a base classifier with a small set of training set and iteratively asks for the labels of the most informative services outside of the initial training set.

Inspired by the above results, this paper introduces semisupervised learning and active learning strategy into collaborative filtering, improving the existing semisupervised learning and active learning algorithms in view of the practical problems existing in collaborative filtering algorithm.

- (2) Use the similarity of user preferences or the similarity of item categories to fill data. For instance, in [18], the similarity is calculated after filling the ratings of the target item and the neighbor item that are not rated together. In [19], the trust model is employed to fill data, and in [20], the similarity is obtained after clustering of users or items. However,

these methods have the same problem: they require a large number of high-quality labeled data, and they do not take into account the users' behavior information, the impact of item, and demographic information on the recommendation effect.

In addition, there are also some methods that are aimed at reducing the computational complexity of recommendation model by using dimension reduction techniques, such as graph-based dimension reduction [21], implicit topic analysis (probabilistic latent semantic analysis, PLSA) [22], potential Dirichlet analysis (LDA) [23], matrix factorization [24], singular value decomposition (SVD) [25], kernel matrix factorization [26], and graph-based methods [27]. To some extent, these methods reduce the time complexity of the model but also lead to the loss of some useful information, meanwhile, ignoring the item information and demographic information.

Based on the above analysis, this paper proposes a recommendation algorithm that combines active learning and semisupervised support vector machines techniques, which considers not only user behavior information but also item information and demographic information. And they are employed to enhance the query and label unlabeled samples and finally result in a better implemented item recommendation.

It should be noted that, during the procedure of analyzing the demographic information and item information, it was found that if users have similar demographic information and favorite item set, they will tend to have similar preferences for many items. It just meets the needs of analysis and clearly means that entities with the similar properties will have the same class label. And the proposed high-quality recommendation system significantly benefits from this data characteristic.

3. Semisupervised Support Vector Machines and Active Learning

3.1. TSVM (Transductive Support Vector Machine). TSVM is a maximum interval classification method based on the hypothesis of low-density segmentation [28]. Similar to the traditional support vector machine, it finds the classification hyperplane with the largest interval as the optimal classification hyperplane; meanwhile, it combines the unlabeled data and labeled data together to train the classification model.

Assume a set of labeled samples with independent and identical distribution:

$$\{(x_1, D_1), \dots, (x_l, D_l)\} \in R^n \times R, i = 1, \dots, l, y_i = \{-1, +1\}. \quad (1)$$

And the unlabeled samples are denoted as follows:

$$\{x_{l+1}, \dots, x_{l+u}\}. \quad (2)$$

Generally, the learning process of TSVM can be considered as the process of solving the following optimization problem:

$$\begin{aligned}
& (y_1, \dots, y_n, \omega, b, \xi_1, \dots, \xi_l, \xi_{l+1}, \dots, \xi_{l+u}) \\
& \min \frac{1}{2} \|\omega\|^2 + C_1 \sum_{i=1}^l \xi_i + C_2 \sum_{i=l+1}^{l+u} \xi_j \\
& \forall_{i=1}^l: y_i [\omega \cdot x_i + b] \geq 1 - \xi_i; \xi_i \geq 0 \\
& \text{s.t.} \\
& \forall_{i=l+1}^{l+u}: y_j [\omega \cdot x_j + b] \geq 1 - \xi_j; \xi_j \geq 0,
\end{aligned} \tag{3}$$

where C_1 and C_2 are set by the user to control the degree of punishment for wrongly classified samples. C_2 is the “impact factor” of unlabeled data during training; $C_2 \xi_j$ is called the “impact term” of the j -th unlabeled sample in the objective function.

The training process of TSVM is as follows:

Step 1. Train the initial classifier by the labeled samples using inductive learning with the specified parameters C_1 and C_2 . During the procedure, the estimated number N of positive samples in unlabeled samples also should be specified.

Step 2. Set C_{temp} as a temporary impact factor and compute the decision function values of all unlabeled samples using the initial classifier. The samples having the N largest decision function values will be labeled as positive, and the remaining unlabeled samples are labeled as negative.

Step 3. Retrain the SVM model based on all labeled samples. And then use the newly trained classifier to switch the labels of one pair of different labeled unlabeled samples, using a certain rule to make the value of the objective function in formula (3) minimized as much as possible. This step is repeated until no pair of examples meet the switching condition.

Step 4. Increase the value of C_{temp} uniformly, and return to Step 3. When $C_{\text{temp}} \geq C_2$, the algorithm is terminated and the labels of all unlabeled samples are output.

3.2. AL (Active Learning). The traditional machine learning method is training and learning over a given set of labeled samples to induce a learning model, which is called “inductive learning.” However, in real applications scenarios, the labeled samples are very limited, and labeling a large number of unlabeled samples is time-consuming, labor-intensive, and tedious. In order to reduce the labeling cost as much as possible and reduce the number of needed training sample sets, active learning method is proposed to solve the problem of the lack of labeled samples and optimize the classification model. During the training of AL learner, it actively identifies the most informative unlabeled samples and submits them to users or domain experts for labeling and then adds the labeled samples into the training set to participate in the next round of training. Therefore, even if the initial training set is small, it still can obtain a relative higher classification accuracy. In this way, the cost of labeling samples and training high-performance classifiers can be reduced [29].

In AL strategies, the main task is to determine which unlabeled sample has the most information or the most uncertain and is inquired, and this inquiry strategy is the focus of research. According to different problem scenarios and sample selection strategies, AL is divided into the following three types: membership query synthesis, stream-based selective sampling, and pool-based sampling.

In item-based recommendations, there is less information about the “user-item” association information (the user label items). TSVM is an effective method to solve the lack of labels problem; it can make better use of unlabeled data to improve the prediction accuracy of the classifier. However, due to its inherent characteristics, its effectiveness in practical applications is not very satisfactory. Inspired by the literature [30–32], this paper proposes a new semisupervised support vector machine method based on AL techniques, which can combine the advantages of these two algorithms to overcome the defects of TSVM and identify the samples that have the greatest impacts on classifier performance, meanwhile, significantly reducing the burden of users’ annotation task.

4. A New TSVM Algorithm Based on Active Learning (AL)

In this section, a new TSVM algorithm based on active learning (AL) named TSVM-(AL + Graph) is proposed, which combines the advantages of semisupervised learning and AL techniques. In the approach, in order to take advantage of the data manifold structure, a regularization term is added to penalize any “abrupt changes” of the evaluated function value. And then, an unlabeled data selection strategy named “maximum-minimum segmentation” method is designed for AL. The detail of TSVM-(AL + Graph) algorithm is described as follows.

4.1. Integrate Manifold Regularization Term into Objective Function. In order to build the TSVM-(AL + Graph) model, it should add a regularization term defined on unlabeled samples into the traditional SVM optimization function, and the TSVM optimization problem is as follows:

$$\min \frac{1}{2} \|\omega\|^2 + C_1 \sum_{i=1}^l H_1(y_i f(x_i)) + C_2 \sum_{i=l+1}^{l+u} H_1(|f(x_i)|), \tag{4}$$

where $H_1(\cdot) = \max(0, 1 - \cdot)$ is the classic Hinge loss function used to penalize labeled data and $H_1(|\cdot|) = \max(0, 1 - |\cdot|)$ is a symmetric Hinge loss function used to penalize unlabeled data. In formula (4), when $C_2 = 0$, the problem turned to be the traditional SVM optimization problem; when $C_2 > 0$, the unlabeled data will be penalized that is inside the margin. However, this optimization problem’s solution space is a nonconvex hat shape, which makes it hard to obtain a satisfactory solution. In order to efficiently solve this problem, the method in [33] is employed: the loss function for unlabeled data is replaced by the Ramp loss function, and it is decomposed into a sum of a Hinge loss

function and a concave loss function. The expression of the Ramp loss function is

$$R_s(z) = H_1(z) - H_s(z) = \min(1 - s, \max(0, 1 - z)), \quad (5)$$

where $H_1(z)$ is the Hinge loss function, $H_s(z)$ is a concave loss function, and its corresponding expression is $H_s(z) = \max(0, s - z)$, s is a preset parameter, and $-1 < s \leq 0$. In this paper, set $s = -0.3$.

In this case, equation (4) can be rewritten as

$$\min \frac{1}{2} \|\omega\|^2 + C_1 \sum_{i=1}^l H_1(y_i f(x_i)) + C_2 \sum_{i=l+1}^{l+2u} R_s(y_i f(x_i)). \quad (6)$$

According to [33], the objective function corresponding to TSVM can be solved by CCCP method as follows:

$$\min \frac{1}{2} \|\omega\|^2 + C_1 \sum_{i=1}^l \xi_i + C_2 \sum_{i=l+1}^{l+2u} \xi_i + \sum_{i=l+1}^{l+2u} \beta_i f(x_i) \quad (7)$$

$$\frac{1}{u} \sum_{i=l+1}^{l+2u} f(x_i) = \frac{1}{l} \sum_{i=1}^l y_i$$

$$\text{s.t.} \quad y_i f(x_i) \geq 1 - \xi_i, \forall 1 \leq i \leq l + 2u$$

$$\xi_i \geq 0, \forall 1 \leq i \leq l + 2u,$$

where β_i is related to the derivative of the loss function and can be expressed as

$$\beta_i = \begin{cases} C_2 R'_s[y_i f(x_i)], & \text{if } i \geq l + 1, \\ 0, & \text{otherwise} \end{cases} \quad (8)$$

$$= \begin{cases} C_2, & \text{if } y_i f(x_i) < s \text{ and } i \geq l + 1, \\ 0, & \text{otherwise.} \end{cases}$$

In order to obtain the geometrical structure of data, a common solution is to define L' as a function of Laplacian graph. In this way, the structure of the data manifold can be explored by adding a regularization term that penalizes any “abrupt changes” of the function values, which is evaluated on neighbor samples in the Laplacian graph. Then, the optimization problem corresponding to TSVM can be expressed as

$$\min \frac{1}{2} \|\omega\|^2 + C_1 \sum_{i=1}^l \xi_i + C_2 \sum_{i=l+1}^{l+2u} \xi_i + \sum_{i=l+1}^{l+2u} \beta_i f(x_i) + C_3 f^T L' f$$

$$\frac{1}{u} \sum_{i=l+1}^{l+2u} f(x_i) = \frac{1}{l} \sum_{i=1}^l y_i$$

$$\text{s.t.} \quad y_i f(x_i) \geq 1 - \xi_i, \forall 1 \leq i \leq l + 2u$$

$$\xi_i \geq 0, \forall 1 \leq i \leq l + 2u, \quad (9)$$

where C_2 controls the influence of unlabeled samples over the objective function and C_3 controls the influence of graph-based regularization term. If $C_3 = 0$, TSVM will ignore the manifold information of the training data.

If the solution to the above optimization problem is ω , then the optimization problem (9) can be rewritten as

$$\min \frac{1}{2} \alpha^T K \alpha + C_1 \sum_{i=1}^l \xi_i + C_2 \sum_{i=l+1}^{l+2u} \xi_i + \sum_{i=l+1}^{l+2u} \beta_i y_i \left(\sum_{j=1}^{l+2u} \alpha_j K(x_i, x_j) + b \right) + C_3 \alpha^T K^T L K \alpha$$

$$\frac{1}{2u} \sum_{i=l+1}^{l+2u} \left(\sum_{j=1}^{l+2u} \alpha_j K(x_i, x_j) + b \right) = \frac{1}{l} \sum_{i=1}^l y_i \quad (10)$$

$$\text{s.t.} \quad y_i \left(\sum_{j=1}^{l+2u} \alpha_j K(x_i, x_j) + b \right) \geq 1 - \xi_i, \xi_i \geq 0.$$

By introducing the Lagrange multiplier and solving its dual problem, we can get the corresponding decision function:

$$f(x) = \sum_{i=1}^{l+2u} (y_i \bar{\rho}_i + \gamma_i) K(x_i, x) + b, \quad (11)$$

where $\bar{\rho} = \rho - \beta$, ρ , and γ_i are Lagrange multipliers.

4.2. *Principle of “Maximum-Minimum Segmentation”.* In equation (4), assuming $R(f, L)$ is the objective function, we can get

$$R(f, L) = \sum_{i=1}^l \max(0, 1 - y_i f(x_i)) + \sum_{i=l+1}^{l+u} \min(1 - s, \max(1 - y_i f(x_i))) + \frac{\lambda}{2} \|f\|_H^2. \quad (12)$$

In order to identify the most informative samples, we select the unlabeled example x^* that leads to a small value for the objective function regardless of its assigned class label y^* (positive or negative labels). Based on this idea, “maximum-minimum segmentation” strategy can be described as follows:

$$\min_{x^* \in u} \max_{y^* \in \{-1, 1\}} R(f, L \cup (x^*, y^*)). \quad (13)$$

Furthermore, it can be expressed as

$$\min_{x_j^* \in u} \max_{y_j^* \in \{-1, 1\}} \min_{f \in H} \left(\sum_{i=1}^l \max(0, 1 - y_i f(x_i)) + \sum_{i \in u \cup \{j\}} \min(1 - s, \max(1 - y_i f(x_i))) + \frac{\lambda}{2} \|f\|_H^2 \right). \quad (14)$$

Assuming the optimal decision function f^* can be obtained from formula (4), then formula (14) can be simplified as

$$\begin{aligned} & \min_{x_j^* \in u} \max_{y_j^* \in \{-1, 1\}} R(f, L \cup (x^*, y^*)) \\ & \approx \min_{x_j^* \in u} \max_{y_j^* \in \{-1, 1\}} \left(\sum_{i=1}^l \max(0, 1 - y_i^* f^*(x_j^*)) + \sum_{i=l+1}^{l+u} \min(1 - s, \max(1 - y_i^* f^*(x_j^*))) \right) \\ & = \min_{x_j^* \in u} \left(\max(0, 1 - f^*(x_j^*), 1 + f^*(x_j^*)) + \min(1 - s, 0, 1 - f^*(x_j^*), 1 + f^*(x_j^*)) \right) \\ & = \min_{x_j^* \in u} \left(1 + |f^*(x_j^*)| \right) \\ & = \min_{x_j^* \in u} |f^*(x_j^*)|. \end{aligned} \quad (15)$$

Through the above analysis, it can be found that the “maximum-minimum segmentation” method is to select the unlabeled samples closest to the optimal hyperplane f^* , which is trained on the current labeled sample set. In the next section, the principle of “maximum-minimum segmentation” will be applied into active learning to construct the proposed TSVM-(AL + Graph) algorithm.

4.3. *TSVM-(AL + Graph) Algorithm.* Given the training sample set and kernel function *Kernel*, the version space is defined as the set of classification hyperplanes; it means the set of all samples that training samples can be divided in the feature space H_{kernel} . Generally, the version space can be defined as

$$\text{Version} = \{f \in H_{\text{Kernel}} | \forall i \in \{1, 2, \dots, l + u\}, y_i f(x_i) > 0\}. \quad (16)$$

The principle of using active learning to choose unlabeled samples for annotation is to identify the samples that lead to the largest reduction of version space. Since formula (14) is equivalent to $\min_{x_j^* \in u} y_j^* f^*(x_j^*)$, thus there exists Proposition 1.

Proposition 1. *Set the version space determined by $l + u$ samples:*

$$\text{Version} = \{f \in H_{\text{Kernel}} | \forall i \in \{1, 2, \dots, l + u\}, y_i f(x_i) > 0\}. \quad (17)$$

Randomly labeled samples (x_{l+2}, y_{l+2}) and (x_{l+3}, y_{l+3}) and then two new version spaces $\text{Version}_{l+2}^{\text{new}}$ and $\text{Version}_{l+3}^{\text{new}}$ can be obtained. If $y_{l+2}f(x_{l+2}) > y_{l+3}f(x_{l+3})$, then $\text{Area}(\text{Version}_{l+2}^{\text{new}}) > \text{Area}(\text{Version}_{l+3}^{\text{new}})$, where $\text{Area}(\text{Version})$ denotes the size of the version space.

Proof. After labeling the samples (x_{l+2}, y_{l+2}) and (x_{l+3}, y_{l+3}) , new version spaces $\text{Version}_{l+2}^{\text{new}}$ and $\text{Version}_{l+3}^{\text{new}}$ are obtained.

Version space $\text{Version}_{l+2}^{\text{new}}$:

$$\text{Version}_{l+2}^{\text{new}} = \left\{ \omega \left| \begin{array}{l} \|\omega\| = 1, \\ y_i(\omega \cdot \phi(x_i) + b) > 0, \quad i = 1, 2, \dots, l+u, \\ y_{l+2}(\omega \cdot \phi(x_{l+2}) + b) > 0. \end{array} \right. \right\} \quad (18)$$

Version space $\text{Version}_{l+3}^{\text{new}}$:

$$\text{Version}_{l+3}^{\text{new}} = \left\{ \omega \left| \begin{array}{l} \|\omega\| = 1, \\ y_i(\omega \cdot \phi(x_i) + b) > 0, \quad i = 1, 2, \dots, l+u, \\ y_{l+3}(\omega \cdot \phi(x_{l+3}) + b) > 0. \end{array} \right. \right\} \quad (19)$$

If $y_{l+2}f(x_{l+2}) > y_{l+3}f(x_{l+3})$, then $y_{l+3}(\omega \cdot \phi(x_{l+3}) + b) > 0$. Further, $y_{l+2}(\omega \cdot \phi(x_{l+2}) + b) > 0$.

In summary, $\text{Version}_{l+3}^{\text{new}} \subset \text{Version}_{l+2}^{\text{new}}$.

Therefore, $\text{Area}(\text{Version}_{l+2}^{\text{new}}) > \text{Area}(\text{Version}_{l+3}^{\text{new}})$.

From Proposition 1, it can be found that, given the sample (x_i, y_i) , if the value of $y_i(x_i)$ is smaller, the labeled sample corresponding to the hyperplane dividing the current version space will reserve the smaller portion. Thus, the sample is more valuable for training the classification model.

The description of the new TSVM algorithm based on AL is shown in Algorithm 1.

In the TSVM-(AL + Graph) algorithm, $y_{\text{previous}}f(x)$ is used instead of $yf(x)$ to measure the sample information, where y_{previous} is not the true label of the sample but is the class label of the previous labeled adjacent sample. The advantage of this approximation strategy is that it does not depend directly on the current classification model; it is based on the relative relationship that similar classification results often have similar class labels. During the procedure, training is restarted only after a certain number of unlabeled samples are annotated. Compared with the traditional method of retraining once for each sample, this method can significantly improve the calculation efficiency.

Furthermore, Algorithm 2 can be obtained by applying the TSVM-(AL + Graph) algorithm to the rating/label prediction, which is shown in Algorithm 2.

5. Experimental Results and Analysis

In this section, firstly, verify the effectiveness of the proposed method based on the UCI dataset; then, apply the verified algorithm to personalized recommendation.

5.1. Experimental Datasets

5.1.1. UCI Dataset. Three datasets (that is, Breast_cancer, WPBC, and Bupa liver) from the UCI machine learning dataset are used to test our proposed algorithm. These datasets have been used in many studies, and they are a binary classification problem. For each dataset, randomly select a number of the data as labeled samples and put them into the labeled sample set L ; remove the labels of all the remaining samples and put them into the unlabeled sample set U . In this way, different sample selection strategies can be used to label unlabeled samples.

5.1.2. MovieLens Dataset. The MovieLens 1M dataset was collected by the University of Minnesota GroupLens research group through MovieLens and contains the anonymous ratings of 3900 movies by 6040 users. In order to facilitate modeling, the movie recommendation problem is converted into two classification problems, that is, “like” and “dislike”; the corresponding class labels are +1 and -1. At the same time, the rating values of 4 and 5 are labeled as +1, and the rating values of 1-3 are labeled as -1. In the experiment, we select 2000 users’ rating data as the experimental data and randomly select 200 data as the test samples; the rest of the data are used as the training set to obtain the classification model. Meanwhile, 5-fold cross-validation was used, and the average of the 5 groups’ data was taken as the experimental result.

5.1.3. Book Dataset. For the personalized book recommendation evaluation, we develop the crawler program and obtain the needed data of book purchase records from jd.com, a well-known e-commerce website in China. The crawled data include user name, user ID, book name, price, purchase time, and user reviews. In this experiment, we also mine review information, selecting and processing real and valuable review information as users’ purchased features are added to training samples. Finally, we train the recommendation model over the adjusted training set for evaluation.

When processing review information, we remove redundant punctuation and pause words and delete those with less than 2 characters, and we manually annotate 5 correct and valuable reviews and 5 spam reviews. For a review to be considered valuable or nonspam, it must meet the following conditions: the review contains a statement; the review expresses some opinions about the book or the characteristics of the book. Six characteristic features and corresponding descriptions of the review information are shown in Table 1.

5.2. Experimental Results on UCI Datasets

5.2.1. Introduction of Comparison Methods. We compare the proposed algorithm TSVM-(AL + Graph) against TSVM-(Random), TSVM, SVM-(AL) [34, 35], and SVM [36]. TSVM-(AL + Graph) algorithm not only exploits the manifold structure of the data to improve the performance

Input:

LDA, UDA /* Labeled sample set, unlabeled sample set
 k /* The number of samples in each round of interaction required labeled

Output:

$f(x)$ /* Classification function

Procedure:

Step 1: set parameters C_1 and C_2 . Select some samples from UDA , annotate them (both positive and negative samples are more than 1), and add them to LDA . Utilizing all labeled samples to establish an initial classification model with inductive learning.

Step 2: calculate values of the decision function for all unlabeled samples. On the basis of the increasing order of $f(x_i)$ values, an unlabeled sequence SDA is formed.

Step 3: select a sample x_i with the minimum objective function value for annotation, that is, $fvalue = \min_{x_i \in UDA} |f(x_i)|$, and record the corresponding label: $y_{previous} = y_i$.

Remove the x_i from UDA and SDA . At the same time, add x_i to LDA :

$UDA \leftarrow UDA - \{x_i\}$, $SDA \leftarrow SDA - \{x_i\}$, $LDA \leftarrow LDA + \{x_i\}$.

Step 4: while $i = 1, 2, \dots, k$

do

if $y_{previous} = 1$, then select the adjacent sample x_{i+p} in the opposite direction of SDA , and label it $y_{previous} = y_{i+p}$, where p can be either a positive or negative value.

if $y_{previous} = -1$, then select the adjacent sample x_{i+p} in the increasing direction of SDA , and label it $y_{previous} = y_{i+p}$, where p can be either a positive or negative value.

Delete the x_{i+p} from UDA and SDA . Simultaneously, add the x_{i+p} to LDA :

$UDA \leftarrow UDA - \{x_{i+p}\}$, $SDA \leftarrow SDA - \{x_{i+p}\}$, $LDA \leftarrow LDA + \{x_{i+p}\}$.

Step 5: retrain the TSVM over the L , and return $f(x)$. If there are still unlabeled examples, return to **Step 2**.

ALGORITHM 1: TSVM based on AL, that is, TSVM-(AL + Graph). The description of TSVM-(AL + Graph) algorithm.

Input:

User-item rating matrix $Recode$, item set $Item = \{i_1, i_2, \dots, i_M\}$, user set $User = \{u_1, u_2, \dots, u_N\}$, rating label $Label = \{c_1, c_2, \dots, c_K\}$.

Output:

The filled user-item rating matrix $Recode$.

Procedure:

Data preprocessing: extract unrated items from the training sample set, and randomly divide these unlabeled data into P datasets. For (Each unlabeled dataset in $DataUnlabel^{User}$)

Step 1: constructing “user-item” features: for unlabeled dataset d_1^{User} and labeled dataset $Data^A$, select m and n attributes from user attributes and item attributes, respectively, to form TSVM-(AL + Graph) features.

Step 2: constructing “user-item” behavior features: combining user preference vector $Perfecet_u = \{c_1, c_2, \dots, c_M\}$ and item attention $Attention_i = \{c_1, c_2, \dots, c_N\}$ vector to construct “user-item” behavior features.

Step 3: rating/label prediction: the features of the unlabeled dataset d_1^{User} and labeled dataset $Data^A$, the “user-item” behavior characteristics, and the labels are all used as the training set of the TSVM-(AL + Graph) algorithm. Then, the algorithm outputs the ratings/labels of the unlabeled data.

Step 4: extending the labeled dataset: after obtaining the ratings/labels of the unlabeled data in **Step 3**, add them to the labeled dataset.

ALGORITHM 2: Rating/label prediction algorithm based on TSVM-(AL + Graph). Rating/label prediction algorithm based on TSVM-(AL + Graph).

of the classifier but also exploits informative examples for human annotator. TSVM-(AL) is the TSVM-(AL + Graph) algorithm without the manifold regularization term. TSVM algorithm initially trains a classifier on both labeled examples and unlabeled examples, which exploits the cluster structure of examples and treats it as prior knowledge about the learning task. SVM algorithm only uses the labeled examples and performs well in the case of a sufficient number of labeled examples, but the performance will be degraded when the labeled examples are scarce.

5.2.2. Classification Results and Analysis. This experiment verifies the effectiveness of the proposed algorithm based on the UCI dataset and compares and analyzes the algorithm from different perspectives.

(1). Set the size of the initial labeled sample set $L = 30$, and the batch sampling size $k = 1$. The main purpose of this experiment is to comprehensively test the performance of the proposed algorithm, including active learning sampling strategy and random sampling strategy and the utilization of manifold structure before and after the introduction of the

TABLE 1: Extracted 6 features and their sample dictionary terms.

Features	Sample dictionary terms	Dictionary size
Opinion phrases	指定用书(textbook), 经典(classic), 高性价比(cost-effective), 很/特别/非常喜欢(like very much), 精装版(hardcover), 内容详实(content full and accurate), 最新版(the latest version), 经典(classical), 学习必备(learning essential), 质量好(good quality), 垃圾(rubbish), ...	400
Question patterns	出版社(where), 怎么样(how about), 作者/译者(who), 出版时间(when), 主要内容(what), ?, ...	25
Language	汉语(Chinese), 英语(English), 日语(Japanese), 俄语(Russian), 法语(French), 德语(German), ...	10
Category of book	电子书(e-book), 教材教辅(course books), 综合性图书(comprehensive books), 励志(inspirational), 人文社科(humanities and social sciences), 生活(life), 经济管理(economics and management), 医药/卫生(medicine and health), 工业技术(industrial technology), 少儿(children's book), ...	15 basic categories and several subcategories
Length of review	The total number of characters in a review, excluding punctuation	-
Product rating	五角星(five-pointed star)	5

manifold regular term. The comparison results are shown in Figures 1 and 2.

- (1) The method of active learning is better than the method of nonactive learning, and the classification accuracy is higher. Traditional SVM has better performance than other classification models in the case of small samples, but it cannot make good use of the information implicit in a large number of unlabeled samples to improve the performance of the classifier. Figure 1 also illustrates this aspect. From Figures 1 and 2, it can be found that as the number of labeled samples increases, the classification performance of TSVM-(AL + Graph) is gradually improving. When a certain percentage is reached, the classification performance exceeds the traditional SVM. This also shows that active learning is effective and reasonable in sample selection strategy, which is of great help to improve the performance of the classifier.
- (2) It can be found from Figures 1 and 2 that, compared with the random sampling strategy, the samples selected by the active learning strategy are more likely to be “support vectors” and can ensure that the selected samples can further improve the performance of the classifier. At the same time, random sampling has a certain degree of randomness, which cannot guarantee that the larger the number of samples, the more obvious the improvement of classifier performance.
- (3) After introducing the manifold regularization term, the proposed method can make better use of the manifold structure of unlabeled samples. Comparing different datasets in Figures 1 and 2, it can be found that, for Brest_cancer dataset, the performance difference between TSVM-(AL + graph) and TSVM-(AL) is slightly smaller. For WPBC dataset, the performance of TSVM-(AL + graph) is slightly higher than that of TSVM-(AL). Therefore, the introduction of manifold regularization term is helpful to improve the classification performance of TSVM.

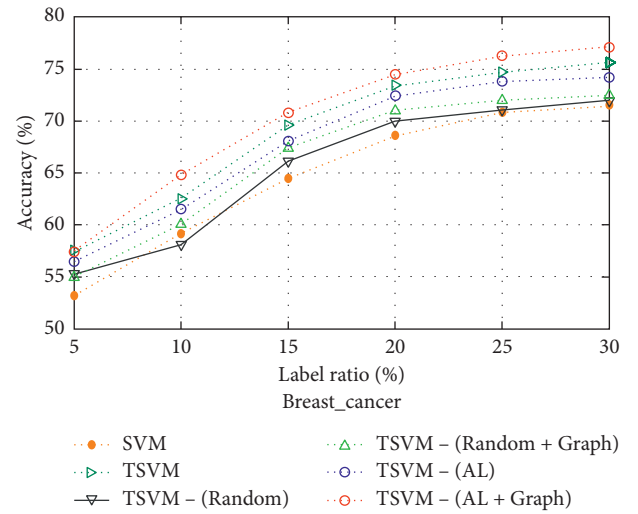


FIGURE 1: The classification accuracy on Breast_cancer dataset as the number of labeled training samples increases.

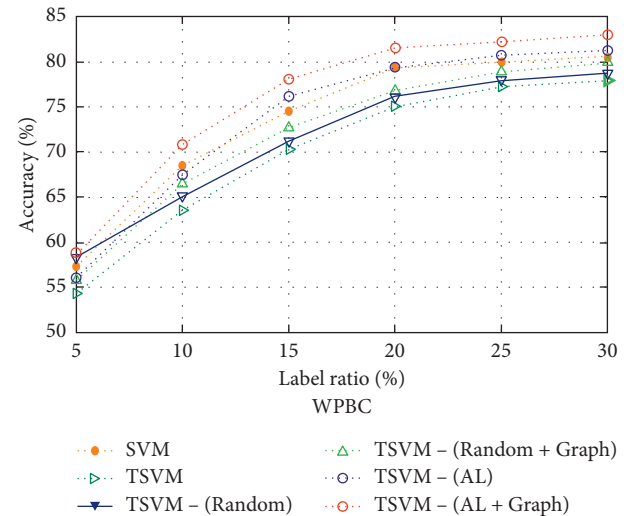


FIGURE 2: The classification accuracy on WPBC dataset as the number of labeled training samples increases.

(2). *The effect of different class label prediction methods on classifier performance.* This experiment compares TSVM-(OAL + Graph) and TSVM-(AL + Graph) and analyzes them on the Bupa liver dataset and WPBC dataset (set the initial labeled sample set $L = 10$), where the TSVM-(OAL + Graph) method adopts the predicted class label using the current classifier as the measure of active learning; the TSVM-(AL + Graph) method adopts the class label of previously labeled adjacent sample, which makes full use of cluster assumption among the data.

From the experimental results in Figures 3 and 4, it can be found that the predictive class labels of adjacent samples labeled previously have more advantages than those predicted by the current classifier in general.

For Bupa liver and WPBC datasets, there is no significant difference in classification performance between the two algorithms, which may be related to the distribution characteristics of the datasets. For Bupa liver dataset, when the proportion of labeled samples is 10%, and when the proportion of labeled samples in the WPBC dataset is 20%, the classification performance of TSVM-(OAL + Graph) exceeds TSVM-(AL + Graph). However, with the increase of labeled sample proportion, the classification performance of TSVM-(AL + Graph) is gradually improved and exceeds TSVM-(OAL + Graph).

5.3. Personalized Recommendation Experiment Results and Analysis. In this section, we implement two personalized recommendations based on real datasets. The first one is a personalized movie recommendation based on MovieLens dataset. In this experiment, the demographic information, user behavior (rating about the movie), and the content of the movie are processed to form a “user-movie” association matrix, and then the model is trained. The result of movies classification is output as the recommendation. According to the classification results, a recommendation list is provided for users instead of the similarity calculation in the traditional collaborative filtering recommendation method. The second evaluation is a personalized book recommendation. This experiment is mainly to analyze the book purchase records, extract the corresponding features, and obtain the personalized recommendation model. In this evaluation, to improve the quality of the book recommendation, the review information that is valuable for improving the performance of the recommendation model is mined and processed to form the users’ purchasing characteristics, and it is then added to the training sample set to train the personalized book recommendation model.

5.3.1. Results and Analysis of Personalized Movie Recommendation. Figure 5 shows the offline experimental results of the recommendation method based on TSVM-(AL + Graph) and the methods in [37], including CF-IWA, PSO-SVM, ItemCF, UserCF, PSO-SVM, GA-SVM, GS-SVM, TSVM, and BP neural network on the MovieLens dataset.

From Figure 5, it can be seen that the classification accuracy of various methods grows with the number of training samples increasing, because with the number of

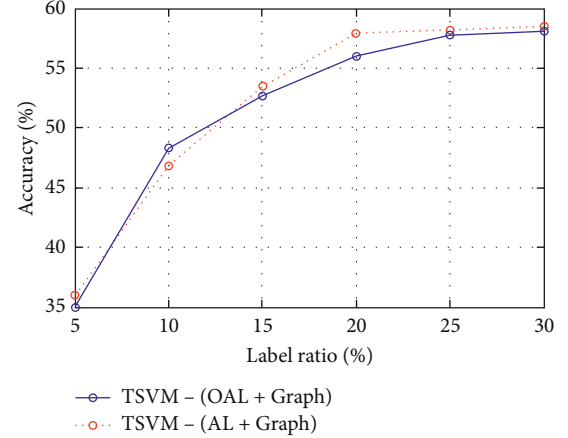


FIGURE 3: The classification accuracy on Bupa liver dataset.

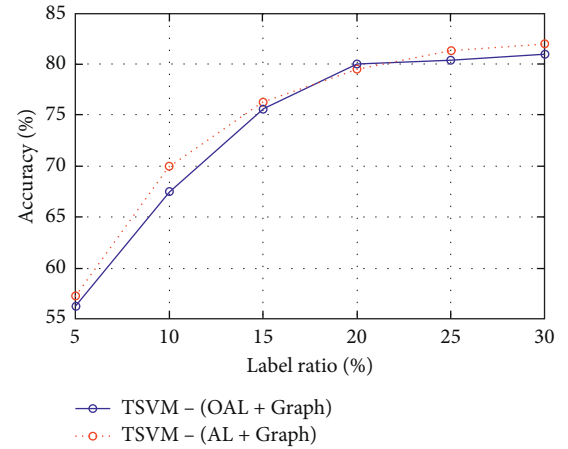


FIGURE 4: The classification accuracy on WPBC dataset.

labeled samples increasing more information can be used for movie recommendation, which provides rich and reliable information for establishing recommendation model. When the labeled training samples account for 20% of the entire training sample set, the performance of the recommendation model based on TSVM-(AL), TSVM-(AL + Graph), and TSVM is not as good as the recommendation model based on traditional SVM, which may be related to the quality and quantity of labeled samples. However, with the number of labeled samples increasing, the advantages of these three methods become more obvious, and the proposed method in this paper is proved to be better than the other six methods. Meanwhile, it can also be found that the model-based method is better than the ItemCF and UserCF methods, which may be caused by the “data sparsity” and “cold start” problems; and the model-based method can make good use of the users’ demographic information, behavior information, and label information, etc., which is useful to alleviate the “data sparsity” and “cold start” problems.

A good recommendation model not only has high accuracy but also has the ability to identify as many items as possible that are interesting to the users (“recall”). An

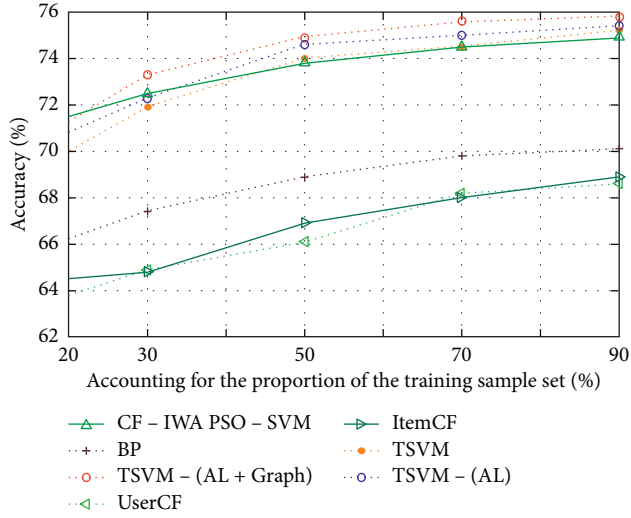


FIGURE 5: Classification accuracy of the seven methods.

important measure of this ability is the F -Score. As shown in Figure 6, the TSVM-(AL + Graph) method has a better F -Score than the other six methods. In particular, when the proportion of training samples accounts for 90% of the entire training set, the F -Score value reaches the highest.

5.3.2. Results and Analysis of Personalized Book Recommendation

(1) *Personalized Recommendation Model Based on TSVM-(AL + Graph) algorithm.* The procedure of the personalized recommendation based on TSVM-(AL + Graph) algorithm is shown in Figure 7.

(2) *User Review Information Preprocessing.* In order to fully explore the advantages of the proposed method, a series of preprocessing of the dataset is conducted. At first, “lexical perspective” preprocessing is conducted. The Chinese word segmentation tool named ICTCLAS is used to segment and annotate the reviews, and then, each review is transformed into a term frequency inverse document frequency (TF-IDF). After that, the “statistical perspective” analysis such as calculating the proportion of keywords and key patterns contained in each review is conducted to form a quantitative matrix.

During the processing, there are six features that can be quantified as follows:

- (1) The proportion of opinion phrases in a review sentence.
- (2) The proportion of question patterns in a review sentence.
- (3) The proportion of language in a review sentence.
- (4) The proportion of book categories mentioned in a review sentence.
- (5) The length of a review sentence.
- (6) The number of “five-pointed stars” given by the user for the overall review of the book (at most 5).

(3) Personalized Book Recommendation Results and Analysis

(1) Mining of book evaluation information.

In order to evaluate the impact of unlabeled samples in different algorithms, the classification performances of TSVM-(AL + Graph), SVM, TSVM, and TSVM-(AL) were compared and analyzed by changing the proportion of labeled samples in the experiment. In this experiment, the range of the proportion of labeled samples is within [2%, 20%], and the total number of unlabeled samples is 1000. Figures 8 and 9 show the classification accuracy caused by the range of the proportion of labeled samples.

As can be seen from Figures 8 and 9, the classification accuracy of TSVM-(AL) and TSVM-(AL + Graph) grows with the proportion of labeled samples increasing. More detailed observation shows that when the number of labeled samples is very few, the classification performance of TSVM-(AL + Graph) is significantly better than SVM and TSVM. For example, in Figure 8, when the proportion of labeled samples is 8.0%, the classification accuracy of TSVM-(AL + Graph) is improved, about 10% better than SVM and 5.0% higher than TSVM. In Figure 9, the classification accuracy of TSVM-(AL + Graph) is about 9.0% higher than SVM and 3.0% higher than TSVM.

Figures 8 and 9 mine the book review information from different perspectives, and the classification accuracy of the “lexical perspective” is slightly higher than “statistical perspective,” which may be related to the inherent statistical characteristics of the model. It is obvious that the classification performance of the method proposed in this paper is better than both SVM and TSVM in these two different perspectives, and the superiority of the proposed method has been sufficiently verified.

(2) Personalized book recommendation method based on user review mining.

In this evaluation, the mined users’ valuable review information is added to the original dataset as the users’ interest feature to form a new dataset, and 70% of data is used for training while the other 30% of data is used for testing; the newly formed “user-book” association data is randomly divided into two parts.

This experiment mainly includes two evaluations. The first one is to compare and analyze the impact of the review information for book recommendation. The other one is to compare the proposed method with other representative methods.

① The effect of the review information.

In order to evaluate the effect of review information during book recommendation, there are four algorithms used for estimation; they are

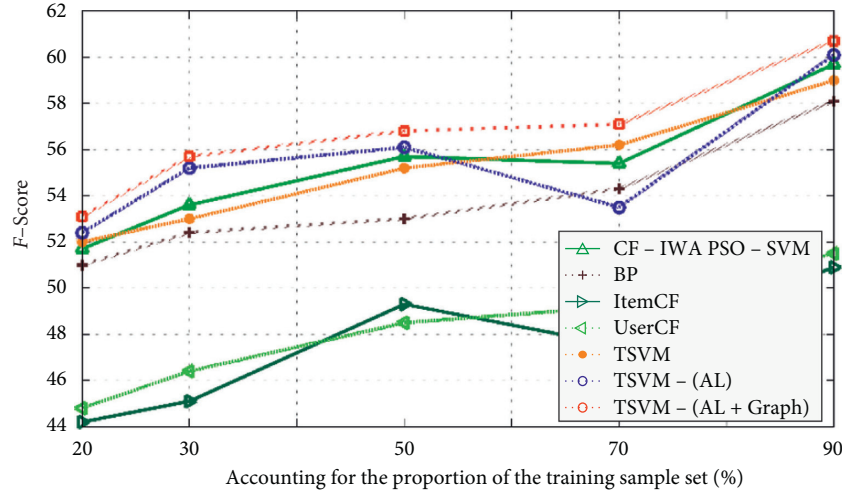


FIGURE 6: F-Score values of the seven methods.

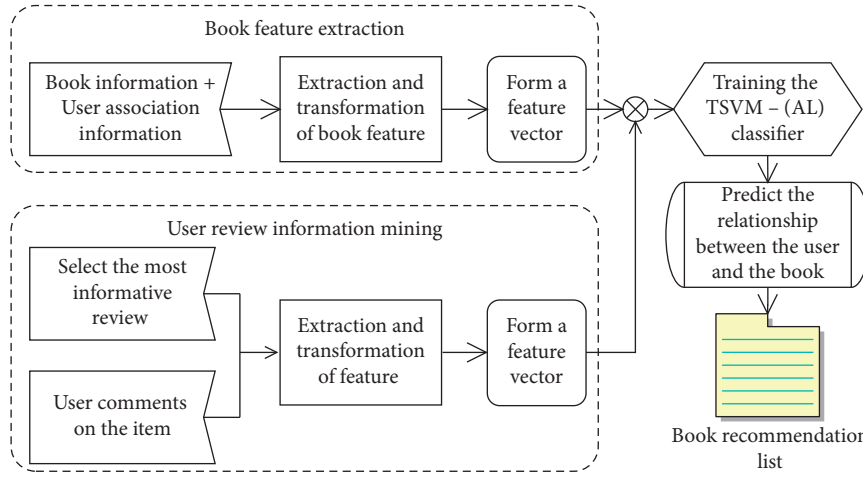


FIGURE 7: The personalized recommendation model based on TSVM-(AL+Graph) algorithm.

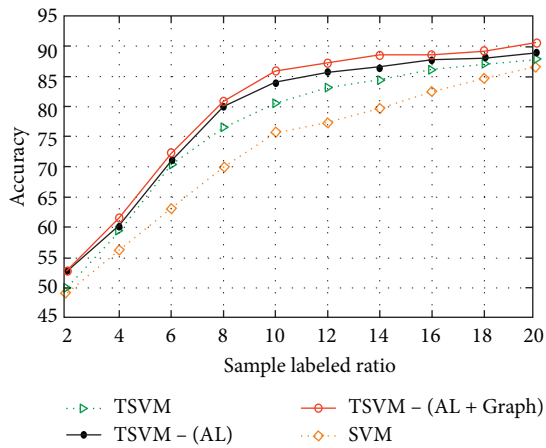


FIGURE 8: Classification accuracy corresponding to "lexical perspective."

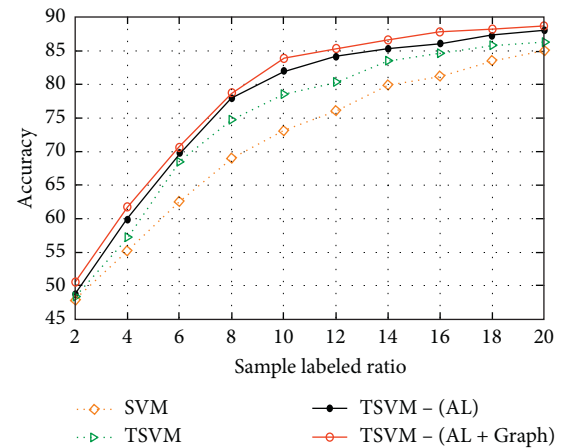


FIGURE 9: Classification accuracy corresponding to "statistical perspective."

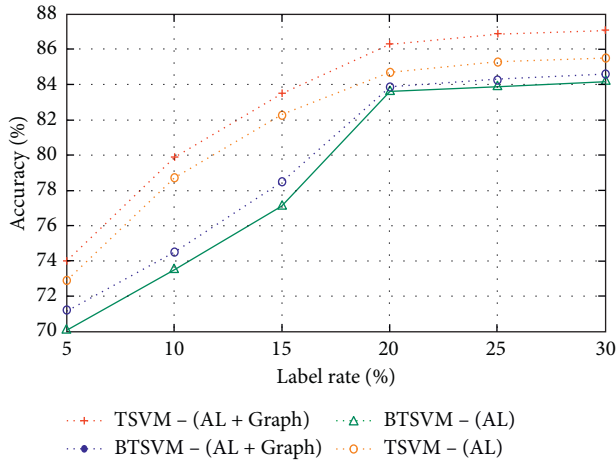


FIGURE 10: The effect of the reviews.

TSVM-(AL+Graph), TSVM-(AL), BTSVM-(AL+Graph), and SVM-(AL). The last two algorithms represent the recommendation methods without utilizing the review information, while TSVM-(AL+Graph) and TSVM-(AL) represent the recommendation methods employing the review information. Figure 10 presents the effectiveness of the four algorithms.

From Figure 10, it can be found that the reviews have a positive impact to improve the recommendation accuracy. It shows that the method of mining the book review proposed in this paper is helpful to improve the recommendation accuracy and is useful to discover users' interests and preferences. Therefore, it is reasonable to integrate users' valuable review information into the training model.

② Performance analysis of different book recommendation methods.

Figure 11 shows the recommendation accuracy of six methods under different labeled sample proportion. The results show that TSVM-(AL+Graph) and TSVM-(AL) methods have relatively high accuracy. This superiority mainly benefits from the following: firstly, the method based on active learning can effectively utilize the small number of labeled samples to explore the unlabeled data. Since the active learning approach will iteratively label those samples that have significant impact on the improvement of the classifier in each iteration and extend them into the training set, the data sparsity and cold start problem will be heavily reduced. Secondly, the manifold regularization term is also employed to discover and utilize the hidden geometric information of the data, which is helpful to reduce the solution space of the nonconvex hat shape; thus, the performance of the classifier is further improved.

The above experimental results show that the proposed method is superior to other approaches in mining users' interests and preferences. The effectiveness of the proposed method in personalized book recommendation scenarios is verified. The experimental data proved that the proposed method can supplement those aspects of interest with sparse

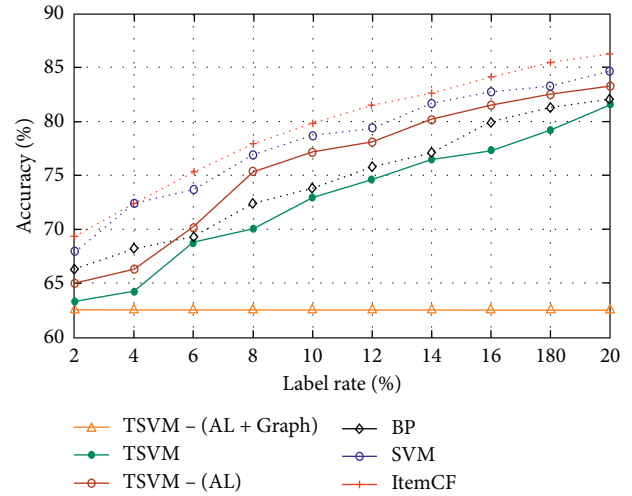


FIGURE 11: The effect of different labeled sample ratios on the recommendation after utilizing the reviews.

data, helping the interest model to be comprehensive, and achieve a better performance of the recommendation system.

6. Conclusion

This paper explores the “data sparsity” (data with labels scarcity), “cold start,” and neglecting demographic characteristics of the traditional collaborative filtering recommendation algorithm in real applications and proposes a new recommendation method based on TSVM and active learning. Firstly, to solve the challenge of using unlabeled data, an active learning strategy is proposed to query and label unlabeled samples. Meanwhile, the manifold regularization term is integrated into the objective function to utilize the distribution characteristics of samples. Secondly, during the construction of the recommendation model, user behavior characteristics, item information, and demographic information are employed to help label and fill the samples to solve the data sparsity and cold start problem. Finally, the proposed algorithm is applied to UCI dataset, personalized movie recommendation, and book recommendation to verify its effectiveness. The experimental results show that the proposed method can effectively mine users' potential preferences, significantly reduce the heavy cost of sample labeling, and lead to a performance improvement of the recommendation system.

Data Availability

The data used to support the findings of the personalized movie recommendation are available from <https://grouplens.org/datasets/movielens/>, and the original data of the precise book review records cannot be released in order to preserve the privacy of individuals.

Conflicts of Interest

The authors declare no conflicts of interest.

Acknowledgments

This work was partially supported by the Technology Foundation of Guizhou Province (grant no. QianKeHeJiChu [2020]1Y269), New Academic Seedling Cultivation and Exploration Innovation Project (grant no. QianKeHe Platform Talents[2017]5789–21), Program for Innovative Talent of Guizhou Province (grant no. QianCaiJiao [2018]190), National Natural Science Foundation of China (grant nos. 71901078 and 71964009), High-Level Talent Project of Guizhou Institute of Technology (grant no. XJGC20190929), and Special Key Laboratory of Artificial Intelligence and Intelligent Control of Guizhou Province (grant no. KY [2020]001).

References

- [1] Z. Zheng, H. Ma, M. R. Lyu et al., “QoS-aware web service recommendation by collaborative filtering,” *IEEE Transactions on Services Computing*, vol. 4, no. 2, pp. 140–152, 2011.
- [2] H. Liu, Z. Hu, A. Mian, H. Tian, and X. Zhu, “A new user similarity model to improve the accuracy of collaborative filtering,” *Knowledge-Based Systems*, vol. 56, pp. 156–166, 2014.
- [3] B. Settles, “Active learning literature survey,” Technical Report 1648, University of Wisconsin-Madison, Madison, WS, USA, 2009.
- [4] J. S. Breese, D. Heckerman, and C. Kadie, “Empirical analysis of predictive algorithms for collaborative filtering,” *Uncertainty in Artificial Intelligence*, vol. 98, no. 7, pp. 43–52, 2013.
- [5] M. Deshpande and G. Karypis, “Item-based top- N recommendation algorithms,” *ACM Transactions on Information Systems*, vol. 22, no. 1, pp. 143–177, 2004.
- [6] J.-H. Su, H.-H. Yeh, P. S. Yu, and V. S. Tseng, “Music recommendation using content and context information mining,” *IEEE Intelligent Systems*, vol. 25, no. 1, pp. 16–26, 2010.
- [7] K. Wang and Y. Tan, “A new collaborative filtering recommendation approach based on naive bayesian method,” in *Proceedings of the Advances in Swarm Intelligence-Second International Conference*, Chongqing, China, June 2011.
- [8] L. Ren and W. Wang, “An SVM-based collaborative filtering approach for Top-N web services recommendation,” *Future Generation Computer Systems*, vol. 78, no. 2, pp. 531–543, 2018.
- [9] J. He, F. Zhuang, Y. Liu, Q. He, and F. Lin, “Bayesian dual neural networks for recommendation,” *Frontiers of Computer Science*, vol. 13, no. 6, pp. 1255–1265, 2019.
- [10] L. Na, L. Ying, T. Xiao-Jun et al., “Improved collaborative filtering algorithm using topic model,” in *Proceedings of the International Conference on Parallel & Distributed Computing*, Taipei, Taiwan, 2017.
- [11] R. Devooght and H. Bersini, *Collaborative filtering with recurrent neural networks*, <https://arxiv.org/abs/1608.07400>, 2016.
- [12] D. G. Bridge and F. Ricci, “Supporting product selection with query editing recommendations,” in *Proceedings of the ACM Conference on Recommender Systems*, Minneapolis, MN, USA, 2007.
- [13] R. Karimi, W. Martin, A. Nanopoulos et al., “Factorized decision trees for active learning in recommender systems,” in *Proceedings of the IEEE International Conference on Tools with Artificial Intelligence*, Herndon, VA, USA, 2013.
- [14] M. Elahi, F. Ricci, and N. Rubens, “Active learning strategies for rating elicitation in collaborative filtering,” *ACM Transactions on Intelligent Systems and Technology*, vol. 5, no. 1, pp. 1–33, 2013.
- [15] M. Elahi, M. Braunhofer, F. Ricci et al., “Personality-based active learning for collaborative filtering recommender systems,” in *Proceedings of the Congress of the Italian Association for Artificial Intelligence*, Turin, Italy, 2013.
- [16] W. Shi, X. Liu, and Q. Yu, “Correlation-aware multi-label active learning for web service tag recommendation,” in *Proceedings of the 2017 IEEE International Conference on Web Services (ICWS)*, Honolulu, Hawaii, 2017.
- [17] X. Liu, S. Agarwal, C. Ding et al., “An LDA-SVM active learning framework for web service classification,” in *Proceedings of the International Conference on Web Services*, pp. 49–56, San Francisco, CA, USA, 2016.
- [18] G. Li, Z. Zhang, L. Wang, Q. Chen, and J. Pan, “One-class collaborative filtering based on rating prediction and ranking prediction,” *Knowledge-Based Systems*, vol. 124, pp. 46–54, 2017.
- [19] L. Wang, H. Zhang, and Y. Chen, “Collaborative filtering recommendation algorithm based on Dice-Euclidean similarity function,” *Application Research of Computers*, no. 10, pp. 2891–2895, 2015.
- [20] U. Liji, Y. Chai, and J. Chen, “Improved personalized recommendation based on user attributes clustering and score matrix filling,” *Computer Standards & Interfaces*, vol. 57, pp. 59–67, 2018.
- [21] M. K. Najafabadi, A. Mohamed, and C. W. Onn, “An impact of time and item influencer in collaborative filtering recommendations using graph-based model,” *Information Processing & Management*, vol. 56, no. 3, pp. 526–540, 2019.
- [22] L. Huang, W. Tan, and Y. Sun, “Collaborative recommendation algorithm based on probabilistic matrix factorization in probabilistic latent semantic analysis,” *Multimedia Tools and Applications*, vol. 78, no. 7, pp. 8711–8722, 2019.
- [23] Z. Gao, Y. Fan, C. Wu et al., “SeCo-LDA: mining service Co-occurrence topics for composition recommendation,” *IEEE Transactions on Services Computing*, vol. 12, no. 3, pp. 446–459, 2019.
- [24] H. Shin, S. Kim, J. Shin, and X. Xiao, “Privacy enhanced matrix factorization for recommendation with local differential privacy,” *IEEE Transactions on Knowledge and Data Engineering*, vol. 30, no. 9, pp. 1770–1782, 2018.
- [25] I. Nouioua, N. Amardjia, and S. Belilita, “A novel blind and robust video watermarking technique in fast motion frames based on SVD and MR-SVD,” *Security and Communication Networks*, vol. 2018, no. 10, pp. 1–17, 2018.
- [26] X. Liu, C. Aggarwal, Y. F. Li et al., “Kernelized matrix factorization for collaborative filtering,” in *Proceedings of the SIAM International Conference on Data Mining*, pp. 378–386, Alberta, Canada, 2016.
- [27] B. Shams and S. Haratizadeh, “Graph-based collaborative rankings,” *Expert Systems with Applications*, vol. 67, pp. 59–70, 2017.
- [28] Y. Chen, G. Wang, and S. Dong, “Learning with progressive transductive support vector machine,” in *Proceedings of the IEEE International Conference on Data Mining*, pp. 67–74, Maebashi, Japan, 2002.
- [29] M. Elahi, F. Ricci, N. Rubens et al., “A survey of active learning in collaborative filtering recommender systems,” *Computer Science Review*, vol. 20, pp. 29–50, 2016.
- [30] Z. Wang, S. Yan, and C. Zhang, “Active learning with adaptive regularization,” *Pattern Recognition*, vol. 44, no. 10-11, pp. 2375–2383, 2011.

- [31] C.-L. Li, C.-S. Ferng, and H.-T. Lin, "Active learning using hint information," *Neural Computation*, vol. 27, no. 8, pp. 1738–1765, 2015.
- [32] K. Moshkbar-Bakhshayesh and M. B. Ghofrani, "Combining supervised and semi-supervised learning in the design of a new identifier for NPPs transients," *IEEE Transactions on Nuclear Science*, vol. 63, no. 3, pp. 1882–1888, 2016.
- [33] R. Collobert, F. Sinz, J. Weston et al., "Large scale transductive SVMs," *Journal of Machine Learning Research*, vol. 7, pp. 1687–1712, 2006.
- [34] C. Campbell, N. Cristianini, and A. J. Smola, "Query learning with large margin classifiers," in *Proceedings of the Seventeenth International Conference on Machine Learning*, pp. 111–118, Kunnamangalam, India, 2000.
- [35] S. Tong and E. Chang, "Support vector machine active learning for image retrieval," in *Proceedings of the Ninth ACM International Conference on Multimedia*, pp. 107–118, Kyongju, Korea, 2001.
- [36] C. Chang and C. Lin, "LIBSVM: a library for support vector machines, science," 2001, <http://www.csie.ntu.edu.tw/~cjlin/libsvm>.
- [37] X. Wang, F. Luo, C. Sang, J. Zeng, and S. Hirokawa, "Personalized movie recommendation system based on support vector machine and improved particle swarm optimization," *IEICE Transactions on Information and Systems*, vol. E100-D, no. 2, pp. 285–293, 2017.

Research Article

Modelling and Analysis of Propagation Behavior of Computer Viruses with Nonlinear Countermeasure Probability and Infected Removable Storage Media

Xulong Zhang  and Yong Li 

School of Computer and Network Engineering, Shanxi Datong University, Datong 037009, China

Correspondence should be addressed to Xulong Zhang; zxl-095@163.com

Received 13 August 2020; Revised 22 September 2020; Accepted 30 September 2020; Published 26 October 2020

Academic Editor: Jianxin Li

Copyright © 2020 Xulong Zhang and Yong Li. This is an open access article distributed under the Creative Commons Attribution License, which permits unrestricted use, distribution, and reproduction in any medium, provided the original work is properly cited.

The dissemination of countermeasures is diffusely recognized as one of the most valid strategies of containing computer virus diffusion. In order to better understand the impacts of countermeasure and removable storage media on viral spread, this paper addresses a dynamical model, which incorporates nonlinear countermeasure probability and infected removable storage media. Theoretical analysis reveals that the unique (viral) equilibrium of the model is globally asymptotically stable. This main result is also illustrated by some numerical experiments. Additionally, the numerical experiments of different countermeasure probabilities are conducted.

1. Introduction

The continual emergence of computer viruses, especially with the growing popularity of the Internet, has brought great troubles and threats to our daily work and life (e.g., [1]). Besides, removable storage media, such as compact disk, removable hard disk, USB flash disk, flash memory card, and so on, which are often used in our daily work provide another spreading route for computer viruses except the Internet. Antivirus software, patches, and firewall are the main technical means of defending against computer viruses, which can weed out all viruses they can recognize that stay in individual electronic devices such as personal computer (PC) and removable storage media. Unfortunately, these techniques seem powerless to the outbreak of a new virus. In order to effectively contain virus spread, one needs to understand the propagation laws of computer viruses, which may provide a theoretical basis for decision making, as well as to use technical measures.

A multitude of propagation models of computer viruses have been presented since 1991, specifically, SIS (susceptible-infected-susceptible) models (e.g., [2, 3]), SIRS (susceptible-

infected-recovered-susceptible) models (e.g., [4, 5]), SLBS (susceptible-latent-breaking-susceptible) model (e.g., [6]), SICS (susceptible-infected-countermeasured-susceptible) models (e.g., [7–9]), and SDIRS (susceptible-delitescent-infected-recovered-susceptible) model (e.g., [10]).

In the field of computer viruses, countermeasures such as warnings, firewall, and software patches can provide a practical approach to avoid virus infection problems. In 2004, Chen and Carley [11] addressed the countermeasure competing (CMC) strategy, which shows that the CMC strategy is more available compared to previous strategies.

Inspired by this work and in order to macroscopically describe the mixed transmission of computer viruses and countermeasures, Zhu et al. [7] presented the first compartment model in this aspect, named as the SICS model, and its global dynamics was fully examined. Afterwards, Yang and Yang [8] extended this model by incorporating the effect of infected *external computers* (i.e., computers outside the Internet) and removable storage media. However, these two models ignore two important facts. On the one hand, they overlook the fact that the linear infection probability is fit well for the real-world situations only when the

countermeasured (or immune) nodes are few. On the other hand, they neglect the fact that countermeasures may be disseminated through networks at different rates, which has been mentioned in Reference [11]. Thus, the assumption of linear countermeasure probability is unreasonable.

To remedy these defects and considering the influences of general countermeasure and infected removable storage media on viral diffusion, this paper studies a new propagation model incorporating generic countermeasure probability and infected removable storage media. The main result, the global stability of the unique (viral) equilibrium, is proved, which is also examined by some numerical experiments. Furthermore, the numerical experiments of different countermeasure probabilities are conducted.

The paper is organized as follows. The model formulation is made in Section 2. Section 3 determines the (viral) equilibrium and investigates its global stability. Numerical experiments are presented in Section 4. This work is summarized in Section 5.

2. Model Description

In this paper, a computer is called external or internal computer determined by whether it is disconnected from or connected to the Internet. All internal computers may have three states: susceptible, infected, and immune (with countermeasures). For brevity, let $S(t)$, $I(t)$, and $C(t)$ (S , I , and C , for short) denote the average numbers of susceptible, infected, and countermeasured computers at time t , respectively. Their entering rates are $\mu_1 > 0$, $\mu_2 > 0$, and $\mu_3 > 0$, respectively. Besides, the following basic assumptions of the model are made.

- (1) Each internal computer leaves the Internet with probability $\delta > 0$.

- (2) Each susceptible internal computer becomes infected by connecting with infected internal computer (or infected removable storage media) with probability $\beta_1 > 0$ (or $\beta_2 > 0$).
- (3) Each infected or susceptible internal computer gains the latest countermeasure with probability $\gamma_1(C(t))$ at time t , where γ_1 is twice continuously differentiable, $\gamma_1' > 0$, $\gamma_1'' < 0$, and $\gamma_1(0) = 0$. The concavity assumption seizes well the saturability of the countermeasure probability.
- (4) By reinstalling the operating system, each countermeasured (or infected) internal computer becomes susceptible with probability $\alpha > 0$ (or $\gamma_2 > 0$).

Now, one can derive the mathematical representation of the model as follows (also see Figure 1):

$$\begin{cases} \frac{dS}{dt} = \mu_1 - \beta_1 SI - \beta_2 S - \gamma_1(C)S + \gamma_2 I + \alpha C - \delta S, \\ \frac{dI}{dt} = \mu_2 + \beta_1 SI + \beta_2 S - \gamma_1(C)I - \gamma_2 I - \delta I, \\ \frac{dC}{dt} = \mu_3 + \gamma_1(C)S + \gamma_1(C)I - \alpha C - \delta C, \end{cases} \quad (1)$$

with initial condition $(S(0), I(0), C(0)) \in \mathbb{R}_+^3$.

3. Theoretical Analysis

Let $N = S + I + C$, and $\mu = \mu_1 + \mu_2 + \mu_3$. Adding up the three equations of system (1), it is easy to get that $\lim_{t \rightarrow \infty} N = (\mu/\delta)$. It follows by the asymptotically autonomous system theory [12] that system (1) is equivalent to the following reduced limiting system:

$$\begin{cases} \frac{dI}{dt} = \mu_2 + \frac{\beta_2 \mu}{\delta} + \left(\frac{\beta_1 \mu}{\delta} - \beta_2 - \gamma_2 - \delta \right) I - \beta_2 C - \beta_1 I^2 - \beta_1 IC - \gamma_1(C)I, \\ \frac{dC}{dt} = \mu_3 + \gamma_1(C) \left(\frac{\mu}{\delta} - C \right) - (\alpha + \delta)C, \end{cases} \quad (2)$$

with initial condition $(I(0), C(0)) \in \Omega$, where

$$\Omega = \left\{ (I, C) \in \mathbb{R}_+^2 : I + C \leq \frac{\mu}{\delta} \right\}, \quad (3)$$

and Ω is positively invariant for system (2).

In the following sections, we just need to investigate the dynamical behavior of system (2).

3.1. Equilibrium

Theorem 1. *There exists a unique (viral) equilibrium $E^* = (I^*, C^*)$ for system (2), where E^* is the single positive solution to the following system:*

$$\begin{cases} \mu_2 + \frac{\beta_2 \mu}{\delta} + \left(\frac{\beta_1 \mu}{\delta} - \beta_2 - \gamma_2 - \delta \right) x - \beta_2 y - \beta_1 x^2 - \beta_1 xy - \gamma_1(y)x = 0, \\ \mu_3 + \gamma_1(y) \left(\frac{\mu}{\delta} - y \right) - (\alpha + \delta)y = 0, \end{cases} \quad (4)$$

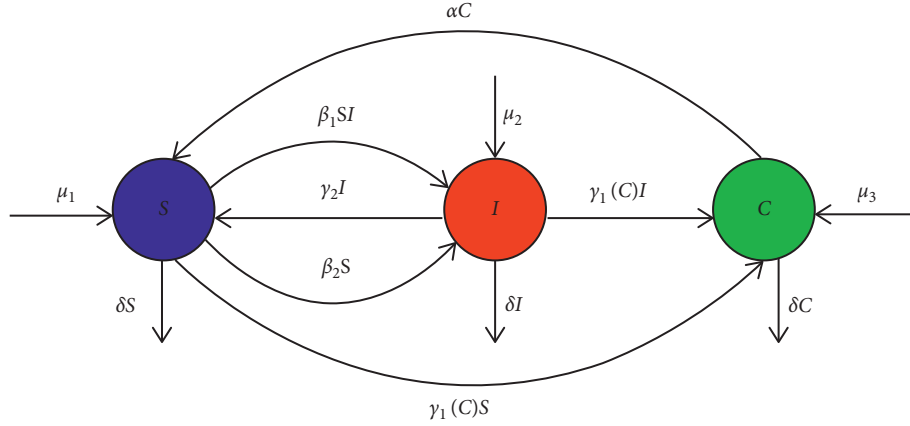


FIGURE 1: Transfer diagram of the new proposed model.

with the initial condition $(x(0), y(0)) \in \Omega$.

Proof. Let us suppose that $E^* = (I^*, C^*)$ is an equilibrium of system (2). Clearly, E^* satisfies system (4). Thus, it suffices to prove that system (4) has a unique positive solution.

Firstly, let us prove that the second equation of system (4) has a unique positive root. Let

$$f(y) = \mu_3 + \gamma_1(y) \left(\frac{\mu}{\delta} - y \right) - (\alpha + \delta)y. \quad (5)$$

As $f(0) = \mu_3 > 0$ and $f(\mu/\delta) = -(\alpha\mu/\delta) - (\mu_1 + \mu_2) < 0$, so f does have a zero located in $(0, (\mu/\delta))$. Besides, notice that

$$f' \left(\frac{\mu}{\delta} \right) = -\gamma_1 \left(\frac{\mu}{\delta} \right) - (\alpha + \delta) < 0, \quad (6)$$

$$f''(y) = \gamma_1''(y) \left(\frac{\mu}{\delta} - y \right) - 2\gamma_1'(y) < 0.$$

We shall consider two possibilities depending upon whether $f'(0)$ is positive or negative.

Case 1: $f'(0) > 0$. Let

$$\bar{y} = \max \left\{ y \in \left[0, \frac{\mu}{\delta} \right] : f'(y) > 0 \right\}. \quad (7)$$

Thus, f is strictly increasing in $[0, \bar{y}]$ and strictly decreasing in $[\bar{y}, (\mu/\delta)]$, which implies that f has a unique zero in $[\bar{y}, (\mu/\delta)]$.

Case 2: $f'(0) \leq 0$. So, f is decreasing and has a unique zero.

It is easily obtained from the above discussions that f does has a single zero. Then, $y = C^*$. Besides, $f'(C^*) < 0$.

Next, let us prove that the first equation of system (4) has a single positive root. Let

$$g(x) = \mu_2 + \beta_2 \left(\frac{\mu}{\delta} - C^* \right) + \left(\frac{\beta_1 \mu}{\delta} - \beta_2 - \gamma_2 - \delta - \beta_1 C^* - \gamma_1(C^*) \right) x - \beta_1 x^2. \quad (8)$$

As $g(0) = \mu_2 + \beta_2 ((\mu/\delta) - C^*) > 0$ and $g((\mu/\delta) - C^*) = -\mu_1 - \alpha C^* - \gamma_2 ((\mu/\delta) - C^*) < 0$, g does have a (positive) zero located in $(0, (\mu/\delta) - C^*)$. Besides, note that

$$g' \left(\frac{\mu}{\delta} - C^* \right) = -\beta_1 \left(\frac{\mu}{\delta} - C^* \right) - (\beta_2 + \gamma_2 + \delta + \gamma_1(C^*)) < 0,$$

$$g''(x) = -2\beta_1 < 0. \quad (9)$$

We shall also proceed by distinguishing two possibilities depending upon whether $g'(0)$ is positive or negative.

Case 1: $g'(0) > 0$. Let

$$\bar{x} = \max \left\{ x \in \left[0, \frac{\mu}{\delta} - C^* \right] : g'(x) > 0 \right\}. \quad (10)$$

Then, g is strictly increasing in $[0, \bar{x}]$ and decreasing in $[\bar{x}, (\mu/\delta) - C^*]$, meaning that g has a single zero in $[\bar{x}, (\mu/\delta) - C^*]$.

Case 2: $g'(0) \leq 0$. Hence, g is decreasing and has a unique zero. Then, g always has a single zero $x = I^*$. Besides, $g'(I^*) < 0$.

Thus, the claimed result follows. \square

3.2. Local Stability

Theorem 2. E^* is locally asymptotically stable.

Proof. The corresponding Jacobian matrix of system (2) at E^* is as follows:

$$\begin{pmatrix} \frac{\beta_1 \mu}{\delta} - \beta_2 - \gamma_2 - \delta - \beta_1 C^* - 2\beta_1 I^* - \gamma_1(C^*) & -\beta_2 - \beta_1 I^* - \gamma_1'(C^*)I^* \\ 0 & \gamma_1'(C^*)\left(\frac{\mu}{\delta} - C^*\right) - \gamma_1(C^*) - (\alpha + \delta) \end{pmatrix}, \quad (11)$$

and its two eigenvalues are

$$\begin{aligned} \lambda_1 &= \frac{\beta_1 \mu}{\delta} - \beta_2 - \gamma_2 - \delta - \beta_1 C^* - 2\beta_1 I^* - \gamma_1(C^*) = g'(I^*) < 0, \\ \lambda_2 &= \gamma_1'(C^*)\left(\frac{\mu}{\delta} - C^*\right) - \gamma_1(C^*) - (\alpha + \delta) = f'(C^*) < 0. \end{aligned} \quad (12)$$

Thus, the claimed result follows from the Lyapunov stability theorem [13]. \square

3.3. Global Stability

Lemma 1. *System (2) has no periodic orbit.*

Proof. Let

$$\begin{aligned} h_1(I, C) &= \mu_2 + \frac{\beta_2 \mu}{\delta} + \left(\frac{\beta_1 \mu}{\delta} - \beta_2 - \gamma_2 - \delta\right)I - \beta_2 C \\ &\quad - \beta_1 I^2 - \beta_1 IC - \gamma_1(C)I, \end{aligned} \quad (13)$$

$$h_2(I, C) = \mu_3 + \gamma_1(C)\left(\frac{\mu}{\delta} - C\right) - (\alpha + \delta)C,$$

$$D(I, C) = \frac{1}{IC}.$$

It can be obtained in the interior of Ω that

$$\begin{aligned} \frac{\partial(Dh_1)}{\partial I} + \frac{\partial(Dh_2)}{\partial C} &= \frac{\beta_1}{C} - \frac{\gamma_1'(C)}{I} - \frac{\mu_2}{I^2 C} - \frac{\mu_3}{IC^2} - \frac{\beta_2}{I^2 C} \left(\frac{\mu}{\delta} - C\right) \\ &\quad + \frac{\mu}{\delta IC^2} (\gamma_1'(C)C - \gamma_1(C)). \end{aligned} \quad (14)$$

Let

$$k(x) = \gamma_1'(x)x - \gamma_1(x). \quad (15)$$

As $k(0) = 0$ and $k'(x) = \gamma_1''(x)x < 0$ for all $x > 0$, $k(C) < 0$. Thus, we have $(\partial(Dh_1)/\partial I) + (\partial(Dh_2)/\partial C) < 0$.

Hence, in the interior of Ω , system (2) has no periodic orbit according to the Bendixson–Dulac criterion [13].

On the boundary of Ω , let (\tilde{I}, \tilde{C}) denote an arbitrary point. Thus, three possibilities may occur.

Case 1: $0 < \tilde{C} < (\mu/\delta)$, $\tilde{I} = 0$. Then, $(dI/dt)|_{(\tilde{I}, \tilde{C})} = \mu_2 + \beta_2((\mu/\delta) - \tilde{C}) > 0$.

Case 2: $0 < \tilde{I} < (\mu/\delta)$, $\tilde{C} = 0$. Then, $(dC/dt)|_{(\tilde{I}, \tilde{C})} = \mu_3 > 0$.

Case 3: $\tilde{I} + \tilde{C} = (\mu/\delta)$, $\tilde{C} \neq 0$, $\tilde{I} \neq 0$. Hence,

$$\frac{d(I + C)}{dt}|_{(\tilde{I}, \tilde{C})} = -\mu_1 - \gamma_2 \tilde{I} - \alpha \tilde{C} < 0. \quad (16)$$

Thus, system (2) has no periodic orbit across the arbitrary point (\tilde{I}, \tilde{C}) . The proof is completed.

In what follows, the main result of this paper will be given as follows. \square

Theorem 3. *E^* is globally asymptotically stable.*

Proof. Based on Theorem 1, Lemma 1, and Theorem 2, the claimed result follows from the generalized Poincaré–Bendixson theorem [13]. \square

4. Numerical Experiments

To illustrate the main result of this paper and the impacts of different countermeasure probabilities on viral spread, some numerical experiments are presented in this section.

Example 1. Consider system (1) with $\mu_1 = 0.55$, $\mu_2 = 0.25$, $\mu_3 = 0.2$, $\alpha = 0.02$, $\beta_1 = 0.05$, $\beta_2 = 0.03$, $\gamma_2 = 0.02$, $\delta = 0.1$, and $\gamma_1(C) = 0.05C/(1 + C)$. The initial condition is $(S(0), I(0), C(0)) = (3, 1, 5)$. In Figure 2, a comparison between the new proposed SICS model and the original SICS model is shown, from which it can be seen that the new proposed model is more reasonable in predicting virus prevalence because computer viruses would not go extinct (i.e., $I \geq 1$), which demonstrates that the linear countermeasure probability overestimates the suppression of countermeasures on virus diffusion when compared to the nonlinear one.

Example 2. Consider system (1) with $\mu_1 = 55$, $\mu_2 = 38$, $\mu_3 = 7$, $\alpha = 0.01$, $\beta_1 = 0.52$, $\beta_2 = 0.015$, $\gamma_2 = 0.01$, $\delta = 0.02$, and $\gamma_1(C) = 0.006C^{0.15}$. Six different initial conditions are listed below.

- (1) $(S(0), I(0), C(0)) = (325, 25, 10)$.
- (2) $(S(0), I(0), C(0)) = (925, 125, 90)$.
- (3) $(S(0), I(0), C(0)) = (1525, 225, 170)$.
- (4) $(S(0), I(0), C(0)) = (2125, 325, 250)$.

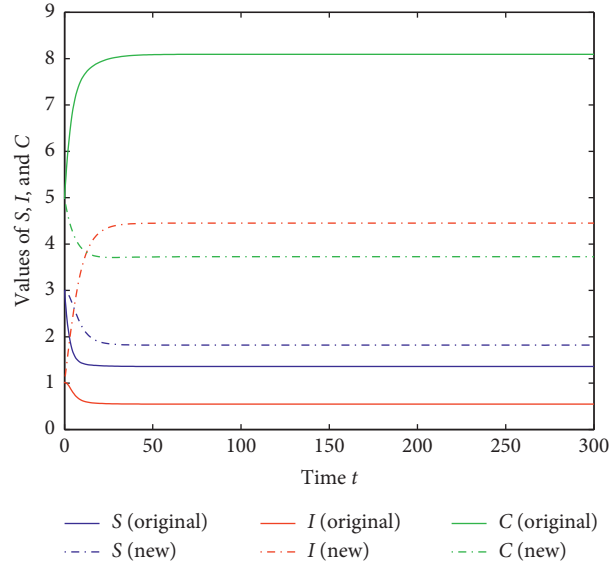


FIGURE 2: A comparison between the new proposed SICS model and the original SICS model.

$$(5) (S(0), I(0), C(0)) = (2725, 425, 330).$$

$$(6) (S(0), I(0), C(0)) = (3325, 525, 410).$$

Figure 3 shows six orbits of system (1) with different initial conditions for a common system. It can be seen from this figure that no matter where the initial state starts, computer viruses would always exist and tend to a steady state, which coincides with the main result. This also reveals that the global stability is independent of the initial state.

Example 3. Consider system (1) with the common initial condition $(S(0), I(0), C(0)) = (1050, 450, 105)$, and six sets of parameters are given in Table 1. Six orbits of system (1) with different system parameters for a common initial condition are shown in Figure 4, from which it can be seen that computer viruses would remain present and tend to a steady state, which accords with the main result. Additionally, this figure reveals that even starting from the same initial state the system would approach to different states for different parameters, which is distinct from the phenomenon in Example 2.

Example 4. Consider system (1) with $\mu_1 = 5.5$, $\mu_2 = 3.8$, $\mu_3 = 0.7$, $\alpha = 0.01$, $\beta_1 = 0.52$, $\beta_2 = 0.015$, $\gamma_2 = 0.01$, and $\delta = 0.02$. The initial condition is $(S(0), I(0), C(0)) = (325, 25, 10)$. Figure 5 shows the influences of the varied countermeasure probabilities on the number of infected computers, where $\gamma_1(C) = 0.08C^{0.2}$, $\gamma_2(C) = (0.08C/(1 + 0.416C))$, and $\gamma_3(C) = (0.08C/(1 + C))$. This figure also demonstrates that the nonlinear countermeasure probabilities which are continuously differentiable up to the second order may have many forms and pose different impacts on viral spread.

5. Summary and Outlook

A new SICS model has been proposed and analyzed in this paper. The global stability of the unique (viral) equilibrium

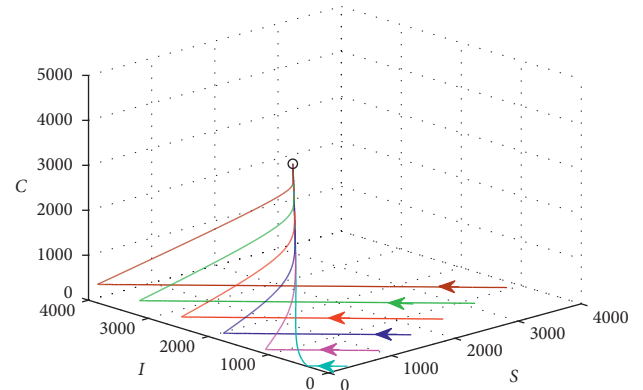


FIGURE 3: Six orbits of system (1) with different initial conditions.

has been proved and illustrated completely. Besides, a comparison between the new proposed model and the original SICS model has been shown, and the effects of varied countermeasure probabilities have also been revealed. The numerical experiments demonstrate that the nonlinear countermeasure probability is more reasonable than the linear one.

Additionally, the follow-up work arrangement is as follows. Firstly, time delays (e.g., [14, 15]), pulses (e.g., [16]), random fluctuations (e.g., [17, 18]), and optimal control strategies (e.g., [19]) can be considered in the new model. Secondly, the new model may be extended on wireless sensor networks (e.g., [20–22]). With the popularity of social networks, individuals' participation has a particularly important effect on information diffusion including propagation of computer viruses. For example, Alduaiji et al. [23] developed an influence propagation model for clique-based community detection in social networks. Li et al. [24] proposed a metric to measure the community-diversified influence in social networks. Therefore, the new model may also be extended in social networks. Finally, the new

TABLE 1: The parameters of system (1) for Example 3.

Parameter	Set 1	Set 2	Set 3	Set 4	Set 5	Set 6
μ_1	55	35	25	15	10	18
μ_2	38	15	25	25	20	19
μ_3	7	10	5	20	25	13
α	0.01	0.03	0.03	0.02	0.02	0.02
β_1	0.52	0.52	0.22	0.72	0.62	0.12
β_2	0.015	0.13	0.01	0.08	0.18	0.02
γ_2	0.01	0.05	0.03	0.02	0.04	0.02
δ	0.02	0.02	0.02	0.03	0.02	0.02
$\gamma_1(C)$	$0.06C^{0.15}$	$0.01C^{0.3}$	$0.1C^{0.1}$	$0.01C^{0.5}$	$0.03C^{0.25}$	$0.05C^{0.05}$

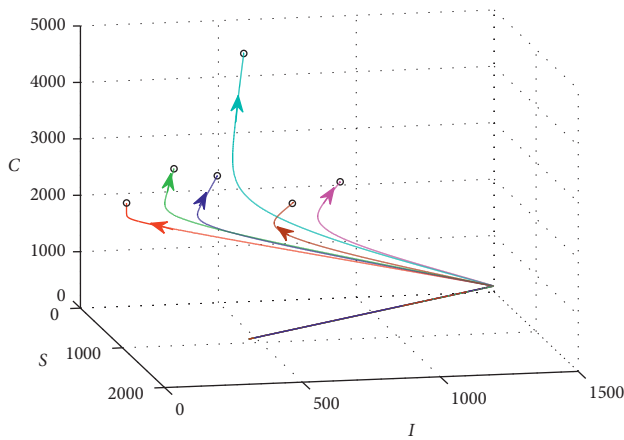
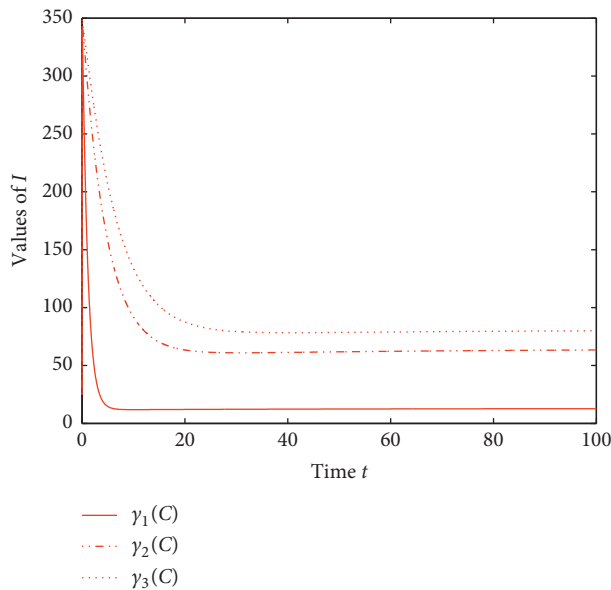


FIGURE 4: Six orbits of system (1) with different system parameters.

FIGURE 5: The impacts of the varied countermeasure probabilities on I .

proposed model can be formulated for cloud computing security (e.g., [25]).

Data Availability

The data included in this study are available from the corresponding author upon request.

Conflicts of Interest

The authors declare that there are no conflicts of interest with regard to the publication of this paper.

Authors' Contributions

Xulong Zhang conceived and designed the study and reviewed and edited the manuscript. Yong Li performed the numerical experiments. All authors read and approved the manuscript.

Acknowledgments

This study was supported by the Natural Science Foundation of Shanxi Province of China under grant nos. 201801D121117 and 201901D111311.

References

- [1] P. Szor, *The Art of Computer Virus Research and Defense*, Addison-Wesley Professional, Boston, MA, USA, 2005.
- [2] J. C. Wierman and D. J. Marchette, "Modeling computer virus prevalence with a susceptible-infected-susceptible model with reintroduction," *Computational Statistics & Data Analysis*, vol. 45, no. 1, pp. 3–23, 2004.
- [3] A. d'Onofrio, "A note on the global behaviour of the network-based SIS epidemic model," *Nonlinear Analysis Real World Applications*, vol. 9, no. 4, pp. 1567–1572, 2008.
- [4] B. K. Mishra and N. Jha, "Fixed period of temporary immunity after run of anti-malicious software on computer nodes," *Applied Mathematics and Computation*, vol. 190, no. 2, pp. 1207–1212, 2007.
- [5] C. Gan, Q. Feng, Q. Zhu, Z. Zhang, Y. Zhang, and Y. Xiang, "Analysis of computer virus propagation behaviors over complex networks: a case study of oregon routing network," *Nonlinear Dynamics*, vol. 100, no. 2, pp. 1725–1740, 2020.
- [6] L.-X. Yang, X. Yang, L. Wen, and J. Liu, "A novel computer virus propagation model and its dynamics," *International Journal of Computer Mathematics*, vol. 89, no. 17, pp. 2307–2314, 2012.
- [7] Q. Zhu, X. Yang, L. Yang, and X. Zhang, "A mixing propagation model of computer viruses and countermeasures," *Nonlinear Dynamics*, vol. 73, no. 7, pp. 1433–1441, 2013.
- [8] L.-X. Yang and X. Yang, "The effect of infected external computers on the spread of viruses: a compartment modeling study," *Physica A: Statistical Mechanics and Its Applications*, vol. 392, no. 24, pp. 6523–6535, 2013.

- [9] X. Zhang and C. Gan, "Global attractivity and optimal dynamic countermeasure of a virus propagation model in complex networks," *Physica A: Statistical Mechanics and Its Applications*, vol. 490, pp. 1004–1018, 2018.
- [10] W. Liu and S. Zhong, "Web malware spread modelling and optimal control strategies," *Scientific Reports*, vol. 7, no. 1, 2017.
- [11] L.-C. Chen and K. M. Carley, "The impact of countermeasure propagation on the prevalence of computer viruses," *IEEE Transactions on Systems, Man and Cybernetics, Part B (Cybernetics)*, vol. 34, no. 2, pp. 823–833, 2004.
- [12] H. R. Thieme, "Convergence results and a poincare-bendixson trichotomy for asymptotically autonomous differential equations," *Journal of Mathematical Biology*, vol. 30, no. 7, pp. 755–763, 1992.
- [13] R. C. Robinson, *An Introduction to Dynamical System: Continuous and Discrete*, Prentice Hall, Englewood Cliffs, NJ, USA, 2004.
- [14] C. Zhang, W. Liu, J. Xiao, and Y. Zhao, "Hopf bifurcation of an improved SLBS model under the influence of latent period," *Mathematical Problems in Engineering*, vol. 2013, Article ID 196214, 2013.
- [15] J. Ren and Y. Xu, "Stability and bifurcation of a computer virus propagation model with delay and incomplete antivirus ability," *Mathematical Problems in Engineering*, vol. 2014, Article ID 475934, 2014.
- [16] Y. Yao, X. D. Feng, W. Yang, W. L. Xiang, and F. X. Gao, "Analysis of a delayed Internet worm propagation model with impulsive quarantine strategy," *Mathematical Problems in Engineering*, vol. 2014, Article ID 369360, 2014.
- [17] C. Zhang, Y. Zhao, Y. Wu, and S. Deng, "A stochastic dynamic model of computer viruses," *Discrete Dynamics in Nature and Society*, vol. 2012, Article ID 264874, 2012.
- [18] J. Amador, "The stochastic SIRA model for computer viruses," *Applied Mathematics and Computation*, vol. 232, pp. 1112–1124, 2014.
- [19] C. Zhang and H. Huang, "Optimal control strategy for a novel computer virus propagation model on scale-free networks," *Physica A: Statistical Mechanics and Its Applications*, vol. 451, pp. 251–265, 2016.
- [20] L. Feng, L. Song, Q. Zhao, and H. Wang, "Modeling and stability analysis of worm propagation in wireless sensor network," *Mathematical Problems in Engineering*, vol. 2015, Article ID 129598, 2015.
- [21] A. Singh, A. K. Awasthi, K. Singh, and P. K. Srivastava, "Modeling and analysis of worm propagation in wireless sensor networks," *Wireless Personal Communications*, vol. 98, no. 3, pp. 2535–2551, 2018.
- [22] Z. Zhang, S. Kundu, and R. Wei, "A delayed epidemic model for propagation of malicious codes in wireless sensor network," *Mathematics*, vol. 7, no. 5, Article ID 396, 2019.
- [23] N. Alduaiji, A. Datta, and J. Li, "Influence propagation model for clique-based community detection in social networks," *IEEE Transactions on Computational Social Systems*, vol. 5, no. 2, pp. 563–575, 2018.
- [24] J. Li, T. Cai, K. Deng, X. Wang, T. Sellis, and F. Xia, "Community-diversified influence maximization in social networks," *Information Systems*, vol. 92, Article ID 101522, 2020.
- [25] C. Gan, Q. Feng, X. Zhang, Z. Zhang, and Q. Zhu, "Dynamical propagation model of malware for cloud computing security," *IEEE Access*, vol. 8, pp. 20325–20333, 2020.

Research Article

Defending against Online Social Network Rumors through Optimal Control Approach

Da-Wen Huang¹, Lu-Xing Yang², Xiaofan Yang³, Yuan Yan Tang⁴ and Jichao Bi⁵

¹College of Computer Science, Sichuan Normal University, Chengdu 610101, China

²School of Information Technology, Deakin University, Melbourne, VIC 3125, Australia

³School of Big Data & Software Engineering, Chongqing University, Chongqing 400044, China

⁴Department of Computer and Information Science, University of Macau, Zhuhai, Macau

⁵State Key Laboratory of Industrial Control Technology, Zhejiang University, Hangzhou 310027, China

Correspondence should be addressed to Da-Wen Huang; hdawen1@gmail.com and Xiaofan Yang; xfyang1964@gmail.com

Received 5 August 2020; Revised 9 September 2020; Accepted 16 September 2020; Published 30 September 2020

Academic Editor: Wei Wang

Copyright © 2020 Da-Wen Huang et al. This is an open access article distributed under the Creative Commons Attribution License, which permits unrestricted use, distribution, and reproduction in any medium, provided the original work is properly cited.

Rumors have been widely spread in online social networks and they become a major concern in modern society. This paper is devoted to the design of a cost-effective rumor-containing scheme in online social networks through an optimal control approach. First, a new individual-based rumor spreading model is proposed, and the model considers the influence of the external environment on rumor spreading for the first time. Second, the cost-effectiveness is recommended to balance the loss caused by rumors against the cost of a rumor-containing scheme. On this basis, we reduce the original problem to an optimal control model. Next, we prove that this model is solvable, and we present the optimality system for the model. Finally, we show that the resulting rumor-containing scheme is cost-effective through extensive computer experiments.

1. Introduction

Nowadays, with the rapid development of Internet technology, online social network (OSN), ranging from Facebook and Twitter to YouTube and LinkedIn, has become a popular platform for people to communicate [1, 2]. On the negative side, harmful rumors can spread rapidly over OSNs, leading to huge losses [3, 4]. In 2013, a false tweet claimed that Barack Obama was injured in an explosion which resulted in a loss of 130 billion US dollars in stock value [5]. In 2015, the rumor of shootouts and kidnappings by drug gangs happening near schools in Veracruz caused severe chaos in the city [6]. The outbreak of rumors has brought many problems, some of which pose threats to our society. Therefore, how to effectively restrain the propagation of rumors over OSNs has been a research hotspot in the field of cybersecurity.

In order to protect the security of cyberspace, it is urgent to propose some effective measures to control the spread of

rumors. In recent years, researchers have suggested many measures to mitigate the impact of rumors, such as blocking or isolating some OSN users to prevent them from further spreading rumors to OSN and releasing convincing rumor-containing messages to OSN users. These measures have been proven to be effective in controlling the spread of rumors [3, 7]. In practice, almost all rumor-containing measures will consume resources (such as money and manpower) during the implementation process, resulting in a certain cost. The cost is generally borne by the OSN platform and government. Since the budget of the OSN platform and government for controlling rumor is limited, it is necessary to study the rumor-containing problem from an economic perspective. However, most of the related research works only discussed the effectiveness (or performance) of rumor-containing measures, and they all ignored the cost of implementing the measures. Different from previous research perspectives, this paper studies rumor-containing problem from an economic perspective. This work not only

considers the losses caused by the spread of rumors but also considers the cost of implementing rumor-contain measures. In this study, we use the total loss caused by rumor to characterize cost-effectiveness. If the total loss is smaller, the cost-effectiveness is better; otherwise, the cost-effectiveness is worse. Based on the definition of cost-effectiveness, cost-effectiveness can be maximized only when the total cost is minimized. This paper will try to find such a rumor-containing scheme that maximizes cost-effectiveness.

From the above discussion, it is noticeable that the rumor-containing agency faces the following challenging problem:

Rumor-containing problem: supposing that a rumor is spreading over an OSN, design a cost-effective rumor-containing scheme.

Designing a cost-effective rumor-containing scheme is a valuable research problem. There are new rumors appearing in OSNs all the time. However, due to the fact that there is no one approach that can completely control the spread of rumors, the rumor-containing problem is essentially a management problem that requires continuous investment of resources. In practice, the budget of the rumor-containing agency is limited. If the economic costs incurred in the process of controlling rumors cannot be managed well, it will be difficult to continuously implement measures to control the spread of rumors.

In this paper, we propose a novel individual-based rumor spreading model, where the effect of the external environment on the spread of the rumor is accounted for. Thereby, we estimate the cost-effectiveness of a rumor-containing scheme. On this basis, we reduce the rumor-containing problem to an optimal control model, where each control stands for a rumor-containing scheme, and the objective functional stands for the cost-effectiveness of a rumor-containing scheme. We prove that this model admits an optimal control, guaranteeing the solvability of the model. We derive the optimality system for the model, which can be used to solve the model. Through extensive comparative experiments, we show that the rumor-containing scheme so obtained is cost-effective.

This paper makes a theoretical study on rumor-containing problem, and the research results can provide some theoretical guidance for taking measures to suppress the spread of rumors. In addition, the research method proposed in this paper can be applied to analyze the cost management of the rumor containment process, and the new model proposed in this paper can be used to study the influence of some parameters on the spread of rumors. Finally, new research ideas can also be extended to other cyberspace security problems, such as malware propagation [8].

The subsequent materials are organized in this fashion: Section 2 reviews the related work. Section 3 establishes an optimal control model of the rumor-containing problem. Sections 4 and 5 solve the model. This work is summarized in Section 6.

2. Related Work

This section is devoted to reviewing the previous work that is related to the present paper. First, rumor-containing problem is introduced. Second, some rumor spreading

models are discussed. Third, the optimal control approach used to deal with rumor-containing problem is introduced.

Rumor-containing problem is devoted to finding effective strategies to control or limit the propagation of rumor in a network, so that the losses caused by rumor can be reduced. In recent years, rumor-containing problem has received significant attention of researchers. Toward this direction, there exist two main types of rumor-containing strategies [3, 9], that is, (a) preventing most influential users or community bridges from being affected by the rumor and (b) spreading convincing messages to clarify the rumor. In the past few years, there has been quite a lot of research on the first type of strategies (also called rumor blocking strategies) [10–15]. The idea of this type of strategies is to find a small set of users or community bridges in the OSN, such that isolating or protecting them will minimize the impact of rumor propagation. However, the rumor-containing strategy ultimately boils down to solving a NP-hard problem and therefore an exact solution is infeasible for large-scale OSNs. Although many heuristic algorithms have been proposed to deal with the problem, they are still too costly for large-scale OSNs. In addition, some isolating or protecting measures may violate human rights. Recently, the second type of rumor-containing strategy has attracted a lot of attention [3, 9]. The essence of the strategy is to model rumor-containing problem as a competitive propagation problem between anti-rumor information and rumor, and this type of strategies has been shown to be effective means of restraining rumor in OSNs [3, 9, 16, 17]. In practice, the above two types of rumor-containing strategies are both effective. However, researchers only studied their effectiveness in controlling rumors but did not consider the cost issues involved in the implementation.

Modeling the spreading process of rumor lays a theoretical basis for studying rumor-containing problem. Existing rumor spreading models can be classified into three categories: *compartmental* models, *network-degree* models, and *individual-based* models. Compartmental rumor spreading models are only suited to homogeneous rumor spreading networks [18–22], and network-degree rumor spreading models only apply to some special types of networks such as scale-free networks [16, 23–26]. In contrast, individual-based rumor spreading models are applicable to all rumor spreading networks [17, 27–30]. The rumor spreading models proposed in [16–22] are all based on the assumption that a rumor can only be received through OSNs. However, in practice, OSN users can also receive rumors from the external environment such as TV programs or tabloid reports [31]. Therefore, previous work may underestimate the propagation ability of rumors. Hence, it is necessary to introduce a rumor spreading model in which the effect of the external environment is accounted for. For our purpose, in the present paper, we aim to establish such an individual-based rumor spreading model.

In recent years, optimal control theory has been applied to deal with rumor-containing problem. Optimal control theory is devoted to finding a control scheme for a dynamical system so that a certain optimality criterion is met [32]. Optimal control has been applied to a variety of areas

such as malware containment [33, 34] and cybersecurity [35]. Based on network-degree rumor spreading models, the rumor-containing problem has been dealt with through optimal control approach [36–39]. Recently, this methodology has been extended to individual-based rumor spreading models. The authors of [30] suggested an isolation-conversion mechanism of restraining rumors. Owing to violation of human rights, the mechanism in [30] may be impracticable. The authors of [17] introduced a rumor-containing message-pushing mechanism, which has two defects: (1) the effect of the external environment on the spread of the rumor was neglected at all and (2) the message-pushing rate function was regarded as a rumor-containing scheme. In practice, this function may not be under direct control of the rumor-containing agency.

In the present paper, we deal with the rumor-containing problem through optimal control approach but from a more practical perspective. First, we consider the influence of external environment on rumor spreading and propose a new rumor spreading model. Second, we regard the growth rate function of the rumor-containing cost as a rumor-containing scheme, and we define the cost-effectiveness of a rumor-containing scheme. Finally, we modeled the rumor-containing problem as the problem of finding the most cost-effective rumor-containing scheme, and we solve the problem by applying the optimal control theory.

3. The Modeling of the Rumor-Containing Problem

This section is devoted to the modeling of the rumor-containing problem. Based on a novel individual-based rumor spreading model, we measure the cost-effectiveness of a rumor-containing scheme. On this basis, we reduce the rumor-containing problem to an optimal control model.

3.1. A Rumor Spreading Model. Consider an OSN of N users denoted u_1 through u_N . Let $G_{\text{net}} = (U, E)$ denote the topological structure of the OSN, i.e., the node set $U = \{u_1, \dots, u_N\}$, and each edge $(u_i, u_j) \in E$ stands for the fact that the users u_i and u_j are mutual OSN friends. Let $\mathbf{A} = (a_{ij})_{N \times N}$ denote the adjacency matrix of G_{net} ; that is, $a_{ij} = 1$ if $(u_i, u_j) \in E$, and $a_{ij} = 0$ otherwise.

Suppose a rumor is spreading over the network G_{net} . In order to mitigate the impact of the rumor, a rumor-containing agency must collect rumor-containing evidence through continuous investment in a prescribed time horizon $[0, T]$. For $0 \leq t \leq T$, let $C(t)$ denote the cumulative rumor-containing cost in the time horizon $[0, t]$. Then $(dC(t)/dt)$ stands for the growth rate of the rumor-containing cost at time t . We refer to the function G defined by $G(t) = (dC(t)/dt)$, $t \in [0, T]$, as a *rumor-containing scheme*. Obviously, this scheme is under control of the rumor-containing agency.

For ease in realization, we assume that all feasible rumor-containing schemes are Lebesgue integrable [40]. Additionally, based on sociological evidence, it can be concluded that $G(t)$ is bounded. Let \bar{G} be the supremum of $G(t)$,

$0 \leq t \leq T$. By combining the above discussions, we get that the set of all feasible rumor-containing schemes is

$$G = \{G(t) \in L[0, T]: G(t) \leq \bar{G}, \quad 0 \leq t \leq T\}, \quad (1)$$

where $L[0, T]$ denotes the set of all Lebesgue integrable functions defined on the interval $[0, T]$.

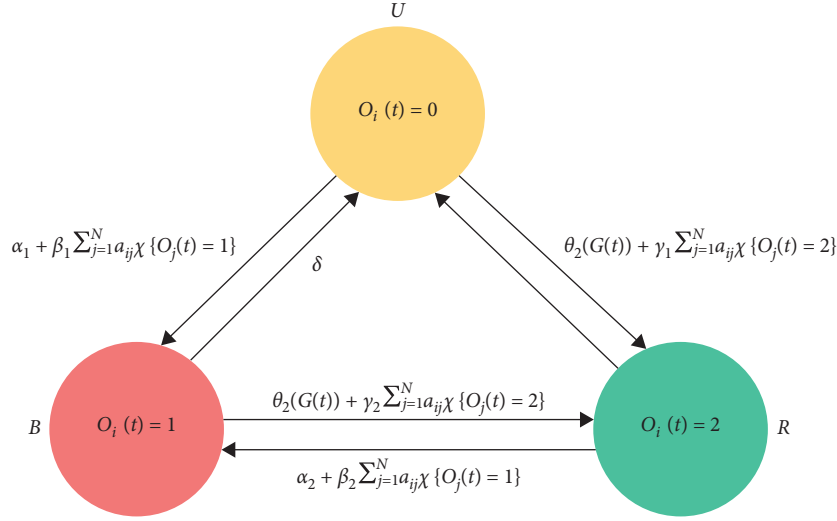
Combined with sociological evidence and rational analysis, we can know that at any time $t \in [0, T]$ each network user is either rumor-uncertain, rumor-believing, or rumor-refusing. Rumor-uncertain means that a user's attitude toward rumor is uncertain. Rumor-believing means that a user believes in a rumor. Rumor-refusing means that a user does not believe in a rumor. Let $O_i(t) = 0, 1$, and 2 stand for the fact that the user u_i is rumor-uncertain, rumor-believing, and rumor-refusing at time t , respectively. We refer to $O_i(t)$ as the state of the user u_i at time t , and the vector

$$O(t) = (O_1(t), \dots, O_N(t)), \quad (2)$$

as the state of the network at time t . The network state evolves over time. In order to describe the evolutionary process of the network state, let us introduce the following notations:

- (i) β_1 (resp., β_2): the probability with which, owing to the influence of a rumor-believing OSN friend, a rumor-uncertain (resp., rumor-refusing) user becomes rumor-believing at any time, and $\beta_1, \beta_2 > 0$.
- (ii) α_1 (resp., α_2): the probability with which, owing to the influence of the external environment, a rumor-uncertain (resp., rumor-refusing) user becomes rumor-believing at any time, and $\alpha_1, \alpha_2 \geq 0$.
- (iii) γ_1 (resp., γ_2): the probability with which, owing to the influence of a rumor-refusing OSN friend, a rumor-uncertain (resp., rumor-believing) user becomes rumor-refusing at any time, and $\gamma_1, \gamma_2 > 0$.
- (iv) δ : the probability with which, owing to the limited memory, a rumor-believing or rumor-refusing user becomes rumor-uncertain at any time, and $\delta > 0$.
- (v) $\theta_1(\bar{G})$ (resp., $\theta_2(\bar{G})$), $\bar{G} \in [0, \infty)$: the probability with which, owing to the growth rate \bar{G} of the rumor-containing cost, a rumor-uncertain (resp., rumor-believing) user becomes rumor-refusing. Obviously, $\theta_1(0) = \theta_2(0) = 0$, θ_1 and θ_2 are strictly increasing.

In practice, the first seven parameters can be estimated through online questionnaire survey, and the last two functions can be approximated through regression based on historical data. In particular, we introduce the parameter α_1 to characterize the effect of the external environment on the spread of rumors, and $\alpha_1 = 0$ refers to the scenario that does not consider the influence of external environment; this scenario has been studied by many researchers [16–30]. In this paper, we will consider a more general case, i.e., $\alpha_1 > 0$. Let $\chi_{\{O_i(t)=1\}}$ and $\chi_{\{O_i(t)=2\}}$ denote the indicator function of the event $O_i(t) = 1$ and the event $O_i(t) = 2$, respectively. Based on the theory of continuous-time Markov chain [41], Figure 1 exhibits the diagram of state transition of the user u_i .

FIGURE 1: The diagram of state transition of the user u_i .

Let $U_i(t)$, $B_i(t)$, and $R_i(t)$ denote the probability that the user u_i is rumor-uncertain, rumor-believing, and rumor-refusing at time t , respectively:

$$\begin{aligned} U_i(t) &= \Pr\{O_i(t) = 0\}, \\ B_i(t) &= \Pr\{O_i(t) = 1\}, \\ R_i(t) &= \Pr\{O_i(t) = 2\}. \end{aligned} \quad (3)$$

Since $U_i(t) = 1 - B_i(t) - R_i(t)$, we refer to the vector

$$E(t) = (B_1(t), \dots, B_N(t), R_1(t), \dots, R_N(t)), \quad (4)$$

as the expected state of the network at time t . Let $E_0 = E(0)$ denote the initial expected network state.

Theorem 1. *The evolutionary process of the expected network state is described by the following system of ordinary differential equations:*

$$\begin{cases} \frac{dB_i(t)}{dt} = \left[\alpha_1 + \beta_1 \sum_{j=1}^N a_{ij} B_j(t) \right] [1 - B_i(t) - R_i(t)] + \left[\alpha_2 + \beta_2 \sum_{j=1}^N a_{ij} B_j(t) \right] R_i(t) - \left[\theta_2(G(t)) + \gamma_2 \sum_{j=1}^N a_{ij} R_j(t) + \delta \right] B_i(t), & 0 \leq t \leq T, i = 1, \dots, N, \\ \frac{dR_i(t)}{dt} = \left[\theta_1(G(t)) + \gamma_1 \sum_{j=1}^N a_{ij} R_j(t) \right] [1 - B_i(t) - R_i(t)] + \left[\theta_2(G(t)) + \gamma_2 \sum_{j=1}^N a_{ij} R_j(t) \right] B_i(t) - \left[\alpha_2 + \beta_2 \sum_{j=1}^N a_{ij} B_j(t) + \delta \right] R_i(t), & 0 \leq t \leq T, i = 1, \dots, N, \\ E(0) = E_0. \end{cases} \quad (5)$$

Proof. Let $\mathbb{E}(\cdot)$ denote the mathematical expectation of a random variable. Then, the rumor-uncertain user u_i becomes rumor-believing at time t at the expected rate

$$\mathbb{E} \left(\alpha_1 + \beta_1 \sum_{j=1}^N a_{ij} \chi_{\{O_j(t)=1\}} \right) = \alpha_1 + \beta_1 \sum_{j=1}^N a_{ij} B_j(t), \quad (6)$$

the rumor-refusing user u_i becomes rumor-believing at time t at the expected rate

$$\mathbb{E} \left(\alpha_2 + \beta_2 \sum_{j=1}^N a_{ij} \chi_{\{O_j(t)=1\}} \right) = \alpha_2 + \beta_2 \sum_{j=1}^N a_{ij} B_j(t), \quad (7)$$

the rumor-believing user u_i becomes rumor-refusing at time t at the expected rate

$$\mathbb{E} \left(\theta_2(G(t)) + \gamma_2 \sum_{j=1}^N a_{ij} \chi_{\{O_j(t)=2\}} \right) = \theta_2(G(t)) + \gamma_2 \sum_{j=1}^N a_{ij} R_j(t), \quad (8)$$

and the rumor-believing user u_i becomes rumor-uncertain at time t at the expected rate δ . The first N equations in system (5) follow. The last N equations in the system can be derived analogously.

System (5) is a novel individual-based rumor spreading model, in which the effect of the external environment is accounted for. For $1 \leq i \leq N$ and $0 \leq t \leq T$, let

$$\begin{aligned} f_i(E(t), G(t)) &= \left[\alpha_1 + \beta_1 \sum_{j=1}^N a_{ij} B_j(t) \right] [1 - B_i(t) - R_i(t)] + \left[\alpha_2 + \beta_2 \sum_{j=1}^N a_{ij} B_j(t) \right] R_i(t) - \left[\theta_2(G(t)) + \gamma_2 \sum_{j=1}^N a_{ij} R_j(t) + \delta \right] B_i(t), \\ f_{N+i}(E(t), G(t)) &= \left[\theta_1(G(t)) + \gamma_1 \sum_{j=1}^N a_{ij} R_j(t) \right] [1 - B_i(t) - R_i(t)] + \left[\theta_2(G(t)) + \gamma_2 \sum_{j=1}^N a_{ij} R_j(t) \right] B_i(t) - \left[\alpha_2 + \beta_2 \sum_{j=1}^N a_{ij} B_j(t) + \delta \right] R_i(t). \end{aligned} \quad (9)$$

For $0 \leq t \leq T$, let

$$f(\mathbf{E}(t), G(t)) = (f_1(\mathbf{E}(t), G(t)), \dots, f_{2N}(\mathbf{E}(t), G(t))). \quad (10)$$

Then, model (5) is abbreviated as

$$\begin{cases} \frac{d\mathbf{E}(t)}{dt} = f(\mathbf{E}(t), G(t)), & 0 \leq t \leq T, \\ \mathbf{E}(0) = \mathbf{E}_0. \end{cases} \quad (11)$$

Next, we show that model (5) is positively invariant.

Theorem 2. Let \mathbf{E} be the solution to model (5). Then, $\mathbf{E}(t) \in [0, 1]^{2N}$, $0 \leq t \leq T$.

Proof. Obviously, $\mathbf{E}(0) \in [0, 1]^{2N}$. For $0 \leq t \leq T$, we proceed by distinguishing among three possibilities.

Case 1. $B_i(t) = 1$. Then, $R_i(t) = 0$. Hence, $(dB_i(t)/dt) = -[\theta_2(G(t)) + \gamma_2 \sum_{j=1}^N a_{ij} R_j(t) + \delta] < 0$.

Case 2. $R_i(t) = 0$. Then, $B_i(t) = 0$. Hence, $(dR_i(t)/dt) = -[\alpha_2 + \beta_2 \sum_{j=1}^N a_{ij} B_j(t) + \delta] < 0$.

Case 3. $0 \leq B_i(t) \leq 1$, $0 \leq R_i(t) \leq 1$, and $B_i(t) + R_i(t) = 1$. Then, $(d[B_i(t) + R_i(t)]/dt) = -\delta < 0$.

Hence, $\mathbf{E}(t) \in [0, 1]^{2N}$, $0 \leq t \leq T$.

In what follows, let

$$\begin{aligned} E(t, G(t)) &= (B_1(t, G(t)), \dots, B_N(t, G(t)), R_1(t, G(t)), \\ &\quad \dots, R_N(t, G(t))), \end{aligned} \quad (12)$$

stand for the solution to model (5).

3.2. The Optimal Control Modeling of the Rumor-Containing Problem. For our modeling purpose, we need to estimate the total loss caused by rumor, and then we will define cost-effectiveness. To this end, let w denote the average loss per unit time of a rumor-believing user. In practice, w can be estimated by assessing the potential consequence of the rumor under consideration.

Theorem 3. The expected total loss of all network users in the time range $[0, T]$ is

$$J_1(G) = w \int_0^T \sum_{i=1}^N B_i(t, G(t)) dt. \quad (13)$$

Proof. Let $dt > 0$ denote an infinitesimal. The average loss of the user u_i in the time range $[t, t + dt]$ is $w dt$ or zero according to whether he is rumor-believing at time t or not. Hence, his expected loss in the time range $[t, t + dt]$ is $w B_i(t, G(t)) dt$. Equation (13) follows.

Theorem 4. The rumor-containing cost in the time range $[0, T]$ is

$$J_2(G) = \int_0^T G(t) dt. \quad (14)$$

Proof. Let $dt > 0$ denote an infinitesimal. The rumor-containing cost in the time range $[t, t + dt]$ is $G(t) dt$. Equation (14) follows.

Based on Theorems 3 and 4, for a rumor-containing scheme G , the total loss caused by a rumor can be measured by the quantity

$$J(G) = J_1(G) + J_2(G) = \int_0^T \left[w \sum_{i=1}^N B_i(t, G(t)) + G(t) \right] dt. \quad (15)$$

In this paper, we use the quantity $J(G)$ to characterize cost-effectiveness, and the smaller the quantity $J(G)$ is, the more cost-effective the rumor-containing scheme will be. In practice, we hope to achieve maximum cost-effectiveness by minimizing the quantity $J(G)$.

Based on the above discussions, we model the rumor-containing problem as the following optimal control problem:

$$\begin{aligned} \min_{G \in \mathcal{G}} J(G) &= \int_0^T F(\mathbf{E}(t), G(t)) dt, \\ \text{subject to } \begin{cases} \frac{d\mathbf{E}(t)}{dt} = f(\mathbf{E}(t), G(t)), & 0 \leq t \leq T, \\ \mathbf{E}(0) = \mathbf{E}_0. \end{cases} \end{aligned} \quad (16)$$

Here, $F(\mathbf{E}(t), G(t)) = w \sum_{i=1}^N B_i(t, G(t)) + G(t)$.

We refer to the optimal control problem as the rumor-containing model. Each instance of the model is given by the 14-tuple as follows:

$$M = (G, \beta_1, \beta_2, \alpha_1, \alpha_2, \gamma_1, \gamma_2, \delta, \bar{G}, w, \theta_1, \theta_2, T, \mathbf{E}_0). \quad (17)$$

4. Dealing with the Rumor-Containing Model

This section aims to deal with the rumor-containing model (16). First, we show that the model is solvable. Second, we derive the optimality system for the model.

4.1. Solvability of the Rumor-Containing Model. The following lemma is a direct corollary of a theorem in [32].

Lemma 1. *The rumor-containing model (16) admits an optimal control if the following six conditions hold simultaneously:*

- (1) \mathcal{G} is closed.
- (2) \mathcal{G} is convex.
- (3) There exists $G \in \mathcal{G}$ such that model (5) is solvable.
- (4) $\mathbf{f}(\mathbf{E}, G)$ is bounded by a linear function in \mathbf{E} .
- (5) $F(\mathbf{E}, G)$ is convex on \mathcal{G} .

(6) There exist $\rho > 1, d_1 > 0$, and d_2 such that $F(\mathbf{E}, G) \geq d_1 G^\rho + d_2$.

We are ready to show the solvability of the rumor-containing model.

Theorem 5. *The rumor-containing model (16) admits an optimal control.*

Proof. First, let G^* be an accumulation point of the set \mathcal{G} . Then, there is a sequence of points, G_1, G_2, \dots , in \mathcal{G} that approaches G^* . On one hand, $G^* \in L[0, T]$ follows from the completeness of $L[0, T]$. On the other hand, $G^* = \lim_{n \rightarrow \infty} G_n(t) \leq \bar{G}$, $0 \leq t \leq T$. Hence, $G^* \in \mathcal{G}$. The closeness of \mathcal{G} is proven. Second, let $G_1, G_2 \in \mathcal{G}$, $0 < \sigma < 1$, and $G^* = (1 - \sigma)G_1 + \sigma G_2$. On one hand, $G^* \in L[0, T]$ follows from the fact that $L[0, T]$ is a vector space. On the other hand, it is obvious that $G^*(t) \leq \bar{G}$, $0 \leq t \leq T$. The convexity of \mathcal{G} is proven. Thirdly, the solvability of the system $(d\mathbf{E}(t)/dt) = \mathbf{f}(\mathbf{E}(t), G)$, $0 \leq t \leq T$, follows from the continuous differentiability of the function $\mathbf{f}(\mathbf{E}, G)$. Fourthly, for $1 \leq i \leq N$, we have

$$\begin{aligned} -\left[\theta_2(\bar{G}) + \gamma_2 \sum_{j=1}^N a_{ij} + \delta\right] B_i &\leq f_i(\mathbf{E}, G) \leq \alpha_1 + \alpha_2 + (\beta_1 + \beta_2) \sum_{j=1}^N a_{ij} B_j, \\ -\left[\alpha_2 + \beta_2 \sum_{j=1}^N a_{ij} + \delta\right] R_i &\leq f_{N+i}(\mathbf{E}, G) \leq \theta_1(\bar{G}) + \theta_2(\bar{G}) + (\gamma_1 + \gamma_2) \sum_{j=1}^N a_{ij} R_j. \end{aligned} \quad (18)$$

Next, the convexity of $F(\mathbf{E}, G)$ on \mathcal{G} follows from its linearity on \mathcal{G} . Finally, we have $F(\mathbf{E}, G) \geq 0 \geq G^2 - \bar{G}^2$. Hence, the claim follows from Lemma 1.

4.2. A Necessary Condition for the Optimal Control. The Hamiltonian of the rumor-containing model (16) is

$$\begin{aligned} H(\mathbf{E}, R, \lambda, \mu) &= w \sum_{i=1}^N B_i + G + \sum_{i=1}^N \lambda_i \left[\left(\alpha_1 + \beta_1 \sum_{j=1}^N a_{ij} B_j \right) (1 - B_i - R_i) + \left(\alpha_2 + \beta_2 \sum_{j=1}^N a_{ij} B_j \right) R_i - \left(\theta_2(G) + \gamma_2 \sum_{j=1}^N a_{ij} R_j + \delta \right) B_i \right] \\ &\quad + \sum_{i=1}^N \mu_i \left[\left(\theta_1(G) + \gamma_1 \sum_{j=1}^N a_{ij} R_j \right) (1 - B_i - R_i) + \left(\theta_2(G) + \gamma_2 \sum_{j=1}^N a_{ij} R_j \right) B_i - \left(\alpha_2 + \beta_2 \sum_{j=1}^N a_{ij} B_j + \delta \right) R_i \right], \end{aligned} \quad (19)$$

where $\lambda = (\lambda_1, \dots, \lambda_N)$ and $\mu = (\mu_1, \dots, \mu_N)$. λ and μ constitute the adjoint of H .

We are ready to present a necessary condition for the optimal control of model (16).

Theorem 6. *Let G be an optimal control for model (16), let \mathbf{E} be the resulting solution to model (5). Then, there exists an adjoint (λ, μ) such that*

$$\begin{aligned}
\frac{d\lambda_i(t)}{dt} &= -w + \left[\alpha_1 + \theta_2(G(t)) + \delta + \sum_{j=1}^N a_{ij}(\beta_1 B_j(t) + \gamma_2 R_j(t)) \right] \lambda_i(t) + \left[\theta_1(G(t)) - \theta_2(G(t)) + (\gamma_1 - \gamma_2) \sum_{j=1}^N a_{ij} R_j(t) \right] \mu_i(t) \\
&\quad + \sum_{j=1}^N \beta_2 a_{ij} R_j(t) \mu_j(t), \\
&\quad - \sum_{j=1}^N a_{ij} [\beta_1 (1 - B_j(t) - R_j(t)) + \beta_2 R_j(t)] \lambda_j(t), \quad 0 \leq t \leq T, i = 1, \dots, N, \\
\frac{d\mu_i(t)}{dt} &= \left[(\alpha_1 - \alpha_2) + \sum_{j=1}^N (\beta_1 - \beta_2) a_{ij} B_j(t) \right] \lambda_i(t) + \sum_{j=1}^N \gamma_2 a_{ij} B_j(t) \lambda_j(t) + \left[\theta_1(G(t)) + \alpha_2 + \delta + \sum_{j=1}^N a_{ij} (\gamma_1 R_j(t) + \beta_2 B_j(t)) \right] \mu_i(t) \\
&\quad - \sum_{j=1}^N a_{ij} [\gamma_1 (1 - B_j(t) - R_j(t)) + \gamma_2 B_j(t)] \mu_j(t), \quad 0 \leq t \leq T, i = 1, \dots, N.
\end{aligned} \tag{20}$$

Moreover, $\lambda(T) = \mu(T) = 0$, and

$$G(t) \in \arg \min_{\tilde{G} \in [0, \tilde{G}]} \left\{ \tilde{G} - \sum_{i=1}^N \lambda_i(t) B_i(t) \theta_2(\tilde{G}) + \sum_{i=1}^N \mu_i(t) [(1 - B_i(t) - R_i(t)) \theta_1(\tilde{G}) + B_i(t) \theta_2(\tilde{G})] \right\}, \quad 0 \leq t \leq T. \tag{21}$$

Proof. It follows from Pontryagin's Minimum Principle [32] that there exists (λ, μ) such that

$$\begin{cases} \frac{d\lambda_i(t)}{dt} = -\frac{\partial H(E(t), G(t), \lambda(t), \mu(t))}{\partial B_i}, & 0 \leq t \leq T, i = 1, \dots, N, \\ \frac{d\mu_i(t)}{dt} = -\frac{\partial H(E(t), G(t), \lambda(t), \mu(t))}{\partial R_i}, & 0 \leq t \leq T, i = 1, \dots, N. \end{cases} \tag{22}$$

System (20) follows by direct calculations. As the terminal cost is unspecified and the final state is free, we have $\lambda(T) = \mu(T) = 0$. Again, by Pontryagin's Minimum Principle, we get

$$G(t) \in \arg \min_{G \in \mathcal{G}} H(E(t), \tilde{G}, \lambda(t), \mu(t)), \quad 0 \leq t \leq T. \tag{23}$$

System (21) follows from direct calculations.

Based on the previous discussions, we get that the optimality system for model (16) comprises system (5), system (20), system (21), and $\lambda(T) = \mu(T) = 0$. The optimality system can be solved by invoking the well-known Forward-Backward Euler Method [42]. We refer to the control obtained in this way as a *promising rumor-containing scheme* for model (16). This is because the scheme may be optimal in terms of cost-effectiveness.

5. The Cost-Effectiveness of the Promising Rumor-Containing Scheme

At the end of the previous section, we proposed the notion of promising rumor-containing scheme. In this section, we

assess the cost-effectiveness of this scheme through comparative experiments.

5.1. Experiment Design. In each of the following experiments, we conduct the following operations: (1) generate an instance of the rumor-containing model (16), (2) obtain a promising rumor-containing scheme for the instance by invoking Forward-Backward Euler Method, and (3) compare this scheme with a set of static rumor-containing schemes in terms of the cost-effectiveness. All the following experiments are carried out on a PC with Inter® Core™ i5-7500 CPU @ 3.40 GHz and 8 GB RAM.

Studies show that some social platforms such as Facebook [43], Twitter [44], and YouTube [45] have provided a way for rumors to generate and spread. To simulate the environment in which rumors spread, we choose three real-world OSNs. First, consider the Facebook network and the Twitter network provided by SNAP, the well-known network library [46]. Due to memory limitation, we randomly choose a subnet of the original network without loss of generality. Choose a 100-node subnet of the original Facebook network (dataset name: ego-Facebook), denoted by G_F , and a 100-node subset of the original Twitter network (dataset name: ego-Twitter), denoted by G_T , respectively. Second, consider the YouTube network in Network Repository [47]. Choose a 100-node subnet of the YouTube network, denoted by G_Y . Figure 2 displays these three networks.

The cost-effectiveness is the focus in this section. Common OSN platforms generally have information security agencies. When rumors break out on OSN, the agency

is responsible for collecting and disseminating truths to dispel rumors, for example, when President Trump declared on Twitter that mail voting would lead to a “rigged election.” In order to control the spread of the rumor, Twitter tagged Trump’s tweets with the label “Getting the facts about mailing votes” and redirected users to a fact-checking page to provide comprehensive investigation information for the misleading article. In practice, the agency’s budget is limited. In order to control the spread of rumors, the agency needs to find a cost-effective rumor control scheme; that is, the scheme can minimize the total loss caused by rumors.

In all the following experiments, let $\bar{G} = 1$, $w = 0.1$, $T = 10$, and $\mathbf{E}_0 = (0.1, \dots, 0.1)$. Let $G^P(t) (0 \leq t \leq T)$ denote the promising rumor-containing scheme, and $G_a(t) = a (0 \leq t \leq T)$ a static rumor-containing scheme. Let

$$\mathbb{M}_i = (G_{\text{net}}^i, \beta_1, \beta_2, \alpha_1, \alpha_2, \gamma_1, \gamma_2, \delta, \bar{G}, w, \theta_1(x), \theta_2(x), T, \mathbf{E}_0), \quad i = 1, 2, 3, \dots, \quad (25)$$

where $G_{\text{net}}^1 = G_F$, $G_{\text{net}}^2 = G_T$, $G_{\text{net}}^3 = G_Y$, $\beta_1 = 0.2$, $\beta_2 = 0.1$, $\alpha_1 = 0$, $\alpha_2 = 0.15$, $\gamma_1 = 0.2$, $\gamma_2 = 0.12$, $\delta = 0.1$, $\bar{G} = 1.0$, $w = 0.1$, $\theta_1(x) = 0.3$, and $\theta_2(x) = 0.2$. In order to show the influence of external environment on the propagation of rumors, we only change the value of α_1 and let $\alpha_1 = 0, 0.1, 0.2, 0.3, 0.4, 0.5$, respectively. Let $B(t)$ denote the expected probability of rumor-believing users in the OSN, and $B(t)$ is given by $B(t) = (1/N) \sum_{i=1}^N B_i(t)$. As shown in Figure 3, compared with the situation that does not consider the effect of external environment (i.e., $\alpha_1 = 0$), increasing α_1 will cause the value of $B(t)$ to increase, especially when t is relatively small. The finding indicates that external environment has a great effect on the expected probability of rumor-believing users in OSNs, especially in the early stages of the spread of rumors, and if we ignore the effect of external environment, the propagation ability of rumors will be seriously underestimated.

$$\mathbb{M} = (G, \beta_1, \beta_2, \alpha_1, \alpha_2, \gamma_1, \gamma_2, \delta, \bar{G}, w, \theta_1, \theta_2, T, \mathbf{E}_0). \quad (26)$$

In practice, the closed-form formula for the functions θ_1 and θ_2 can be approximated through regression based on historical data, and both θ_1 and θ_2 are monotonically increasing functions. Supposing that there is a rumor spreading on the network G_F , we consider three different forms of θ_1 and θ_2 , and the experimental settings are as follows.

Experiment 2. Consider three instances of the rumor-containing model:

$$\mathbb{M}_F^i = (G_F, \beta_1, \beta_2, \alpha_1, \dots, \theta_2^i(x), T, \mathbf{E}_0), \quad i = 1, 2, 3, \dots, \quad (27)$$

where $\beta_1 = 0.2$, $\beta_2 = 0.1$, $\alpha_1 = 0.2$, $\alpha_2 = 0.15$, $\gamma_1 = 0.2$, $\gamma_2 = 0.12$, $\delta = 0.1$, $\bar{G} = 1.0$, $w = 0.1$, $\theta_1^1(x) = 0.3x$, $\theta_1^2(x) = 0.2x$, $\theta_1^3(x) = 0.3x^{(1/2)}$, $\theta_2^1(x) = 0.2x^{(1/2)}$, $\theta_2^2(x) = (1.5x/4 + x)$, and $\theta_2^3(x) = (x/4 + x)$. Let G^P denote the promising rumor-containing scheme. By applying the

$$A = \{G_a: a = 0, 0.1, 0.2, \dots, 1.0\}. \quad (24)$$

In particular, the static rumor-containing scheme $G_a(t) = 0$ stands for taking no rumor-containing scheme; that is, let the rumors spread freely.

5.2. Experimental Results

Experiment 1. For the rumor-containing model $\mathbb{M} = (G, \beta_1, \beta_2, \alpha_1, \dots, \theta_2, T, \mathbf{E}_0)$, $\alpha_1 = 0$ stands for ignoring the influence of external environment on the propagation of a rumor. Consider three instances as follows:

approach introduced in Section 4.2, we get a promising control G^P , which is shown in Figure 4. It is seen that the promising rumor-containing scheme G^P of the three instances first stays at the maximum allowable rate and then drops to the zero rates.

Furthermore, we compare the cost-effectiveness between the promising control strategy G^P and a group of static control strategies $A = \{G_a: 0, 0.1, 0.2, \dots, 1.0\}$. The comparison result can be found in Figure 5. It is seen that $J(G^P) < J(G_a)$, $G_a \in A$. The result shows that our proposed rumor-containing scheme G^P obtains the highest cost-effectiveness; hence, it performs much better than all the static rumor-containing schemes.

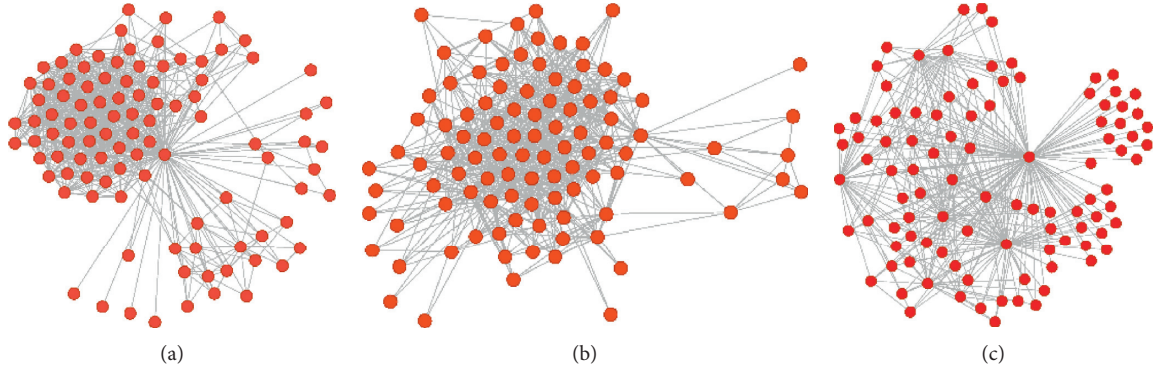
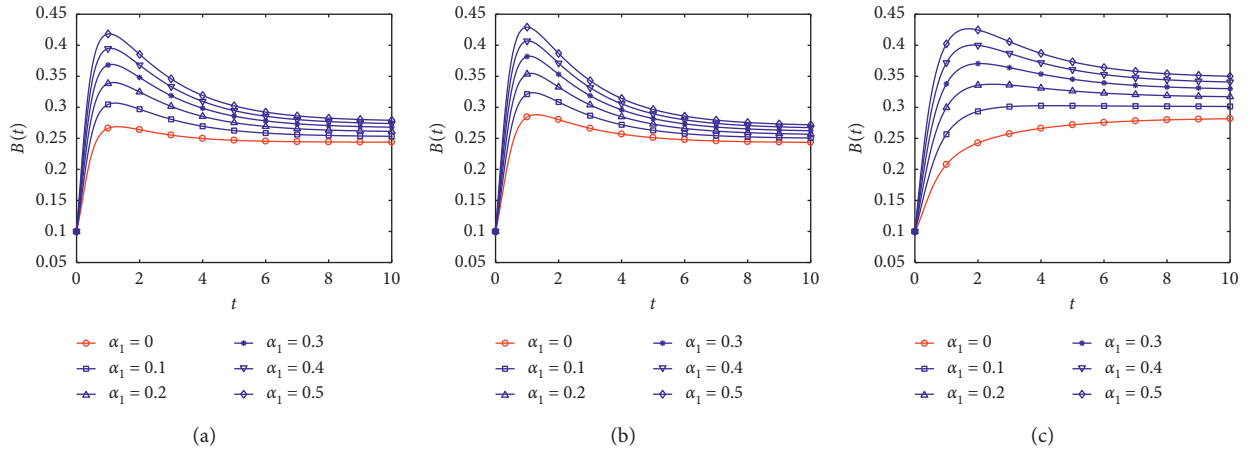
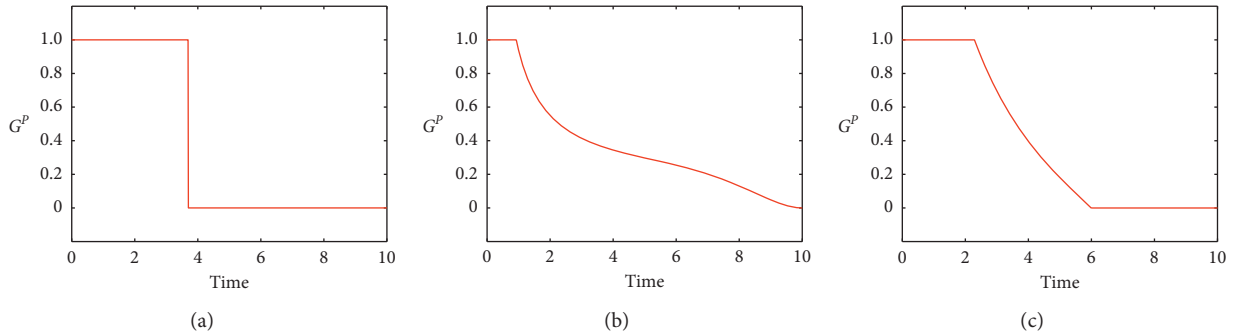
Similarly, supposing that there is a rumor spreading on the network G_T , we consider three different forms of θ_1 and θ_2 , and the experimental settings are as follows.

Experiment 3. Consider three instances of the rumor-containing model:

$$\mathbb{M}_T^i = (G_T, \beta_1, \beta_2, \alpha_1, \alpha_2, \gamma_1, \gamma_2, \delta, \bar{G}, w, \theta_1^i(x), \theta_2^i(x), T, \mathbf{E}_0), \quad i = 1, 2, 3, \dots, \quad (28)$$

where $\beta_1 = 0.15$, $\beta_2 = 0.1$, $\alpha_1 = 0.15$, $\alpha_2 = 0.12$, $\gamma_1 = 0.2$, $\gamma_2 = 0.1$, $\delta = 0.1$, $\bar{G} = 1.0$, $w = 0.1$, $\theta_1^1(x) = 0.4x$, $\theta_1^2(x) = 0.3x$, $\theta_1^3(x) = 0.4x^{(1/2)}$, $\theta_2^1(x) = 0.3x^{(1/2)}$, $\theta_2^2(x) = (0.8x/1 + x)$, and $\theta_2^3(x) = (0.6x/1 + x)$. Let G^P denote the promising rumor-containing scheme. By applying the approach introduced in Section 4.2, we get a promising control G^P , which is shown in Figure 6. It is seen that the promising rumor-containing scheme G^P of the three instances first stays at the maximum allowable rate and then drops to the zero rates.

Furthermore, we compare the cost-effectiveness between the promising control strategy G^P and a group of static control strategies $A = \{G_a: 0, 0.1, 0.2, \dots, 1.0\}$. The comparison result can be found in Figure 7. It is seen that $J(G^P) < J(G_a)$, $G_a \in A$. The result shows that our proposed

FIGURE 2: Three real-world OSNs: (a) G_F , (b) G_T , and (c) G_Y .FIGURE 3: The effect of α_1 on $B(t)$ for the three OSNs: (a) Facebook network G_F , (b) Twitter network G_T , and (c) YouTube network G_Y .FIGURE 4: The promising rumor-containing scheme G^P for three pairs of $(\theta_1(x), \theta_2(x))$ functions: (a) $\theta_1(x) = \theta_1^1(x)$ and $\theta_2(x) = \theta_2^1(x)$, (b) $\theta_1(x) = \theta_1^2(x)$ and $\theta_2(x) = \theta_2^2(x)$, and (c) $\theta_1(x) = \theta_1^3(x)$ and $\theta_2(x) = \theta_2^3(x)$.

rumor-containing scheme G^P obtains the highest cost-effectiveness; hence, it performs much better than all the static rumor-containing schemes.

Again, supposing that there is a rumor spreading on the network G_Y , we consider three different forms of θ_1 and θ_2 , and the experimental settings are as follows.

Experiment 4. Consider three instances of the rumor-containing model:

$$\mathbb{M}_Y^i = (G_Y, \beta_1, \beta_2, \alpha_1, \alpha_2, \gamma_1, \gamma_2, \delta, \bar{G}, w, \theta_1^i(x), \theta_2^i(x), T, E_0), \quad i = 1, 2, 3, \dots, \quad (29)$$

where $\beta_1 = 0.15$, $\beta_2 = 0.13$, $\alpha_1 = 0.15$, $\alpha_2 = 0.16$, $\gamma_1 = 0.2$, $\gamma_2 = 0.1$, $\delta = 0.1$, $\bar{G} = 1.0$, $w = 0.1$, $\theta_1^1(x) = 0.3x$, $\theta_1^2(x) = 0.2x$, $\theta_1^3(x) = 0.3x^{(1/4)}$, $\theta_2^1(x) = 0.2x$, $\theta_2^2(x) = 0.2x^{(1/4)}$, $\theta_2^3(x) = (1.5x/4 + x)$, and $\theta_2^4(x) = (x/4 + x)$. Let G^P denote the promising rumor-containing scheme. By applying the approach introduced in Section 4.2, we get a promising control

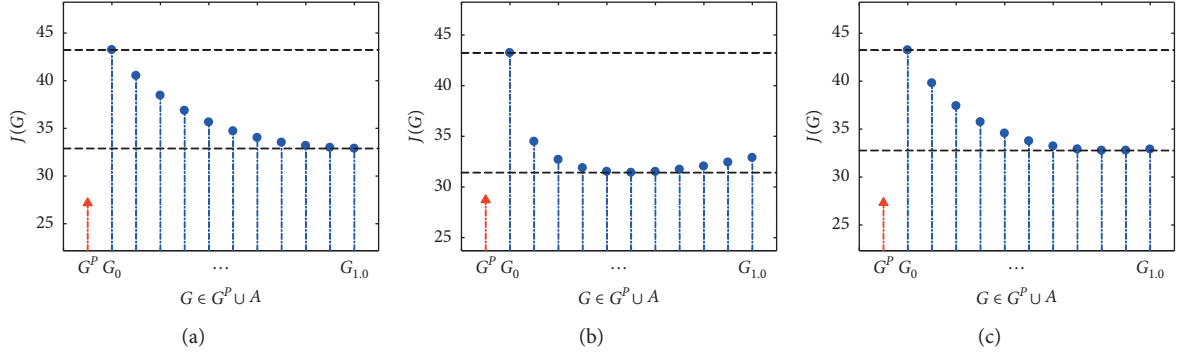


FIGURE 5: A comparison between the three promising controls G^P in Figure 2 and the set of static controls A in terms of total cost.

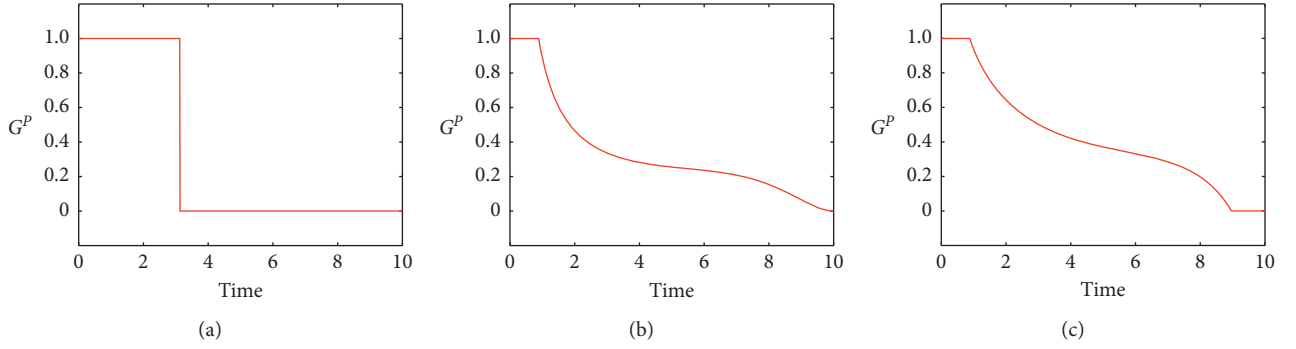


FIGURE 6: The promising rumor-containing scheme G^P for three pairs of $(\theta_1(x), \theta_2(x))$ functions: (a) $\theta_1(x) = \theta_1^1(x)$ and $\theta_2(x) = \theta_2^1(x)$, (b) $\theta_1(x) = \theta_1^2(x)$ and $\theta_2(x) = \theta_2^2(x)$, and (c) $\theta_1(x) = \theta_1^3(x)$ and $\theta_2(x) = \theta_2^3(x)$.

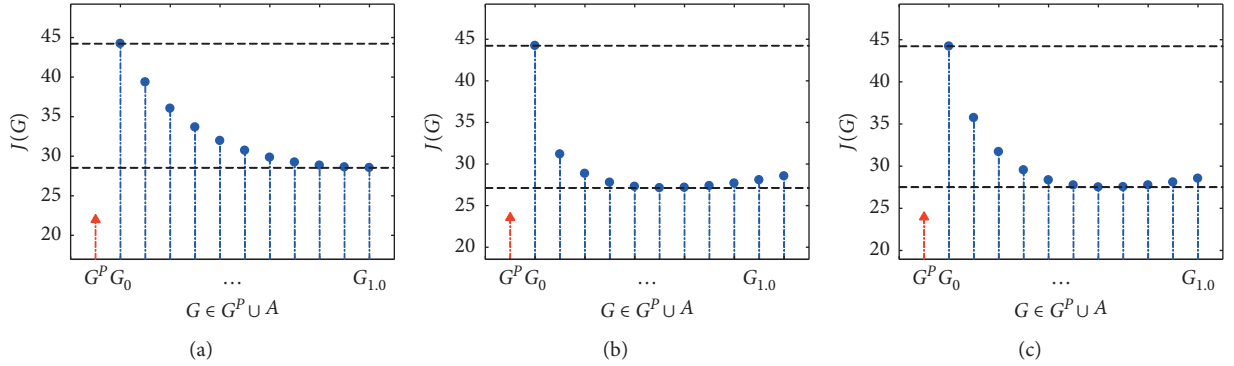


FIGURE 7: A comparison between the three promising controls G^P in Figure 4 and the set of static controls A in terms of total cost.

G^P , which is shown in Figure 8. It is seen that the promising rumor-containing scheme G^P of the three instances first stays at the maximum allowable rate and then drops to the zero rates.

Furthermore, we compare the cost-effectiveness between the promising control strategy G^P and a group of static control strategies $A = \{G_\alpha: 0, 0.1, 0.2, \dots, 1.0\}$. The comparison result can be found in Figure 9. It is seen that $J(G^P) < J(G_\alpha)$, $G_\alpha \in A$. The result shows that our proposed rumor-containing scheme G^P obtains the highest cost-effectiveness; hence, it performs much better than all the static rumor-containing schemes.

Based on the results of Experiments 2–4, we can draw some conclusions as follows: (a) if we do not take any rumor-containing scheme, the spread of rumors will cause great losses, and (b) the proposed rumor-containing scheme can greatly mitigate the impact of rumor and performs much better than all the static rumor-containing schemes in terms of the cost-effectiveness. Apart from the above three experiments, we conduct 1,000 similar experiments as well. In all these experiments, we obtain similar and consistent results. Therefore, we conclude that the promising rumor-containing scheme is cost-effective.

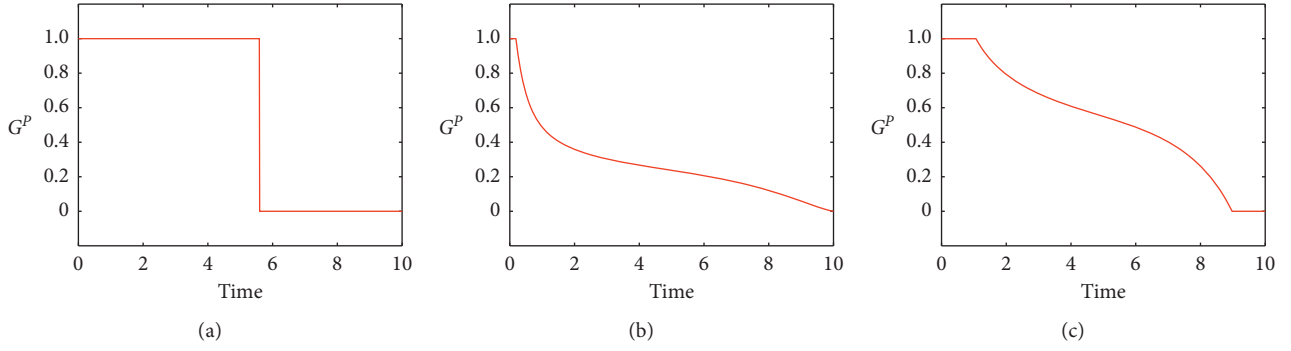


FIGURE 8: The promising rumor-containing scheme G^P for three pairs of $(\theta_1(x), \theta_2(x))$ functions: (a) $\theta_1(x) = \theta_1^1(x)$ and $\theta_2(x) = \theta_2^1(x)$, (b) $\theta_1(x) = \theta_1^2(x)$ and $\theta_2(x) = \theta_2^2(x)$, and (c) $\theta_1(x) = \theta_1^3(x)$ and $\theta_2(x) = \theta_2^3(x)$.

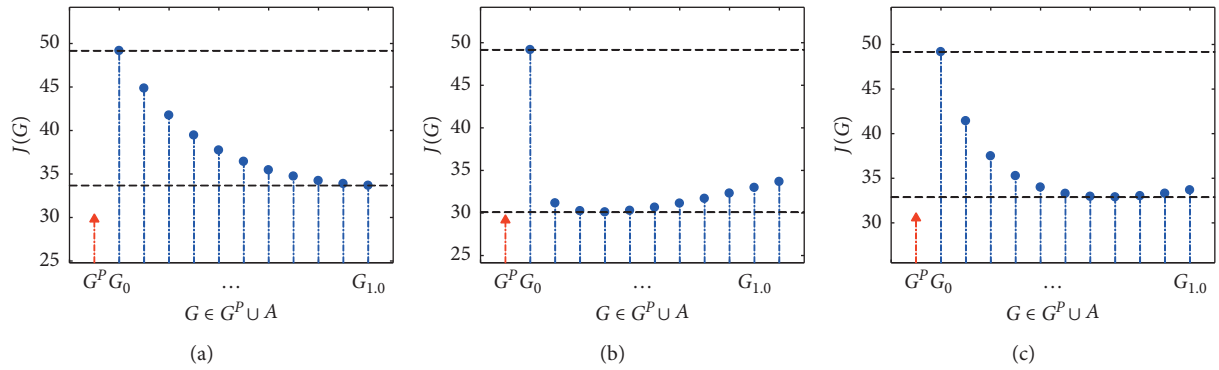


FIGURE 9: A comparison between the three promising controls G^P in Figure 6 and the set of static controls A in terms of total cost.

6. Concluding Remarks

In this study, we have studied the problem of developing a cost-effective rumor-containing scheme. Based on a node-level rumor spreading model that takes account of the effect of external environment, we have measured the impact of rumors. On this basis, we have modeled the rumor-containing problem as an optimal control problem. The optimization goal of the problem is to find a rumor-containing scheme that minimizes the total loss, and simulation results show that the proposed scheme is cost-effective. This work has studied the propagation of rumor from theoretical modeling and cost management perspectives. The research results can provide some theoretical guidance for taking measures to suppress the spread of rumors. The new model proposed in this paper can be used to study the influence of some parameters on the spread of rumors, and the research ideas can also be applied to study other cyberspace security problems.

The spread of rumors in the real world may be more complicated, and there are some open problems. First, since there is more than one OSN in the real world [48, 49], the rumor-containing problem should be extended to multiplex OSNs. Second, since realistic OSNs are varying over time [50, 51], it is necessary to study the rumor-containing problem with dynamic OSNs. Thirdly, in some application scenarios, the spread of a rumor can be captured by a system of partial differential equations [52–54]; it is worth adapting this work to these situations. Next, it is necessary to apply

our methodology to some other areas such as disease spreading [55, 56], malware propagation [57, 58], and cybersecurity [59, 60]. Finally, in this work, the rumor-monger is assumed to be nonstrategic. In practice, however, the rumor-monger may well be strategic. In this situation, the rumor-containing problem should be treated in the framework of game theory [61–63].

Data Availability

The data used to support the findings of this study are available, and the sources of the datasets have been given in the paper.

Conflicts of Interest

The authors declare that there are no conflicts of interest.

Authors' Contributions

Da-Wen Huang contributed to formal analysis, software, and roles/writing of the original draft. Lu-Xing Yang contributed to formal analysis, investigation, and validation. Xiaofan Yang contributed to supervision, methodology, and writing, reviewing, and editing of the paper. Yuan Yan Tang contributed to supervision and writing, reviewing, and editing of the paper. Jichao Bi contributed to writing, reviewing, and editing of the paper.

References

- [1] P. Verduyn, O. Ybarra, M. Résibois, J. Jonides, and E. Kross, "Do social network sites enhance or undermine subjective well-being? A critical review," *Social Issues and Policy Review*, vol. 11, no. 1, pp. 274–302, 2017.
- [2] D. J. Kuss and M. D. Griffiths, "Social networking sites and addiction: ten lessons learned," *International Journal of Environmental Research and Public Health*, vol. 14, no. 3, p. 311, 2017.
- [3] S. Wen, J. Jiang, Y. Xiang, S. Yu, W. Zhou, and W. Jia, "To shut them up or to clarify: restraining the spread of rumors in online social networks," *IEEE Transactions on Parallel and Distributed Systems*, vol. 25, no. 12, pp. 3306–3316, 2014.
- [4] S. Vosoughi, D. Roy, and S. Aral, "The spread of true and false news online," *Science*, vol. 359, no. 6380, pp. 1146–1151, 2018.
- [5] K. Rapoza, *Can 'Fake News' Impact the Stock Market?*, Forbes, New Jersey, NJ, USA, 2017, <http://www.forbes.com/sites/kenrapoza/2017/02/26/can-fake-news-impact-the-stock-market/>.
- [6] J. Ma, W. Gao, P. Mitra et al., "Detecting rumors from microblogs with recurrent neural networks," in *Proceedings of the 25th International Joint Conference on Artificial Intelligence*, pp. 3818–3824, New York, NY, USA, January 2016.
- [7] A. J. Kimmel, *Rumors and Rumor Control: A Manager's Guide to Understanding and Combatting Rumors*, Routledge, Abingdon, UK, 2012.
- [8] C. Gan, Q. Feng, Q. Zhu, Z. Zhang, Y. Zhang, and Y. Xiang, "Analysis of computer virus propagation behaviors over complex networks: a case study of Oregon routing network," *Nonlinear Dynamics*, vol. 100, no. 2, pp. 1725–1740, 2020.
- [9] K. Sharma, F. Qian, H. Jiang, N. Ruchansky, M. Zhang, and Y. Liu, "Combating fake news," *ACM Transactions on Intelligent Systems and Technology*, vol. 10, no. 3, pp. 1–42, 2019.
- [10] C. Budak, D. Agrawal, and A. E. Abbadi, "Limiting the spread of misinformation in social networks," in *Proceedings of the 20th International Conference on World Wide Web*, pp. 665–674, Hyderabad, India, March 2011.
- [11] N. P. Nguyen, G. Yan, M. T. Thai, and S. Eidenbenz, "Containment of misinformation spread in online social networks," in *Proceedings of the 4th Annual ACM Web Science Conference on—WebSci '12*, pp. 213–222, Evanston, IL, USA, June 2012.
- [12] L. Fan, Z. Lu, W. Wu, B. Thuraisingham, H. Ma, and Y. Bi, "Least cost rumor blocking in social networks," in *Proceedings of the 2013 33rd International Conference on Distributed Computing Systems*, pp. 540–549, Philadelphia, PA, USA, July 2013.
- [13] G. A. Tong, W. Wu, L. Guo et al., "An efficient randomized algorithm for rumor blocking in online social networks," *IEEE Transactions on Network Science and Engineering*, vol. 14, 2017.
- [14] B. Wang, G. Chen, L. Fu, L. Song, and X. Wang, "DRIMUX: dynamic rumor influence minimization with user experience in social networks," *IEEE Transactions on Knowledge and Data Engineering*, vol. 29, no. 10, pp. 2168–2181, 2017.
- [15] L. Yang, Z. Li, and A. Giua, "Containment of rumor spread in complex social networks," *Information Sciences*, vol. 506, pp. 113–130, 2019.
- [16] Z. He, Z. Cai, J. Yu, X. Wang, Y. Sun, and Y. Li, "Cost-efficient strategies for restraining rumor spreading in mobile social networks," *IEEE Transactions on Vehicular Technology*, vol. 66, no. 3, pp. 2789–2800, 2016.
- [17] J. Chen, L.-X. Yang, X. Yang, and Y. Y. Tang, "Cost-effective anti-rumor message-pushing schemes," *Physica A: Statistical Mechanics and Its Applications*, vol. 540, Article ID 123085, 2020.
- [18] L. Zhao, J. Wang, Y. Chen, Q. Wang, J. Cheng, and H. Cui, "SIHR rumor spreading model in social networks," *Physica A: Statistical Mechanics and Its Applications*, vol. 391, no. 7, pp. 2444–2453, 2012.
- [19] L. Zhao, J. Wang, and R. Huang, "Immunization against the spread of rumors in homogeneous networks," *PLoS One*, vol. 10, no. 5, Article ID e0124978, 2015.
- [20] J. Xu, M. Zhang, and J. Ni, "A coupled model for government communication and rumor spreading in emergencies," *Advances in Difference Equations*, vol. 208, no. 1, pp. 1687–1847, 2016.
- [21] Z.-J. Zhao, Y.-M. Liu, and K.-X. Wang, "An analysis of rumor propagation based on propagation force," *Physica A: Statistical Mechanics and Its Applications*, vol. 443, pp. 263–271, 2016.
- [22] L. A. Huo and N. Song, "Dynamical interplay between the dissemination of scientific knowledge and rumor spreading in emergency," *Physica A: Statistical Mechanics and Its Applications*, vol. 461, pp. 73–84, 2016.
- [23] Y. Moreno, M. Nekovee, and A. F. Pacheco, "Dynamics of rumor spreading in complex networks," *Physical Review E*, vol. 69, no. 6, Article ID 066130, 2004.
- [24] M. Nekovee, Y. Moreno, G. Bianconi, and M. Marsili, "Theory of rumour spreading in complex social networks," *Physica A: Statistical Mechanics and Its Applications*, vol. 374, no. 1, pp. 457–470, 2007.
- [25] L. Zhao, W. Xie, H. O. Gao, X. Qiu, X. Wang, and S. Zhang, "A rumor spreading model with variable forgetting rate," *Physica A: Statistical Mechanics and Its Applications*, vol. 392, no. 23, pp. 6146–6154, 2013.
- [26] J. Ma and H. Zhu, "Rumor diffusion in heterogeneous networks by considering the individuals' subjective judgment and diverse characteristics," *Physica A: Statistical Mechanics and Its Applications*, vol. 499, pp. 276–287, 2018.
- [27] L.-X. Yang, P. Li, X. Yang, Y. Wu, and Y. Y. Tang, "On the competition of two conflicting messages," *Nonlinear Dynamics*, vol. 91, no. 3, pp. 1853–1869, 2018.
- [28] L.-X. Yang, T. Zhang, X. Yang, Y. Wu, and Y. Yan Tang, "Effectiveness analysis of a mixed rumor-quelling strategy," *Journal of the Franklin Institute*, vol. 355, no. 16, pp. 8079–8105, 2018.
- [29] C. Pan, L.-X. Yang, X. Yang, Y. Wu, and Y. Y. Tang, "An effective rumor-containing strategy," *Physica A: Statistical Mechanics and Its Applications*, vol. 500, pp. 80–91, 2018.
- [30] J. Zhao, L.-X. Yang, X. Zhong, X. Yang, Y. Wu, and Y. Y. Tang, "Minimizing the impact of a rumor via isolation and conversion," *Physica A: Statistical Mechanics and Its Applications*, vol. 526, Article ID 120867, 2019.
- [31] S. Zannettou, M. Sirivianos, J. Blackburn, and N. Kourtellis, "The web of false information," *Journal of Data and Information Quality*, vol. 11, no. 3, pp. 1–37, 2019.
- [32] D. Liberzon, *Calculus of Variations and Optimal Control Theory: A Concise Introduction*, Princeton University Press, Princeton, NJ, USA, 2012.
- [33] S. Eshghi, M. H. R. Khouzani, S. Sarkar, and S. S. Venkatesh, "Optimal patching in clustered malware epidemics," *IEEE/ACM Transactions on Networking*, vol. 24, no. 1, pp. 283–298, 2016.
- [34] W. Liu and S. Zhong, "Web malware spread modelling and optimal control strategies," *Scientific Reports*, vol. 7, Article ID 42308, 2017.

- [35] V. M. Preciado, M. Zargham, C. Enyioha, A. Jadbabaie, and G. J. Pappas, "Optimal resource allocation for network protection against spreading processes," *IEEE Transactions on Control of Network Systems*, vol. 1, no. 1, pp. 99–108, 2014.
- [36] L. Huo, T. Lin, C. Fan, C. Liu, and J. Zhao, "Optimal control of a rumor propagation model with latent period in emergency event," *Advances in Difference Equations*, vol. 54, 2015.
- [37] Y. D. Jeong, K. S. Kim, and I. H. Jung, "Optimal control strategies depending on interest level for the spread of rumor," *Discrete Dynamics in Nature and Society*, vol. 2018, Article ID 9158014, 15 pages, 2018.
- [38] L. Huo and C. Ma, "Optimal control of rumor spreading model with consideration of psychological factors and time delay," *Discrete Dynamics in Nature and Society*, vol. 2018, Article ID 9314907, 12 pages, 2018.
- [39] X. Wang, X. Wang, F. Hao, G. Min, and L. Wang, "Efficient coupling diffusion of positive and negative information in online social networks," *IEEE Transactions on Network and Service Management*, vol. 16, no. 13, pp. 1226–1239, 2019.
- [40] E. M. Stein and R. Shakarchi, *Real Analysis: Measure Theory, Integration, and Hilbert Spaces*, Princeton University Press, Princeton, NJ, USA, 2005.
- [41] W. J. Stewart, *Probability, Markov Chains, Queues, and Simulation: The Mathematical Basis of Performance Modeling*, Princeton University Press, Princeton, NJ, USA, 2009.
- [42] K. Atkinson, W. Han, and D. Stewart, *Numerical Solution of Ordinary Differential Equation*, Wiley, Hoboken, NJ, USA, 2009.
- [43] A. Y. K. Chua and S. Banerjee, "Rumor verifications on facebook: click speech of likes, comments and shares," in *Proceedings of the 2017 Twelfth International Conference on Digital Information Management (ICDIM)*, pp. 257–262, Fukuoka, Japan, September 2017.
- [44] N. Grinberg, K. Joseph, L. Friedland, B. Swire-Thompson, and D. Lazer, "Fake news on Twitter during the 2016 U.S. presidential election," *Science*, vol. 363, no. 6425, pp. 374–378, 2019.
- [45] J. Allen, B. Howland, M. Mobius, D. Rothschild, and D. J. Watts, "Evaluating the fake news problem at the scale of the information ecosystem," *Science Advances*, vol. 6, no. 14, p. 3539, 2020.
- [46] J. McAuley and J. Leskovec, "Learning to discover social circles in ego networks," in *Proceedings of the Advances in Neural Information Processing Systems*, pp. 539–547, Lake Tahoe, NV, USA, December 2012.
- [47] R. A. Rossi and N. K. Ahmed, "The network data repository with interactive graph analytics and visualization," in *Proceedings of the 29th AAAI Conference on Artificial Intelligence*, pp. 4292–4293, Austin, TX, USA, January 2015.
- [48] W. Wang, M. Tang, H. E. Stanley, and L. A. Braunstein, "Social contagions with communication channel alternation on multiplex networks," *Physical Review E*, vol. 98, no. 6, Article ID 062320, 2018.
- [49] Y. Zhou, J. Zhou, G. Chen, and H. E. Stanley, "Effective degree theory for awareness and epidemic spreading on multiplex networks," *New Journal of Physics*, vol. 21, no. 3, Article ID 035002, 2019.
- [50] G. Miritello, E. Moro, and R. Lara, "Dynamical strength of social ties in information spreading," *Physical Review E*, vol. 83, no. 4 Pt 2, Article ID 045102, 2011.
- [51] V. Sekara, A. Stopczynski, and S. Lehmann, "Fundamental structures of dynamic social networks," *Proceedings of the National Academy of Sciences*, vol. 113, no. 36, pp. 9977–9982, 2016.
- [52] H. Zhao and L. Zhu, "Dynamic analysis of a reaction-diffusion rumor propagation model," *International Journal of Bifurcation and Chaos*, vol. 26, no. 6, Article ID 1650101, 2016.
- [53] L. Zhu, H. Zhao, and H. Wang, "Complex dynamic behavior of a rumor propagation model with spatial-temporal diffusion terms," *Information Sciences*, vol. 349–350, pp. 119–136, 2016.
- [54] L. Zhu, H. Zhao, and H. Wang, "Partial differential equation modeling of rumor propagation in complex networks with higher order of organization," *Chaos*, vol. 29, no. 5, Article ID 053106, 2019.
- [55] C.-Y. Xia, Z. Wang, J. Sanz, S. Meloni, and Y. Moreno, "Effects of delayed recovery and nonuniform transmission on the spreading of diseases in complex networks," *Physica A: Statistical Mechanics and Its Applications*, vol. 392, no. 7, pp. 1577–1585, 2013.
- [56] C. Xia, Z. Wang, C. Zheng et al., "A new coupled disease-awareness spreading model with mass media on multiplex networks," *Information Sciences*, vol. 471, pp. 185–200, 2019.
- [57] L. Feng, X. Liao, Q. Han, and H. Li, "Dynamical analysis and control strategies on malware propagation model," *Applied Mathematical Modelling*, vol. 37, no. 16–17, pp. 8225–8236, 2013.
- [58] L. Feng, L. Song, Q. Zhao, and H. Wang, "Modeling and stability analysis of worm propagation in wireless sensor network," *Mathematical Problem in Engineering*, vol. 2015, Article ID 129598, 8 pages, 2015.
- [59] S. Xu, W. Lu, and H. Li, "A stochastic model of active cyber defense dynamics," *Internet Mathematics*, vol. 11, no. 1, pp. 23–61, 2015.
- [60] L. X. Yang, P. Li, X. Yang, Y. Xiang, and Y. Y. Tang, "Effective quarantine and recovery scheme against advanced persistent threat," *IEEE Transactions on Systems, Man, and Cybernetics*, 2019.
- [61] M. J. Osborne, *An Introduction to Game Theory*, Oxford University Press, Oxford, UK, 2003.
- [62] L.-X. Yang, P. Li, Y. Zhang, X. Yang, Y. Xiang, and W. Zhou, "Effective repair strategy against advanced persistent threat: a differential game approach," *IEEE Transactions on Information Forensics and Security*, vol. 14, no. 7, pp. 1713–1728, 2019.
- [63] L. X. Yang, P. Li, X. Yang, Y. Xiang, and Y. Y. Tang, "Simultaneous benefit maximization of conflicting opinions: modeling and analysis," *IEEE Systems Journal*, vol. 99, pp. 1–2, 2020.

Research Article

A Configurable Semantic-Based Transformation Method towards Conceptual Models

Tiexin Wang^{1,2}, Jingwen Cao,¹ Chuanqi Tao,¹ Zhibin Yang,^{1,2} Yi Wu,¹ and Bohan Li¹

¹College of Computer Science and Technology, Nanjing University of Aeronautics and Astronautics, Nanjing 211106, China

²Key Laboratory of Safety-Critical Software (Nanjing University of Aeronautics and Astronautics), Ministry of Industry and Information Technology, Nanjing 211106, China

Correspondence should be addressed to Tiexin Wang; tiexin.wang@nuaa.edu.cn

Received 12 May 2020; Accepted 16 June 2020; Published 27 September 2020

Guest Editor: Jianxin Li

Copyright © 2020 Tiexin Wang et al. This is an open access article distributed under the Creative Commons Attribution License, which permits unrestricted use, distribution, and reproduction in any medium, provided the original work is properly cited.

Conceptual models are built to depict and analyze complex systems. They are made of concepts and relationships among these concepts. In a particular domain, conceptual models are helpful for different stakeholders to reach a clear and unified view of domain problems. However, the process of building conceptual models is time-consuming, tedious, and expertise required. To improve the efficiency of the building process, this paper proposes a configurable semantic-based (semi-) automatic conceptual model transformation methodology (SbACMT) that tries to reuse existing conceptual models to generate new models. SbACMT contains three parts: (i) a configurable semantic relatedness computing method building on the structured linguistic knowledge base “ConceptNet” (SRCM-CNet), (ii) a specific meta-model, which follows the Ecore standard, defines the rules of applying SRCM-CNet to different conceptual models to automatically detect transformation mappings, and (iii) a multistep matching and transformation process that employs SRCM-CNet. A case study is carried out to detail the working mechanism of SbACMT. Furthermore, through a systematically analysis of this case study, we validate the performance of SbACMT. We prove that SbACMT can support the automatic transformation process of conceptual models (e.g., class diagrams). The scalability of SbACMT can be improved by adapting the meta-model and predefined syntax transformation rules.

1. Introduction

Conceptual models, which are mainly built to represent the static characteristics of a system, can be used to refer to models formed after a conceptualization or generalization process [1]. A conceptual model represents concepts (entities) and relationships between them; it helps different stakeholders reach a clear and unified overview of a particular system or domain being modeled. In artificial intelligence field, a typical usage of conceptual models is to build expert systems and knowledge-based systems.

To achieve different kinds of purposes, several kinds of conceptual models (with modeling languages) have been proposed, such as “class diagrams,” “data flow models,” “entity-relationship models,” and “business process models.” Considering diverse research fields and practical

cases, conceptual modeling theories are defined and relevant modeling tools are employed.

In practice, conceptual models have been built for various purposes, such as simulating groundwater system [1] and improving environmental science curriculum [2]. In the context of computer science, especially in the software engineering field, a typical kind of conceptual models is “class diagrams.”

Class diagrams are built in the requirement analysis phase and being refined in the system design phase; they are defined with the UML (Unified Modeling Language) notations. Based on the object-oriented theories, a class diagram is a complete mapping of the subjects and their relations of a particular domain being analyzed.

Domain-specific conceptual models can be used to generate domain ontologies and knowledge graph (since

ontologies can be regarded as the schema of knowledge graph). The creation of semantic web can also benefit from qualified domain-specific (or domain-cross) conceptual models.

However, conceptual modeling is a time-consuming and iteratively evolve process, which is expertise required. Since conceptual models are useful to help solve complex problems, more and more specific conceptual models (in different domains, with diverse modeling languages and for different purposes) have to be built. Consequently, how to effectively build conceptual models attracts attention from both academics and industrial.

An intuitive idea is to merge/integrate the existing qualified conceptual models to get new ones. To realize this idea, model transformation methods shall be adopted. However, there are three main challenges in adopting model transformation methods to solve this problem:

- (1) Ch1: conceptual models may have different structures and formats. Furthermore, they are defined on different abstract levels. How to deal with the heterogeneous problem?
- (2) Ch2: the semantic content conveyed in conceptual models is complex and may be ambiguous. How to find the same or similarity concepts automatically?
- (3) Ch3: how to ensure and validate the correctness of the model transformation process and the new generated model?

Considering the three challenges, we propose a configurable semantic-based (semi-) automatic conceptual model transformation method (SbACMT). The main contributions of this work are as follows:

- (1) Con1: focusing on generating new class diagrams (a kind of conceptual models), we define a meta-model on a higher abstract level to unify the structure and format (syntax).
- (2) Con2: considering the semantic conveyed in class diagrams, we propose a semantic relatedness computing method to automatically detect potential transformation mappings.
- (3) Con3: we propose an integrated transformation process that combines the meta-model-based transformation theory and the semantic relatedness computing method.

SbACMT is a general-purpose model transformation methodology. It aims at serving to the transformations among different kinds of conceptual models, instead of focusing on two specific kinds of conceptual models.

This paper is organized in 7 sections. Section 2 presents the preliminaries of this work. Section 3 introduces the meta-model defined in SbACMT and illustrates the semantic relatedness computing method "SRCM-CNet." Section 4 details the integrated transformation process. Section 5 shows a case study and evaluates the performance of SbACMT. Section 6 gives the related work, while Section 7 draws a conclusion.

2. Preliminaries

2.1. Model and Model Transformation. Model and model transformation are two pilots of model-driven approaches, such as model-driven engineering (MDE), model-driven architecture (MDA), and model-based testing (MBT). These approaches have been adopted by various domains (e.g., enterprise engineering [3–5] and software engineering [6–8]).

Focusing on a specific viewpoint, a model provides abstractions of a system that allow people to have a better understanding of and to reason about it [9–11].

Models have been divided into different categories. Depending on existing forms, there are mathematical models, graph models, text models, etc. In the context of MDA [12], models are categorized as four abstraction levels: meta-meta-model, meta-model, model, and system (subject). Depending on precision, models are divided into three levels, namely: conceptual models, specification models, and implementation models [13]. Also, in MDA, a similar classification is as follows: computation-independent model (CIM), platform-independent model (PIM), and platform-specific model (PSM).

As another pilot of model-driven approaches, model transformation is a process which contains a sequence of activities operating on models. The aim of model transformation is to generate target models based on source models [14–16].

Two systematic classifications of model transformation methods are given in [17, 18]. According to the content conveyed in models, model transformations can be divided into two groups: model-to-model and model-to-text.

Depending on the abstraction level of source and target models, model transformation can be divided as follows: horizontal transformation (source and target models belong to the same abstraction level, e.g., CIM and CIM) and vertical transformation (e.g., transform CIMs to PIMs).

Model transformation methods are defined by leveraging certain model transformation technologies, such as XSLT [19], VIATRA [20], QVT [21], and ATL [22]. Table 1 illustrates briefly the above four model transformation technologies.

As stated in [22], "a vast number of model transformations are being developed and organized in complex patterns." On the one hand, some model transformation technologies provide a wide range of functions but require certain effort to learn to use them properly. On the other hand, some other transformation technologies are capable to be executed automatically; however, the precondition of applying them is strict and the transformation practices built on them have low reusability.

Besides the above model transformation technologies, some other technologies, such as Kermet (extension of EMOF) [31], MOFM2T (model-to-text) [32], JTL (EMF-based tool) [33], Tefkat (special for MOF models) [34], and MOMENT [35] (model merging), are also being used in practice.

TABLE 1: Model transformation languages and technologies.

Languages	Characteristic	Relevant standards & technologies	Instances	Note
XSLT	Expressed as well-formed XML document; associating patterns with templates	XML, XMI [23]	[27]	Text based, text-to-text
VIATRA2	based on graph transformation techniques	VPM meta-modeling approach [24]	[28]	Graph models
QVT	Meta-models shall be conformed to MOF standards	MOF 2.0 [21]; OCL [25]	[29]	Not well tool supported
ATL	Supported by mature software tools	KM3 [26]	[30]	Requiring manual effort

SbACMT focuses on conceptual model transformation. To serve to different kinds of conceptual models, SbACMT is designed to be configurable. It belongs to the horizontal classification. SbACMT aims at finding automatically the shared and same (similar) or relevant concepts (entities) between different conceptual models.

Considering the model transformation theories, SbACMT is meta-model based and employs semantic relatedness computing method as the detecting technology.

2.2. Semantic Relatedness Computing Methods. Semantic relatedness is a form of measurement that quantitatively identifies the relationship between words or concepts based on the similarity or closeness of their meaning [36].

Semantic relatedness computing methods have been widely adopted. For instance, in natural language processing field, they are used to do semantic information retrieval, keyword extraction, etc.

To develop semantic relatedness computing methods, knowledge resource such as semantic thesaurus (e.g., WordNet and Wikipedia) or corpus (e.g., classics and speech drafts) is needed. Furthermore, depending on different kinds of knowledge resources, various computing methods, such as graph based and information content based, have been proposed.

A systematically classification about the knowledge resources is given in [37]. Figure 1 shows a general idea of this classification.

Comparing with the “web-based” resources, both the “linguistically constructed” and “collaboratively constructed” resources provide more precise and credible content.

Considering the development of semantic relatedness computing methods, the linguistically constructed knowledge resources are commonly used in practice.

As stated in [38], the computing methods can be divided into three groups, namely, “graph based,” “context based,” and “temporal.” Table 2 shows a general illustration of this classification.

Many research works employ WordNet as the semantic thesaurus. However, WordNet is no longer continuously updated and maintained. As an evolved semantic thesaurus, ConceptNet is built partially upon WordNet.

Considering the precision issue, this paper employs ConceptNet as the knowledge resource and adopts a graph-

based computing method to do semantic relatedness computing method to do semantic relatedness computing.

3. Foundations

3.1. SbACMT_MM. A meta-model is a model that defines modeling rules. It is built by leveraging the meta-modeling languages. Currently, three mature meta-modeling languages are as follows: MOF [21], KM3 [26], and Ecore [43].

Ecore is a lightweight version of MOF, and it is well tool supported. Comparing with KM3, Ecore is more widely used. Focusing on the transformation of UML class diagrams, we define a meta-model “SbACMT_MM” conforming to the Ecore standard.

Different kinds of conceptual models have different structures and formats. The structures and formats of conceptual models concern on the syntax aspect, which is easy to handle (comparing to the semantic aspect). The purpose of defining a meta-model is to unify structure and format, which may affect the transformation accuracy, and is to apply the semantic checking rules in a general way. The risk of adjusting syntax transformation rules is lower than adapting semantic checking rules.

As shown in Figure 2, SbACMT_MM contains three packages: class diagram, semantic relatedness, and mapping rule. The “class diagram” package shows the composition of a class diagram in model transformation context. The “semantic relatedness” package defines how to do semantic relatedness computing between a pair of concepts. The “mapping rule” package defines the mechanism of selecting concept mapping pairs based on semantic relatedness computing results.

A class diagram can be defined as a six-tuple.

3.1.1. $CD = \langle Domain, Class, Attribute, Relationship, Type, Object \rangle$. “Domain” represents the problem domain that a class diagram built for; it defines the context of a class diagram. “Class” corresponds to a group of the same or similar objects within a domain. “Attribute” can be regarded as additional information to clearly explain the “Class.” “Relationship” stands for the relations between classes, which has four instances “generalization,” “association,” “aggregation,” and “dependency.” “Attribute” owns “Type,” which stands for a predefined set of types (e.g., integer and string). “Object” stands for the instances of “Class.” The names of

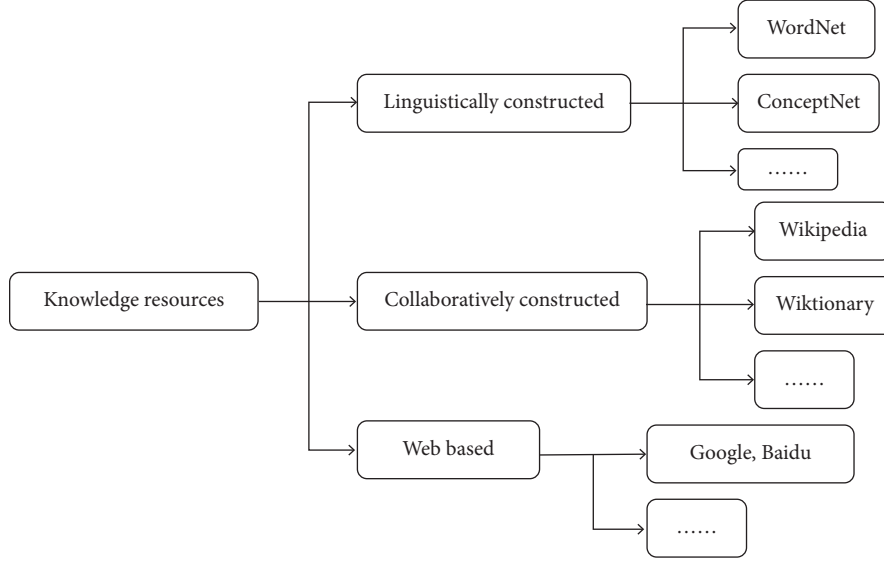


FIGURE 1: Knowledge resource classification (adapted from [37]).

TABLE 2: Semantic relatedness computing method.

Method	Instances	Research work	Note
Graph based	Path based	[37]	Shortest
	Random walk	[38]	Probability
	Co-occurrence based	[39]	WordNet glosses
Context based	Vector based	[40]	WordNet glosses
	Information theoretic	[41]	WordNet
Temporal		[42]	Time series

“Domain,” “Class,” “Attribute,” and “Relationship” correspond to “Concept” defined in the “Semantic Relatedness” package.

In the “Semantic Relatedness” package, there are four core modeling elements defined as a four-tuple.

3.1.2. $SR = \langle \text{Concept}, \text{SemanticRelation}, \text{Type}, \text{CalculationRules} \rangle$. “Concept” relates to the names (attribute) used in “class diagram” package. “Semantic relation” stands for a set of semantic relations (e.g., hyponym and part of) between concepts. Semantic relations are divided into two groups: direct semantic relations and iterative semantic relations. Each of the direct semantic relations has an enumeration type, whereas iterative semantic relations are combinations of the direct semantic relations. A concrete value or a specific computing rule, which is represented as “calculation rules,” is assigned to each of the semantic relations.

In the “mapping rule” package, there are two modeling elements: “MappingPair” and “Threshold.” “MappingPair” stands for all the potential mapping concept pairs, i.e., class-to-class, class-to-attribute, and attribute-to-attribute. For each kind of the mapping pairs, two thresholds (as instances

of “Threshold”) are defined to distinguish potential mapping levels, i.e., acceptable, considerable, and impossible.

3.2. *Semantic Relatedness Computing in SbACMT.* ConceptNet is a semantic network based on information from the OMCS (Open Mind Common Sense) database. It is represented as a directed graph whose nodes are concepts and edges are common sense assertions about these concepts. The concepts represent a closely related set of natural language phrases, e.g., noun phrases, verb phrases, adjective phrases, and clauses.

Currently, the latest version of ConceptNet is 5.7, which contains 304 kinds of languages and maintains 34 kinds of semantic relations among concepts.

Figure 3 is a simple illustration of the structure of ConceptNet. As shown in Figure 3, each arrow indicates a start node and an end node of an edge. In the middle of an edge, the relationship and weight between two nodes are shown. The weight means the credibility of the assertion. Between two nodes (concepts), there may exist several edges (semantic relations).

In the SbACMT context, we select 15 (out of 34) semantic relations from ConceptNet to be used to detect the potential mappings (the same or similar concepts).

As shown in Table 3, a value is assigned to each of the relations.

The selection of these fifteen semantic relations and value assigning are completed through a three-step process. First, we invited seven researchers to vote independently and to choose the relations that they thought are appropriate for judging similar and relevant concepts. The semantic relationships that have no fewer than 4 votes are finally selected. Next, we asked the seven researchers to assign a corresponding value to each of these relations based on their experience. Finally, we carried out tests based on the gold standard “RG-65” [40] to adjust these values.

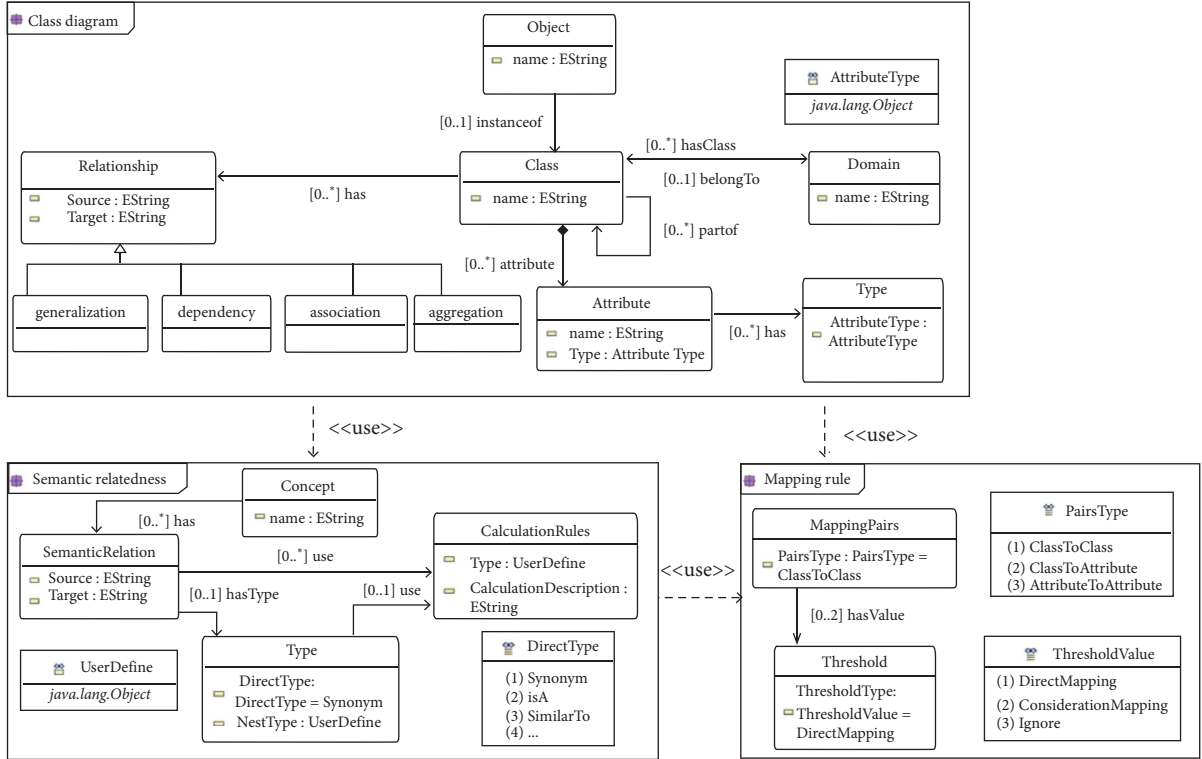


FIGURE 2: A brief illustration of SbACMT_MM.

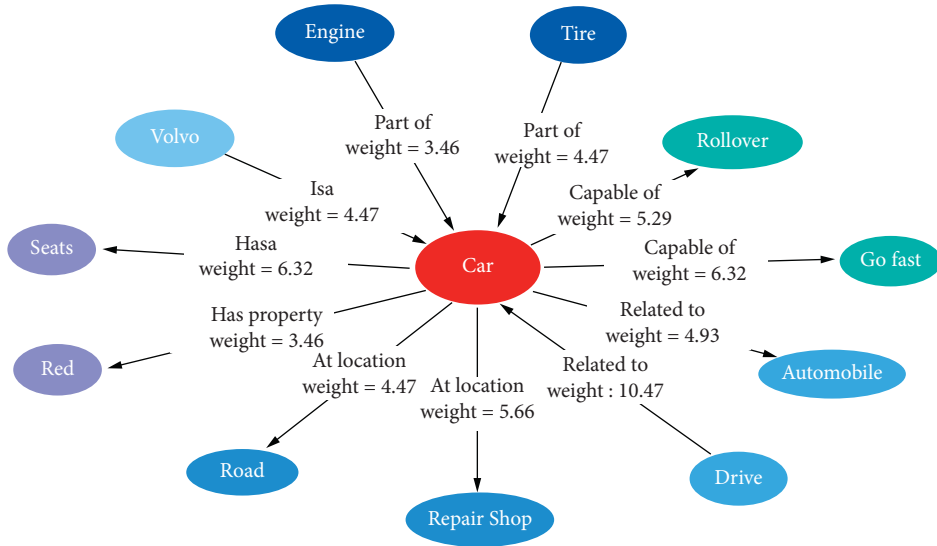


FIGURE 3: A simple illustration of ConceptNet.

For each of the comparing concept pairs, we define two algorithms to compute the semantic relatedness. Algorithm 1 detects if a direct semantic relation exists, whereas Algorithm 2 detects if an iterative semantic relation exists. The pseudocode of the two algorithms is shown as follows.

If a comparing concept pair cannot be located, a lexical analysis function will be executed first. This function aims to transform the input concept (word) to its origin form, and it deals with two main situations: words with delimiters and anagram (e.g., plural and tense).

“SR_V” is short for semantic relatedness value, which is computed between a pair of comparing concepts (string A and string B).

4. Selecting Potential Mapping Pairs

“SR_V” ranges from 0 to 1. Thresholds on “SR_V” are defined to distinguish potential mapping pairs. Table 4 shows three sets of these thresholds.

TABLE 3: The selected semantic relations.

Semantics relation	Sev	Example
Synonym	0.95	Sunlight \longleftrightarrow sunshine
Similar to	0.9	Mixer \longleftrightarrow food processor
Is a	0.7	Car \longrightarrow vehicle
Related to	0.6	Car \longleftrightarrow motor
Defined as	0.6	Peace \longrightarrow absence of war
Distinct from	0.5	Red \longleftrightarrow blue
Derived from	0.45	Pocketbook \longrightarrow book
Part of	0.45	Tire \longrightarrow car
Made of	0.45	Bottle \longrightarrow plastic
Created by	0.45	Tree \longrightarrow fruit
Etymologically related to	0.4	Folkmusiikki \longleftrightarrow folk music
Has a	0.4	Car \longrightarrow seat
Has context	0.4	Astern \longrightarrow ship
At location	0.4	Car \longrightarrow road
Located near	0.4	Table \longleftrightarrow chair

The thresholds are adjusted and assigned through a similar process as the one of the selecting semantic relations from ConceptNet.

For a comparing concept pair, if their SR_V is bigger than “* * -t1,” we assume the two concepts can be matched directly (acceptable). If the SR_V is between “* * -t1” and “* * -t2,” the users or domain experts shall be asked to make the matching judgment (considerable). If the SR_V is less than “* * -t2,” we assume no mapping shall be built. All the considerable mapping pairs will be listed out as potential mapping. Without manual judgments, the potential mappings will be used as transformation rules.

4.1. Matching Process. In SbACMT, model transformation process is divided into two phases: building potential mappings and executing transformations.

Figure 4 illustrates briefly the transformation process. After taking in two models, SbACMT extracts and classifies two groups of “Class” and “Attribute.” The first phase “building potential mappings” contains three main steps: building matching pairs among classes, building matching pairs between classes and attributes, and building matching pairs among attributes. The three steps are executed in sequence. After getting the potential mappings, a manual verification step can be added optionally. Then, the transformation phase, which concerns on those mappings, is to be executed.

4.2. Class-to-Class Mapping Step. The name of a class is regarded as a specific domain concept. A class may own a set of attributes. Classes are connected with each other by relations, which can be regarded as class’s attributes. While comparing two classes, their names are taken into account.

Equation (1) is defined to compute the semantic relatedness between two classes:

$$C2C_SRV_{(i,j)} = SR_V(C_i, C_j). \quad (1)$$

In equation (1), $C2C_SRV_{(i,j)}$ stands for the SR_V between $Class_i$ (C_i) and $Class_j$ (C_j), whereas $Class_i$ comes from

the source conceptual model and $Class_j$ comes from the target conceptual model. $C2C_SRV_{(i,j)}$ equals to $SR_V(C_i, C_j)$, the SR_V between two class names. All the $C2C_SRV_{(i,j)}$ values (calculated automatically) will be compared with thresholds “c2c-t1” and “c2c-t2” to generate potential mappings.

4.3. Class-to-Attribute Mapping Step. After executing the first matching step, some classes may be left unmatched. This step aims to build potential cross-level (granularity) mappings between classes and attributes. Equation (2) is used:

$$C2C_SRV_{(i,j)} = SR_V(C_i, A_j), \text{ or } SR_V(A_k, C_j). \quad (2)$$

Take one class (or attribute) from the source conceptual model and one attribute (or class) from the target conceptual model, and then apply semantic relatedness computing algorithm between their names. $C2C_SRV_{(i,j)}$ stands for the cross-level comparing result between a specific pair of Concept C_i (or C_j) and attribute A_j (or A_i).

4.4. Attribute-to-Attribute Mapping Step. After executing the two former matching steps, some classes and attributes may still be left unmatched. For the unmatched classes, we regard them as specific parts that cannot be transformed or merged. For the unmatched attributes, equation (3) is used to build potential mappings among them:

$$A2A_SRV = SR_V(A_i, A_j). \quad (3)$$

The potential attribute matching pairs are only built between those attributes that belong to the potential matched classes. In equation (3), assuming A_i is an attribute of $Class_n$ (C_n) and A_j is an attribute of $Class_m$ (C_m), the matching algorithm only needs to be executed if there is a potential mapping between C_n and C_m .

4.5. Verification of Potential Mappings. To generate transformation rules, the potential mappings have to be verified. In SbACMT, we propose two ways “verification based on relations” and “manual verification.”

The relations defined in the source conceptual models (class diagrams) are used to verify the automatically generated potential mappings:

- (1) For the relation “generalization/specialization (is a or is a kind of)”, if the father class is matched then all its children classes should be matched to the same class (or its children classes) in the target class diagram.
- (2) For the “aggregation/composition (has a or part of)” relation, the classes owning this relation can be matched to the same class in the target class diagram.
- (3) For the “dependency” and “association” relations, we regard them as “user-defined” type. They are not used as verification measurements.

For instance, if in the source class diagram, two classes C_i and C_n have a generalization relation, and a potential mapping is built between C_i and C_j (from the target class


```

/*initialize corresponding values of semantic relations and values*/
Semantic_Relation_Values = {(synonym, 0.95), (similar, 0.9), ( ), ( ), ...}
/* Algorithm 1 detect direct semantic relations*/
Function detecting direct Semantic Relation (String A, String B){
    int SR_V=0;
    for (int i=0; i < Semantic_Relation_Values.size (); i++){
        if (Semantic_Relation_Value.get (i).get Relation (Concept Net (A, B))){
            if (Semantic_Relation_Value.get (i).get Value ()>SR_V)
                SR_V= Semantic_Relation_Value.get(i).get Value();
        }
    }
    return SR_V;
}

```

ALGORITHM 1: The algorithm of detecting direct semantic relations.

```

/* Algorithm 2 detect iterative semantic relations*/
Function detecting iterative Semantic Relation (String A, String B){
    int temp1, temp2, SR_V=0;
    string [] inter Strings= Concept Net (A);
    for (int i=0; i < inter Strings.size (); i++){
        for(j=0; j < Semantic_Relation_Values.size (); j++){
            if (Semantic_Relation_Value.get (j).get Relation (inter Strings.get (i), B)){
                temp1= Semantic_Relation_Value.get (j).get Value ();
                temp2= Semantic_Relation_Value.get (i).get Value();
                if (temp1*temp2> SR_V)
                    SR_V= temp1*temp2;
            }
        }
    }
    return SR_V;
}

```

ALGORITHM 2: The algorithm of detecting iterative semantic relations.

TABLE 4: Thresholds for judging mapping pairs.

Group	Threshold	Value
Class-to-class	c2c-t1	0.75
	c2c-t2	0.50
Class-to-attribute	c2a-t1	0.70
	c2a-t2	0.50
Attribute-to-attribute	a2a-t1	0.80
	a2a-t2	0.60

diagram), we will verify that if a mapping between C_n and C_j is automatically generated. This verification step is executed automatically.

For the “manual verification,” a visual interface is provided to the users (or experts) to show the automatically generated mappings. These mappings are divided as two groups: “acceptable” and “considerable.” If there is no manual judgment, all these mappings will be used directly as transformation rules.

5. Use Case

5.1. Use Case Illustration. We evaluate the performance of SbACMT with the following use case. In the use case, two

conceptual models (UML class diagrams) “vehicle management” and “traffic management” conforming to Ecore standard are involved. Figure 5 shows the two class diagrams.

The class diagram “vehicle management” contains three classes “person” (with seven attributes), “driving license” (with six attributes) and “vehicle” (with five attributes). The (association) relations between them are as follows: “person” possesses “vehicle” and “driving license.”

The class diagram of “traffic management” contains three classes “automobile” (with four attributes), “ticket” (with five attributes), and “driver” (with four attributes). The relationships are as follows: “ticket” concerns “automobile” and “driver” pays for the “ticket” and drives “automobile.”

SbACMT takes the two class diagrams as inputs and generates the potential mappings (pairs) between them automatically.

5.2. Transforming Process. The first matching step focuses on classes. A compound word (the class name) will be split into single words and then compared with potential target, respectively. For instance “driving license” is split as “driving” and “license”.

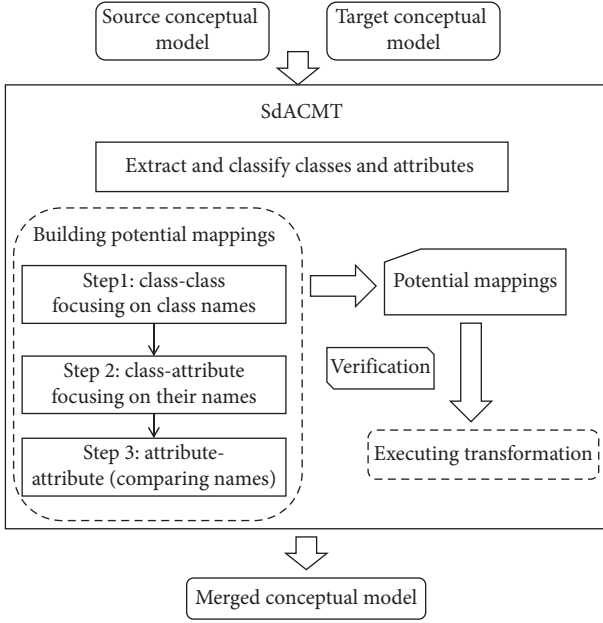


FIGURE 4: An overview of the matching process.

Table 5 shows the computing results. All three classes “person,” “driving license,” and “vehicle” are mapped with classes of the target class diagram. Since no classes left unmatched, the second matching step is skipped.

The third matching step focuses on attributes. In this step, all the attributes belonging to the already matched classes are taken into consideration. Tables 6–9 show the computing results.

6. Evaluation

The evaluation of SbACMT contains two dimensions: (1) focusing on the semantic relatedness computing method (parameters and constraints) and (2) focusing on the correctness of the automatically generated mappings.

6.1. Adjusting SRCM-CNet with Gold Standard RG-65. We use the “RG-65 gold standard” data set to test SRCM-CNet. The testing results are measured with Spearman’s rank correlation coefficient.

As stated in [36], a semantic relatedness computing method is considered reliable if an inter-rater agreement (computing results) of it is over 75%.

Considering Spearman’s rank correlation coefficient, we compare SRCM-CNet with three other semantic relatedness computing methods. Table 10 shows the testing results. SRCM-CNet gets Spearman’s rank correlation coefficient “0.9,” which is better than the other methods.

6.2. Correctness Evaluation. We evaluate the correctness of SbACMT on basis of the use case presented above.

The quantitative evaluation focuses on class-class and attribute-attribute mappings. The retrieved mappings and expected mappings are shown in Tables 11 and 12, respectively.

As shown in Table 12, according to the computing results, the attributes “id” and “name” (both from class “person”) match with the attribute “id” (from class “driver”). However, we only build the mapping between attributes “id” and “id,” since they have a higher SR_V.

Inspired by the work stated in [45], performance measures are based on three indicators: precision, recall, and F-measure:

- (1) The precision (P) evaluates the quality of the automatic built transformation mappings.
- (2) The recall (R) evaluates the sufficiency of the automatic built mappings.
- (3) The F-measure (F) is the weighted harmonic average of P and R. A higher value of F is preferred.

Equation (4) shows the computing rules of “precision,” “recall,” and “F-measure”:

$$P = \frac{|\text{retrieved} \cap \text{expected}|}{|\text{retrieved}|},$$

$$R = \frac{|\text{retrieved} \cap \text{expected}|}{|\text{expected}|}, \quad (4)$$

$$F = \frac{2 \times P \times R}{P + R}.$$

The evaluation results of SbACMT are shown in Figure 6.

The performance evaluation has been performed on a computer with 2.4 GHz, i5-6200U CPU, and 8 G RAM (with Windows 10 OS and Java 9 JDK).

Generally, the precision rate and the recall rate affect each other. Considering the attribute mapping pairs, the quality of the automatic built mappings is high. The precision of automatically built class mappings is mediocre (the number of classes involved in the use case is small).

7. Related Works

This section presents the related works in three aspects: the usage of meta-models in practice, semantic relatedness computing methods adopted in practice, and our previous relevant work [47].

7.1. Meta-Model Usage. Meta-models, which are a special kind of models, define the rules of building models and can be used to verify the correctness of the models conforming to them.

Meta-models have been defined in various domains. In [48], a meta-model is defined to adopt organizational concepts to help analyze and design multiagent systems. In [49], a meta-model, which is made of four smaller meta-models, is defined to formalize software protection from man-at-the-end attacks. In [50], an accident process meta-model is defined to describe the hazard-accident process by fault propagation. In [51], a meta-model is defined to argue about compliance of requirements models and to keep track of compliance decision through the requirement modeling.

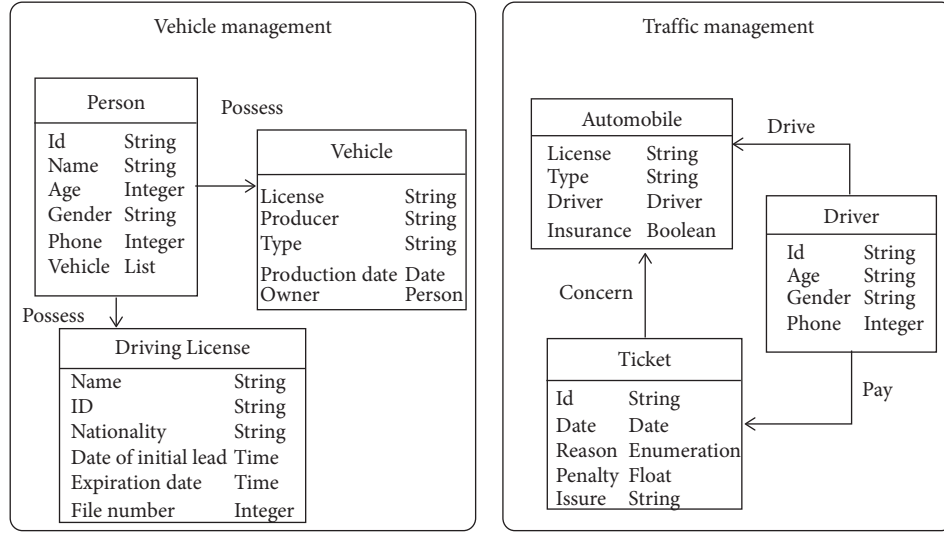


FIGURE 5: An illustration of the use case.

TABLE 5: Matching between concepts.

Vehicle\traffic	Automobile	Driver	Ticket
Person	0.0	0.6	0.36
Vehicle	0.90	0.57	0.57
Driving license	0.6	0.6	0.57

TABLE 6: Matching between attributes, Set 1.

Vehicle\automobile	License	Type	Driver	Insurance
License	1	—	—	—
Producer	0.49	0.2	0	0
Type	0.49	1	—	—
Production date	0.14	0	0.1	0
Owner	0	0	0.49	0

TABLE 7: Matching between attributes, Set 2.

Person\driver	Id	Age	Gender	Phone
Id	1	—	—	—
Name	0.92	—	—	—
Age	0.38	0.8	—	—
Gender	0.2	0.29	1	—
Phone	0	0.18	0	1
Address	0.2	0.29	0.49	0.58
Vehicle	0	0	0	0.23

TABLE 8: Matching between attributes, Set 3.

Driving license\automobile	License	Type	Driver	Insurance
Name	0.49	0.66	0	0.23
Id	0.2	0.66	0	0
Nationality	0	0.42	0	0.36
Date of initial lead	0.36	0.36	0.36	0
Expiration date	0.36	0	0	0
File number	0.36	0.57	0.36	0.36

TABLE 9: Matching between attributes, Set 4.

Driving license\driver	Id	Age	Gender	Phone
Name	0.92	—	—	—
Id	1	—	—	—
Nationality	0	0.42	0.36	0.42
Date of initial lead	0.57	0.6	0.36	0.36
Expiration date	0.36	0	0	0
File number	0.57	0.6	0.36	0.6

TABLE 10: Spearman’s rank correlation coefficient with RG-65.

Relatedness measure	RG-65
SRCM-CNet	0.90
Extended gloss overlaps [44]	0.8
Resnik [45]	0.72
Lin [46]	0.72

In [52], a meta-model is defined to help effectively build interenterprise collaborations.

The majority of current existing meta-models are defined without strict semantics or syntax. They are presented as class-based graphs or activity diagrams, and natural language is used to describe the context and the constraints, etc. Researchers and engineers focus on the content conveyed by meta-models more than meta-modeling theories and languages, which leads to the low reusability and poor readability of these meta-models. Table 13 presents the comparing results of the above meta-models.

We define SbACMT_MM conforming to the Ecore standard, which ensures the unified semantics and syntax. In the “semantic-based conceptual model transformation” context, SbACMT_MM sets the theoretical foundation.

7.2. Semantic-Based Matching Methods. Employing semantic-based analysis to determine similarity between concepts (entities) is a common research topic in various fields, such as ontology matching and data schemas matching. A certain number of semantic relatedness computing theories and methods are proposed.

In [53], semantic analysis is used to lift meta-models into ontologies to integrate eventually modeling languages. In [54], towards data integration, an automatic schema matching method built on probabilistic lexical annotation technique is proposed. In [55], a new semantic matching method is adopted to find the corresponding entities via similarity matrices. In [56], a two-step method built on state-of-the-art methods is proposed to improve ontology matching by enriching ontology mappings.

Table 14 presents the above research works and shows a comparison between them.

To support general-purpose usage, a certain number of semantic reasoners are proposed and are used in practice. In Table 15, five semantic reasoners are listed and analyzed.

Agreement maker uses different matching algorithms to aggregate their matching results, which is usually called parallel combination.

STROMA uses linguistic, structural techniques to deal with ontology matching. It adopts five matching strategies and weights the results. The system is generic as it can be used for different domains.

ASMOV utilizes lexicographic, structural, and instance-based techniques and WordNet. It incorporates a semantic validation process, which increases the accuracy of the system.

S-Match represents the ontology entity as a logical formula; the matching problem is reduced to the proposition validity problem. The input of the S-Match system is two graph structure patterns. The output is the logical relation between the nodes in the graph.

Compared with existing computing methods and semantic reasoners, we adapted ConceptNet as semantic knowledge base (with rich semantic relations and assertions). Furthermore, focusing on conceptual model (class diagrams) transformation, we tailor the semantic relations defined in ConceptNet and quantify the adopted relations with the RG-65 gold standard. The rules of applying SRCM-CNet are defined in SbACMT_MM.

7.3. Relevant Previous Works. Compared with our previous work [47], the main novelty of this paper is reflected in three aspects.

First, it is the new meta-model “SbACMT_MM”. Towards conceptual model transformation, we define this meta-model by employing the Ecore standard. SbACMT_MM consists of three parts “class diagram,” “semantic relatedness,” and “mapping pair”; it builds the foundation of combining SRCM-CNet into automatic model transformation process.

Second, it is the adopted semantic knowledge base. In our previous work, WordNet is adapted as the basic semantic resources. In this paper, we adapted ConceptNet as the semantic knowledge base and built a local semantic thesaurus (with Neo4J) based on it. Comparing to WordNet, ConceptNet contains more content (e.g., words and semantic relations), being constantly updated and supports multilanguages.

Third, it is the evaluation part. In previous work, we evaluated the performance of the automatic generated transformation mappings only based on manual judgments. In this paper, we adopted the RG-65gold standard and Spearman’s rank correlation coefficient, which is more persuasive.

TABLE 11: Mapping built between classes.

Potential entity mappings	Retrieved mappings	Expected mappings
Person-driver	Yes	Yes
Vehicle-automobile	Yes	Yes
Driving license-driver	Yes	No

TABLE 12: Mapping built between attributes.

Potential entity mappings	Retrieved mappings	Expected mappings
Person: id-driver: id	Yes	No
Person: age-driver: age	Yes	Yes
Person: gender-driver: gender	Yes	Yes
Person: phone-driver: phone	Yes	Yes
Vehicle: license-automobile: license	Yes	Yes
Vehicle: type-automobile: type	Yes	Yes
Vehicle: owner-automobile: owner	No	Yes
Driving license: id-driver: id	Yes	No

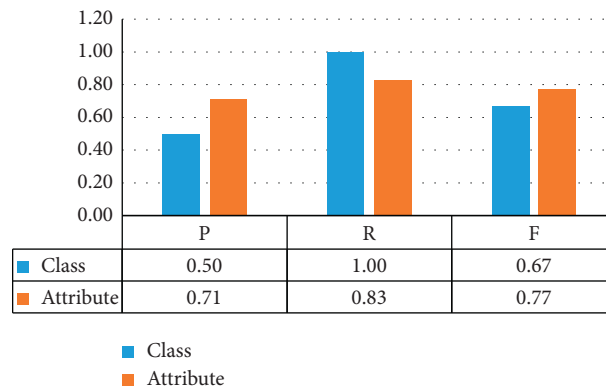


FIGURE 6: “P,” “R,” and “F” evaluation results.

TABLE 13: Meta-models defined in practice.

Ref.	Serving domain	Meta-modeling language adopted	Existing form
[48]	Software engineering	No	Graph & nature and mathematical languages description
[49]	Software protection	No	Class diagram & nature language description
[50]	System engineering	SysML from implementation view	Graphs + natural language description
[51]	Requirements engineering	No	Class-based description
[52]	Enterprise engineering	No	Class-based diagram and natural language description

TABLE 14: Research works concerning semantics.

Ref.	Serving filed	Semantics resource & adopted methods	Note
[53]	Software development	Manual	Ecore to OWL
[54]	Data integration	Word net	Combing lexical annotation
[55]	Ontology matching	Concept net	Syntax & semantic
[56]	Ontology matching	Adopted mature semantic reasoner	Two-step approach

In social network field, as presented in [57–59], semantic checking technologies are also adapted to build connections between entities (e.g., events, persons, and comments).

TABLE 15: Existing semantic reasoners.

Name	Semantic relations	Semantic source	Note
Agreement maker [60]	Is a	WordNet	Hybrid pattern matching system
STROMA [56]	Equal, is a, part of, related	WordNet, UMLS, Open Thesaurus	Two steps (1) initial matching (2) semantic enrichment
ASMOV [61]	Equal, is a	WordNet	One step Linguistic, structural, instance-based techniques
S-Match [62]	Equal, is a, related	WordNet	One step Pattern layer based matching system

8. Conclusion

There are many kinds of conceptual models defined and used in diverse domains. Reusing and merging existing conceptual models to generate new conceptual models are always required in practice.

To accelerate the building process of conceptual models, this paper proposes a general configurable (semi-) automatic conceptual model (class diagrams) transformation method. A semantic relatedness computing method, which is mainly built on the structured knowledge base ConceptNet, is employed as the potential mapping-detecting technology.

SbACMT follows the meta-model based model transform theory. A specific meta-model “SbACMT-MM” defines the rules of applying SRCM-Net to generate mappings between conceptual models. Considering the granularity of conceptual models, we also propose an integrated mapping and transformation process in which three matching steps are divided. User effort can be optionally involved in this process at certain points, such as judging the intermediate potential mapping pairs.

SbACMT is configurable in two aspects. First, by adapting the “class diagram” part of SbACMT-MM, SbACMT can support other kinds (besides class diagrams) of conceptual model transformations. Second, by adapting the thresholds assigned in Table 4, SbACMT can serve for customized transformation. Moreover, the values assigned to semantic relationships can also be adjusted by users.

SbACMT aims to serve to transformations of different kinds of conceptual models. It can accelerate the process of building new conceptual models in general.

SbACMT is well tool supported. As shown with the evaluation of the use case, SbACMT can achieve automatic conceptual model transformation with effective performance. A potential research direction of SbACMT concerns about contextual information. While calculating the semantic relatedness between concept pairs, the contextual information shall be taken into account. Two possible solutions are as follows: making use of the assertions (on the edges) of ConceptNet and combining other semantic resources together with ConceptNet.

Data Availability

The data set RG-65 was used to support the findings of this study.

Conflicts of Interest

The authors declare that they have no conflicts of interest.

Acknowledgments

This work was supported by the “Fundamental Research Funds for the Central Universities (no. 3082018NS2018057).”

References

- [1] D. Haynes, J. Brodie, J. Waterhouse, Z. Bainbridge, D. Bass, and B. Hart, “Assessment of the water quality and ecosystem health of the great barrier reef (Australia): conceptual models,” *Environmental Management*, vol. 40, no. 6, pp. 993–1003, 2007.
- [2] K. P. J. Fortuin, C. S. A. Van Koppen, and R. Leemans, “The value of conceptual models in coping with complexity and interdisciplinarity in environmental sciences education,” *Bioscience*, vol. 61, no. 10, pp. 802–814, 2011.
- [3] D. Chen, G. Doumeingts, and F. Vernadat, “Architectures for enterprise integration and interoperability: past, present and future,” *Computers in Industry*, vol. 59, no. 7, pp. 647–659, 2008.
- [4] K. Kosanke, F. Vernadat, and M. Zelm, “CIMOSA: enterprise engineering and integration,” *Computers in Industry*, vol. 40, no. 2-3, pp. 83–97, 1999.
- [5] F. Benaben, W. Mu, N. Boissel-Dallier et al., “Supporting interoperability of collaborative networks through engineering of a service-based Mediation information system (MISE 2.0),” *Enterprise Information Systems*, vol. 9, no. 5-6, pp. 556–582, 2015.
- [6] T. Yue, L. C. Briand, and Y. Labiche, “Facilitating the transition from use case models to analysis models,” *ACM Transactions on Software Engineering and Methodology*, vol. 22, no. 1, pp. 1–38, 2013.
- [7] F. Rademacher, J. Sorgalla, and S. Sachweh, “Challenges of domain-driven microservice design: a model-driven perspective,” *IEEE Software*, vol. 35, no. 3, pp. 36–43, 2018.
- [8] C. Vögele, A. van Hoorn, E. Schulz, W. Hasselbring, and H. Krcmar, “WESSBAS: extraction of probabilistic workload specifications for load testing and performance prediction—a model-driven approach for session-based application systems,” *Software & Systems Modeling*, vol. 17, no. 2, pp. 443–477, 2018.
- [9] A. W. Brown, “Model driven architecture: principles and practice,” *Software and Systems Modeling*, vol. 3, no. 4, pp. 314–327, 2004.
- [10] T. Kühne, “Matters of (meta-) modeling,” *Software & Systems Modeling*, vol. 5, no. 4, pp. 369–385, 2006.

- [11] J. Bézuvin, "Model driven engineering: an emerging technical space," *International Summer School on Generative and Transformational Techniques in Software Engineering*, pp. 36–64, Springer, Berlin, Germany, 2005.
- [12] S. J. Mellor, K. Scott, A. Uhl et al., *MDA Distilled: Principles of Model-Driven Architecture*, Addison-Wesley Professional, Boston, MA, USA, 2004.
- [13] M. Fowler, K. Scott, and G. Booch, "UML distilled, object oriented series," 1999.
- [14] M. Belaunde, C. Casanave, D. DSouza et al., "MDA guide version 1.0," 2003.
- [15] A. G. Kleppe, J. Warmer, J. B. Warmer et al., *MDA Explained: The Model Driven Architecture: Practice and Promise*, Addison-Wesley Professional, Boston, MA, USA, 2003.
- [16] L. Tratt, "Model transformations and tool integration," *Software & Systems Modeling*, vol. 4, no. 2, pp. 112–122, 2005.
- [17] K. Czarnecki and S. Helsen, "Classification of model transformation approaches," *Proceedings of the 2nd OOPSLA Workshop on Generative Techniques in the Context of the Model Driven Architecture*, vol. 45, no. 3, pp. 1–17, 2003.
- [18] T. Mens and P. Van Gorp, "A taxonomy of model transformation," *Electronic Notes in Theoretical Computer Science*, vol. 152, pp. 125–142, 2006.
- [19] Objects X S L F, "W3C recommendation," 1999.
- [20] D. Varró and A. Balogh, "The model transformation language of the VIATRA2 framework," *Science of Computer Programming*, vol. 68, no. 3, pp. 214–234, 2007.
- [21] Q. V. T. Omg, "Meta object facility (mof) 2.0 query/view/transformation specification," 2008.
- [22] F. Jouault, F. Allilaire, J. Bézuvin et al., "ATL: a model transformation tool," *Science of Computer Programming*, vol. 72, no. 1–2, pp. 31–39, 2008.
- [23] OMG X M L, "Metadata interchange (XMI) specification," version," 2000.
- [24] D. Varró and A. Pataricza, "VPM: a visual, precise and multilevel metamodeling framework for describing mathematical domains and UML (the mathematics of metamodeling is metamodeling mathematics)," *Software & Systems Modeling*, vol. 2, no. 3, pp. 187–210, 2003.
- [25] J. Cabot and M. Gogolla, "Object constraint language (OCL): a definitive guide," *International School on Formal Methods for the Design of Computer, Communication and Software Systems*, pp. 58–90, Springer, Berlin, Germany, 2012.
- [26] F. Jouault and J. Bézuvin, "KM3: a DSL for metamodel specification," *International Conference on Formal Methods for Open Object-Based Distributed Systems*, pp. 171–185, Springer, Berlin, Germany, 2006.
- [27] J. Kovse and T. Härder, "Generic XMI-based UML model transformations," *International Conference on Object-Oriented Information Systems*, pp. 192–198, Springer, Berlin, Germany, 2002.
- [28] D. Varró and A. Pataricza, "Generic and meta-transformations for model transformation engineering," *International Conference on the Unified Modeling Language*, pp. 290–304, Springer, Berlin, Germany, 2004.
- [29] V. De Castro, E. Marcos, and J. M. Vara, "Applying CIM-to-PIM model transformations for the service-oriented development of information systems," *Information and Software Technology*, vol. 53, no. 1, pp. 87–105, 2011.
- [30] M. Tisi, J. Cabot, and F. Jouault, "Improving higher-order transformations support in ATL," *International Conference on Theory and Practice of Model Transformations*, pp. 215–229, Springer, Berlin, Germany, 2010.
- [31] J. M. Jézéquel, O. Barais, and F. Fleurey, "Model driven language engineering with kermeta," *International Summer School on Generative and Transformational Techniques in Software Engineering*, pp. 201–221, Springer, Berlin, Germany, 2009.
- [32] J. Oldevik, T. Neple, R. Grønmo et al., "Toward standardised model to text transformations," *European Conference on Model Driven Architecture-Foundations and Applications*, pp. 239–253, Springer, Berlin, Germany, 2005.
- [33] A. Cicchetti, D. Di Ruscio, R. Eramo et al., "JTL: a bidirectional and change propagating transformation language," *International Conference on Software Language Engineering*, pp. 183–202, Springer, Berlin, Germany, 2010.
- [34] M. Lawley and J. Steel, "Practical declarative model transformation with Tefkat," in *Satellite Events at the MoDELS 2005 Conference, Lecture Notes in Computer Science*, J. M. Bruehl, Ed., Vol. 3844, Springer, Berlin, Germany, 2006.
- [35] A. Boronat, J. Carsí, and I. Ramos, "Exogenous model merging by means of model management operators," *Electronic Communication of the European Association*, vol. 20, 2006.
- [36] Y. Feng, E. Bagheri, F. Ensan et al., "The state of the art in semantic relatedness: a framework for comparison," *The Knowledge Engineering Review*, vol. 32, 2017.
- [37] M. Jarmasz and S. Szpakowicz, "Roget's thesaurus and semantic similarity," in *Proceedings of Conference on Recent Advances in Natural Language Processing (RANLP 2003)*, pp. 212–219, Borovets, Bulgaria, September 2003.
- [38] T. Hughes and D. Ramage, "Lexical semantic relatedness with random graph walks," in *Proceedings of the 2007 joint conference on empirical methods in natural language processing and computational natural language learning (EMNLP-CoNLL)*, pp. 581–589, Prague, Czechia, June 2007.
- [39] R. L. Cilibrasi and P. M. B. Vitanyi, "The google similarity distance," *IEEE Transactions on Knowledge and Data Engineering*, vol. 19, no. 3, pp. 370–383, 2007.
- [40] T. Pedersen, "Duluth: measuring degrees of relational similarity with the gloss vector measure of semantic relatedness," in *Proceedings of the Sixth International Workshop on Semantic Evaluation (SemEval 2012)*, pp. 497–501, Montréal, Canada, June 2012.
- [41] N. Seco, T. Veale, and J. Hayes, "An intrinsic information content metric for semantic similarity in WordNet," in *Proceedings of the European Conference on Artificial Intelligence*, Trento, Italy, August 2004.
- [42] K. Radinsky, E. Agichtein, E. Gabrilovich et al., "A word at a time: computing word relatedness using temporal semantic analysis," in *Proceedings of the 20th international conference on World wide web*, pp. 337–346, Hyderabad, India, April 2011.
- [43] D. Steinberg, F. Budinsky, E. Merks et al., *EMF: Eclipse Modeling Framework*, Pearson Education, London, UK, 2008.
- [44] S. Banerjee and T. Pedersen, "Extended gloss overlaps as a measure of semantic relatedness," in *Proceedings of the International Joint Conferences on Artificial Intelligence*, pp. 805–810, Acapulco, Mexico, August 2003.
- [45] P. Resnik, "Using information content to evaluate semantic similarity in a taxonomy," 1995, <http://arxiv.org/abs/9511007>.
- [46] D. Lin, "An information-theoretic definition of similarity," *International Conference on Machine Learning*, vol. 98, pp. 296–304, 1998.
- [47] T. Wang, S. Truptil, F. Benaben et al., "A meta-model based automatic conceptual model-to-model transformation methodology," in *Proceedings of the 6th International*

- Conference of MODELSWARD*, pp. 586–593, Funchal, Portugal, January 2018.
- [48] J. Ferber and O. Gutknecht, “A meta-model for the analysis and design of organizations in multi-agent systems,” in *Proceedings International Conference on Multi Agent Systems (Cat. No. 98EX160)*, pp. 128–135, IEEE, Paris, France, July 1998.
 - [49] C. Basile, D. Canavese, L. Regano, P. Falcarin, and B. D. Sutter, “A meta-model for software protections and reverse engineering attacks,” *Journal of Systems and Software*, vol. 150, pp. 3–21, 2019.
 - [50] Q. Wei, J. Jiao, S. Zhou et al., “Research on accident process meta-modeling based on SysML,” in *Proceedings of the 2015 First International Conference on Reliability Systems Engineering (ICRSE)*, IEEE, HoChiMinh City, Vietnam, pp. 1–6, October 2015.
 - [51] A. Siena, A. Perini, A. Susi et al., “A meta-model for modelling law-compliant requirements,” in *Proceedings of the 2009 Second International Workshop on Requirements Engineering and Law*, IEEE, Atlanta, GA, USA, pp. 45–51, September 2009.
 - [52] A. Montarnal, W. Mu, F. Benaben, J. Lamothe, M. Luras, and N. Salatge, “Automated deduction of cross-organizational collaborative business processes,” *Information Sciences*, vol. 453, pp. 30–49, 2018.
 - [53] G. Kappel, E. Kapsammer, H. Kargl et al., “Lifting metamodels to ontologies: a step to the semantic integration of modeling languages,” *International Conference on Model Driven Engineering Languages and Systems*, pp. 528–542, Springer, Berlin, Germany, 2006.
 - [54] L. Po and S. Sorrentino, “Automatic generation of probabilistic relationships for improving schema matching,” *Information Systems*, vol. 36, no. 2, pp. 192–208, 2011.
 - [55] M. Keshavarz and Y. H. Lee, “Ontology matching by using ConceptNet,” in *Proceedings of the Asia Pacific Industrial Engineering & Management Systems Conference*, pp. 1917–1925, Phuket, Thailand, December 2012.
 - [56] P. Arnold and E. Rahm, “Enriching ontology mappings with semantic relations,” *Data & Knowledge Engineering*, vol. 93, pp. 1–18, 2014.
 - [57] J. Li, C. Liu, and M. Islam, “Keyword-based correlated network computation over large social media,” in *Proceedings of the 30th IEEE International Conference on Data Engineering (ICDE)*, pp. 268–279, Chicago, IL, USA, April 2014.
 - [58] J. Li, C. Liu, J. X. Yu, Y. Chen, T. Sellis, and J. S. Culpepper, “Personalized influential topic search via social network summarization,” *IEEE Transactions on Knowledge and Data Engineering*, vol. 28, no. 7, pp. 1820–1834, 2016.
 - [59] J. Li, T. Cai, K. Deng et al., “Community-diversified influence maximization in social networks,” *Information Systems*, vol. 92, pp. 1–12, 2020.
 - [60] I. F. Cruz, F. P. Antonelli, and C. Stroe, “Agreement maker,” *Proceedings of the VLDB Endowment*, vol. 2, no. 2, pp. 1586–1589, 2009.
 - [61] Y. Jean-Mary and M. Kabuka, “Asmov: Ontology alignment with semantic validation,” in *Proceedings of the Joint SWDB-ODBS Workshop*, pp. 15–20, Vienna, Austria, September 2007.
 - [62] F. Giunchiglia, P. Shvaiko, and M. Yatskevich, “S-Match: an algorithm and an implementation of semantic matching,” *European Semantic Web Symposium*, pp. 61–75, Springer, Berlin, Germany, 2004.

Research Article

The Influence of Network Structural Preference on Link Prediction

Yongcheng Wang,¹ Yu Wang,¹ Xinye Lin,¹ and Wei Wang^{ID}²

¹National Key Laboratory of Science and Technology on Blind Signal Processing, Chengdu 610041, China

²Cybersecurity Research Institute, Sichuan University, Chengdu 610065, China

Correspondence should be addressed to Wei Wang; wwzqbx@hotmail.com

Received 4 May 2020; Accepted 15 June 2020; Published 26 September 2020

Guest Editor: Chenquan Gan

Copyright © 2020 Yongcheng Wang et al. This is an open access article distributed under the Creative Commons Attribution License, which permits unrestricted use, distribution, and reproduction in any medium, provided the original work is properly cited.

Link prediction in complex networks predicts the possibility of link generation between two nodes that have not been linked yet in the network, based on known network structure and attributes. It can be applied in various fields, such as friend recommendation in social networks and prediction of protein-protein interaction in biology. However, in the social network, link prediction may raise concerns about privacy and security, because, through link prediction algorithms, criminals can predict the friends of an account user and may even further discover private information such as the address and bank accounts. Therefore, it is urgent to develop a strategy to prevent being identified by link prediction algorithms and protect privacy, utilizing perturbation on network structure at a low cost, including changing and adding edges. This article mainly focuses on the influence of network structural preference perturbation through deletion on link prediction. According to a large number of experiments on the various real networks, edges between large-small degree nodes and medium-medium degree nodes have the most significant impact on the quality of link prediction.

1. Introduction

Complex networks play an important role in modeling and analyzing complex systems such as the social system, biological system, and information system [1]. Generally, individuals, such as human beings, biological elements, and computers, are represented by nodes, while links represent the relations or interaction between nodes [2]. The theory of complex networks offers new insight into the connection in the real world. Related research studies focus not only on single-layer networks, such as clustering [3], link prediction [4], and community discovery [5, 6] but also multilayer networks [7] as well, such as cascade [8, 9], communication [10–13], synchronization [14], and game [15–17].

Link prediction in a complex network includes prediction on links unknown or to be built in a given network. Based on the structure and attributes of a public network, link prediction is intended to predict the possibility of link generation between two nodes, which have not been

connected yet [18]. For a given undirected network, as shown in Figure 1, the solid lines signify known edges in the network, while the dotted lines signify the unknown edges or those to be built in the future. What we need to do here is to predict the unknown edges denoted by the dotted lines through known nodes and edges accurately. As one of the research directions of data mining, link prediction can be applied to various fields. For instance, in social networks, link prediction can recommend new friends to users by predicting whether two strangers online are acquaintances offline. In biology, predicting protein-protein interaction will significantly reduce the cost of experiments. Besides, researchers have applied the idea and method of link prediction on node classification, such as determining the type of an article in an academic network [19].

Researchers have made considerable efforts to enhance the accuracy of link prediction. Many link prediction algorithms are based on the similarity between nodes, assuming that the more similar two nodes are, the more likely

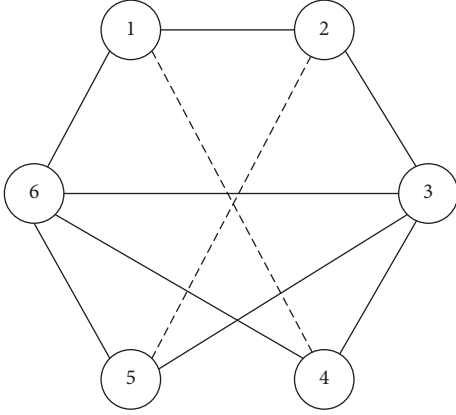


FIGURE 1: Diagram of link prediction.

that there is a link between them. The index describing the similarity between nodes can be roughly classified into the local index, global index, and quasi-local index. The local index is the most commonly used among the methods based on node similarity, due to its simplicity and adaptability for considerably large networks. There are other link prediction algorithms which could be based on maximum likelihood estimation, and they have better performance when dealing with networks with a distinct hierarchical structure, such as a grassland food chain [20]. Some algorithms may also employ probabilistic models for link prediction, during which information processed covers not only the network structure but also the attributes of nodes. These algorithms are characterized by higher prediction accuracy but, at the same time, greater calculation complexity [21].

Link prediction is usually proven useful in biological networks. In social networks, however, they may raise concerns about privacy and security, in that our data are valuable not only for enterprises and public entities but also for an increasing number of cybercriminals conducting network analysis for malicious purposes. Through the link prediction algorithm, cybercriminals can accurately predict the friends of a social account user and even the owner of that account according to his or her relationships. If they dig further, criminals may find the name, age, address, bank account, and other private information of a social account's corresponding entity.

Considering what has been mentioned above, it is urgent to improve privacy protection. However, currently, there lacks intensive research on how to prevent identification of link prediction algorithms utilizing concealing, changing, or adding edges through network structural disturbance at a small cost. Based on the perturbation of the adjacency matrix, Lu et al. [22] studied the influence of structural consistency on link predictability. Waniek et al. [23] studied how to conceal sensitive relations in the network through reconnection strategy, proposing a heuristic method in achieving it. Wu et al. [24] proposed an active learning algorithm and applied perturbation on the most symbolic links in the network, to adjust the structure predictability of the graph.

Based on the previous research, this article focuses on the influence of network structural preference disturbance

through deletion on link prediction. According to a large number of experiments on the various real networks, edges between large-small degree nodes and medium-medium degree nodes have the most significant impact on the performance of link prediction. In the real-world network, the connection choice between nodes is not uniform, but there is an obvious preference, which leads to a certain correlation between nodes in the network. Based on this connection correlation between nodes, people put forward the concept of homogeneity and heterogeneity to distinguish the connection preference between nodes. Therefore, the heterogeneity of complex network nodes is a measure of the uniform distribution of nodes. If the nodes tend to connect similar nodes, they will form homogeneous network; if the high nodes and low nodes have certain probability to connect, they will form heterogeneous network.

2. Model Demonstration

In this section, some basic terminologies used in this article will be first introduced, based on which official definitions will be made. Then, we will present the method of network structural preference perturbation. Finally, the pseudocode of this method will be given.

2.1. Definition. A complex network: a given biological or social network can be modeled as a graph, $G = (V, E)$, in which V denotes the set of nodes in the network, E denotes the set of edges, and A denotes the adjacent matrix of the network. When there is a link $(i, j) \in E$ between node v_i and v_j , the elements from matrix A satisfy $e_{ij} = 1$; otherwise, they satisfy $e_{ij} = 0$. We can use source and target to describe the relationship between nodes, thus dividing networks into directed and undirected networks. In directed networks, the link, by the name of arc, is built from a source node to a target node. In undirected networks, there is no distinction between source nodes and target nodes in a link, by the name of edge. This article will mainly focus on undirected networks, which can be further applied to directed networks conveniently.

Link prediction: in a given network $G = (V, E)$, N denotes the number of nodes and M denotes the number of edges. Therefore, the total number of node pairs is $((N(N-1))/2)$. If the universal set U denotes the set of all pairs of nodes in a network, link prediction works as follows: any pair of nodes, denoted by $(v_i, v_j) \in (U - E)$, which does not belong to the network, will be assigned a particular score through a certain kind of algorithm. Then, based on scores assigned to the pairs of nodes, the largest K pairs will be chosen as edges for prediction.

Network structural preference perturbation: in a given network $G = (V, E)$, network structural preference perturbation aims at executing one or more operations among adding, changing, and deleting towards the edges of a network at a lower cost based on the set of edges E . The aim of these operations is that when a new network $G^* = (V, E^*)$ is formed eventually, the edges lost or to be built in G are

barely predictable through the operations demonstrated above.

2.2. Method of Perturbation. The method of network structural preference perturbation mainly consists of one or more operations among adding, changing, and deleting towards the edges of a network. This article will focus on deletion, trying to identify the particular quality of edges that are significant in influencing the effect of link prediction. For a given network $G = (V, E)$, the set of edges E can be divided into a train set E^T and test set E^P . The network structural preference perturbation mainly happens in train sets. After the perturbation, edge prediction can be made in the training network through an algorithm of link prediction. The performance of link prediction can thus be calculated by comparing the edges predicted and those in the test set. The given network in the following passages refers to a training network.

When a training network has been divided from the original one, we start to apply perturbation on it. For any edge denoted by e_{ij} , its deletion value can be calculated through the following formula:

$$w_{ij} = \frac{e_{ij} \cdot (k_i \cdot k_j)^\alpha}{\sum_{a=1}^{|V|} \sum_{b=1}^{|V|} e_{ab} \cdot (k_a \cdot k_b)^\alpha}. \quad (1)$$

In this formula, k_i and k_j denote, respectively, the degree of node v_i and v_j . α is used to control the preference of edge selection. When α is specified as a specific value, the weight of each edge selected will be calculated. For example, when α is slightly greater than 0, the connection between large and small nodes and medium and medium nodes has a larger weight, which means it is easier to be selected. α is an adjustable parameter. Formula (1) makes sure that the sum of deletion value of all the edges equals 1.

After acquiring the deletion value of every edge, we set up a parameter of proportion f , in order to randomly pick out edges by the number of $f \cdot |E^T|$ and delete them. It is noteworthy that the degree of some nodes in the edge may change after the edge has been deleted, and hence, the deletion value of every node, w_{ij} , will be changed. In an ideal situation, the deletion value of the remaining edges should be recalculated every time an edge is deleted. However, the time complexity of the perturbation algorithm would be enormous in this way. To reduce time complexity, a parameter of the proportional interval is set by the name of f_{interval} , meaning that the calculation of deletion value is only redone after every $f_{\text{interval}} \cdot |E^T|$ edges are deleted.

The pseudocode of the proposed method is as follows. (see Algorithm 1).

3. Experiment

3.1. Experimental Setup. We have experimented on four real networks, whose statistics are shown in Table 1. During the experiment, four algorithms of link prediction are used, including RA [29], AA [30], CN [31], and PA [32]. For a random given node v_i , with $\Gamma(i)$ denoting the set of its

adjacent nodes, the calculation formula of the four algorithms can be expressed as follows:

Resource allocation (RA) is

$$s_{ij}^{\text{RA}} = \sum_{z \in \Gamma(i) \cap \Gamma(j)} \frac{1}{\log k_z}. \quad (2)$$

Adamic-Adar (AA) index is

$$s_{ij}^{\text{AA}} = \sum_{z \in \Gamma(i) \cap \Gamma(j)} \frac{1}{k_z}. \quad (3)$$

Common neighbor (CN) is

$$s_{ij}^{\text{CN}} = |\Gamma(i) \cap \Gamma(j)|. \quad (4)$$

Preferential attachment (PA) is

$$s_{ij}^{\text{PA}} = |k_i \cdot k_j|. \quad (5)$$

We here choose precision as the index of the performance of link prediction. For a given group of edges that has not been observed, precision is defined as the ratio of successfully predicted edges to the top L predicted edges. Suppose that L_r is the number of successfully predicted edges among the top L predicted edges; then, the calculation formula for precision can be expressed as follows:

$$\text{precision} = \frac{L_r}{L}. \quad (6)$$

For a given network, the train set and test set will be divided by the ratio of 9: 1. In order to test the performance of prediction, perturbation will be applied on the train set under different α and f . Then, predictions will be made through the four algorithms of link prediction, and the result will be compared with the test set. Every experiment will be repeated 100 times.

3.2. Experiment Result. First, the experiment supposes that f equals 0.01, 0.1, 0.2, 0.3, and 0.4, respectively, and $f_{\text{interval}} = 0.01$. The precision calculated through four algorithms on four data sets will be tested, under the condition that α ranges from -20 to 20 , with an interval of 1. As shown in Figure 2, the result indicates that when α is slightly larger than 0, the minimum value of precision is achieved, signifying the best effect of network perturbation. The result shown in the cases (a), (e), and (i) from Figure 3 suggests that edges between large-small degree nodes and medium-medium degree nodes have the largest influence on the performance of link prediction.

Then, α is set to be -20 , -10 , 0 , 10 , and 20 , respectively, and $f_{\text{interval}} = 0.01$. The precision calculated through four algorithms on four data sets will be tested under the condition that f ranges from 0.01 to 0.4, with an interval of 0.01. As shown in Figure 4, in most cases, the precision decreases as f increases for all four methods of the algorithm. Because the larger the f is, the larger the ratio of deleted edges will be, and the fewer edges are remained in the network, thus reducing the quality of prediction of the different algorithms of link prediction. However, there are cases in metabolic and

```

(1) Input: adjacent matrix of the original network  $A$ , parameter  $f$ , parameter  $f_{\text{interval}}$ , and parameter  $\alpha$ 
(2) for  $i = 1; i \leq (f/f_{\text{interval}}); i++$  do
(3)    $A = \text{DELETE-EDGE}(A, f_{\text{interval}}, \alpha)$ 
(4) end for
(5) function  $\text{DELETE-EDGE}(A, f_{\text{interval}}, \alpha)$ 
(6)    $|E| = \text{sum}(\text{sum}(A))$ ;
(7)   Initialize the value matrix:  $W \leftarrow 0$ ;
(8)   for  $i = 1; i \leq \text{size}(A); i++$  do
(9)     for  $j = 1; j \leq \text{size}(A); j++$  do
(10)      Calculate the value of each element  $w_{ij}$  in  $W$  using formula (1);
(11)    end for
(12)  end for
(13)  for  $k = 1; k \leq f_{\text{interval}} * |E|; k++$  do
(14)    Randomly choose a position  $(i, j)$  based on the value matrix  $W$ ;
(15)     $A_{ij} = 0$ 
(16)  end for
(17)  return  $A$ ;
(18) end function
(19) Output: the adjacent matrix after the perturbation  $A^* = A$  has been applied

```

ALGORITHM 1: Perturbation algorithm.

TABLE 1: Statistical features of four real networks, including the number nodes $|V|$, the number of edges $|E|$, average degree $\langle k \rangle$, average shortest path $\langle d \rangle$, clustering coefficient C [28], assortativity coefficient r [33], and heterogeneity of node degree H ($H = (\langle k^2 \rangle / \langle k \rangle^2)$).

Networks	$ V $	$ E $	$\langle k \rangle$	$\langle d \rangle$	C	r	H
Jazz [25]	198	2,742	27.697	2.235	0.618	0.020	1.396
Macaques [26]	62	1,187	38.290	1.380	0.667	-0.073	1.039
Metabolic [27]	453	2,025	8.940	2.664	0.647	-0.226	4.485
Neural [28]	297	2,148	14.465	2.455	0.292	-0.163	1.801

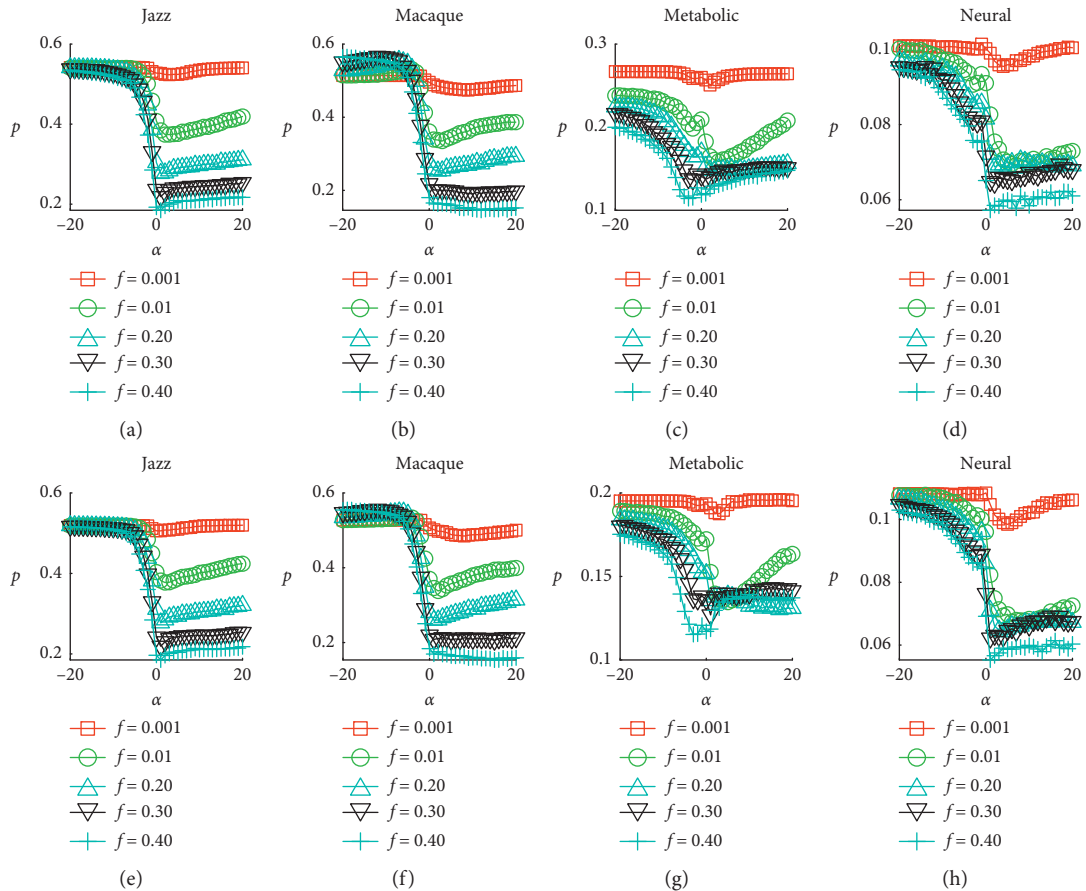


FIGURE 2: Continued.

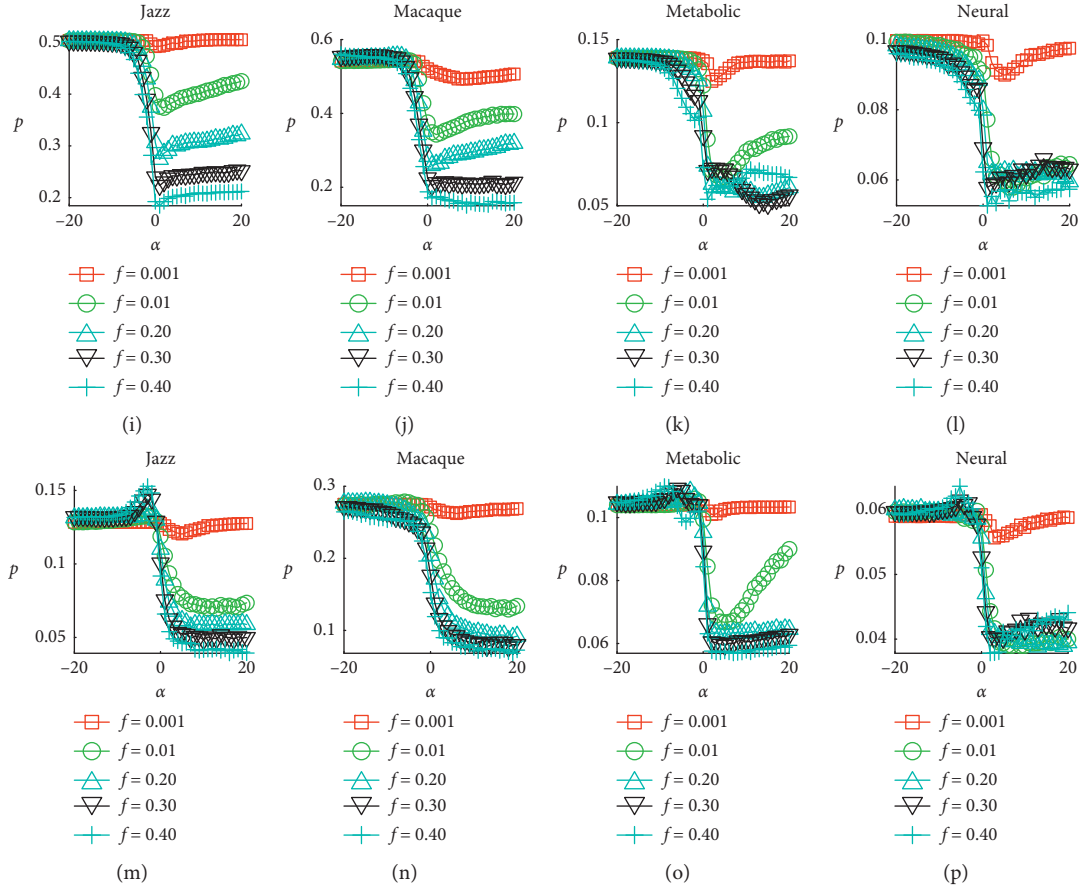


FIGURE 2: Precision under different α . From the top to bottom, results are shown through four methods of RA, AA, CN, and PA. From left to right, results are shown from four networks of jazz, macaque, metabolic, and neural.

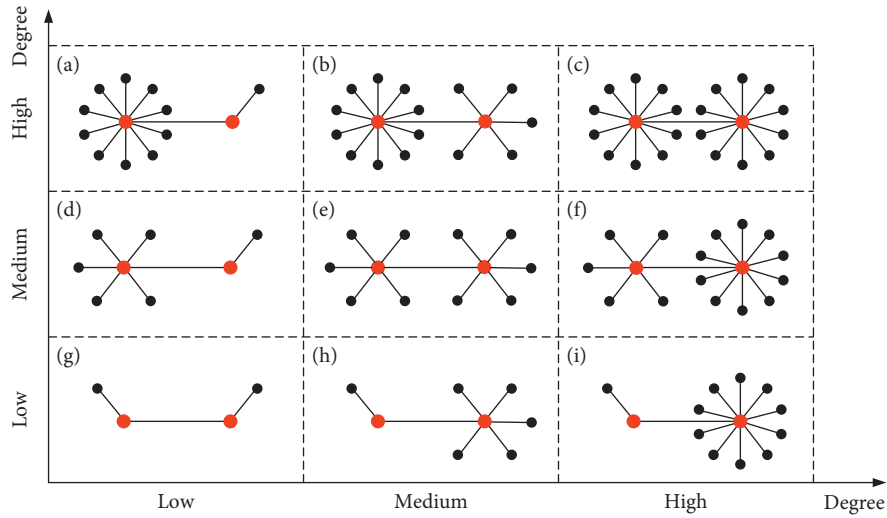


FIGURE 3: Analysis of the reason why perturbation effect reaches its peak when α is slightly larger than 0. (a) Connection of large-small degree nodes; (b) connection of large-medium degree nodes; (c) connection of large-large degree nodes; (d) connection of medium-small degree nodes; (e) connection of medium-medium degree nodes; (f) connection of medium-large degree nodes; (g) connection of small-small degree nodes; (h) connection of small-medium degree nodes; (i) connection of small-large degree nodes.

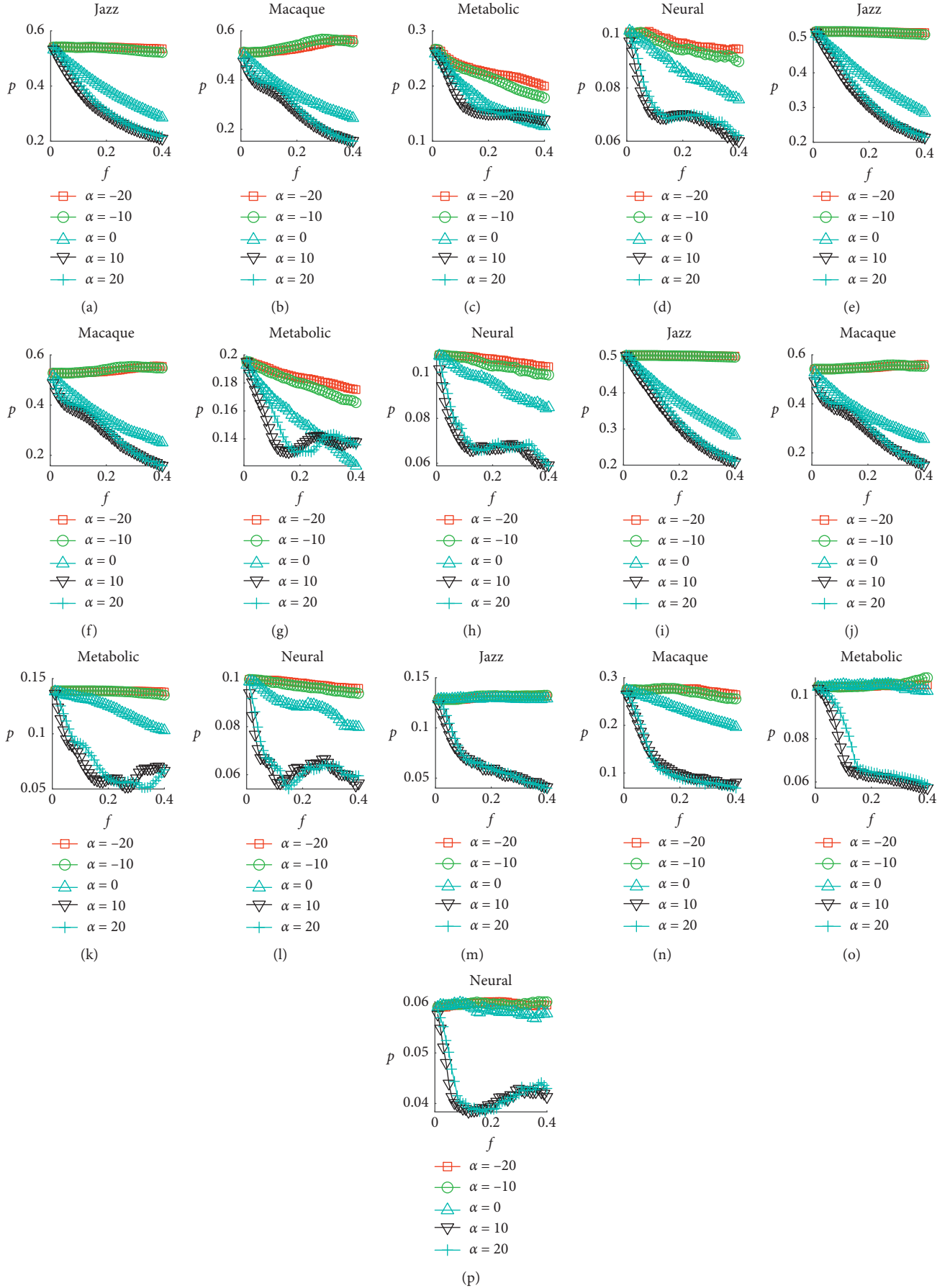


FIGURE 4: Precision under the condition of various f . From the top to bottom, results are shown through four methods of RA, AA, CN, and PA. From left to right, results are shown from four networks of jazz, macaque, metabolic, and neural.

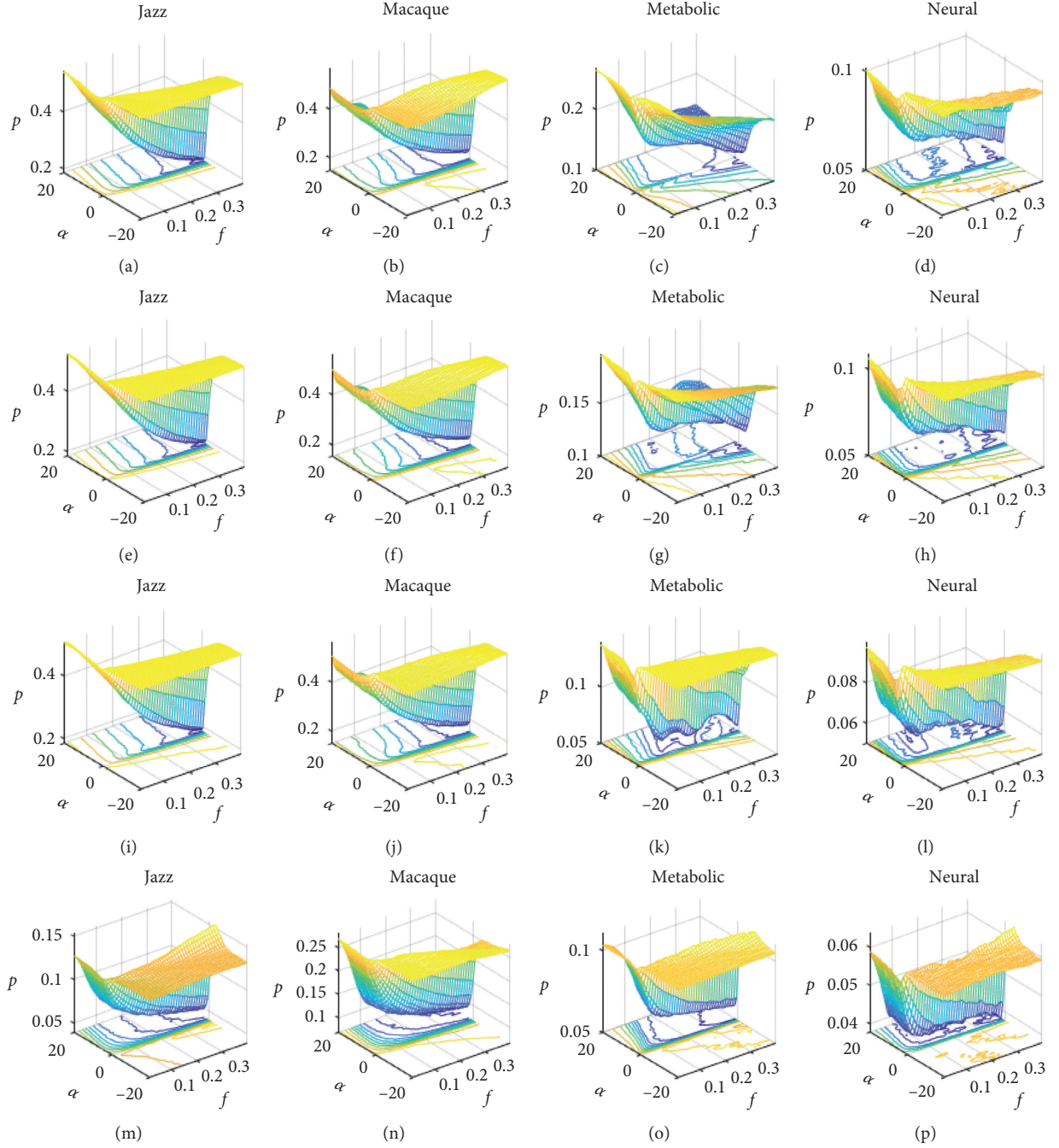


FIGURE 5: Precision under the condition of various α and f . From the top to bottom, results are shown through four methods of RA, AA, CN, and PA. From left to right, results are shown from four networks of jazz, macaque, metabolic, and neural. Curves in the horizontal planes are isolines.

neural networks where precision increases as f increases, which could result from the fact that metabolic and neural networks have higher heterogeneity of node degree.

In order to better demonstrate the influence network structural preference perturbation has on link prediction, we have also tested the precision calculated through four algorithms on four data sets, under the condition that α ranges from -20 to 20 , with an interval of 1 , f ranges from 0.01 to 0.4 , with an interval of 0.01 , and $f_{\text{interval}} = 0.01$. The

experimental results are shown in Figure 5, where curves in the horizontal planes are isolated.

4. Conclusion

In this article, the influence of network structural preference perturbation by a deletion on link prediction is analyzed. By using an interactive criterion to determine node degree, we first assign a perturbation value through the calculation to

every edge in a given network. Then, we apply perturbation through deletion on edges selected according to perturbation value. This procedure will be repeated until a certain proportion of edges have experienced perturbation. After that, we make link prediction on networks before and after perturbation, using four methods including RA, AA, CN, and PA, compared to the different influence types of connection and the ratio of deletion has on the performance of link prediction.

Massive experiments on various real networks indicate that the edges between large-small degree nodes and those between medium-medium degree nodes have the most significant influence on the performance of link prediction. By deleting the specific link in the network, we can resist the impact of link prediction on privacy protection. The above strategies can not only protect privacy in the field of social networks but also be worth promoting and applying in other fields. For example, in the design of computer communication topology, to minimize the connection between large and small nodes, medium and medium nodes can resist topology estimation, so as to better protect our own network; in the field of counter-terrorism, we should pay more attention to the connection between the leader node and leaf node, which often means the vulnerability of the terrorist team in communication connection.

Data Availability

The data can be obtained upon request to the corresponding author.

Conflicts of Interest

The authors declare that they have no conflicts of interest.

Acknowledgments

This work was partially supported by the National Natural Science Foundation of China (Grant no. 61903266), China Postdoctoral Science Foundation (Grant no. 2018M631073), China Postdoctoral Science Special Foundation (Grant no. 2019T120829), Fundamental Research Funds for the Central Universities, and Sichuan Science and Technology Program (No. 20YYJC4001).

References

- [1] R. Albert and A.-L. Barabási, "Statistical mechanics of complex networks," *Reviews of Modern Physics*, vol. 74, no. 1, pp. 47–97, 2002.
- [2] M. Newman, *Networks: An Introduction*, Oxford University Press, New York, NY, USA, 2010.
- [3] X. Han, L. Wang, C. Cui, J. Ma, and S. Zhang, "Linking multiple online identities in criminal investigations: a spectral co-clustering framework," *IEEE Transactions on Information Forensics and Security*, vol. 12, no. 9, pp. 2242–2255, 2017.
- [4] K. Chi, G. Yin, Y. Dong, and H. Dong, "Link prediction in dynamic networks based on the attraction force between nodes," *Knowledge-Based Systems*, vol. 181, 2019.
- [5] G. Yin, K. Chi, Y. Dong, and H. Dong, "An approach of community evolution based on gravitational relationship refactoring in dynamic networks," *Physics Letters A*, vol. 381, no. 16, pp. 1349–1355, 2017.
- [6] Z. Zhao, C. Li, X. Zhang, F. Chiclana, and E. H. Viedma, "An incremental method to detect communities in dynamic evolving social networks," *Knowledge-Based Systems*, vol. 163, pp. 404–415, 2019.
- [7] R. Tang, S. Jiang, X. Chen, H. Wang, W. Wang, and W. Wang, "Interlayer link prediction in multiplex social networks: an iterative degree penalty algorithm," *Knowledge-Based Systems*, vol. 194, p. 105598, 2020.
- [8] J. Gao, S. V. Buldyrev, H. E. Stanley, and S. Havlin, "Networks formed from interdependent networks," *Nature Physics*, vol. 8, no. 1, pp. 40–48, 2011.
- [9] J. Gao, S. V. Buldyrev, S. Havlin, and H. E. Stanley, "Robustness of a network of networks," *Physical Review Letters*, vol. 107, no. 19, 2011.
- [10] C. Granell, S. Gómez, and A. Arenas, "Dynamical interplay between awareness and epidemic spreading in multiplex networks," *Physical Review Letters*, vol. 111, no. 12, p. 128701, 2013.
- [11] W. Wang, M. Tang, H. Yang, Y. Younghae Do, Y.-C. Lai, and G. Lee, "Asymmetrically interacting spreading dynamics on complex layered networks," *Scientific Reports*, vol. 4, no. 1, p. 5097, 2014.
- [12] W. Wang, Q.-H. Liu, S.-M. Cai, M. Tang, L. A. Braunstein, and H. E. Stanley, "Suppressing disease spreading by using information diffusion on multiplex networks," *Scientific Reports*, vol. 6, no. 1, Article ID 29259, 2016.
- [13] W. Wang, Q.-H. Liu, J. Liang, Y. Hu, and T. Zhou, "Co-evolution spreading in complex networks," Ithaca, NY, USA, Physics Reports.
- [14] X. Zhang, S. Boccaletti, S. Guan, and Z. Liu, "Explosive synchronization in adaptive and multilayer networks," *Physical Review Letters*, vol. 114, no. 3, Article ID 038701, 2015.
- [15] Z. Wang, A. Szolnoki, and M. Perc, "Optimal interdependence between networks for the evolution of cooperation," *Scientific Reports*, vol. 3, no. 1, p. 2470, 2013.
- [16] Z. Wang, A. Szolnoki, and M. Perc, "Interdependent network reciprocity in evolutionary games," *Scientific Reports*, vol. 3, p. 1183, 2013.
- [17] Z. Wang, A. Szolnoki, and M. Perc, "Self-organization towards optimally interdependent networks by means of co-evolution," *New Journal of Physics*, vol. 16, no. 3, Article ID 033041, 2014.
- [18] vol. 39, no. 5, pp. 651–661, 2010.
- [19] B. Gallagher, H. Tong, T. Eliassi-Rad, and C. Faloutsos, "Using ghost edges for classification in sparsely labeled networks," in *Proceedings of the 14th ACM SIGKDD International Conference on Knowledge Discovery and Data Mining*, pp. 256–264, Las Vegas, NEV, USA, August 2008.
- [20] A. Clauset, C. Moore, and M. E. J. Newman, "Hierarchical structure and the prediction of missing links in networks," *Nature*, vol. 453, no. 7191, pp. 98–101, 2008.
- [21] B. Taskar, M.-F. Wong, P. Abbeel, and D. Koller, "Link prediction in relational data," *Advances in Neural Information Processing Systems*, pp. 659–666, 2004.
- [22] L. Lü, T. Zhou, Y.-C. Zhang, and H. E. Stanley, "Toward link predictability of complex networks," *Proceedings of the National Academy of Sciences*, vol. 112, no. 8, pp. 2325–2330, 2015.
- [23] M. Waniek, K. Zhou, Y. Vorobeychik, E. Moro, T. P. Michalak, and T. Rahwan, "How to hide ones relationships from link

- prediction algorithms,” *Scientific Reports*, vol. 9, no. 1, pp. 1–10, 2019.
- [24] T. Wu, G. Ming, X. Xian, W. Wang, S. Qiao, and G. Xu, “Structural predictability optimization against inference attacks in data publishing,” *IEEE Access*, vol. 7, pp. 92119–92136, 2019.
 - [25] P. M. Gleiser and L. Danon, “Community structure in jazz,” *Advances in Complex Systems*, vol. 06, no. 4, pp. 565–573, 2003.
 - [26] Y. Takahata, *Diachronic Changes in the Dominance Relations of Adult Female Japanese Monkeys of the Arashiyama B Group, the Monkeys of Arashiyama*, pp. 123–139, State University of New York Press, New York, NY, USA, 1991.
 - [27] J. Duch and A. Arenas, “Community detection in complex networks using extremal optimization,” *Physical Review E*, vol. 72, no. 2, Article ID 027104, 2005.
 - [28] D. J. Watts and S. H. Strogatz, “Collective dynamics of “small-world” networks,” *Nature*, vol. 393, no. 6684, pp. 440–442, 1998.
 - [29] Q. Ou, Y.-D. Jin, T. Zhou, B.-H. Wang, and B.-Q. Yin, “Power-law strength-degree correlation from resource-allocation dynamics on weighted networks,” *Physical Review E*, vol. 75, no. 2, Article ID 021102, 2007.
 - [30] L. A. Adamic and E. Adar, “Friends and neighbors on the web,” *Social Networks*, vol. 25, no. 3, pp. 211–230, 2003.
 - [31] M. E. Newman, “Clustering and preferential attachment in growing networks,” *Physical Review E*, vol. 64, no. 2, Article ID 025102, 2001.
 - [32] L. Lü and L. Lü, “Link prediction in complex networks: a survey,” *Physica A: Statistical Mechanics and Its Applications*, vol. 390, no. 6, pp. 1150–1170, 2011.
 - [33] M. E. Newman, “Assortative mixing in networks,” *Physical Review Letters*, vol. 89, no. 20, Article ID 208701, 2002.

Research Article

Influence of Student Depression on the Spread of Public Opinion in University

Nie Min, Yang Lei, Luo Weimin, Guowu Yang, and Hu Xia 

Big Data Research Center, University of Electronic Science and Technology of China, Chengdu 610054, China

Correspondence should be addressed to Hu Xia; xiahu@uestc.edu.cn

Received 2 June 2020; Revised 29 June 2020; Accepted 6 July 2020; Published 23 September 2020

Guest Editor: Qingyi Zhu

Copyright © 2020 Nie Min et al. This is an open access article distributed under the Creative Commons Attribution License, which permits unrestricted use, distribution, and reproduction in any medium, provided the original work is properly cited.

In this study, we examined the impact of college students' mental health on their social behavior. A social network was identified based on the behavior of college students sharing a meal. We analyzed the impact of depression on the structure of this network and found that students without obvious depressive symptoms, based on the test data of the SCL-90 Assessment Scale, were better at socializing than students with obvious depressive symptoms. We proposed a public opinion spreading model on social networks and formulated a heterogeneous mean-field theory to describe it. Further, using computer simulation experiments, we studied the impact of students' mental health on the process of information propagation in college. The results of the experiments showed that students without obvious depressive symptoms were more likely to receive information than students with obvious depressive symptoms. Based on the results of our study, college psychological consultants can actively identify students who may be at risk of mental illness and give them attention and guidance.

1. Introduction

In the present self-media era, people can communicate online with friends through various platforms such as WeChat, QQ, Weibo, and BBS [1–4]. College students are interested in novelty and are the main users of various social platforms. On the one hand, students can communicate through these platforms to improve their studies. On the other hand, various views and opinions held by disgruntled members of colleges and universities also pass through these social platforms as public opinion and have a significantly negative impact on students. Therefore, understanding the principles and mechanisms of public opinion dissemination in colleges and universities has become a focus of intensive research study. The core of these studies lay in analyzing information dissemination on social networks [5–12].

Structurally, online social networks often have characteristics such as small-world and scale-free properties and high clustering coefficient [13–17]. These characteristics have a strong influence on the information propagation process, propagation range, and burst threshold [18–23]. Watts [24], a well-known network science scholar, analyzed

the spread of news stories, videos, and pictures on Twitter and found that the propagation process showed a substantial structural diversity; “hot” events, which spread quickly over the social network, often have both viral propagation and broadcast characteristics. Lu and Zhou [4] found that it was easier to spread information on high-cluster coefficient networks. For high-risk information (such as political information), single dissemination cannot eliminate the risks and uncertainties caused by the dissemination of the information; multiple confirmations become particularly important [25, 26]. Zheng et al. [27] proposed complex propagation dynamics based on multiple confirmations to characterize the information propagation process in social networks. It was found that the smaller the average, the higher the difference in the spread of information on regular and random networks. Because of the limited risk of redundant information to eliminate the propagation [28], Wu et al. [29–31] further analyzed information propagation on multilayered social networks based on the theory of edge division [32]. During the dissemination process, it was found that the multilayer network structure is comparatively more conducive to information dissemination. Shu et al. [33]

found that the interlayer network structure is particularly crucial to information spread.

In the dissemination of public opinion in colleges and universities, different students have different roles. For example, students who frequent the library may have short online communication times. By contrast, students who live in dormitories may have an extended online learning and communication time, which leads to differences in the influence of different student attributes on colleges' public opinion communication attributes. In this study, we constructed a public opinion spreading model to determine whether students with apparent symptoms of depression influence the spread of public opinion in colleges and universities.

2. Data Descriptions

To quantify the impact of college students' mental health on their social relationships in school, we collected data from 4955 freshmen in a college, including the SCL-90 Assessment Scale (hereafter referred to as the SCL-90 form) of 20188 swipe-card data in October 21–31, 2018. The data used in the article, which could only be used for statistical analysis to obtain certain macrostatistical characteristics, were all processed through anonymization; hence, it is impossible to identify specific students. Derogatis proposed the SCL-90 table in 1975. The table is deployed for comprehensively scoring people's mental health on multiple levels, such as feelings, emotions, thoughts, consciousness, behavior, lifestyle, interpersonal relationships, diet, and sleep, and quantifying multiple depression. Related test indicators include somatization, obsessive-compulsive symptoms, interpersonal sensitivity, depression, anxiety, hostility, terror, paranoia, and psychosis. Based on the respondent's answer, the degree of depressive symptoms is established on a scale of 1 to 5, which indicates "none," "very light," "moderate," "heavy," and "serious." The overall score range of the respondents was [13–65]. Based on their scores, respondents can be divided into five categories: none (no symptoms), mild (symptomatic but infrequent), moderate (symptomatic and frequent), heavy (symptomatic and severe), and severe (symptomatic and very serious). To simplify the research, in this follow-up study, the subjects were divided into two categories based on whether they had or did not have obvious depressive symptoms. The overall score range of students without apparent symptoms of depression was [13–26]. Students with moderate, heavy, and severe symptoms, with an overall score range of [27–65], were categorized as those with apparent symptoms of depression.

Among the 4955 students, 3879 were male and 1076 were female. The minimum age was 16.1 years (as of October 1, 2018), the maximum was 25.1, the average was 18.5, and the median was 18.4. Dining in the cafeteria is a typical behavior of college students that can reflect students' social behavior to a certain extent. Therefore, we built a social network using the swiping-card data from the student canteen. The graph $G(V, E)$ was used to represent a social network, where V represents a set of nodes and E represents a set of connected edges. The nodes represented students, with the edges

representing the social relationships between them. We inferred that there was a link between two students that met the following three conditions at the same time: (1) they spent a similar length of time on a credit card machine; (2) their spending time interval was less than two minutes; (3) During the entire observation time (August 21 to October 31, 2018), the number of times conditions (1) and (2) were met was greater than the threshold T .

3. Propagation Model Description

The college students' social network G could further determine whether the students had obvious symptoms of depression. Students with obvious depressive symptoms were recorded as G_H , and those without obvious depressive symptoms were recorded as G_N . Mathematically, the social network G and the network W are adjacent weights; $w_{ij} = n_{ij}$ represents the number of meals the two categories of students have in a short period. The greater w_{ij} , the closer the relationship between student i and student j .

To describe the propagation process of public opinion in universities, we proposed a generalized susceptible-infected-recovered (SIR) model. The susceptible students were those that did not know the news but were likely to come to know it. The infected students were those that already knew the news and were willing to share it with friends. The recovered students were those that were not interested in the information. At the initial moment, a student was randomly selected as infected. At a specific moment t , there was a certain probability of each infected student i informing a susceptible neighbor. To consider the spread of student depression arising from public opinion information in universities, we assumed that the probability of students passing information to students with depression and those without depression was heterogeneous and could be specifically divided into the following four cases:

- (i) If the student i had no obvious depressive symptoms, the probability that he would pass the information to a friend without obvious depressive symptoms j was λ_{NN} , where N indicates no obvious symptoms of depression. Specifically, λ_{NN} is expressed as follows:

$$\lambda_{NN} = 1 - (1 - \lambda_{nn})^{w_{ij}}. \quad (1)$$

- (ii) If the student i had no obvious symptoms of depression, the probability that he would pass the information to a friend with obvious symptoms of depression j was λ_{NH} , where the subscript H indicates the presence of obvious symptoms of depression. Similarly, λ_{NH} is expressed as follows:

$$\lambda_{NH} = 1 - (1 - \lambda_{nh})^{w_{ij}}. \quad (2)$$

- (iii) If the student i had obvious depressive symptoms, the probability that he would pass the information

to a friend without obvious depressive symptoms j was

$$\lambda_{HN} = 1 - (1 - \lambda_{hn})^{w_{ij}}. \quad (3)$$

- (iv) If the student i had no obvious symptoms of depression, the probability that he would pass the information to a friend with obvious symptoms of depression j was

$$\lambda_{HH} = 1 - (1 - \lambda_{hh})^{w_{ij}}. \quad (4)$$

Students' depression has different effects on the transmission of different types of information. The probability of each student losing interest in the news was γ . The propagation dynamics evolved until there were no infected students in the system.

4. Theoretical Analysis

In this section, we propose a set of heterogeneous mean-field theories to characterize the public opinion propagation model. The degree of distribution of the network G is denoted as $P(k_H, k_N)$, which indicates that a randomly selected node i has k_H friends with obvious depressive symptoms and k_N friends with no obvious depressive symptoms. $S_X(k_H, k_N, t)$, $\rho_X(k_H, k_N, t)$, and $R_X(k_H, k_N, t)$ were used to indicate that students with degree (k_H, k_N) were in the susceptible, infected, and recovered states, respectively, where $X \in \{H, N\}$ indicates whether the student had obvious symptoms of depression. At the initial time, that is, $t = 0$, we have $S(k_H, k_N, t) = (1 - 1/n)$, $\rho(k_H, k_N, t) = (1/n)$, and $R(k_H, k_N, t) = 0$, where n represents the number of nodes in the network G .

A student i_H with obvious depressive symptoms with degree (k_H, k_N) is in a susceptible state and needs to satisfy two conditions at the same time: (1) he is not infected by a friend with obvious symptoms and (2) he is not infected by a friend without obvious symptoms. For condition (1), the probability that the student i_H is connected to an infected friend with obvious symptoms is

$$c_{HN} = \frac{\sum_{k'_H} P(k'_H, K'_N) k'_{HH} \rho_H(k'_H, K'_N)}{\langle k_H \rangle}. \quad (5)$$

where $\langle k_H \rangle$ indicates the number of students with obvious depressive symptoms. Therefore, the probability of the student i_H not getting infected by a friend with obvious depressive symptoms is

$$\eta_{HH}(t) = 1 - S_H(k_H, k_N, t) \lambda_{HH} c_{HH}. \quad (6)$$

Similarly, we can obtain the probability of satisfying condition (2), that is, the probability of the student i_H not being infected by a friend without obvious depressive symptoms, as follows:

$$\eta_{HN}(t) = 1 - S_H(k_H, k_N, t) \lambda_{HN} c_{HN}, \quad (7)$$

where c_{HN} represents the probability of the student i_H being connected to an infectious friend without obvious symptoms, which is expressed as follows:

$$c_{HN} = \frac{\sum_{k'_N} P(k'_H, K'_N) k'_{HN} \rho_H(k'_H, K'_N)}{\langle k_{HN} \rangle}, \quad (8)$$

where $\langle k_{HN} \rangle$ represents the number of students with obvious depressive symptoms who have no obvious depressive symptoms.

Considering conditions (1) and (2) comprehensively, the probability of student i_H being infected at t was

$$\chi_H(t) = 1 - (1 - \eta_{HH}(t))(1 - \eta_{HN}(t)). \quad (9)$$

Therefore, we can obtain the evolution equation of $S_H(k_H, k_N, t)$ as

$$\frac{dS_H(k_H, k_N, t)}{dt} = -\chi_H(t). \quad (10)$$

For those infected with obvious depressive symptoms, this growth stems from the infection of the susceptible nodes by neighbors, and the decrease comes from recovery. Therefore, the state evolution equation of $\rho_H(k_H, k_N, t)$ is

$$\frac{d\rho_H(k_H, k_N, t)}{dt} = \chi_H(t) - \gamma \rho_H(k_H, k_N, t). \quad (11)$$

The state evolution equation of $R_H(k_H, k_N, t)$ is

$$\frac{dR_H(k_H, k_N, t)}{dt} = \gamma \rho_H(k_H, k_N, t). \quad (12)$$

Similar to the aforementioned discussion, it can be observed that the degree of the nodes indicating students without obvious depressive symptoms is (k_H, k_N) ; the evolution equations in the susceptible, infected, and recovered states, respectively, were

$$\frac{dS_N(k_H, k_N, t)}{dt} = -\chi_N(t), \quad (13)$$

$$\frac{d\rho_N(k_H, k_N, t)}{dt} = \chi_N(t) - \gamma \rho_N(k_H, k_N, t), \quad (14)$$

with

$$\frac{dR_N(k_H, k_N, t)}{dt} = \gamma \rho_N(k_H, k_N, t), \quad (15)$$

where

$$\chi_N(t) = 1 - (1 - \eta_{NN}(t))(1 - \eta_{NH}(t)). \quad (16)$$

The probability of a student without obvious depressive symptoms i_N connecting to an infected friend without obvious symptoms was

$$c_{NN} = \frac{\sum_{k'_N} P(k'_H, K'_N) k'_{NN} \rho_N(k'_H, K'_N)}{\langle k_N \rangle}. \quad (17)$$

where $\langle k_N \rangle$ represents the number of students with no obvious depressive symptoms connected to those without obvious depressive symptoms and c_{NH} indicates the probability of the student i_N connecting to an infected friend with obvious symptoms, which is expressed as follows:

$$c_{NH} = \frac{\sum_{k'_H} P(k'_H, K'_N) k'_H \rho_H(k'_H, K'_N)}{\langle k_{NH} \rangle}. \quad (18)$$

where $\langle k_{NH} \rangle$ represents the ratio of students with obvious depressive symptoms to those without obvious depressive symptoms.

We have presented the evolution equations of students with and without obvious depressive symptoms in various states. It is not difficult to obtain the proportion of various nodes in the SIR states in this system, as follows:

$$\begin{aligned} S(t) &= \sum_{k_H, k_N} P(k_H, k_N) [S_H(k_H, k_N, t) + S_N(k_H, k_N, t)], \\ \rho(t) &= \sum_{k_H, k_N} P(k_H, k_N) [\rho_H(k_H, k_N, t) + \rho_N(k_H, k_N, t)], \end{aligned} \quad (19)$$

$$R(t) = \sum_{k_H, k_N} P(k_H, k_N) [R_H(k_H, k_N, t) + R_N(k_H, k_N, t)], \quad (20)$$

respectively.

Next, we determined the outbreak threshold of public opinion. At $t \rightarrow 0$, only a few nodes in the network were informed; consequently, $\rho_H(t) \rightarrow 0$, and $\rho_N(t) \rightarrow 0$. Therefore, we can obtain the Jacobian matrix of the equations (11) and (14) as H . The dimension of the matrix H is $k_H^{\max} k_N^{\max} \times k_H^{\max} k_N^{\max}$. The critical condition to be met by the outbreak threshold is as follows:

$$\lambda_c = \frac{1}{\Lambda(H)}, \quad (21)$$

where $\Lambda(H)$ represents the maximum eigenvalue of the matrix H .

4.1. Numerical Simulation. In this section, we applied the public opinion information dissemination model on the real-world social network and randomized network and analyzed the influence of the network structure on information dissemination. We set the threshold as $T = 2$. The randomized null model was constructed as follows. (1) Two connected edges, e_1 and e_2 , were randomly selected. e_1 was connected to nodes i and j , and e_2 was connected to the nodes m and n . If the network does not have double edges and self-loops, when the nodes connected by the two connected edges are exchanged, then the nodes were exchanged; otherwise, the nodes were left as they were. (2) Step (1) was repeated until the $10E$ step, where E represents the number of edges.

In the experimental simulation process, we calculated the probability of propagating information between nodes of the same type as equal, denoted as λ_{in} ; the probability of propagation between nodes of different types was equal,

denoted as $\lambda_{between}$. Using the same parameters, we conducted, at least, 1000 experimental simulations to calculate the average values.

First, we analyzed the network topology of the social network. In Figure 1(a), the relationship between students without obvious depressive symptoms is shown. Compared with the zero model of stochastic networks, large-degree nodes in real networks tend to connect with small-degree nodes. In Figure 1(b), we also observed a similar phenomenon in the context of a meal-sharing social network. Only a few large-degree nodes dined together; the connection was more of a star-shaped knot, that is, large-degree nodes were connected to more small-degree nodes.

Figure 2 shows the clustering coefficients of students with or without obvious depressive symptoms. We found that the clustering coefficient c_k decreased with k , regardless of whether the students had obvious depressive symptoms. Compared to the null model, when $k \leq 400$, the students had a high clustering coefficient, which indicated that nodes with a small degree were more inclined to have a group meal with three people, while nodes with a high degree had few meals.

In Figure 3, we show the proportion of susceptible, infectious, and recovered states over time of students with and without obvious depressive symptoms. In the figure, $\lambda_{in} = 0.004$, $\lambda_{between} = 0.006$, and the recovery probability $\gamma = 0.1$. For students without obvious depressive symptoms, we found that the real network was not conducive to information dissemination. This phenomenon may be attributable to the following reasons. Compared with the random network, the real network has a higher cluster coefficient. When the information dissemination rate is high, information in the network with a high clustering coefficient always passes to the surrounding nodes, and as it is not easy to reach nodes beyond the surrounding ones, this environment is not conducive to information dissemination. Similarly, among students without obvious depressive symptoms, it was more difficult to disseminate information on the real network compared to the random ones, as shown in Figure 3(b).

In Figure 4, we present a graph of the evolution of the state of the nodes in the network over time. Figures 4(a)–4(c) show that $t = 0$, $t = 5$, and $t = t_{\max}$ on the random network in Figure 3. Students with significant depressive symptoms were infected. In the figure, green indicates the susceptible state, red indicates the infected state, and blue indicates the recovered state. Similarly, Figures 4(d)–4(f) show students without obvious depressive symptoms on random networks at $t = 0$, $t = 5$, and $t = t_{\max}$. Figures 4(g)–4(i) show students with obvious depressive symptoms on the real network, when $t = 0$, $t = 5$, and $t = t_{\max}$. Figures 4(j)–4(l) show the state of students who have no obvious depressive symptoms on the real network at time $t = 0$, $t = 5$, and $t = t_{\max}$.

In Figure 5, we show the spread of information among students on real social networks in detail. In the figure, we set the recovery probability to $\gamma = 1.0$. Through numerous experimental simulations, we found that varying the value of γ did not qualitatively change the propagation phenomenon. Figure 5(a) shows the proportion of students without significant depressive symptoms receiving information R_N as a

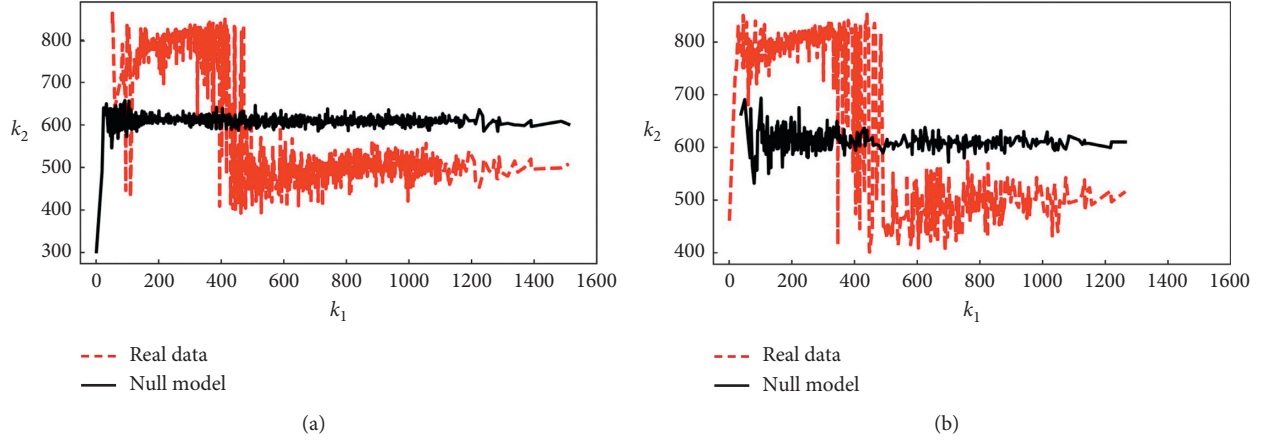


FIGURE 1: Degree correlation for (a) real-world network and (b) null model network.

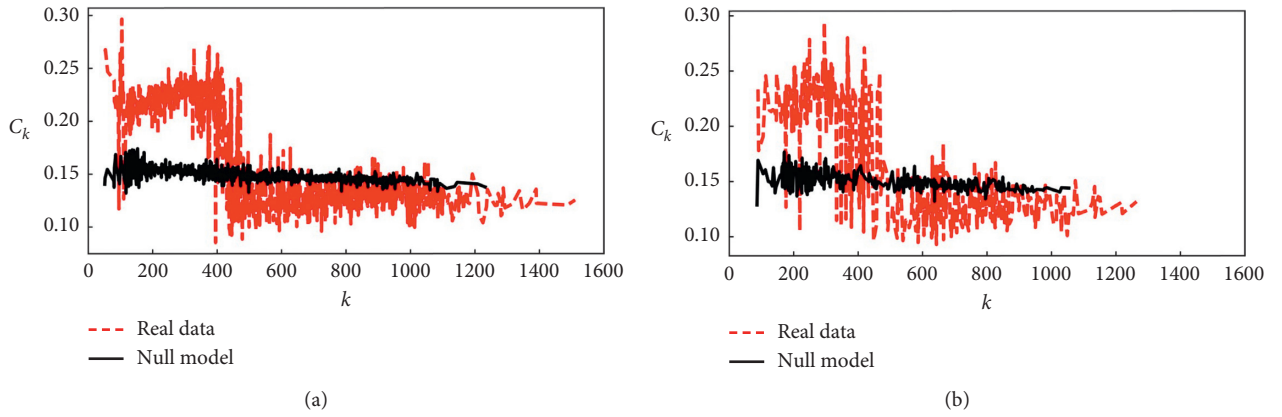


FIGURE 2: Clustering for (a) real-world network and (b) null model network.

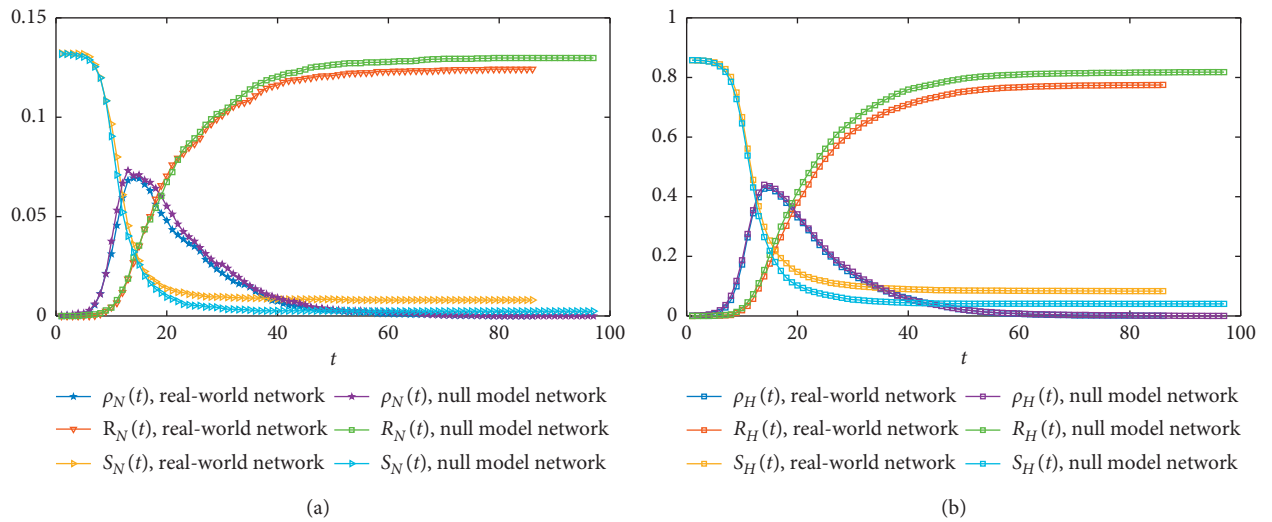


FIGURE 3: The status of various students evolves over time on social network (a) with and (b) without obvious depressive symptoms.

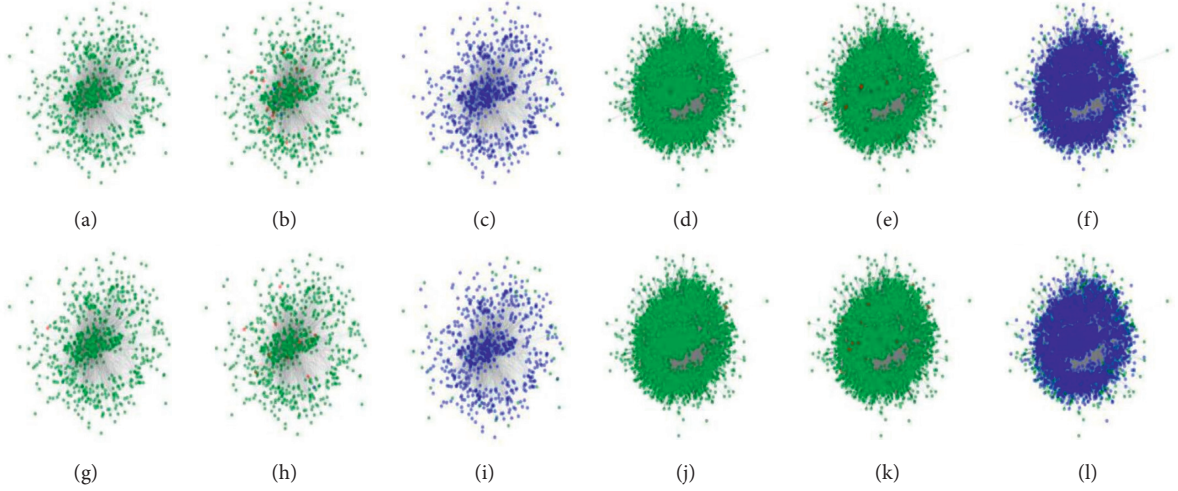


FIGURE 4: Node state on different time steps.

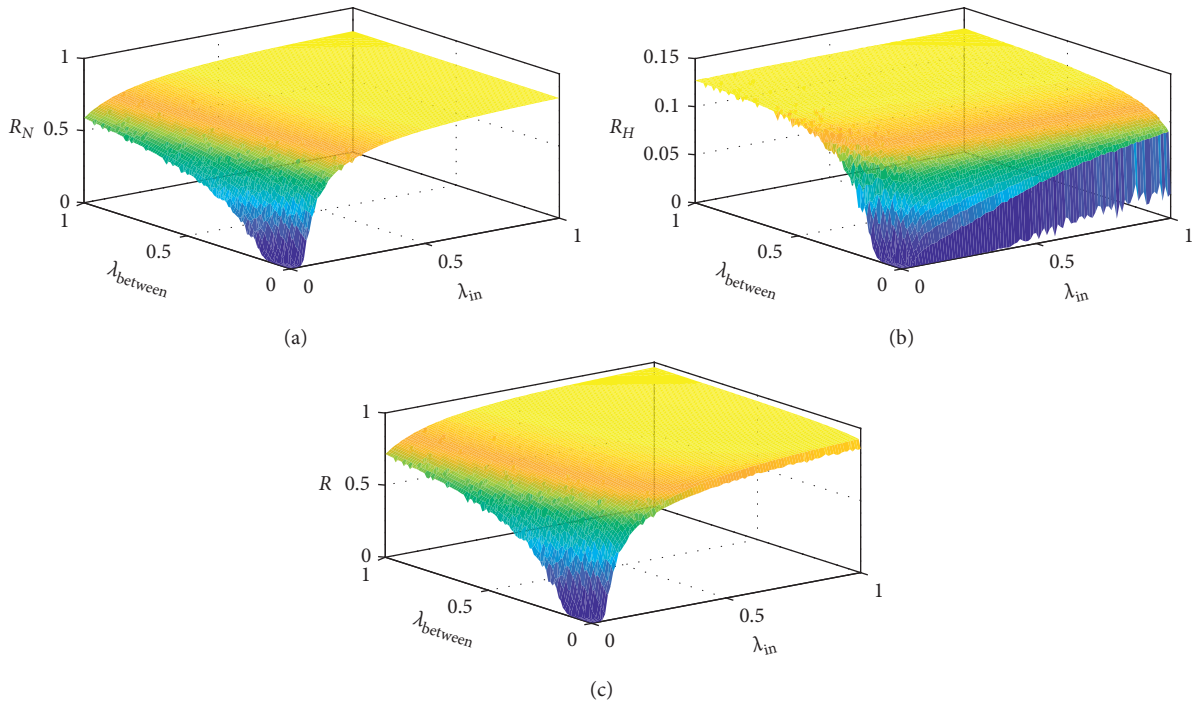


FIGURE 5: Information spreading on real-world networks.

function of λ_{in} and $\lambda_{between}$. As λ_{in} and $\lambda_{between}$ increased, R_N also increased. When both λ_{in} and $\lambda_{between}$ were less than their outbreak threshold (can be predicted by using equation (21)), it was almost impossible for students without obvious symptoms of depression to receive information. When λ_{in} or $\lambda_{between}$ was greater than the outbreak threshold, a large number of students without obvious depressive symptoms could receive the message. When λ_{in} ($\lambda_{between}$) was sufficiently large, $\lambda_{between} = 0$ ($\lambda_{in} = 0$) could cause global information bursts. We observed a similar phenomenon in Figures 5(b) and 5(c), which show R_H and R with λ_{in} and $\lambda_{between}$, respectively.

Figure 6 shows the spread of public opinion on the corresponding null model random network. Among them, the three subgraphs show the changes in R_N , R_H , and R with λ_{in} and $\lambda_{between}$. From the three figures, a phenomenon similar to Figure 3 can be observed.

To further compare the impact of the real network structure on information dissemination, we show the difference in the spread of information on real and random networks in Figure 7. For students without obvious depressive symptoms, the difference in the spread was defined as

$$\Delta R_N = R_N^{\text{real}} - R_N^{\text{random}}, \quad (22)$$

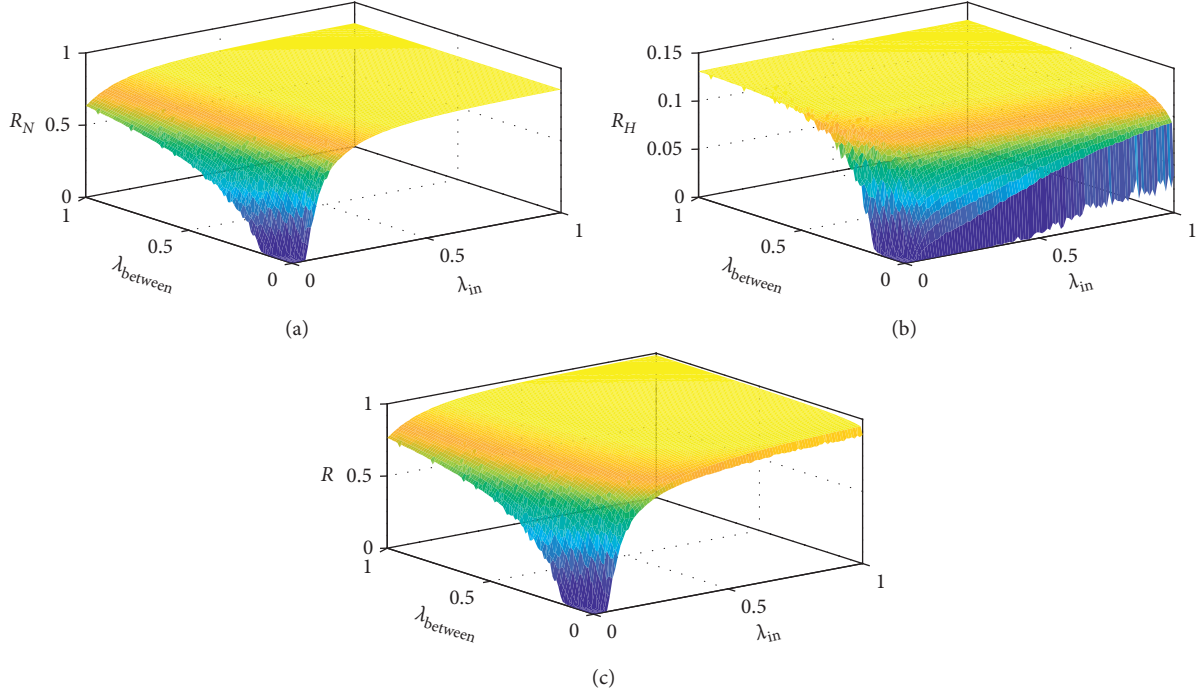


FIGURE 6: Information spreading on null model networks.

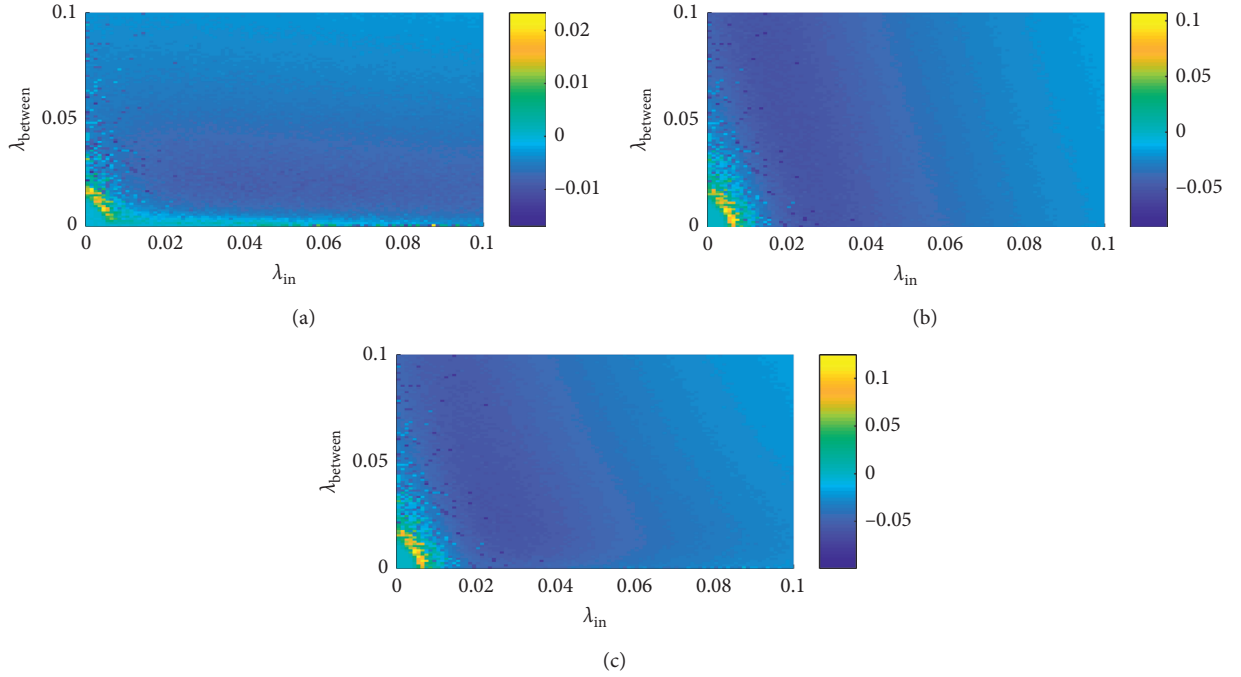


FIGURE 7: Difference of information spreading on real-world and null model networks.

where R_N^{real} and R_N^{random} represent the spread of information on real and random networks, respectively. Similarly, the difference in the spread of the proportion of students with significant depressive symptoms receiving information and the proportion of all students receiving information was ΔR_H and ΔR . Figures 7(a)–7(c) show ΔR_N , ΔR_H , and ΔR along with λ_{in} and λ_{between} changes. We found

that when λ_{in} and λ_{between} were small, ΔR_N , ΔR_H , and ΔR were all greater than zero, which indicates that the true network structure was not conducive to information dissemination. Because the real network had a high clustering coefficient, it was conducive to the spread of information in a local range. With increase in λ_{in} and λ_{between} , ΔR_N , ΔR_H , and ΔR were all less than zero, that is,

the real network was not conducive to information dissemination.

5. Conclusions

We proposed a model of public opinion information dissemination based on the SIR model. In the model, the students were divided into two categories based on whether they had obvious depressive symptoms or not. We proposed a heterogeneous mean-field theory to characterize the model. Several computer simulations revealed that students without obvious depressive symptoms were more likely to receive information than students with obvious depressive symptoms. Further, due to the existence of high clustering coefficients in real social networks, there were two scenarios of information propagation. When the information dissemination rate was low, it was easier to disseminate information on real social networks than on random networks. The results help us to have a deeper understanding of the effects of student depression on the spread of public opinion. In big data era, the online data about the student activity should be taken into consideration when building their social network and the effects of student depression on the spread of public opinion in university should be further investigated.

Data Availability

No data were used to support this study.

Conflicts of Interest

The authors declare that they have no conflicts of interest.

References

- [1] S. Pei and H. A. Makse, "Spreading dynamics in complex networks," *Journal of Statistical Mechanics: Theory and Experiment*, vol. 2013, no. 12, p. P12002, 2013.
- [2] T. R. Zaman, R. Herbrich, J. Van Gael, and D. Stern, "Social media's perspective on industry 4.0: a twitter analysis," in *Proceedings of the Workshop on Computational Social Science and the Wisdom of Crowds*, Whistler, Canada, December 2010.
- [3] D. Wang, Z. Wen, H. Tong, C.-Y. Lin, C. Song, and A.-L. Barabási, "Information spreading in context," in *Proceedings of the 20th International Conference on World Wide Web (2011)*, pp. 735–744, Hyderabad, India, March 2011.
- [4] L. Lü and T. Zhou, "The small world yields the most effective information spreading," *New Journal of Physics*, vol. 13, no. 12, p. 123005, 2011.
- [5] M. Zanin, D. Papo, P. A. Sousa et al., "Combining complex networks and data mining: why and how," *Physics Reports*, vol. 635, pp. 1–44, 2016.
- [6] A. L. Lloyd and R. M. May, "Epidemiology: how viruses spread among computers and people," *Science*, vol. 292, no. 5520, pp. 1316–1317, 2001.
- [7] Z.-K. Zhang, C. Liu, X.-X. Zhan, X. Lu, C.-X. Zhang, and Y.-C. Zhang, "Dynamics of information diffusion and its applications on complex networks," *Physics Reports*, vol. 651, pp. 1–34, 2016.
- [8] X.-X. Zhan, A. Hanjalic, and H. Wang, "Information diffusion backbones in temporal networks," *Scientific Reports*, vol. 9, p. 1, 2019.
- [9] R. Pastor-Satorras and C. Castellano, "Distinct types of eigenvector localization in networks," *Scientific Reports*, vol. 6, p. 18847, 2016.
- [10] Y. Moreno, J. B. Gómez, and A. F. Pacheco, "Epidemic incidence in correlated complex networks," *Physical Review E*, vol. 68, Article ID 035103, 2003.
- [11] D. M. J. Lazer, M. A. Baum, Y. Benkler et al., "The science of fake news," *Science*, vol. 359, no. 6380, pp. 1094–1096, 2018.
- [12] M. A. Porter and J. P. Gleeson, "Dynamical systems on networks," 2016, <http://arxiv.org/abs/1403.7663>.
- [13] A.-L. Barabási and R. Albert, "Emergence of scaling in random networks," *Science*, vol. 286, no. 5439, pp. 509–512, 1999.
- [14] M. Newman, *Networks: An Introduction*, Oxford University Press, Oxford, UK, 2010.
- [15] A. Clauset, C. R. Shalizi, and M. E. J. Newman, "Power-law distributions in empirical data," *SIAM Review*, vol. 51, no. 4, pp. 661–703, 2009.
- [16] S. Boccaletti, V. Latora, Y. Moreno, M. Chavez, and D. Hwang, "Complex networks: structure and dynamics," *Physics Reports*, vol. 424, no. 4–5, pp. 175–308, 2006.
- [17] R. Cohen and S. Havlin, *Complex Networks: Structure, Robustness and Function*, Cambridge University Press, Cambridge, UK, 2010.
- [18] Z. Wang, C. Xia, Z. Chen, and G. Chen, "Epidemic propagation with positive and negative preventive information in multiplex networks," *IEEE Transactions on Cybernetics*, vol. 99, 2020.
- [19] Q. Shao, C. Xia, L. Wang, and H. Li, "A new propagation model coupling the offline and online social networks," *Nonlinear Dynamics*, vol. 98, no. 3, pp. 2171–2183, 2019.
- [20] Z. Wang, Q. Guo, S. Sun, and C. Xia, "The impact of awareness diffusion on SIR-like epidemics in multiplex networks," *Applied Mathematics and Computation*, vol. 349, pp. 134–147, 2019.
- [21] C. Gan, Q. Feng, Q. Zhu, Z. Zhang, Y. Zhang, and Y. Xiang, "Analysis of computer virus propagation behaviors over complex networks: a case study of oregon routing network," *Nonlinear Dynamics*, vol. 1, 2020.
- [22] C. Gan, L. Wang, Z. Zhang, and Z. Wang, "Sparse attention based separable dilated convolutional neural network for targeted sentiment analysis," *Knowledge-Based Systems*, vol. 188, p. 104827, 2020.
- [23] Y. Yi, Z. Zhang, L. T. Yang, C. Gan, X. Deng, and L. Yi, "Blockchain empowered cooperative authentication with data traceability in vehicular edge computing," *IEEE Transactions on Network Science and Engineering*, vol. 69, 2020.
- [24] S. Goel, A. Anderson, J. Hofman, and D. J. Watts, "The structural virality of online diffusion," *Management Science*, vol. 62, p. 180, 2016.
- [25] D. Centola, "An experimental study of homophily in the adoption of health behavior," *Science*, vol. 334, no. 6060, pp. 1269–1272, 2011.
- [26] D. Centola and M. Macy, "Complex contagions and the weakness of long ties," *American Journal of Sociology*, vol. 113, no. 3, pp. 702–734, 2007.
- [27] M. Zheng, L. Lü, M. Zhao et al., "Spreading in online social networks: The role of social reinforcement," *Physical Review E*, vol. 88, Article ID 012818, 2013.
- [28] W. Wang, M. Tang, H.-F. Zhang, and Y.-C. Lai, "Dynamics of social contagions with memory of nonredundant information," *Physical Review E*, vol. 92, Article ID 012820, 2015.

- [29] J. Wu, M. Zheng, Z.-K. Zhang, W. Wang, C. Gu, and Z. Liu, "A model of spreading of sudden events on social networks," *Chaos: An Interdisciplinary Journal of Nonlinear Science*, vol. 28, Article ID 033113, 2018.
- [30] J. Wu, M. Zheng, K. Xu, and C. Gu, "Effects of two channels on explosive information spreading," *Nonlinear Dynamics*, vol. 99, no. 3, pp. 2387–2397, 2020.
- [31] J. Wu, M. Zheng, W. Wang, H. Yang, and C. Gu, "Double transition of information spreading in a two-layered network," *Chaos: An Interdisciplinary Journal of Nonlinear Science*, vol. 28, Article ID 083117, 2018.
- [32] W. Wang, M. Tang, H.-F. Zhang, H. Gao, Y. Do, and Z.-H. Liu, "Epidemic spreading on complex networks with general degree and weight distributions," *Physical Review E*, vol. 90, Article ID 042803, 2014.
- [33] P. Shu, Q.-H. Liu, S. Wang, and W. Wang, "Social contagions on interconnected networks of heterogeneous populations," *Chaos: An Interdisciplinary Journal of Nonlinear Science*, vol. 28, no. 11, p. 113114, 2018.

Research Article

Weibo Rumor Recognition Based on Communication and Stacking Ensemble Learning

Yu Wu ¹, Yan Zeng,² Jie Yang,² and Zhenni Zhao²

¹*School of Cyber Security and Information Law, Chongqing University of Posts and Telecommunications, Chongqing 400065, China*

²*School of Computer Science and Technology, Chongqing University of Posts and Telecommunications, Chongqing 400065, China*

Correspondence should be addressed to Yu Wu; wuyu@cqupt.edu.cn

Received 5 June 2020; Revised 23 August 2020; Accepted 2 September 2020; Published 18 September 2020

Academic Editor: Wei Wang

Copyright © 2020 Yu Wu et al. This is an open access article distributed under the Creative Commons Attribution License, which permits unrestricted use, distribution, and reproduction in any medium, provided the original work is properly cited.

Research on the identification of rumors in cyberspace helps to discover social issues that are of concern to the public and are not easily found, and it also can help to purify cyberspace and to maintain social stability. However, the real complexity of rumors makes it difficult for its recognition technology to bridge the semantic gap between qualitative description and quantitative calculation of rumors. Firstly, the existing rumor definitions are mostly qualitative descriptions, so we propose a technical definition of Internet rumors to facilitate quantitative calculations. Secondly, since the feature set used in rumor recognition research is not effective, by combining with communication, we construct a more suitable feature set for rumor recognition. Thirdly, aiming at the problem that traditional classification algorithms are not suitable for complex rumor information recognition, a rumor recognition method based on Stacking ensemble learning is proposed. Our experiment results show that the proposed method has higher accuracy, less algorithm execution time, and better practical application effect.

1. Introduction

Nowadays, the Internet is full of various information like Internet rumors, malware, and fake news, and it is difficult for people to tell the truth of that information. With the development of cyberspace, the researches on Internet misinformation have gradually mainly focused on Internet rumor recognition, Internet rumor propagation, malware and virus propagation, fake news detection, and water army detection.

The research on malware and virus propagation focused on modeling the spread of malicious malware to predict the spreading behaviour of it [1], while the research on water army is mainly about detecting water army among a large number of social media users in an online topic and preventing the negative effect on the development of the public opinion [2]. The spread of rumors may affect personal reputation, invade public privacy, or cause chaos in public order, lead to group events, and endanger the stability of the country. Therefore, modeling the propagation of Internet

rumors in social network to help control the spread of the misinformation is of great importance [3]. However, it is also vital to figure out what are Internet rumors and how to recognize them in a more effective way.

In paper [4], Peterson et al. proposed that rumor, in general, refers to an unverified account or explanation of events, circulating from person to person and pertaining to an object, event, or issue of public concern. Since then, rumors have been given some specific characteristics, such as ambiguity, transmissibility, and timeliness. With the development of the Internet, the spread of information has accelerated, and Internet rumors are derived. In paper [5], Chao et al. considered that Internet rumors were unconfirmed information transmitted by Internet users in specific ways. Most scholars believe that the spread of Internet rumors is carried out on the Internet, because the network connection is wide and arbitrary, which makes the spread of Internet rumors faster, the coverage of influence wider, and the extent of damage bigger [6]. However, the existing definitions cannot accurately describe the technical

characteristics of Internet rumors and other elements from the perspective of computability.

At present, on the one hand, the research on Internet rumors recognition focuses on extracting feature set that can be used to detect rumors. On the other hand, the classification modeling of Internet rumors, which does not need various features but a large amount of data, has become a research hotspot. However, feature selection of Internet rumors is more suitable for a small number of datasets.

The feature set used in current Internet rumor recognition is based on the features proposed by Castillo et al. [7] and Qazvinian et al. [8]. Generally, the feature set is divided into three types: content feature, user feature, and propagation feature; sometimes it is further subdivided into time feature, network feature, and combination of the two. These features are usually simple statistical characteristics, and the deep semantics of the text information are not mined. Therefore, the recognition accuracy is affected by the lack of key features. In paper [9], Kwon et al. applied RNN to learn the deep meaning between messages. Based on the protection mechanism, Chen et al. [10] proposed a new RNN model to recognize the Internet rumor by using time sequence to obtain the potential contextual change. Although the neural network model can overcome the problem of sparse features by using continuous vectors to represent text, it has too many parameters and slow convergence speed and needs a lot of corpus.

The classification algorithms often used in rumor recognition research include SVM, Decision Tree, Naive Bayes, and Neural Networks. For example, in paper [11], Duan et al. used SVM to detect fake information from the comment perspective of the source Weibo. In paper [12], Chen et al. used the regression method to recognize the online food safety rumors. However, this method is limited by the topic type of the rumor and can only determine whether the article is related to the rumor. In paper [13], Lu et al. proposed an improved method based on the Co-Forest algorithm, which improved the accuracy of prediction for unlabelled samples, to solve the problem of data imbalance.

Due to the fact that the dataset is difficult to obtain, the current research tends to extract the statistical characteristics of text information. Moreover, new experimental methods in which features are added on the basis of previous researches make the feature dimension continuously increase and lead to the inaccurate model parameter. Besides, classical algorithms such as SVM, Decision Tree, and Naive Bayes are no longer suitable for recognizing Internet information with complex content. In specific problems and scenarios, each model has its advantages and disadvantages. The results of recognition might be better by combining the advantages of multiple models [14]. For example, in paper [15], Xie et al. proposed a high-precision EEG emotion recognition model by integrating LightGBM, XGBoost, and Random Forest. In paper [16], Duan et al. classified the sentiment of Weibo text by using the Stacking ensemble learning method, and the accuracy rate was as high as 93%.

In this paper, we give the definition of Internet rumor based on communication's 5W Formula, and three characteristics of User Credibility, Emotional Consistency, and

Regional Correlation are constructed. Then, we verify the validity of the feature by using Chi-square, so as to better filter the feature set. Finally, analysing the existing classification algorithms, adopting the Stacking ensemble learning, we propose a rumor recognition method combined with different models and optimized using cross validation. Finally, the experiments are conducted among different methods and datasets.

The structure of this paper is as follows: the related work is introduced in the first part. The design of the Stacking model, which includes features construction and selection, and the construction of the model are described in the second part. In the third part, we conduct the experiments and analyse the results. The conclusion of this paper and the introduction of future work are given in the last part.

2. Related Work

2.1. Ensemble Learning and Stacking. For different problems, the speed, accuracy, and generalization ability of machine learning models are different. To obtain a model with strong generalization ability and high robustness, the ensemble learning method is proposed. The current mainstream methods are Boosting (typically AdaBoost, GBDT, and XGBoost), Bagging (typically Random Forest), and Stacking. The Stacking model applied in this paper has a layered framework. The original training dataset is inputted into multiple primary learners in the first layer, and the first layer's prediction results are used as the input training set for the next layer of learners. Finally, the prediction results obtained in the previous layer are inputted into the final metalearners to get the final prediction result (see Figure 1).

2.2. Other Methods. SVM [17] is a binary classification model that uses the margin maximization strategy. It minimizes the structured risk, the empirical risk, and confidence range to improve the generalization ability. Therefore, in a small statistical dataset, it can also get good statistical regularity.

Decision Tree J48 [8] is based on C4.5. It uses a divide-and-conquer strategy and has high credibility; and its results are easy to understand.

Random Forest [18] is one of the ensemble learning methods. By combining multiple weak classifiers, the final result is obtained by voting or calculating mean value. The model has high accuracy and generalization performance.

Logistic regression [19] is one of the generalized linear models, as well as a classical classification method used to solve the optimization problem with the likelihood function as the objective function.

3. Weibo Rumor Recognition

3.1. Rumor Definition. Based on the existing rumor definitions, this paper combines the 5W's of communication to divide the elements of rumor transmission into communicators, content, objects, effects, and channels. The communicator could be an individual or an organization. The content is the information that the communicator wants to

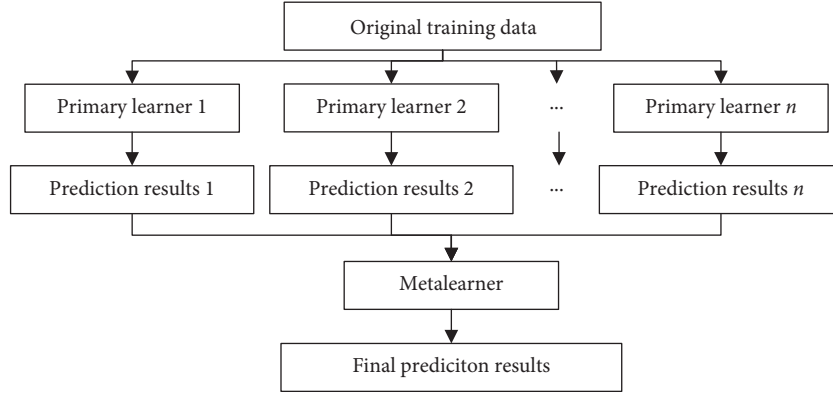


FIGURE 1: Stacking principle.

pass to the audience. The object is the receiver of information or the communicator of information processing. The effect is that the audience is affected by the message sent by the communicator, causing changes in their ideas, behaviours, and so forth. The channel is the mean by which communication is achieved. Sometimes the object of Internet rumors is also the communicator, so we combine them as the same element for analysis. Therefore, the qualitative definition of Internet rumor given in this paper is shown in Definition 1.

Definition 1. Internet rumors: internet rumors refer to the information published by Internet users through online media platforms, which is ambiguous in content, unconfirmed by the official, and to some extent harmful to the society. Its expressions include text, pictures, audio, and video.

The research object of this paper is Weibo. Weibo rumor, which can be divided into pure text, picture not matching the text, and fake images, is a type of the Internet rumors. Since most of Weibo contains text, the current recognition of Weibo rumors mainly focuses on text. In order to facilitate the recognition of Internet rumors, as shown in Definition 2, this paper gives its formal definition from computability.

Definition 2. Weibo rumors: the object of rumor recognition is a Weibo set $\mathbf{W}\{\mathbf{m}_1, \mathbf{m}_2, \mathbf{m}_3, \dots, \mathbf{m}_n\}$, and $\mathbf{m}_i = \langle \mathbf{X}_i, y_i, f \rangle$. $\mathbf{X}_i\{\mathbf{U}_i, \mathbf{T}_i, \mathbf{P}_i\}$ is the feature set of each Weibo. The user feature set $\mathbf{U}_i\{f_{u_1}, f_{u_2}, f_{u_3}, \dots, f_{u_n}\}$ represents the attributes of the i -th Weibo's publisher. The content feature set $\mathbf{T}_i\{f_{t_1}, f_{t_2}, f_{t_3}, \dots, f_{t_n}\}$ represents the attributes of the i -th Weibo's text. The propagation feature set $\mathbf{P}_i\{f_{p_1}, f_{p_2}, f_{p_3}, \dots, f_{p_n}\}$ represents the propagation attributes of the i -th microblog. y_i is the confidence value of whether \mathbf{m}_i is a rumor, and $y_i = f(\mathbf{X}_i)$, $(0 \leq y_i \leq 1)$. When y_i is closer to 1, the probability of \mathbf{m}_i being a rumor is higher and vice versa.

3.2. Rumor Recognition Process. At present, the research on rumor recognition mainly focuses on feature construction, and the method of adding new features based on previous

research work would make the feature dimension increase and estimation of model parameters inaccurate. Therefore, using the Chi-square test to test the validity of new features could obtain a feature set that is more suitable for Internet rumors recognition. Internet rumor recognition is regarded as a binary classification problem. In this paper, it is considered to use the idea of Stacking ensemble learning to build a new classification model because each algorithm has its advantages (see Figure 2).

3.3. Feature Construction. Combining the research studies of paper [8] and paper [20], we select 24 basic features, which are divided into content feature (CONT), user feature (USER), and propagation feature (TRAN). The content feature includes the length of text, the number of @, the number of #, the number of question/exclamation marks, whether there are pictures or URLs, and the number of positive/negative words. The user feature includes the length of username, gender, the number of friends, the number of followers, the number of mutual followers, the number of microblog posts, the number of favourite microblogs, certification information, personal description, and user's own influence. The propagation feature includes the number of reposts, the number of comments, the number of likes, the interval between user registration time and microblog post time, and microblog's attention.

The above features are mostly statistical features; in order to recognize Weibo rumor more effectively, this paper constructs new features in three aspects, user, content, and propagation features, to mine the hidden meaning behind text information.

Definition 3. User Credibility (UCRE): the user's credibility is determined by many factors. By integrating information such as the number of users' friends, followers, mutual followers, the number of microblogs posted, and certification information, the user's influence and activity are constructed to calculate the user's credibility. The more credible a user is, the more credible the information he/she posts. The calculation formula of the user's credibility is as follows:

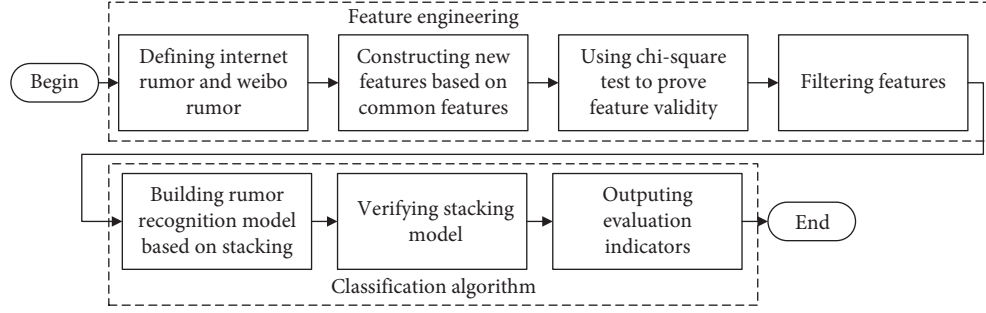


FIGURE 2: Rumor recognition flowchart.

$$f_{\text{credibility}}(u_i) = f_{\text{verified}}(u_i) + f_{\text{influence}}(u_i) + f_{\text{InfoIntegrity}}(u_i), \quad (1)$$

where $f_{\text{influence}}(u_i)$ is the user's influence, f_{verified} is the user's certification information, and $f_{\text{InfoIntegrity}}$ is whether the user's information is complete; the user's information includes username, gender, personal description, registration place, and profile photo. The greater the user's influence, the greater the impact of the microblog they posted within a certain time and space. The user's influence is mainly determined by the number of users' followers and the number of mutual followers. The calculation formula is as follows:

$$f_{\text{influence}}(u_i) = \frac{C_{\text{bifollowers}}(u_i)}{C_{\text{followers}}(u_i)},$$

$$f_{\text{verified}}(u_i) = \begin{cases} 0, & \text{unverified,} \\ 1, & \text{verified,} \end{cases} \quad (2)$$

$$f_{\text{InfoIntegrity}}(u_i) = \begin{cases} 0, & \text{complete,} \\ 1, & \text{incomplete,} \end{cases}$$

where u_i is user who posts i -th microblog, $C_{\text{bifollower}}$ is the number of u_i 's mutual followers, and C_{follower} is the number of u_i 's followers.

Definition 4. Emotion consistency (ECON): emotion consistency is whether the sentiment of the microblog is consistent with the sentiment of the microblog's comment. When the microblog shows a strong emotion, it may incite others' emotions; then the microblog is more likely to be a rumor. By segmenting the \mathbf{m}_i 's text and comments, we obtain the text's term vector set $\mathbf{V}_i\{v_1, v_2, v_3, \dots, v_n\}$, where v_i is the processed word, and the i -th microblog's j -th comment's term vector set $\mathbf{C}_j^i\{c_1, c_2, c_3, \dots, c_n\}$, where c_i is the processed word.

The number of positive/negative words is calculated by using Affective Lexical Ontology [21]. The specific formula is as follows:

$$S = C_{\text{pos}} - C_{\text{neg}}, \quad (3)$$

where S is the emotion of the term vector set, C_{pos} is the number of positive words, and C_{neg} is the number of

negative words. Then we can get the final emotion SO as follows:

$$SO = \begin{cases} 1, & S > 0, \\ 0, & S = 0, \\ -1, & S < 0, \end{cases} \quad (4)$$

where 1 represents positive, -1 represents negative, and 0 represents neutral. Calculating the emotion of each comment, the overall emotion of the comments is calculated as follows:

$$SO(c^i) = \begin{cases} 1, & \sum_{j=1}^n SO(c_j^i) > 0, \\ 0, & \sum_j SO(c_j^i) = 0, \\ -1, & \sum_j SO(c_j^i) < 0. \end{cases} \quad (5)$$

Comparing the emotions of \mathbf{m}_i and c^i , the emotion consistency of \mathbf{m}_i is calculated as follows:

$$SC = \begin{cases} 0, & SO(m_i) \neq SO(c^i), \\ 1, & SO(m_i) = SO(c^i). \end{cases} \quad (6)$$

Definition 5. Regional correlation (RCO): regional correlation refers to the distance between the place mentioned in the microblog and the user's registration place. The longer the distance is, the less credible the microblog is. This paper uses Euclidean distance to calculate the distance. The formula is as follows:

$$\text{dist}(x, y) = \sqrt{\sum_{i=1}^n (x_i - y_i)^2}, \quad (7)$$

where $\text{dist}(x, y)$ is the distance between city x and city y , the coordinate of city x is (x_1, x_2) , and the coordinate of city y is (y_1, y_2) . Calculating the distance between cities in China, the distance matrix is shown as follows:

$$\mathbf{M} = \begin{bmatrix} 0 & 96.06 & \cdots & 2433.9 & 2666.29 \\ 96.06 & 0 & \cdots & 2525.47 & 2759.9 \\ \cdots & \cdots & 0 & \cdots & \cdots \\ 2433.9 & 2525.47 & \cdots & 0 & 310.74 \\ 2666.29 & 2759.92 & \cdots & 310.74 & 0 \end{bmatrix}. \quad (8)$$

According to the difference between the user registration place and the place mentioned by microblog, it can be divided into 4 cases: ① Both the user registration place and the place mentioned in microblog are in China. ② The user registration place is in China, but the place mentioned in microblog is not. ③ The user registration place is not in China, but the place mentioned in microblog is. ④ Neither the user registration place nor the place mentioned in microblog is in China. Since most of Weibo rumors occur in China, the current research is mainly focused on case ①. In cases ②, ③, and ④, the distance would be set to 10000, which indicates the maximum threshold.

3.4. Feature Selection. In order to test the validity of the basic features and new features, we use Chi-square test to obtain the feature ranking results, as shown in Table 1.

As shown in Table 1, the Regional Correlation, Emotional Consistency, and User Credibility are ranked 3rd, 5th, and 9th, so the three new features we constructed are valid.

Two sets of control experiments are conducted on different models. One is that which is based on the new features and adds features one by one according to the features ranking results. In the other experiment, feature sets are added one by one according to the features ranking results. The experimental results are shown in Figures 3 and 4.

As illustrated in Figures 3 and 4, as the number of features in the feature set increases, the model's recognition accuracy gradually increases, but when the features exceed a certain number, the model's recognition accuracy tends to decrease.

In Figure 3, the accuracy of Naive Bayes is highest when the number of features is increased to 15; and when the number of features is increased from 3 to 12, the accuracy of SVM is significantly higher than that of Decision Tree. When the number of added features exceeds 12, the accuracy of Decision Tree starts to exceed SVM. As the number of features continues to increase, the accuracy of the Random Forest model continues to increase, but the accuracy decreases as the number of features exceeds 21. In general, the results of each model are the best when the number of features is around 13–14.

In Figure 4, the result is not much different from the result of Figure 3. The number of features in the feature set with better results is mostly around 16. In summary, we use the first 16 features shown in Table 1 as the feature set. The final feature set used in rumor recognition is shown in Figure 5.

3.5. Classification Algorithm. The Stacking method is adopted as a combination strategy of ensemble learning in

TABLE 1: Features ranking results.

Ranking	Description	Score
1	Verified	477.060
2	Time span	358.353
3	Regional correlation	305.972
4	The number of friends	268.123
5	Emotional Consistency	255.905
6	User Influence	159.063
7	The number of microblogs	147.373
8	The number of #	78.590
9	User Credibility	65.372
10	The number of mutual followers	47.535
11	The number of followers	36.855
12	The number of @	25.129
13	The number of reports	10.981
14	Picture	6.679
15	The length of text	6.468
16	The number of likes	5.991
17	The number of exclamation marks	5.841
18	The number of negative words	5.722
19	User information integrity	3.279
20	Personal description	3.279
21	The length of username	2.824
22	The number of positive words	2.058
23	Gender	1.604
24	The number of comments	1.546
25	The number of question marks	1.160
26	The number of favourite microblogs	0.652
27	User activity	0.309

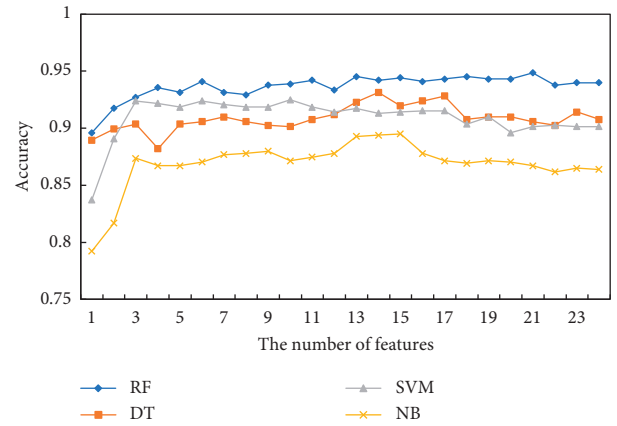


FIGURE 3: Based on the new features.

this paper. We select SVM, Random Forest, and Naive Bayes as the primary learners and logistic regression as the meta-learner. SVM uses the hinge loss function to calculate surrogate loss, which makes it sparse. At the same time, it considers the minimization of the empirical risk and the structural risk to make it stable [22], so it has better generalization ability and a smaller computational cost when using kernel function [17]. Random Forest can estimate missing data and balance errors for imbalanced data [18]. When the correlation between attributes is small, the performance of the NB model is better. The model construction is shown in Figure 6.

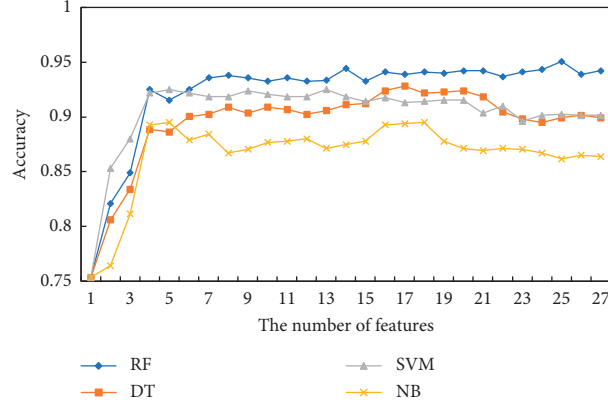


FIGURE 4: According to the features ranking.

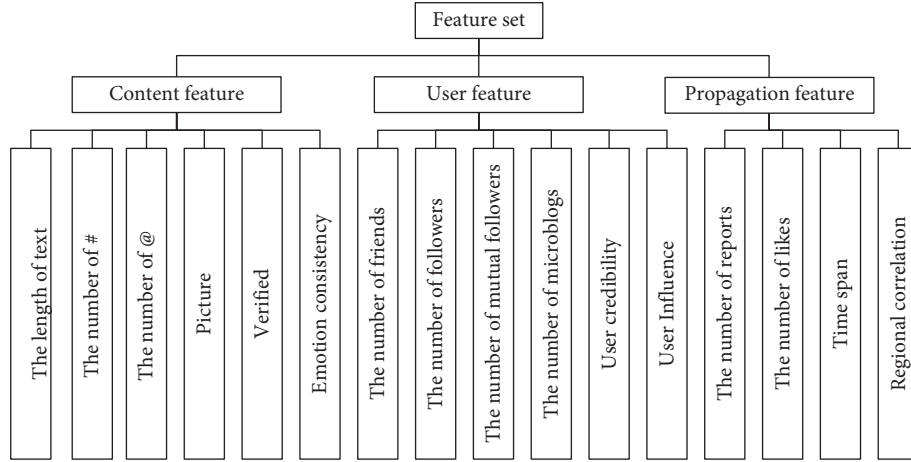


FIGURE 5: Final feature set.

The specific algorithm is described in Algorithm 1.

While time complexities of random forest and logistic regression model are $O(n \log n)$ and $O(n \cdot k + k)$ (where k is the number of features), that of SVM determined by the kernel function and Naive Bayes can reach $O(n^3)$. According to the strategy of the Stacking model, its time complexity equals the maximum value among the primary learners and metalearner. Therefore, the time complexity of Algorithm 1 is $O(n^3)$.

4. Experiment and Analysis

4.1. Dataset. We use the data from Ma et al. [23], which contain 2313 rumor events and 2351 nonrumor events, about 3.8 million pieces of microblog information, and 2.7 million pieces of user information. In the experiment, we split the dataset into training set and test set according to the proportion of 8:2.

At the same time, in order to verify the validity of the method in this paper on actual network data, we collected data on the Weibo platform and established an empirical database. The datasets used for empirical study in this paper are shown in Table 2.

4.2. Algorithm for Comparison. To verify the validity of the method proposed in this paper, we compare the following methods with our models: tanh-RNN [23], the method used in the paper where the data source is; SVM [20], the first method used in Weibo rumor recognition; Decision Tree J48 [8], the first method used in Twitter fake information recognition; AdaBoost and Random Forest, representative ensemble learning methods; and the method proposed in this paper. SVM and Decision Tree J48 are usually used as a benchmark for Internet rumor recognition in most research works.

4.3. Experimental Procedures

- Feature set comparison: based on the recognition model proposed in this paper, we conduct experiments on different feature sets to verify the validity of the new features proposed in this paper
- Algorithm comparison: in order to measure the accuracy and generalization ability of the recognition method proposed in this paper, we compared different algorithms through the accuracy, precision, recall, and F1-score

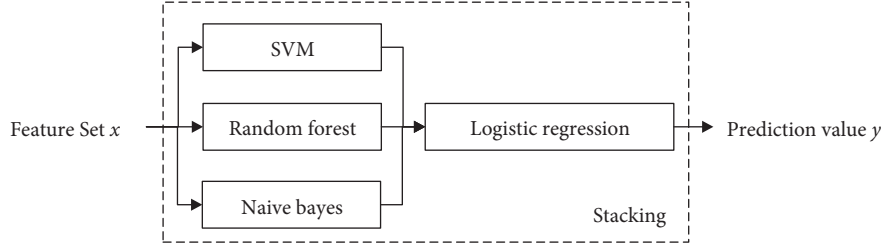


FIGURE 6: The model construction.

Input: a Weibo set $\mathbf{W}\{\mathbf{m}_1, \mathbf{m}_2, \mathbf{m}_3, \dots, \mathbf{m}_n\}$

Output: the confidence value y_i of \mathbf{m}_i

Step 1: extract features of \mathbf{m}_i as shown in Figure 5

Step 2: calculate user credibility of \mathbf{m}_i

Step 3: segment \mathbf{m}_i and its comments, and calculate emotion consistency of \mathbf{m}_i

Step 4: calculate regional correlation of \mathbf{m}_i

Step 5: standardize each feature of \mathbf{m}_i

Step 6: split the preprocessed data set into train set, test set and validation set, and input them into SVM, RF, and Naïve Bayes model

Step 7: input the new feature set in step 6 into logistic regression model

Step 8: calculate the accuracy, precision, recall and F1-score of the Stacking model

ALGORITHM 1: Weibo rumor recognition method based on stacking.

TABLE 2: Empirical study data.

Event	The number of Weibo	The number of users
Doctor accident	3,057	1,424
2019-nCoV	3,091	1,223
Community fire	2,447	896

- (c) Algorithm execution time comparison: we compare the training time and test time in different models to analyse model performance
- (d) Empirical analysis: the practicality of the recognition method proposed in this paper is verified by conducting experiments on the latest events

4.4. Feature Set Comparison. In this paper, we compare different feature sets by using the recognition model proposed in this article. The experimental results are shown in Table 3 (\mathbf{F}_{CONT} is the Content Features set, \mathbf{F}_{USER} is the User Features set, \mathbf{F}_{PROP} is the Propagation Features set, UCRE is the User Credibility, ECON is the Emotional Consistency, ROC is the Regional Correlation, and \mathbf{F}_{SIFT} is the Features Set shown in Figure 5).

Table 3 shows that the accuracy rate of using \mathbf{F}_{CONT} for Weibo rumor recognition is as low as 70%, which indicates that it is difficult to detect rumors in the more complicated content. Compared with only relying on \mathbf{F}_{CONT} for recognition, the recognition results by using \mathbf{F}_{USER} and \mathbf{F}_{PROP} are better; in particular, the accuracy is improved by 20%. In the experimental results of $\mathbf{F}_{\text{CONT+TRAN}}$, $\mathbf{F}_{\text{USER+TRAN}}$, and $\mathbf{F}_{\text{CONT+USER}}$, we can see that their accuracy is 0.2%, 1.9%, and 2.6% lower than that of \mathbf{F}_{SIFT} , respectively. The accuracy of $\mathbf{F}_{\text{CONF+SENT+LOC}}$, which is composed of only three new features constructed in this paper, is as high as 90.8%, which shows that the three new

features of User Credibility, Emotional Consistency, and Regional Correlation constructed in this paper have good effect on Weibo rumor recognition. However, the experimental results of $\mathbf{F}_{\text{SIFT-CONF-SENT-LOC}}$ without three new features are lower than those of \mathbf{F}_{SIFT} , and the accuracy of \mathbf{F}_{SIFT} is 93%. The accuracy and recall rate of rumor and nonrumor recognition are all over 90%, and the F1-score is also stable at 93%. The feature set proposed in this paper has higher values than other feature sets, which indicates that our feature set is more effective to detect Weibo rumors.

In order to validate the effectiveness of each feature in \mathbf{F}_{SIFT} selected in this paper, applying the rumor recognition method based on Stacking, we conduct 16 different experiments on \mathbf{F}_{SIFT} with one feature removed every time. The results are shown in Table 4.

As is shown in Tables 3 and 4, the accuracy in each experiment is lower than that of \mathbf{F}_{SIFT} ; and the rumor recognition accuracy based on the feature set without the regional correlation is the lowest, which indicates that the Regional Correlation has the biggest impact on the recognition results. In conclusion, the 16 features selected in this paper have a positive effect on rumor recognition.

4.5. Algorithm Comparison. We compare different algorithms with the rumor recognition model proposed in this paper to illustrate the accuracy and generalization ability of the model we proposed. The results are shown in Table 5.

As shown in Table 5, compared with tanh-RNN, SVM, and Decision Tree J48, the Stacking model has the highest accuracy rate of 93.5%. The Stacking model can recognize rumor with 96.5% recall rate and 91.4% precision, which shows that the model can recognize more rumors; and the Stacking model can recognize nonrumor events with 93%

TABLE 3: Feature set comparison results.

Feature set	Class	Accuracy	Precision	Recall	F1-score
F_{CONT}	N	0.704	0.662	0.783	0.717
	R		0.760	0.631	0.690
F_{USER}	N	0.913	0.938	0.877	0.906
	R		0.893	0.947	0.919
F_{PROP}	N	0.921	0.954	0.877	0.914
	R		0.895	0.961	0.927
$F_{\text{USER+PROP}}$	N	0.932	0.960	0.897	0.927
	R		0.911	0.933	0.932
$F_{\text{CONT+PROP}}$	N	0.916	0.945	0.877	0.910
	R		0.894	0.953	0.922
$F_{\text{CONT+USER}}$	N	0.909	0.929	0.877	0.902
	R		0.892	0.938	0.915
$F_{\text{SIFT-UCRE-ECON-RCO}}$	N	0.922	0.950	0.884	0.915
	R		0.899	0.957	0.927
$F_{\text{UCRE+ECONS+RCO}}$	N	0.908	0.909	0.897	0.903
	R		0.907	0.918	0.912
F_{SIFT}	N	0.935	0.960	0.902	0.930
	R		0.914	0.965	0.939

TABLE 4: The effectiveness of each feature in F_{SIFT} .

Ranking	Removed	Class	Accuracy	Precision	Recall	F1-score
1	The number of friends	N	0.9344	0.9573	0.9038	0.9298
		R		0.9159	0.9630	0.9388
2	The number of #	N	0.9344	0.9552	0.9060	0.9300
		R		0.9175	0.9609	0.9387
3	Emotional Consistency	N	0.9343	0.9531	0.9083	0.9301
		R		0.9191	0.9588	0.9386
4	The number of mutual followers	N	0.9335	0.9577	0.9028	0.9294
		R		0.9131	0.9630	0.9373
5	The number of followers	N	0.9334	0.9551	0.9038	0.9287
		R		0.9157	0.9609	0.9378
6	The number of @	N	0.9334	0.9487	0.9105	0.9292
		R		0.9206	0.9547	0.9374
7	Picture	N	0.9334	0.9529	0.9060	0.9289
		R		0.9173	0.9588	0.9376
8	Verified	N	0.9332	0.9508	0.9083	0.9291
		R		0.9190	0.9568	0.9375
9	User Credibility	N	0.9332	0.9508	0.9083	0.9291
		R		0.9190	0.9568	0.9375
10	The number of microblogs	N	0.9331	0.9541	0.9060	0.9294
		R		0.9180	0.9612	0.9391
11	The length of text	N	0.9325	0.9507	0.9060	0.9278
		R		0.9172	0.9568	0.9366
12	User Influence	N	0.9325	0.9550	0.9016	0.9275
		R		0.9139	0.9609	0.9368
13	The number of reports	N	0.9303	0.9505	0.9016	0.9254
		R		0.9136	0.9568	0.9347
14	The number of likes	N	0.9303	0.9401	0.9128	0.9262
		R		0.9218	0.9465	0.9340
15	Time span	N	0.9293	0.9441	0.9060	0.9247
		R		0.9167	0.9506	0.9333
16	Regional Correlation	N	0.9175	0.9405	0.8837	0.9112
		R		0.8986	0.9486	0.9229

TABLE 5: Algorithm comparison results.

Algorithm	Class	Accuracy	Precision	Recall	F1-score
SVM	N	0.917	0.917	0.911	0.914
	R		0.918	0.924	0.921
NB	N	0.813	0.819	0.815	0.817
	R		0.808	0.812	0.810
RF	N	0.935	0.945	0.917	0.931
	R		0.926	0.951	0.938
LR	N	0.905	0.918	0.873	0.898
	R		0.893	0.928	0.910
J48	N	0.923	0.916	0.931	0.920
	R		0.933	0.922	0.926
tanh-RNN	N	0.873	0.956	0.782	0.861
	R		0.816	0.964	0.884
DT-rank	N	0.732	0.726	0.749	0.737
	R		0.738	0.715	0.726
CAMI	N	0.933	0.945	0.921	0.932
	R		0.921	0.945	0.933
Stacking	N	0.935	0.960	0.902	0.930
	R		0.914	0.965	0.939

TABLE 6: Algorithm execution time results.

Time Algorithm	Training time (ms)	Testing time (ms)
SVM	2434.3073	24.2662
J48	32.0261	0.3138
NB	1.9568	0.9729
LR	15.342	0.2064
AdaBoost	2544.4393	31.1073
RF	532.5212	16.4673
Stacking	7954.252	0.0765

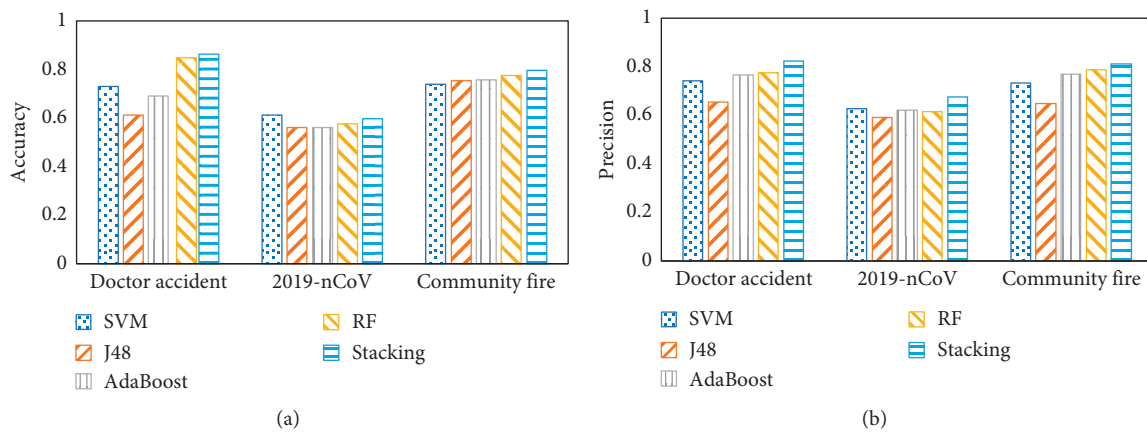


FIGURE 7: Continued.

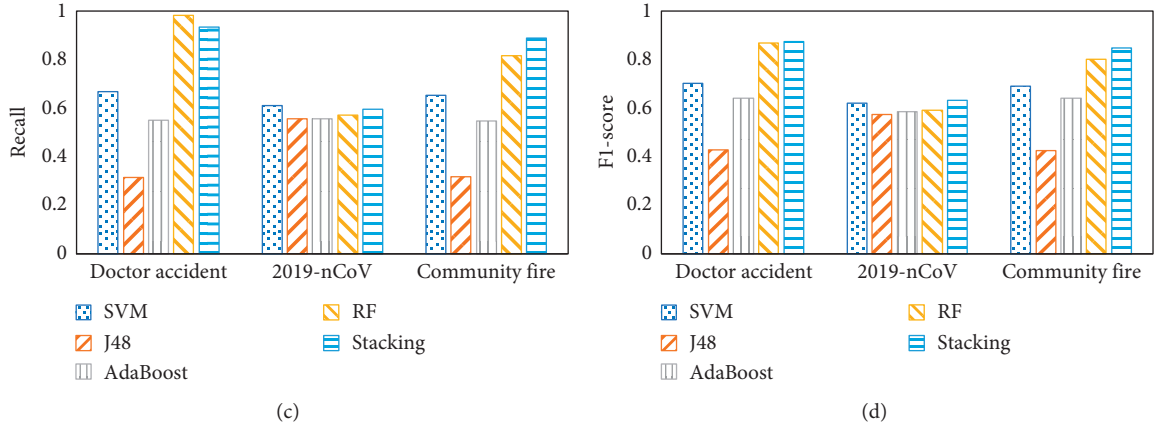


FIGURE 7: Empirical analysis results-Stacking.

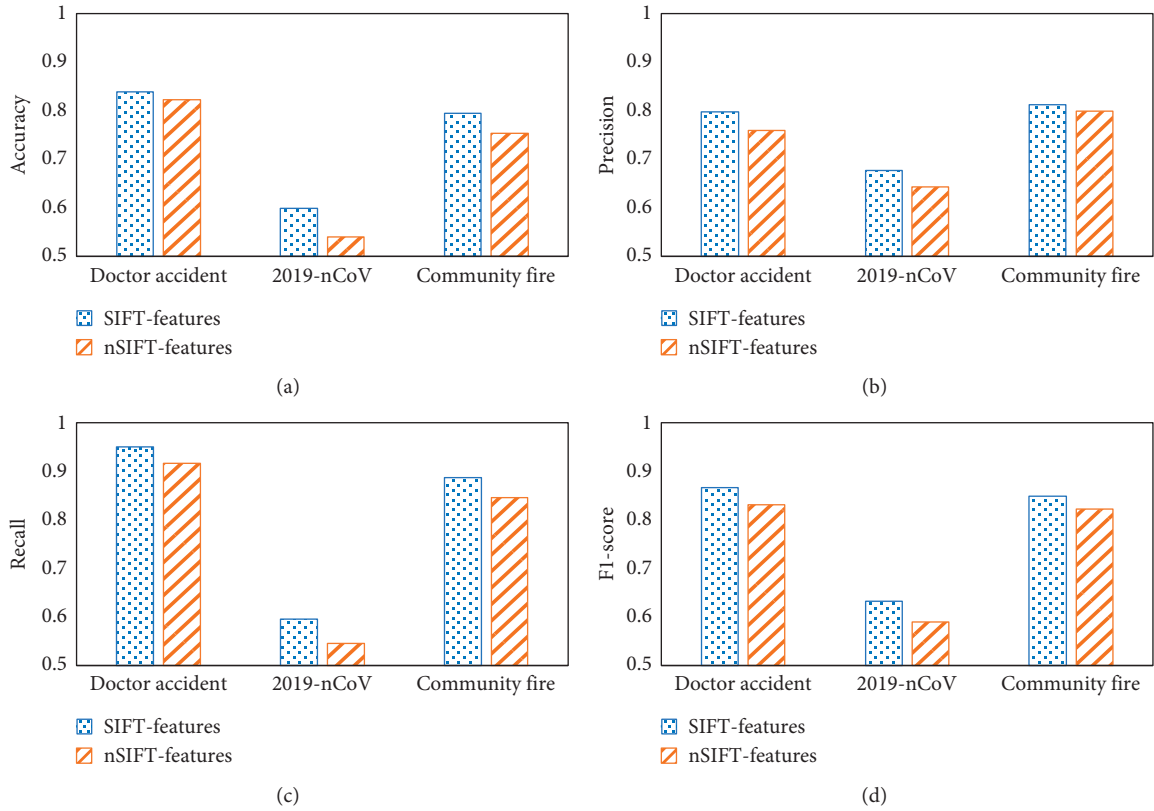


FIGURE 8: Empirical analysis results-feature set.

F1-score and recognize rumor with 93.9% F1-score, which are higher compared with other algorithms. The above results show that the Stacking model proposed in this paper has the best recognition effect.

4.6. Algorithm Execution Time. We calculate the training time and test time of each algorithm separately, and the results are shown in Table 6.

Table 6 shows that the Naive Bayes algorithm takes the shortest time in training, but the Stacking model proposed in

this paper takes the longest time in training because it ensembled multiple algorithms. In the testing phase, the Stacking model takes the shortest time, which only accounts for 7.8% of Naive Bayes, and the second shortest logistic regression model is 2.7 times longer than the Stacking model.

4.7. Empirical Analysis. In order to verify the practicability of the Weibo rumor recognition method proposed in this paper, we use three events for experimenting (see Table 2), and the results are shown in Figure 7.

Figure 7 shows that, in different events, the performance of each model is a little different. RF has 98% recall and 77% accuracy, which indicates that the RF model may recognize most nonrumor Weibo as rumor. Although the Stacking model has 93% recall and 80% accuracy, it is higher than other models. Therefore, the model proposed in this paper is relatively effective in actual recognition.

Besides, in order to verify the effectiveness of the new features proposed in this paper, the comparative experiments are conducted on the feature set with UCRE, ECON, and RCO, and the feature set excludes them. The results are shown in Figure 8.

As illustrated in Figure 8, evaluating on the accuracy, precision, recall, and F1-score, the Stacking model implemented on the feature set with UCRE, ECON, and RCO performs better. In conclusion, the new features proposed in this paper are suitable for actual rumor recognition.

5. Conclusion

In this paper, based on previous studies, three new features are constructed by combining the 5W's Formula in communication; and we obtain the optimal feature set of Weibo rumor recognition through the Chi-square test and other methods. Then, based on the idea of the Stacking method, we select SVM, Random Forest, and Naive Bayes as the primary learner and logistic regression as the metalearner to model and analyse the Weibo rumor recognition. The experimental results show that the features constructed in this paper and the proposed recognition method can effectively detect rumors in Weibo.

However, there are still some shortcomings in this paper. For example, in the case of 2019-nCov, while the content information is more complex and the amount of information is larger, the performance of the algorithm proposed in this paper is worse than that of the other two events. Therefore, it is necessary to carry out deeper semantic mining of microblog text content; for example, the content and emotion of the text using phonetic transcription abbreviations need to be specially processed. In addition, designing a more suitable and effective integration strategy of classification algorithms for Weibo rumor recognition is one of the future works. Besides, detecting rumors with Weibo text information is worthy of further study.

Data Availability

The experiment was conducted with open dataset, which can be downloaded at <http://alt.qcri.org/wgao/data/rumdect.zip>.

Conflicts of Interest

The authors declare that there are no conflicts of interest regarding the publication of this paper.

Acknowledgments

This work was supported by the Research on Cyber Group Events Management and Pre-Warning Mechanism, National Social Science Fund of China (17XFX013).

References

- [1] W. P. Liu and S. M. Zhong, "Web malware spread modelling and optimal control strategies," *Science Reports*, vol. 7, p. 42, 2017.
- [2] Z. H. Xie, Y. Zhang, and L. Zhang, "The recognition of public opinion viruses of micro-blog based on logistic regression," *Microcomputer & Its Applications*, vol. 36, no. 16, pp. 67–69, 2017.
- [3] W. Liu, X. Wu, W. Yang, X. Zhu, and S. Zhong, "Modeling cyber rumor spreading over mobile social networks: a compartment approach," *Applied Mathematics and Computation*, vol. 343, pp. 214–229, 2019.
- [4] W. A. Peterson and N. P. Gist, "Rumor and public opinion," *American Journal of Sociology*, vol. 57, no. 2, pp. 159–167, 1951.
- [5] N. P. Chao and X. Huang, "Research on "rumors" phenomenon in Internet communication," *Information Studies: Theory & Application*, vol. 27, no. 6, pp. 586–589, 2004.
- [6] G. He, X. Q. Lv, Z. Li, and L. P. Xu, "Automatic rumor identification on Microblog," *Library and Information Service*, vol. 57, no. 23, pp. 114–120, 2013.
- [7] C. Castillo, M. Mendoza, and B. Poblete, "Information credibility on twitter," in *Proceedings of the 20th International Conference on World Wide Web*, pp. 675–684, New York, NY, USA, 2011.
- [8] V. Qazvinian, E. Rosengren, D. R. Radev, and Q. Z. Mei, "Rumor has it: identifying misinformation in Microblogs," in *Proceedings of the 2011 Conference on Empirical Methods in Natural Language Processing*, pp. 1589–1599, New York, NY, USA, 2011.
- [9] S. Kwon, M. Cha, and K. Jung, "Rumor detection over varying time windows," *PLoS One*, vol. 12, no. 1, pp. 1–19, 2017.
- [10] T. Chen, X. Li, H. Yin, and J. Zhang, "Call attention to rumors: deep attention based recurrent neural networks for early rumor detection," *Lecture Notes in Computer Science*, vol. 41, pp. 40–52, 2018.
- [11] D. G. Duan, C. S. Wang, Z. M. Han, and B. Li, "A rumor detection model based on Weibo's reviews," *Computer Simulation*, vol. 33, no. 1, pp. 386–390, 2016.
- [12] Y. F. Chen, X. Y. Zhou, and L. Zhang, "Research on the methods to identify online food safety rumor-related documents based on semantic co-occurrence matching," *Information Studies: Theory & Application*, vol. 41, no. 6, pp. 130–136, 2018.
- [13] T. Q. Lu, B. Shi, and Z. M. Yan, "Semi-supervised learning algorithm applied to Microblog rumors detection," *Application Research of Computers*, vol. 33, no. 3, pp. 744–748, 2016.
- [14] W. Dong and X. H. Yue, "The weighted multiple meta-models stacking method for regression problem," *Proceedings of the 38th Chinese Control Conference*, vol. 33, pp. 7511–7516, 2019.
- [15] Q. Xie, Z. T. Liu, and X. W. Ding, "Electroencephalogram emotion recognition based on a stacking classification model," *Proceeding of the 37th Chinese Control Conference*, vol. 41, pp. 5544–5548, 2018.
- [16] J. D. Duan, S. R. Liu, K. Ma, and R. Y. Sun, "Text sentiment classification method based on ensemble learning," *Journal of Jinan University (Natural Science Edition)*, vol. 33, no. 6, pp. 43–488, 2019.
- [17] K. P. Kota and G. V. S. R. Anjaneyulu, "A comparative analysis of support vector machines & logistic regression for propensity based response modeling," *Social Science Electronic Publishing*, vol. 4, no. 3, pp. 7–16, 2015.

- [18] C. Su, S. Ju, Y. Liu, and Z. Yu, "Improving random forest and rotation forest for highly imbalanced datasets," *Intelligent Data Analysis*, vol. 19, no. 6, pp. 1409–1432, 2015.
- [19] H. Li, *Statistical Learning Methods*, Tsinghua University Press, Beijing, China, 2016.
- [20] F. Yang, X. H. Yu, Y. Liu, and M. Yang, "Automatic detection of rumor on sina Weibo," *Proceedings of the ACM SIGKDD Workshop on Mining Data Semantics*, vol. 19, pp. 13–20, 2012.
- [21] L. H. Xu, H. F. Lin, Y. Pan, and H. Ren, "Constructing the affective lexicon ontology," *Journal of the China Society for Scientific and Technical Information*, vol. 27, no. 2, pp. 180–185, 2008.
- [22] Z. H. Zhou, *Machine Learning*, Tsinghua University Press, Beijing, China, 2016.
- [23] J. Ma, W. Gao, P. Mitra, and S. Kwon, "Detecting rumors from Microblogs with recurrent neural networks," *Proceedings of the 25th International Joint Conference on Artificial Intelligence*, vol. 27, pp. 3818–3824, 2016.

Research Article

A Subjective Expressions Extracting Method for Social Opinion Mining

Mingyong Yin ^{1,2} Haizhou Wang ^{3,4} Xingshu Chen ^{3,4} Hong Yan,^{3,4} and Rui Tang³

¹College of Computer Science, Sichuan University, Chengdu, China

²Institute of Computer Application, Mianyang, China

³College of Cybersecurity, Sichuan University, Chengdu, China

⁴Cybersecurity Research Institute, Sichuan University, Chengdu, China

Correspondence should be addressed to Haizhou Wang; whzh.nc@scu.edu.cn

Received 3 May 2020; Accepted 29 May 2020; Published 26 August 2020

Guest Editor: Qingyi Zhu

Copyright © 2020 Mingyong Yin et al. This is an open access article distributed under the Creative Commons Attribution License, which permits unrestricted use, distribution, and reproduction in any medium, provided the original work is properly cited.

Opinion mining plays an important role in public opinion monitoring, commodity evaluation, government governance, and other areas. One of the basic tasks of opinion mining is to extract the expression elements, which can be further divided into direct subjective expression and expressive subjective expression. For the task of subjective expression extraction, the methods based on neural network can learn features automatically without exhaustive feature engineering and have been proved to be efficient for opinion mining. Constructing adequate input vector which can encode sufficient information is a challenge of neural network-based approach. To cope with this problem, a novel representation method that combines the different features with word vectors is proposed. Then, we use neural network and conditional random field to train and predict the expressions and carry out comparative experiments on different methods and features combinations. Experimental results show the performance of the proposed model, and the F value outperforms other methods in comparative experimental dataset. Our work can provide hint for further research on opinion expression extraction.

1. Introduction

Information retrieved from social network not only includes the objective facts of events but also contains the opinions expressed by the people, organizations, or the media. Sometimes, the relevant opinions of events are worthier than the events themselves. The main opinions on events often need to be tracked, analyzed, and extracted manually, which is time-consuming and laborious. It is difficult to quickly locate and extract the views conveyed in news events from huge amounts of information. If we can automatically mine and extract all relevant opinion information of these news events and then dig out the main viewpoints, it will be helpful to understand the attitudes and positions of related parties towards the events, so that public opinion monitoring and analysis can go deep into the viewpoint level from the facts level and then further improve the monitoring and

understanding of public opinion on events. In a word, the opinion mining is of great significance to the monitoring and analysis of public opinion in social network.

The level of opinion mining can be divided into word level, sentence level, and text level. Word level methods tend to focus on the attitudes, opinions, and sentiment polarity contained in the words themselves. The common mechanisms are to search approximate words heuristically according to the existing opinion word seeds, expand the original opinion lexicon, and then judge view sentences according to the vocabulary. Text-level mining methods often evaluate the emotional tendency by extracting viewpoint sentences from the text and synthesizing multiple viewpoint sentences.

Sentence-level opinion mining methods not only make better use of context but also find out subjectivity expression elements, opinion holders, entities, view content, sentiment polarity, and emotional strength in more detail. Therefore,

this paper uses sentence to carry out the research of opinion expression extraction.

In general, the elements of opinion sentences include subjective expression elements, opinion holders, entities, opinion content, sentiment polarity, and emotional intensity [1]. Among them, subjective expression is the core of opinion; it expresses the personal attitude and emotion towards related event of opinion holders, which is composed of words or phrases that contain emotional, evaluative, and speculative information. There may be more than one viewpoint in an opinion sentence. These viewpoints are marked by subjective expressive elements and have emotional tendencies and intensity. Moreover, the subjective expressive elements can be divided into direct subjective expressions (DSE) and expressive subjective expressions (ESE). Contrary to the subjective expressive elements, objective expression is used to state objective facts. Figure 1 shows the classification of expression elements.

The key difference between DSE and ESE is that the former explicitly gives a subjective expression and its source, while the latter presupposes a subjective expression and its source but does not introduce them. For instance, the sentence “She insists that the screen of the new phone is so cool” is typical DSE. When annotating and identifying these elements, they need to be closely combined with the context to avoid ignoring more implicit elements.

Due to the diversity of linguistic expressions and the missing of opinion elements, identifying and extracting freely or implicitly subjective expression is hard to tackle. Automatic recognition of subjective expression extraction is still a challenging task that needs to be further researched.

The main contributions of this paper are summarized as follows:

- (1) A subjective factor extraction model based on neural network and CRF is proposed, which can support DSE and ESE extraction, and achieves better recognition results on open data sets.
- (2) This paper proposes a semantic representation method based on word vectors, which combines lexical and named entity features. It can capture sentence information and input it into the neural network model for feature recognition.
- (3) Contrast experiments are carried out on the experimental data, and the differences, advantages, and disadvantages of different subjective factor extraction methods are fully compared and analyzed, which can provide reference for the follow-up study.

The article is organized as follows. Section 2 gives a brief introduction to the related research. Section 3 focuses on the methods proposed in this paper. In Section 4, the experiment and analysis are carried out, and the conclusion is given in Section 5.

2. Related Work

News report is generally objective; it can describe the objective facts, the opinions of the parties concerned, and even

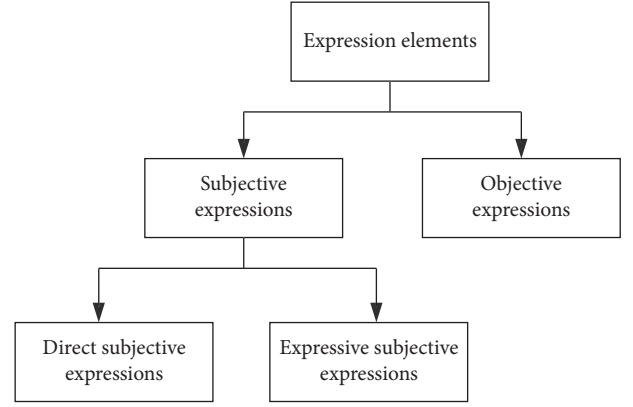


FIGURE 1: Schematic diagram of expressive elements classification.

the attitude and tendency of the authors themselves. Generally, a news report may include multiple opinions from many opinion holders on different targets. Extracting opinion sentences and searching for subjective expression elements, opinion holders, target objects, sentiment polarity, and intensity are the subtasks of opinion mining [2–5].

Kim and Hovy first use semisupervised method to mine opinion words, sentiment polarity, and opinion holders [6]. They use WordNet to find the closest synonyms from the seed vocabulary with three emotional polarities, identify the viewpoint words and their polarities in the text, and then use the maximum entropy classifier to identify the viewpoint holder according to the syntactic characteristics. Another work they contributed is to identify opinion expression elements, opinion holders, and content through semantic role tagging (SRT) [7]. First, they summarize the semantic roles of the three elements and construct corpus. Then, they determine the semantic roles of words in the text through maximum entropy classifier and then determine the three opinion elements in news text.

Weibe et al. define opinion sentences in news texts as sentences that express private state for opinion holders [1]. Private state is often expressed by words or phrases, which are called subjective expressive elements with certain sentiment polarity and intensity. According to the definition, they tagged Multiperspective Question Answering (MPQA) corpus of news text for opinion mining and made many subsequent studies based on MPQA. Breck et al. [8] transform the recognition of subjective expressive elements of views into sequential tagging task. Conditional random field (CRF) is used to identify subjective expressive elements by combining word features, part-of-speech features, lexical features, and WordNet. It is found that the characteristics of WordNet play a significant role in improving the recall rate, and subjective expression factors often appear in a pile.

Yang and Cardie [5] used Semi-Markov Conditional Random Field (Semi-CRF) to identify subjective expressive elements in sentences, which is innovative in dealing with phrase level rather than word level. Semi-CRF allows the acquisition of features from clause sequences. It can deal with the boundary better, but the time complexity of the method is relatively high.

Later research extends to a variety of opinion elements, not only to the identification of subjective expression elements, but also to the identification of elements such as sentiment polarity,

intensity, opinion holders, and target entities. Fine-grained elements extraction further deepens the research level of opinion mining. Johansson and Moschitti combined syntactic and semantic features to identify subjective expression elements and their polarity [9]. With more and more research on extraction of multiple opinion elements, many joint extraction methods have been proposed. Choi et al. [10, 11] proposed two methods: one is to combine CRF with Integer Linear Programming (ILP) and the other is to use hierarchical parameter sharing technology CRF.

With the breakthrough of deep learning in the field of natural language processing, researchers have applied it to opinion mining. Irsoy et al. introduce recursive neural network (RNN) to identify subjective expression elements, opinion holders, and target objects. The experimental results show that the combination of bidirectional recursive neural network and bidirectional recurrent neural network can perform better in multiple subtasks. Then a multilayer cyclic neural network model [4] is proposed to identify the subjective expression elements, and it is found that the relatively narrow and deep cyclic neural network performs better.

Wang et al. [12] use bidirectional long short-term memory (BiLSTM) to identify subjective expression elements and explored the internal mechanism of long short-term memory (LSTM). It was found that LSTM has better adaptability to context than regular RNN. Du et al. used the model of multilayer BiLSTM combined with attention mechanism [13] to detect subjective expression factors. Experiments show that attention mechanism helps to link information in context. Zhang et al. [14] proposed a model based on encoder-decoder to jointly mine the relationship between opinion elements.

Compared with traditional machine learning methods, the method of extracting opinion elements based on neural network usually uses word vectors as features directly and does not need to construct a large number of complex features artificially, so as to reduce the dependence of the model on the features artificially constructed. Based on the compound model of bidirectional long-term and short-term memory network and conditional random field, this paper combines the advantages of both to extract more accurate subjective expression elements.

To sum up, whether based on CRF, neural network model, or combine different levels of lexical and syntactic features, subjectivity expression extraction will confront the problem of insufficient comprehensiveness and accuracy. How to make full use of the advantages of various methods and more rich features to improve extraction performance still needs to be further researched.

3. Subjective Expression Extraction Model

In this section, we go deep into the construction of subjective expression extraction model, using combination of BiLSTM and CRF with multiple features to predict the optimal tag sequence of opinion elements according to the context of each sentence in the document. The flow chart is shown in Figure 2. It is divided into four steps, which are described as follows:

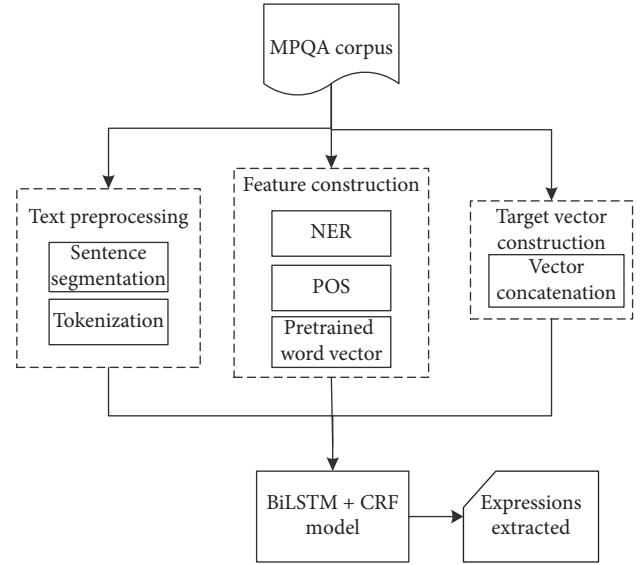


FIGURE 2: Elements extraction flow of opinion expression.

- (1) Text preprocessing: the CoreNLP natural language processing tool of Stanford University is used for sentence cut, tokenization, and stemming of the documents in the corpus.
- (2) Feature construction: we adopt pretrained word vectors, part of speech (PoS), and Named Entity Recognition (NER) as sentence feature for semantic representation. The CoreNLP tool is used to identify PoS and NER types of words in text and transform them into corresponding feature vectors. In this paper, we use the 300-dimensional word vectors published by Google Word2vec, whose training corpus is the Google News dataset containing hundreds of billions of words.
- (3) Target vector construction: we take subjective expression extraction task as a sequential annotation problem and the input vector can keep the order information of sentence by concatenation of three features. By encoding each feature with numerical vector, we can convert the sentence of each text into the target vector for model training.
- (4) Model training: we use the constructed features and target vectors to fit the model and obtain the optimal parameters by iteration. Then, the optimal model is acquired and can be used to expression extraction task.

3.1. Feature Construction

3.1.1. Word Vector Feature. After text preprocessing, each sentence is composed of word sequences $[w_1, w_2, \dots, w_i, \dots, w_n]$, w_i representing the i th word in the sentence, and the total number of words in sentence is n . The word sequence is transformed into the word vector sequence by mapping the word vector matrix W^{word} . The word vector of the first word in the vocabulary is calculated as follows:

$$r_j^{\text{word}} = W^{\text{word}} \times v_j. \quad (1)$$

The matrix W^{word} represents all the word vectors in the corpus vocabulary with size $|j|$; each column represents the word vector of the j th word in the vocabulary with dimension 300; v_j is a vector with size $|V|$, except the index position j of w_j in the corresponding vocabulary which is 1; the other rows are 0, that is, a one-hot vector. The word vector matrix is expressed as the parameters of the model, which can be obtained when training the model, and the pretrained word vector can be expressed as the initial word vector matrix so that word w_i in a sentence is transformed into word vector r_i^{word} in the above way.

However, not all words in the document are included in the vocabulary. This phenomenon is noted as out of vocabulary (OOV). The initial word vectors of these extra-set words will be represented by a unified UNK word vector. In this paper, a 300-dimensional word vector $[-0.01, 0.01]$ is randomly generated with normal distribution to represent UNK words. In the process of training the model, all the word vectors in the corpus are trained and fine-tuned as model parameters.

3.1.2. POS and NER Feature. Word vectors are trained with large-scale corpus, which can effectively capture the characteristics of words. Moreover, the pretrained word vectors include a certain extent of contextual information, because the pretrained word vector model usually chooses contextual words as input, such as CBOW model [15]. However, limited by corpus and training method, it is difficult to represent enough semantic information, so extra features are introduced for promotion, and then experiments will be conducted to determine whether and which is necessary to introduce other feature vectors.

Part of speech determines whether a word is a verb, noun, adjective, or another part of speech based on context information. In this paper, the CoreNLP (<http://stanfordnlp.github.io/CoreNLP/>) POS Tagger Annotator tool of Stanford University is used to annotate the POS tag of each word in the corpus text. Table 1 shows the lexical information of subjective expression elements and opinion holder elements in MPQA corpus. From Table 1, we can see that the proportion of lexical parts of DSE subjective expression elements is as high as one-half of verbs. The proportion of ESE subjective expression elements is about 40% of verbs, adjectives, and adverbs. Therefore, it is reasonable to adopt POS for the identification of opinion elements.

The POS tags of each word are obtained from POS tagging result of the dataset. For example, “Bush rejected the Kyoto pact last March” is labeled as [NNP, VBD, DT, NNP, NN, JJ, NNP]. Our research actually utilizes 45 types of POS tags.

The POS tags of each word are transformed into feature vectors using one-hot representation. Assume the corresponding part-of-speech feature vector of a word w_i is

$$r_i^{\text{pos}} = [\text{pos}_1, \text{pos}_2, \dots, \text{pos}_i, \dots, \text{pos}_n]. \quad (2)$$

TABLE 1: Part-of-speech ratio of subjective expressive elements.

POS type	DSE (%)	ESE (%)
Verb	50.29	17.71
Adverb	5.19	10.45
Adjective	5.86	13.55

The calculation of each dimension of the vector is as shown in the following:

$$\text{pos}_j = \begin{cases} 1, & \text{POS type ID of } w_i \text{ is } j, \\ 0, & \text{others.} \end{cases} \quad (3)$$

Named entity labels of each word are transformed into named entity feature vectors using one-hot representation. The feature vector of the named entity corresponding to the word w_i is $r_i^{\text{ns}} = [\text{ne}_1, \text{ne}_2, \dots, \text{ne}_j, \dots, \text{ne}_m]$, the way in which each dimension of the vector is shown in the following:

$$\text{ner}_j = \begin{cases} 1, & \text{NER type ID of } w_i \text{ is } j, \\ 0, & \text{others.} \end{cases} \quad (4)$$

NER can identify text fragments that represent specific types of entities, such as person, place, institution, and proper noun [16]. Opinion holders are people or organizations that express their opinions, so their words are more likely to belong to named entities. The CoreNLP NER tool is used to identify named entities in the corpus, the statistic proportion of named entity type about opinion holders in MPQA corpus is counted, and the results are numbered.

It can be found that nearly one-half of the opinion holder is named entity. Therefore, using type of named entity as a feature of words can be in favor of the recognition of opinion holder elements being a reasonable speculation. Twenty-four named entity types are actually used in this paper.

The table represents the number of named entity types, with value of 24 in this article. The sequence of named entity features of a sentence is expressed as $[r_1^{\text{ne}}, r_2^{\text{ne}}, \dots, r_i^{\text{ne}}, \dots, r_n^{\text{ne}}]$.

The three lexical features of each word, word vector, POS feature, and NER are concatenated in series to construct the features of the word. By doing that, a sentence is represented as a feature sequence.

3.2. Target Vector Construction. In this paper, subjective expression extraction is considered as a sequential annotation problem. A sentence denotes a sequence in which each word has a corresponding tag for the opinion element, and nonviewpoint elements have their tag “O.” Most opinion elements are phrases or even clauses; therefore, the label of viewpoint elements not only identifies the category but also identifies the location of the word in the elements. In this paper, BIO tagging method [17] is used to represent the label of words. The type of label has B-prefix which represents the first word of opinion element and I-prefix which represents the nonheader word of opinion element. Figure 3 is an example of the BIO tag sequence corresponding to the word sequence of a sentence in DSE subjective expression element recognition, which is transformed into the target vector

[illegible]

After obtaining the tag sequence of the sentence, by transforming the sequence into the target vector in the same way with POS feature vectors and NER feature vectors construction, we can acquire the target output of the model. Each word is represented as a one-hot vector y_i , and the sequence of target vectors of sentences can be expressed as a one-hot vector. DSE subjective expression elements and ESE subjective expression elements are considered as a three-class annotation problem, so the length is set as 3.

3.3. Model Construction. The opinion extraction model we proposed is based on neural network and conditional random field, and its structure is shown in Figure 4. In this paper, feature vector $Y = [y_1, y_2, \dots, y_j, \dots, y_n]$ is used to represent sentence $[w_1, w_2, \dots, w_i, \dots, w_n]$. Context information of a text is often bidirectional and target words are related not only to previous texts but also to subsequent texts. BiLSTM is more powerful than unidirectional long- and short-term memory network in many tasks. The forward LSTM network receives the feature sequence of the order, and the output of the time t is \vec{h}_t ; the reverse LSTM network receives the input of the feature sequence in reverse order, and the output of the time t is \overleftarrow{h}_t .

The output of BiLSTM at time t is $h_t = [h_t^{\rightarrow}; h_t^{\leftarrow}]$ obtained in series. The output sequence of BiLSTM network is $H = [h_1, h_2, \dots, h_j, \dots, h_n]$. Then the context feature sequence is extracted through a linear layer using sigmoid as activation function using the following formula:

$$l_t = \sigma(W_l h_t + b_l). \quad (5)$$

In the output layer of general BiLSTM model, the output y_t of time t is decided by the current hidden unit h_t and input x_t but is independent with the output of other time. For moment t , the model expects finding the most probable label y_t based on the current input and context information. However, the label y_{t_1} at other moments has no impact on the label y_t . If there is a strong dependency relationship (for example, B-DSE should be I-DSE after B-DSE), BiLSTM cannot model these kinds of constraints, and its ultimate effect will be limited. So linear-CRF is introduced to study the relationship between tag sequences.

Line-CRF can effectively capture the relationship between adjacent elements in the output sequence. Moreover, it can find a sequence $Y = [y_1, y_2, \dots, y_j, \dots, y_n]$ with the highest probability based on $p(y_1, y_2, \dots, y_n | x)$ optimization. The result is an optimal output sequence rather than the optimal stitching of each moment, which is not available in the recurrent neural network. Our model combines the advantages of both.

The conditional probability of linear-CRF under the condition of input feature sequence and target vector sequence is defined as follows:

$$P(Y | L) = \frac{\prod_{i=1}^N \psi_i(y_{i-1}, y_i, L)}{\sum_{y' \in f(L)} \prod_{i=1}^N \psi_i(y'_{i-1}, y'_i, L)}. \quad (6)$$

The $\psi_i(y_{i-1}, y_i, L)$ is eigenfunction of linear-CRF, y_i represent the i th target vector in the target vector sequence Y , and $y' \in f(L)$ is the predicted output sequence. In training phase, the maximum likelihood estimation is used to maximize the conditional probability of formula (6). When predicting, we use Viterbi algorithm to find the most probable tag sequence, and then we acquire the output sequence of opinion elements prediction of a sentence.

The super parameters of the model are set as follows: the number of hidden units of BiLSTM is 25, the dropout of hidden layer is 0.5, and the linear layer unit is 25. These parameters are optimized through many repeated experiments. The number of iteration rounds is set to 50; we use early stopping method to monitor for preventing overfitting and stochastic gradient descent algorithm for optimization.

4. Experiment Result and Analysis

4.1. MPQA Corpus Introduction. The dataset used in the experiment is MPQA1.2 opinion mining corpus, which is constructed jointly by the University of Pittsburgh and Cornell University. It contains 535 news articles from multiple media sources, about the news events occurring between 2001 and 2002. The text fragments of each document are labeled as multiple types of tags.

4.1.1. Corpus Analysis. Before conducting experiment, we investigate the subjective expression elements in the corpus. Table 2 presents some of their statistical information. DSE represents the subjective expression elements of DSE and ESE represents the subjective expression elements of ESE.

DSE and ESE subjectivity elements account for about half of all sentences. It can be seen that news corpus does convey a considerable amount of subjective opinions. The average number of subjective elements of DSE in opinion sentences is 1.56, and more than half of the general opinion sentences have more than one DSE element. We find that a sentence often conveys its opinion information by speech events, so the number of DSEs in an opinion sentence is more than 1. The expression of ESE is flexible, and its word length is from 1 to 40. More abundant and free expression forms bring more difficult problems that need to be handled.

4.1.2. Corpus Division. This paper divides 535 articles into 400 training validation sets and 135 test sets in the same way as [13]. The training verification set is divided into training set and verification set 10 times in a 9:1 way. The test set is used for evaluation effect of the model, which is calculated by the average value of the tenfold cross-validation model.

Word	It	is	very	regrettable	that	the	United	States	has	taken
BIO tag	O	O	O	O	O	O	O	O	B-DSE	I-DSE
Target vector	[1,0,0]	[1,0,0]	[1,0,0]	[1,0,0]	[1,0,0]	[1,0,0]	[1,0,0]	[1,0,0]	[0,1,0]	[0,0,1]

Word	a	negative	stand	Masaaki	Nakajima	of	the	Earth	Japan	said
BIO tag	I-DSE	I-DSE	I-DSE	O	O	O	O	O	O	B-DSE
Target vector	[0,0,1]	[0,0,1]	[0,0,1]	[1,0,0]	[1,0,0]	[1,0,0]	[1,0,0]	[1,0,0]	[1,0,0]	[0,1,0]

FIGURE 3: Illustration of conversion from word to target vector.

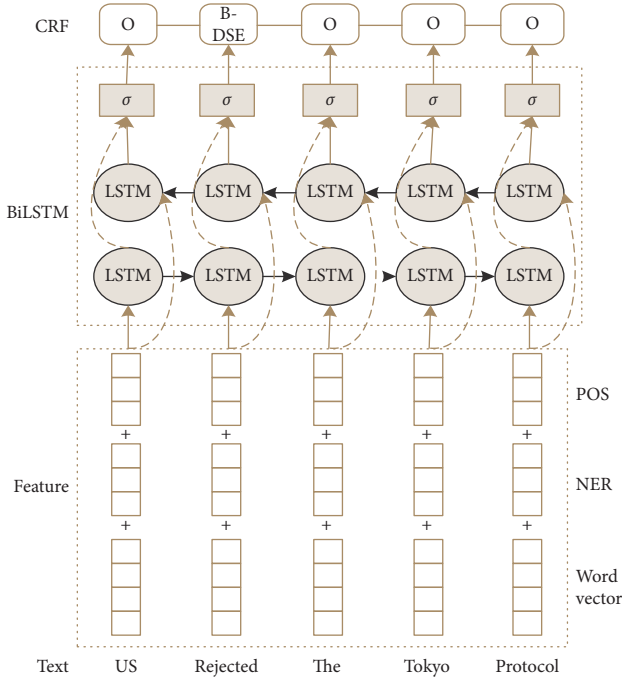


FIGURE 4: Model architecture diagram.

4.2. Evaluation Method. This paper evaluates the performance of the model by using the measurement method widely used in the field of opinion mining. In the process of annotating MPQA corpus, the annotator finds that the boundary of opinion elements cannot be determined strictly [8]. So Breck et al. [9] and Johansson and Moschitti [17] proposed two soft metrics: Binary Overlap and Proportional Overlap. Compared with the commonly used measurement methods of label boundary matching, these two methods are more efficient in evaluating the extraction effect.

In Binary Overlap metrics, if the boundaries of predictive tags and manual tags overlap, then this is a correct tag. The accuracy, recall, and F-measure of Binary Overlap are calculated by the following formulas:

$$P_{\text{binary}} = \frac{|\{p \mid p \in P \wedge \exists c \in C \text{ s.t. overlap}(c, p)\}|}{|P|}, \quad (7)$$

$$R_{\text{binary}} = \frac{|\{c \mid c \in C \wedge \exists p \in P \text{ s.t. overlap}(c, p)\}|}{|C|}, \quad (8)$$

$$F_{\text{binary}} = \frac{2P_{\text{binary}}R_{\text{binary}}}{P_{\text{binary}} + R_{\text{binary}}}. \quad (9)$$

Among them, C and P , respectively, represent the correct label set of manual labeling and the label set of model prediction and $||$ represent the number of labels of a certain expression element in each set.

Proportional Overlap measurement pays more attention to the proportion of prediction and golden label overlap than Binary Overlap measurement. It starts with measuring the degree of overlap cvrg between two markers s and s' :

$$\text{cvrg}(s, s') = \frac{|s \cap s'|}{|s'|}. \quad (10)$$

Here, $|S|$ denotes the length of the tagged word. Then, the overlap rate CVRG of two tag sets S and S' is calculated:

$$\text{CVRG}(S, S') = \sum_{s_j \in S} \sum_{s'_k \in S'} \text{cvrg}(s_j, s'_k). \quad (11)$$

Finally, the accuracy, recall rate, and F value of Proportional Overlap measure are calculated by

$$P_{\text{proportional}} = \frac{\text{CVRG}(P, C)}{|P|}, \quad (12)$$

$$R_{\text{proportional}} = \frac{\text{CVRG}(C, P)}{|C|}, \quad (13)$$

$$F_{\text{proportional}} = \frac{2P_{\text{proportional}}R_{\text{proportional}}}{P_{\text{proportional}} + R_{\text{proportional}}}. \quad (14)$$

In formulas (12) and (13), the number of markers for a certain element in each set is represented as $||$.

4.3. Multifeature Contrast Experiment. We compare the effects of each feature on the recognition of each opinion element through experiments and pursue an effective combination of features suitable for each opinion element recognition. This paper briefly describes the meanings of some words and symbols in the following experiments:

- (1) +Pretrained word vector: model with pretrained word vector as feature.
- (2) +Fine-tuning the pretrained word vector: using the pretrained word vector as the feature but in the phase

TABLE 2: MPQA corpus statistic information.

Property	DSE	ESE
Total number	9840	12273
The proportion of the opinion sentences	56.86%	55.80%
Minimum number of opinion expressions	1	1
Maximum number of expressions	8	15
Average number of opinion expressions	1.56	1.98
Minimum length of expression words	1	1
Average length of expression words	1.81	3.30
Maximum length of expression words	15	40

of model training, word vectors are updated as model parameters.

- (3) +Part-of-speech feature: the model of adding POS feature.
- (4) +Entity features: the model incorporates named entity features.

4.3.1. Subjective Expression Element Recognition of DSE. Firstly, the model is applied to the recognition of DSE subjective expression elements. Table 3 shows the result of Binary Overlap and Property Overlap when the model is combined with word vector, part-of-speech feature, named entity feature, and part-of-speech entity feature. The bold numbers represent the highest score of an evaluation method.

By looking further into Table 4, we compare the impact of each feature as follows.

- (1) The influence of fine-tuning word vectors: the accuracy of pretrained word vectors is higher without fine-tuning, but the recall rate is lower and fine-tuning has reverse effect, higher recall rate, and lower accuracy. While in DSE recognition task, the fine-tuning word vector performs slightly better than that in the case of no fine-tuning. So the trained word vectors are fine-tuned in combination with other features in later experiment.
- (2) The influence of part-of-speech features: after fine-tuning the pretrained word vector and adding part-of-speech features, the recall rate is the highest among all feature combinations with the two measurement methods, the F value under the Binary Overlap measure is the highest, and the F value under the Proportional Overlap measure is the second highest. Part-of-speech features promote the recognition effect of DSE elements.
- (3) The influence of named entity features: after fine-tuning the pretraining word vector and adding named entity features, the recall rate and F value are slightly improved under the two measures. Compared with the part-of-speech feature, it plays a less important role.
- (4) The influence of combination of part of speech and named entity features: after fine-tuning the pre-trained word vector and adding part of speech and

named entity features, the recall rate slightly increased under the two measures, the F value under Proportional Overlap was the highest, and the F value under Binary Overlap was the second highest. It is similar to the function of part of speech.

In general, the combination of fine-tuning pretraining word vectors and part-of-speech features is adequate in the recognition of DSE subjective expression elements. The combination of lexical and entity features is similar to that of individual lexical features, while named entity features have little impact on DSE recognition. Moreover, considering the complexity of the model, the additional features in the recognition of DSE subjective expression elements are only part-of-speech features. It is presumed that the DSE elements are generally shorter and the part of speech is more obvious, so the part of speech features are effective after they are added.

4.3.2. ESE Subjective Expressive Element Recognition. This paper combines the model with a variety of feature combinations and applies them to the recognition of ESE subjective expression elements. Table 3 shows the effect of using Binary Overlap and Proportional Overlap measures when the model is combined with word vector, part of speech, and named entity features to identify ESE subjective expression elements. The bold numbers represent the highest score of an evaluation method. As shown in Table 5, the impact variety of each feature can be seen.

- (1) The influence of fine-tuning word vectors: the accuracy of pretrained word vectors is higher without fine-tuning, the recall rate is lower, and the reverse is true for fine-tuning. From the F value of the two measures, the fine-tuning word vector of ESE feature recognition task is slightly more than that of non-fine-tuning task by about 3 and 2 percentage points, respectively, and the recall rate is increased by about 6 to 7 percentage points. Finely tuning the pre-training words vector improves the recognition effect of ESE elements. So the trained word vectors are fine-tuned in combination with other features.
- (2) The influence of part-of-speech characteristics: on the basis of fine-tuning the pretrained word vector and adding part-of-speech features, the accuracy of the two measures has only increased by about 1 percentage point, while the others have decreased. It is not necessary to add part-of-speech features alone.
- (3) The influence of named entity features: on the basis of fine-tuning the pretraining word vector, adding named entity features, the accuracy of the two measures only increased by about one percentage point, while the others decreased. It is not necessary to add named entity features alone.
- (4) The influence of the combination of part of speech and named entity features: after fine-tuning the pretraining word vector and adding part of speech

TABLE 3: Measurement of ESE recognition model under different feature combinations.

Feature combination	Binary Overlap			Proportional Overlap		
	Accuracy (%)	Recall (%)	F value (%)	Accuracy (%)	Recall (%)	F value (%)
+Pretrained word vectors	82.83	48.79	61.24	67.11	43.14	52.27
+Fine-tuning word vectors	75.55	56.27	64.39	60.70	49.66	54.48
+Fine-tuning word vectors + POS	76.82	54.74	63.82	62.16	48.22	54.16
+Fine-tuning word vectors + NER	76.26	54.49	63.49	62.59	47.33	53.76
+Fine-tuning word vectors + POS + NER	75.56	57.52	65.15	60.80	50.85	55.07

TABLE 4: Measurement of DSE recognition model under different feature combinations.

Feature combination	Binary Overlap			Proportional Overlap		
	Accuracy (%)	Recall (%)	F value (%)	Accuracy (%)	Recall (%)	F value (%)
+Pretrained word vectors	79.84	62.19	69.88	74.81	56.48	64.32
+Fine-tuning word vectors	75.61	65.67	70.24	70.62	59.21	64.35
+Fine-tuning word vectors + POS	74.64	67.67	70.94	69.54	61.32	65.10
+Fine-tuning word vectors + NER	74.65	67.50	70.85	69.52	61.12	65.00
+Fine-tuning word vectors + POS + NER	75.09	67.17	70.85	70.01	61.04	65.13

and named entity features, the accuracy, recall rate, and F value of the two measures are improved, and F value is the highest of all feature combinations.

In general, fine-tuning the combination of pretraining word vector, part of speech, and named entity is an effective feature in ESE subjective expression element recognition. ESE elements are generally long and contain clauses expressing opinions implicitly. These long sentences may have many types of POS and named entity phrases occurrence which can enrich context information; we presume this is the reason why named entities and part-of-speech features work together effectively.

4.4. Contrast Experiment with Other Methods

4.4.1. *Baseline Model.* This paper chooses four methods as the baseline model, listed as follows:

- (1) CRF-OE: Breck et al. [8] use conditional random fields to solve the problem of extracting subjective expression elements. Word feature (one-hot vector), syntactic feature, and semantic feature (WordNet lexicon) are used.
- (2) RecursiveNN: Irsoy and Cardie [18] use structural recurrent neural networks to identify opinion holder elements.
- (3) BSRNN: Irsoy and Cardie [4] use a multilayer bi-directional recurrent neural network (RNN) to solve the problem of extracting subjective expression elements. Except that the number of layers of bi-directional RNN is set to three layers, the hyperparameters and word vectors are maintained as well as the method in this paper.
- (4) BiLSTM: Wang et al. [12] use the BiLSTM network model to extract two subjective expression elements and super-parameters and word vectors are maintained the same.

4.4.2. *Contrast and Analysis.* The deep neural network model is compared with the baseline model in identifying the corresponding opinion elements. The results are shown in Table 5.

The experimental results show that the model we proposed has the best recognition effect on DSE, and BLSTM, BSRNN, and CRF-OE are less effective. The results show that this model is better than BSRNN model in recognizing DSE elements in nested opinion sentences. BSRNN model sometimes omits a part of DSE elements and misjudges ESE elements as DSE elements.

In ESE recognition, the most effective is our model and BSRNN. The proposed model is higher than BSRNN in Proportional Overlap metric and lower than BSRNN in Binary Overlap metric. The performance of BLSTM model is worse than that of the former two. Compared with BLSTM and BSRNN models, this model is good at correctly identifying ESE elements, and BSRNN and BLSTM are have an advantage to identify short ESEs as DSE elements.

This paper is slightly improved compared with other models. Therefore, by analyzing the recognition results of multiple models, it is found that the number of opinion elements identified in this model is more than that of other models. But the length is obviously longer than that of BSRNN, which is closer to the result of manual labeling. It is shown that the quality of viewpoint elements identified by this model is higher when the number of viewpoint elements identified is similar. It is observed that the effect of boundary determination is better than BSRNN and BLSTM models.

Although this model is superior to the baseline model in opinion expression extraction to some extent, but the recognition performance still needs to be improved. Compared with the manual tagging of corpus, several problems are summarized:

- (1) Similar ESE subjective expression elements may be merged
- (2) Shorter ESE subjectivity expression factors are easily neglected

TABLE 5: The contrast of three expression extraction models and baseline methods in this paper.

Type	Model	Binary Overlap			Proportional Overlap		
		Accuracy (%)	Recall (%)	<i>F</i> value (%)	Accuracy (%)	Recall (%)	<i>F</i> value (%)
DSE	CRF-OE [9]	82.28	52.99	64.45	74.96	46.98	57.74
	BSRNN [13]	65.66	73.61	69.30	61.78	63.87	62.69
	BiLSTM ^[25]	70.63	68.74	69.60	67.84	59.48	63.30
	Our model	74.64	67.67	70.94	69.54	61.32	65.10
ESE	CRF-OE	68.36	51.84	58.85	56.09	42.26	48.10
	BSRNN	63.82	68.95	66.05	56.19	52.45	53.88
	BiLSTM	71.58	57.60	63.75	65.72	42.99	51.85
	Our model	75.56	57.52	65.15	60.80	50.85	55.07

- (3) A few of the subjectivity expression elements identified by DSE are shorter than those labeled by hand

5. Conclusion

In this paper, we studied the extraction method of subjective expression elements and proposed a compound model based on multifeature deep neural network and conditional random field. Then we described the various features used in the model, the reasons for selecting these features, and the way of feature construction. We carried out experiments on subjectivity expression elements (DSE and ESE) with multifeature combination, the effect of each feature combination mode on the corresponding subtask is tested, and the most suitable feature combination for the corresponding subtask model is recommended.

Experimental results show that the proposed opinion elements extraction model can effectively extract viewpoint elements and has better accuracy, recall rate, and *F* value. However, the experiment also showed that the extraction effect of the model is restricted when the opinion elements are short and similar, which we will carry on in future work. In a word, our work can provide reference for the follow-up research on the extraction of subjective expression elements.

Data Availability

The experiment was conducted with open dataset MPQA Opinion Corpus v1.2, which can be downloaded at http://mpqa.cs.pitt.edu/corpora/mpqa_corpus/mpqa_corpus_1_2/.

Conflicts of Interest

The authors declare that there are no conflicts of interest regarding the publication of this paper.

Acknowledgments

This work was supported in part by the National Natural Science Foundation of China (NSFC) under Grant nos. 61272447 and 61802271 and in part by the Fundamental Research Funds for the Central Universities under Grant nos. SCU2018D018 and SCU2018D022.

References

- [1] J. Wiebe, T. Wilson, and C. Cardie, "Annotating expressions of opinions and emotions in language," *Language Resources and Evaluation*, vol. 39, no. 2-3, pp. 165–210, 2005.
- [2] L. Wang, H. Raghavan, C. Cardie et al., "Query-focused opinion summarization for user-generated content," in *Proceedings of the COLING 2014, the 25th International Conference on Computational Linguistics: Technical Papers*, Dublin, Ireland, August 2014.
- [3] B. Yang and C. Cardie, "Joint modeling of opinion expression extraction and attribute classification," *Transactions of the Association for Computational Linguistics*, vol. 2, pp. 505–516, 2014.
- [4] O. Irsoy and C. Cardie, "Opinion mining with deep recurrent neural networks," in *Proceedings of the 2014 Conference on Empirical Methods in Natural Language Processing (EMNLP)*, Doha, Qatar, October 2014.
- [5] B. Yang and C. Cardie, "Extracting opinion expressions with semi-markov conditional random fields," in *Proceedings of the 2012 Joint Conference on Empirical Methods in Natural Language Processing and Computational Natural Language Learning*, Jeju Island, Korea, July 2012.
- [6] S.-M. Kim and E. Hovy, "Identifying and analyzing judgment opinions," in *Proceedings of the Main Conference on Human Language Technology Conference of the North American Chapter of the Association of Computational Linguistics*, New York, NY, USA, June 2006.
- [7] S. Kim and E. Hovy, "Extracting opinions, opinion holders, and topics expressed in online news media text," in *Proceedings of the Workshop on Sentiment and Subjectivity in Text*, Sydney, Australia, July 2006.
- [8] E. Breck, Y. Choi, and C. Cardie, "Identifying expressions of opinion in context," in *Proceedings of the 20th international joint conference on Artificial Intelligence*, Hyderabad, India, January 2007.
- [9] R. Johansson and A. Moschitti, "Extracting opinion expressions and their polarities--exploration of pipelines and joint models," in *Proceedings of the 49th Annual Meeting of the Association for Computational Linguistics: Human Language Technologies*, Portland, Oregon, June 2011.
- [10] Y. Choi, E. Breck, and C. Cardie, "Joint extraction of entities and relations for opinion recognition," in *Proceedings of the 2006 Conference on Empirical Methods in Natural Language Processing*, Sydney, Australia, July 2006.
- [11] Y. Choi and C. Cardie, "Hierarchical sequential learning for extracting opinions and their attributes," in *Proceedings of the ACL 2010 conference short papers*, Uppsala, Sweden, July 2010.

- [12] X. Wang, Y. Liu, M. Liu, C. Sun, and X. Wang, "Understanding gating operations in recurrent neural networks through opinion expression extraction," *Entropy*, vol. 18, no. 8, p. 294, 2016.
- [13] J. Du, L. Gui, and R. Xu, "Extracting opinion expression with neural attention," in *Proceedings of the Social Media Processing: 5th National Conference, SMP*, Nanchang, China, October 2016.
- [14] M. Zhang, Q. Wang, and G. Fu, "End-to-end neural opinion extraction with a transition-based model," *Information Systems*, vol. 80, pp. 56–63, 2019.
- [15] T. Mikolov, K. Chen, G. Corrado et al., "Efficient estimation of word representations in vector space," 2013, <http://arxiv.org/abs/1301.3781>.
- [16] G. Lample, B. Miguel, S. Subramanian et al., "Neural architectures for named entity recognition," in *Proceedings of the NAACL-HLT*, San Diego, CA, USA, June 2016.
- [17] E. F. Sang and J. Veenstra, "Representing text chunks," in *Proceedings of the ninth conference on European chapter of the Association for Computational Linguistics*, Bergen, Norway, June 1999.
- [18] O. Irsoy and C. Cardie, "Bidirectional recursive neural networks for token-level labeling with structure," 2013, <http://arxiv.org/abs/1312.0493>.

Research Article

Modeling a Rumor Propagation in Online Social Network: An Optimal Control Approach

Rachid Ghazzali ¹, **Amine El Bhih** ¹, **Adil El Alami Laaroussi** ^{1,2} and **Mostafa Rachik**¹

¹Laboratory of Analysis Modeling and Simulation, Department of Mathematics and Computer Science, Faculty of Sciences Ben M'Sik, Hassan II University Casablanca, BP 7955, Sidi Othman, Casablanca, Morocco

²Laboratory of Applied Sciences and Didactics, Higher Normal School Tetouan, Abdelmalek Essaadi University, Tetouan, Morocco

Correspondence should be addressed to Rachid Ghazzali; ghazzalirachid@gmail.com

Received 29 May 2020; Accepted 14 July 2020; Published 11 August 2020

Guest Editor: Jianxin Li

Copyright © 2020 Rachid Ghazzali et al. This is an open access article distributed under the Creative Commons Attribution License, which permits unrestricted use, distribution, and reproduction in any medium, provided the original work is properly cited.

We propose to model the phenomenon of the spread of a rumor in social networks in this paper. From an existing SIR model, we manipulate a new one that is based on the model of cholera in order to take into account professional pages that specialize in spreading rumors. In the second part, we introduce a control strategy to fight against the diffusion of the rumor. Our main objective is to characterize the three optimal controls that minimize the number of spreader users, fake pages, and the corresponding costs. For that matter, using the maximum principle of Pontryagin, we prove the existence and we give characterization of our controls. Numerical simulations are given to concretize our approach.

1. Introduction

The phenomenon of rumor is a complex phenomenon that has eluded man since ancient times, where it intersects many factors and interventions, including what is natural, sociological, economic, and psychological. Communities have known over the years the emergence of many rumors that have spread widely among them; it was also the focus of interaction and analysis by the commanders of these societies throughout history [1]; human beings have fabricated rumors and disseminated them for political, economic, and social purposes [2], where they are exploited to achieve commercial profits or to achieve victories in wars by dissolving fear and surrender within the enemy or with holding confidence in their leaders. The phenomenon of rumor has known many changes in its composition, in line with the change that societies know and the development of daily life in general with the increasing use of technological instruments and modern technologies in communication within communities. This phenomenon has witnessed a dramatic rise and an increase in the speed of its spread. This increase contributes significantly to huge consequences on the other

hand. The development of the phenomenon of rumors and the strength of their influence and impact within societies gave this phenomenon another dimension [3], as it became used by the media and intelligence in competition between countries and what is known as propaganda and polemic or buzz by publishing some false news in whole or in part to influence the opinions of voters by raising or decreasing the popularity of politicians [4] as happened in the elections between Trump and Hillary where Hillary was the most popular and was the favorite to win until the last weeks before the presidential election [5], where some of the specialized communication agencies published many news about Hillary contributed significantly to influence public opinion tendency to Trump, who eventually won. Jennifer et al. in their article [6] did a study in order to understand the dynamics of this exceptional campaign in which social media played a major role. The website [7] gives a variety of Trump's Tweets grouped by topic (people, places, and things Trump has insulted on Twitter). In 2018, Russian authorities have considered starting to block sites like Telegram [8] because of the danger on national security. And if some rumors arouse ridicule, such as saying that Nicolas Cage was

Dracula, others were of great danger; to see more in this regard, we guide the reader to the beautiful book [9].

Mathematical modeling is one of the most important applications of mathematics that contribute to the representation and simulation of social, economic, biological, and ecological phenomena and convert them into mathematical equations that are formulated, studied, analyzed, and interpreted [10]. In this context, many researchers have developed different mathematical models representing the dynamics of the rumor [11] and the elements interfering with its spread [12–15], and especially [16] in the work [17], authors gave a review and a study of several mathematical models of rumor's propagation.

1.1. Related Work. In 1964, Goffman and Newill developed in their article titled “Generalization of Epidemic Theory: An Application to the Transmission of Ideas” [18] a new concept for modeling the transmission of ideas within a society based on the mathematical model SIR due to the great similarity between the two phenomena. This model was previously used to model the transmission of diseases and epidemics within communities; in the introduction of their work, the authors stated that “the process already described does not take into account the almost endless number of complexities which actually arise” [18]. Based on the previous work, Daley and Kendall in their letter titled “Epidemics and Rumors” suggested applying the previous idea to modeling the spread of rumors within communities [19]. With the development of societies and the emergence of modern technological means (transport communication), new factors have emerged that further complicate the phenomenon of rumor and contribute to the large spread of rumors; this has led many researchers to think about developing the previous model. As an example, in the work done by Luis M.A. Bettencourt et al. [20], they proposed a new model taking into account new factors by extending the SIR model to a SEIZR model with two additional compartments. In the same context and to give time factor more importance in the process of spread of the phenomenon, Laarabi et al. [21] had developed another model using a delayed rumor propagation model. This is in addition to many recent works that have recently been produced that take into account several factors involved in the development of a concept that truly simulates the dynamics of rumor propagation; to take a broader view, the reader is referred to the article [22]. With the emergence of social networks and their impacts on communication within communities where they are taking more and more space within the community, it became clear that they must be taken into account as major intervening in the spread of rumors; in this context many of the works that adopted this hypothesis have been produced. To take an idea of some of these works, see the article [23]. For example, in the work [24], authors had implemented a mathematical model in order to model the dynamics of a rumor in social network by adding three new compartments: reviewers, sharers, and collectors who are reviewing the message, collecting the message, sharing the message, or giving no response to the message, respectively, but in the work [25], the authors were limited to highlight the role of users of the

network and ignore the impact of the network itself, especially the role of pages that spread the rumor within the network. The loading of false information in these pages is a source of rumor between browsers and considered as a big factor which helps in the rapid spread of rumors, such as rivers and valleys, which store bacteria and microbes and are a hotbed for the multiplication and growing bacteria that transmit diseases to humans through the use of the water of those rivers. A good example of this similarity is the cholera epidemic. In this paper and based on the previous hypothesis, we will exploit the mathematical model that has been formulated to represent the cholera epidemics [26] and combine it with the previous work model by adding a new compartment F which represents page's rumor. Other models from population dynamics and optimal controls can be found in [3, 27].

Recently, a significant amount of prior works exists in the study of rumor detection in social networks. For example, in [28], the authors propose a GCN-based model for rumor detection on social media, called Bi-GCN, and they discuss several variants of Bi-GCN to model the propagation patterns. Ma et al. in [29] discuss the same topic involving a novel approach to capture the temporal characteristics based on the time series of rumor's life cycle, for which time series modeling technique is applied to incorporate various social context information, while Han Guo et al. [30] propose a novel hierarchical neural network combined with social information (HSA-BLSTM) for rumor detection and they test their model on two real-world datasets from Weibo and Twitter demonstrating outstanding performance in both rumor detection and early detection scenarios. Li et al. [31] give another approach, the personalized influential topic search by proposing two random-walk based approaches in order to measure the influence of a topic on a query user. Moreover, Li et al. in [32] studied the problem from another side, influence maximization; the aim is to find a limited number of users which can influence the maximum number of users in social networks. Li et al. in [33] continue to improve their work by taking into account the physical locations of the users since location is an important factor in this process. The same approach was discussed by Cai et al. in [34], where they formulate a new problem of holistic influence maximization, denoted as HIM query, for targeted advertisements in a spatial social network.

1.2. Problem Definition. In [35], where the authors subdivide the population into three compartments representing the main actors in the dynamics of the propagation of a rumor, these compartments are ignorant individuals, the spreaders, and the stiflers. As we mentioned before, many agencies specialized in propaganda dissemination have become using social media to facilitate the spread of rumor and large volume of users. For this purpose, special pages are created to spread a rumor about a specific subject or target person. This page is promoted by fictitious users that are created for this purpose. They create a private network of friends; their friends are the first victims; every time they like or comment on what is posted by the page or fictitious people, this activity is displayed to all their friends or perhaps friends of

their friends inadvertently which is promoted by this rumor passively by them, while studies indicate that the number of users of the networks is rising at a tremendous rate and it has become one of the basics in the field of communication and publicity, according to statistics [4]. It treated millions of rumors spread daily in social networks, starting from this model, and by adding an additional compartment, named F as Fakes, we will build our own model which describes the propagation of a rumor through a social network. Our idea is to combine the classical model $ISpSt$ with another mathematical model that describes the dynamics of cholera in order to highlight the importance of fake page which are specified in spreading fake news; in other words, since there is a similarity between these two phenomena, we can consider a fake page as a contaminated river which contains bacteria; these bacteria are false information in our case. We can use this model in order to describe the dynamics of the rumor between the different individuals as well as bringing out the contribution of fake pages in this process [36]. In this paper and based on the previous hypothesis, we will exploit the mathematical model that has been formulated to represent the cholera epidemics [36] and combine it with the previous work model by adding a new compartment F which represents page's rumor.

In this paper, in Section 2, we propose a continuous mathematical model IS_pS_tF that describes the dynamics of a population that reacts in the spread of the rumor in a social network positivity, and the boundness of the model is discussed. In 3, we present an optimal control problem for the proposed model where we give some results concerning the existence of the optimal control, and we characterize the optimal controls using the Pontryagin maximum principle in discrete time. Numerical simulations through MATLAB are given in Section 3.2. Finally, we conclude the paper in Section 4.

1.2.1. IS_pS_tF . In this section, we will describe our model IS_pS_tF which consists of four compartments representing the subdivision of the population that reacts in the spread of the rumor in a social network. I , ignorant, represents users who do not know the rumor and are susceptible to be informed, S_p , spreader, represents users who spread the rumor, S_t , stifter, represents individuals who refuse to spread the rumor, and F , rumor's page, represents the page specialized in spreading the rumor. The compartment I represents the number of users who do not know the rumor and who are susceptible to be informed; this population increases with the rate μN which represents the new users created; an ignorant inquires about the rumor through two ways: either by consulting a specialized page in the diffusion of the rumor or directly by the contact with a spreader. Some of these users deactivate their account at a rate μI . Thus, in this compartment, we have an incoming flux equal to μN and an outgoing flux equal to $\alpha_h S_p I + \alpha_e I (F/\kappa + F) + \mu I$.

The compartment S_p represents the number of people who spread the rumor either directly or by sharing one-page publications or by creating new publications. Thus, we have an incoming flux equal to $\theta(\alpha_h S_p I + \alpha_e I (F/\kappa + F))$ which represents the proportion of the new users who will spread

the rumor. After the contact between two spreaders, one of them decides not to diffuse the information at a rate γS_p^2 , and after the contact of a spreader and a stifter, the stifter succeeds to convince him that the information is false at a rate $\lambda S_t S_p$; after a certain period, a portion of the spreaders decide not to spread the rumor at a rate βS_p .

The compartment S_t represents the number of stiflers who refuse to spread the rumor. This number increases at a rate $(1 - \theta)(\alpha_h S_p I + \alpha_e I (F/\kappa + F))$ which represents the portion of users who knew that the information is wrong, in addition to the flux that left the S_p compartment $S_p(\gamma S_p + \lambda S_t) + \beta S_p$, and decreases with the rate μS_t of stiflers who have deactivated their accounts.

The compartment F represents the page specialized in the diffusion of the rumor. This page contains malicious publications about the rumor; in this page, S_p have the right to publish and share these publications at rates $\delta_1 S_p$ and $\varepsilon_2 S_p$, respectively, and the ignorants who consult the page also share these publications at a rate $\varepsilon_1 I$.

The following diagram will demonstrate the flux directions of individuals among the compartments (Figure 1).

The dynamics of this model are governed by the following nonlinear system:

$$\begin{cases} \frac{dI}{dt} = \mu N - \alpha_h S_p I - \alpha_e I \frac{F}{\kappa + F} - \mu I, \\ \frac{dS_p}{dt} = \theta \left(\alpha_h S_p I + \alpha_e I \frac{F}{\kappa + F} \right) - \beta S_p - S_p (\gamma S_p + \lambda S_t), \\ \frac{dS_t}{dt} = (1 - \theta) \left(\alpha_h S_p I + \alpha_e I \frac{F}{\kappa + F} \right) + S_p (\gamma S_p + \lambda S_t) + \beta S_p - \mu S_t, \\ \frac{dF}{dt} = \delta_1 S_p + \varepsilon_1 I + \varepsilon_2 S_p. \end{cases} \quad (1)$$

With initial values, $I(0)$, $S_p(0)$, $S_t(0)$, and $F(0)$ are nonnegatives $F/\kappa + F$: logistic capacity (concentration of rumors).

In order to demonstrate the effectiveness of the model we have proposed, we will present a numerical simulation with the following figure so that we can see how well the model adapts to reality. Initial values are approximate data that we suggested after studying and researching some statistics about the users of social networks; the values are attached in the table.

From Figure 2, we note that there is no significant effect until the 30th day, 30 days after the launch of the rumor; the number of ignorants decreases sharply; in contrast, there is a significant rise of spreaders and the numbers of stiflers and pages is rising on average. These changes indicate that after 30 days trading rumor has become more and more due to the continuous publication of it.

1.2.2. Model Basic Properties

Theorem 1. If $I(0) \geq 0$, $S_p(0) \geq 0$, $S_t(0) \geq 0$, and $F(0) \geq 0$, the solutions $I(t)$, $S_p(t)$, $S_t(t)$, and $F(t)$ of system (1) are positive for all $t \geq 0$.

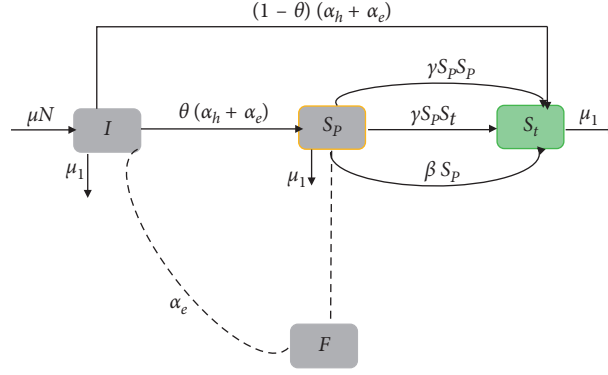


FIGURE 1: Description diagram of the rumor dynamics.

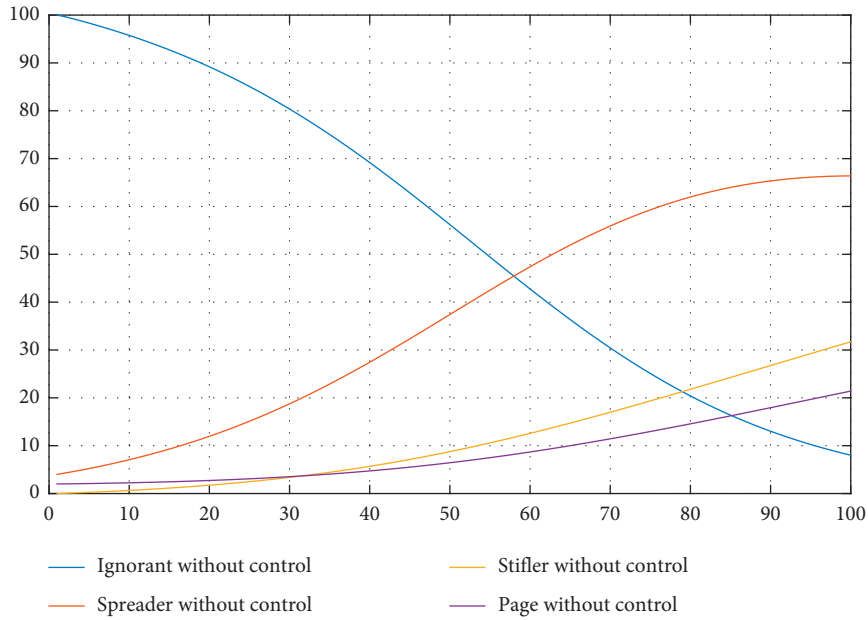


FIGURE 2: Dynamics without control strategy.

Proof.

$$\begin{aligned} \frac{dI(t)}{dt} &= \mu N - \alpha_h S_p I - \alpha_e I \frac{F}{\kappa + F} - \mu I \\ &\geq -\alpha_h S_p I - \alpha_e I \frac{F}{\kappa + F} - \mu I \\ \frac{dI(t)}{dt} + \left(\alpha_h S_p + \alpha_e \frac{F}{\kappa + F} + \mu \right) I &\geq 0. \end{aligned} \quad (2)$$

where $G(t) = \alpha_h S_p + \alpha_e (F/\kappa + F) + \mu$. Both sides in the last inequality are multiplied by $\exp\left(\int_0^t G(s)ds\right)$.

We obtain

$$\exp\left(\int_0^t G(s)ds\right) \cdot \frac{dI(t)}{dt} + G(t) \exp\left(\int_0^t G(s)ds\right) \cdot I(t) \geq 0. \quad (3)$$

Then

$$\frac{d}{dt} \left(I(t) \exp\left(\int_0^t G(s)ds\right) \right) \geq 0. \quad (4)$$

Integrating this inequality from 0 to t gives

$$\int_0^t \frac{d}{ds} \left(I(s) \exp\left(\int_0^s \left(\alpha_h S_p + \alpha_e \frac{F}{\kappa + F} + \mu \right) ds \right) \right) ds \geq 0. \quad (5)$$

Then

$$I(t) \geq I(0) \exp\left(\int_0^t -\left(\alpha_h S_p + \alpha_e \frac{F}{\kappa + F} + \mu \right) ds\right) \quad (6)$$

$$\implies I(t) \geq 0.$$

Similarly, we prove that $I(t) \geq 0$, $S_p(t) \geq 0$, $S_t(t) \geq 0$, and $F(t) \geq 0$.

1.2.3. Boundedness of the Solutions

Theorem 2. *The set*

$$\Omega = \left\{ \frac{(I, S_p, S_t, F) \in \mathbb{R}_+^4}{0 \leq I + S_t + S_p + F \leq 1} \right\} \quad (7)$$

is positively invariant under system (1) with initial conditions $I(0) \geq 0$, $S_p(0) \geq 0$, $S_t(0) \geq 0$, and $F(0) \geq 0$ being positively invariant for system (1).

2. The Model with Controls

Now, we introduce our controls into system (1). As control measures to fight the spread of rumor, we extend our system by including three kinds of controls u , v , and w . The first control u is to tell users that the information or publication is false and contains a malicious rumor. The second control v is through the admin where he deactivates an account after learning that it is fake or aimed at spreading the rumor. The last one w is also applied by the admin, this time by deactivating the page intended to spread the rumor after the arrival of a certain number of complaints.

With the aim of better understanding the effects of any control measure of these strategies, we introduce three new variables: π_i , where $i = 1, 2, 3$, $\pi_i = 0$ in the absence of control, and $\pi_i = 1$ in the presence of control. One has

$$\begin{cases} \frac{dI}{dt} = \mu N - \alpha_h S_p I - \alpha_e I \frac{F}{\kappa + F} - \mu I - \pi_1 u I, \\ \frac{dS_p}{dt} = \theta \left(\alpha_h S_p I + \alpha_e I \frac{F}{\kappa + F} \right) - (\beta) S_p - S_p (\gamma S_p + \lambda S_t) \\ \quad - \pi_2 v S_p, \\ \frac{dS_t}{dt} = (1 - \theta) \left(\alpha_h S_p I + \alpha_e I \frac{F}{\kappa + F} \right) + S_p (\gamma S_p + \lambda S_t) \\ \quad + \beta S_p - \mu S_t + \pi_1 u I, \\ \frac{dF}{dt} = \delta_1 S_p + \varepsilon_1 I + \varepsilon_2 S_p - \pi_3 w F. \end{cases} \quad (8)$$

3. Optimal Control Problem

We define the objective functional as follows:

$$J(u, v, w) = \int_0^T \left(S_p(t) + \frac{1}{2} A u^2(t) + \frac{1}{2} B v^2(t) + \frac{1}{2} C w^2(t) \right) dt, \quad (9)$$

where $A > 0$, $B > 0$, and $C > 0$ are the cost coefficients:

$$J(u^*, v^*, w^*) = \min \left\{ \frac{J(u, v, w)}{(u, v, w) \in U_{ad}} \right\}, \quad (10)$$

where U_{ad} is the set of admissible controls defined by

$$U_{ad} = \left\{ \frac{(u, v, w)}{u_{\min} \leq u(t) \leq u_{\max}, v_{\min} \leq v(t) \leq v_{\max}, w_{\min} \leq w(t) \leq w_{\max} t \in [0, T]} \right\}, \quad (11)$$

and $(u_{\min}, v_{\min}, w_{\min}, u_{\max}, v_{\max}, w_{\max}) \in (]0, 1[)^6$.

Theorem 3. *Consider the control problem with system (8).*

There exists an optimal control $(u^*, v^*, w^*) \in U_{ad}^3$ such that

$$J(u^*, v^*, w^*) = \min_{(u, v, w) \in U_{ad}^3} J(u^*, v^*, w^*). \quad (12)$$

If the following conditions are met:

- (1) The set set of controls and the corresponding state variables is nonempty.
- (2) The control set U_{ad} is convex and closed.
- (3) The right-hand side of the state system is bounded by a linear function in the state and control variables.
- (4) The integrand $L(I, S_p, S_t, F, u, v, w)$ of the objective functional is convex on U_{ad} and there exist constants c_1 and c_2 such that

$$L(I, S_p, S_t, F, u, v, w) \geq c_1 + c_2 (|u|^2 + |v|^2 + |w|^2)^{\beta/2}. \quad (13)$$

Proof. The existence of the optimal control can be obtained using a result by Fleming and Rishel [37], checking the following step:

Condition 1: To prove that the set of controls and the corresponding state variables is nonempty, we will use a simplified version of an existence result ([38], Theorem 7). Let $\dot{I} = f_I(t, I, S_p, S_t, F)$, $\dot{S}_p = f_{S_p}(t, I, S_p, S_t, F)$, $\dot{S}_t = f_{S_t}(t, I, S_p, S_t, F)$, and $\dot{F} = f_F(t, I, S_p, S_t, F)$, where f_I, f_{S_p}, f_{S_t} , and f_F form the right-hand side of the system of 8. Let $u(t) = c_1$, $v(t) = c_2$, and $w(t) = c_3$, for some constants, and since all parameters are constants and I, S_p, S_t , and F are continuous, then f_I, f_{S_p}, f_{S_t} , and f_F are also continuous. Additionally, the partial derivatives $\partial f_I / \partial I, \partial f_I / \partial S_p, \partial f_I / \partial S_t, \partial f_I / \partial F, \partial f_{S_p} / \partial I, \partial f_{S_p} / \partial S_p, \partial f_{S_p} / \partial S_t, \partial f_{S_p} / \partial F, \partial f_{S_t} / \partial I, \partial f_{S_t} / \partial S_p, \partial f_{S_t} / \partial S_t, \partial f_{S_t} / \partial F, \partial f_F / \partial I, \partial f_F / \partial S_p, \partial f_F / \partial S_t$, and $\partial f_F / \partial F$ are all continuous. Therefore, there exists a unique solution (I, S_p, S_t, F) that satisfies the initial conditions. Therefore, the set of controls and the corresponding state variables is nonempty and condition 1 is satisfied.

Condition 2: By definition, U_{ad} is closed. Take any control $u_1, u_2 \in U_{ad}$ and $\lambda \in [0, 1]$. Then $\lambda u_1 + (1 - \lambda) u_2 \geq 0$.

Additionally, we observe that $\lambda u_1 \leq \lambda (1 - \lambda) u_2 \leq (1 - \lambda)$; then $\lambda u_1 + (1 - \lambda) u_2 \leq \lambda + (1 - \lambda) = 1$.

Hence,

$$0 \leq \lambda u_1 + (1 - \lambda)u_2 \leq 1, \quad \text{for all } u_1, u_2 \in U_{\text{ad}} \text{ and } \lambda \in [0, 1]. \quad (14)$$

Therefore, U_{ad} is convex and condition 2 is satisfied.

Condition 3: All the right-hand sides of equations of system are continuous, bounded above by a sum of bounded control and state, and can be written as a linear function of u, v , and w with coefficients depending on the time and state. Therefore, condition 3 is satisfied.

Condition 4: The integrand in the objective functional (9) is convex on U_{ad} . It rests to show that there exist constants $c_1, c_2 > 0$, and $\beta > 1$ such that the integrand $L(I, S_p, S_t, F, u, v, w)$ of the objective functional satisfies

$$\begin{aligned} L(I, S_p, S_t, F, u, v, w) &= S_p(t) + \frac{A}{2}u^2(t) + \frac{B}{2}v^2(t) + \frac{C}{2}w^2(t) \\ &\geq c_1 + c_2(|u|^2 + |v|^2 + |w|^2)^{\beta/2}. \end{aligned} \quad (15)$$

The state variables are bounded; let $c_1 = S_p$, $c_2 = \inf(A/2, B/2, C/2)$, and $\beta = 2$; then it follows that

$$L(I, S_p, S_t, F, u, v, w) \geq c_1 + c_2(|u|^2 + |v|^2 + |w|^2)^{\beta/2}. \quad (16)$$

Then, from Fleming and Rishel [37], we conclude that there exists an optimal control.

3.1. Characterization of the Optimal Controls. In this section, we apply Pontryagin's maximum principle [26]. The key idea is introducing the adjoint function to attach the system of differential equations to the objective functional resulting in the formation of a function called the Hamiltonian. This principle converts the problem of finding the control to optimize the objective functional subject to the state of differential equations with initial condition to find the control to optimize Hamiltonian pointwise (with respect to the control).

Now, we have the Hamiltonian of the optimal problem given by

$$\begin{aligned} H &= S_p + \frac{1}{2}Au^2 + \frac{1}{2}Bv^2 + \frac{1}{2}Cw^2 + \lambda_1 \left(\mu N - \alpha_h S_p I - \alpha_e I \frac{F}{\kappa + F} - \mu I - \pi_1 u I \right) \\ &\quad + \lambda_2 \left(\theta \left(\alpha_h S_p I + \alpha_e I \frac{F}{\kappa + F} \right) - (\beta) S_p - S_p (\gamma S_p + \lambda S_t) - \pi_2 v S_p \right) \\ &\quad + \lambda_3 \left((1 - \theta) \left(\alpha_h S_p I + \alpha_e I \frac{F}{\kappa + F} \right) + S_p (\gamma S_p + \lambda S_t) + \beta S_p - \mu S_t + \pi_1 u I \right) \\ &\quad + \lambda_4 (\delta_1 S_p + \varepsilon_1 I + \varepsilon_2 S_p - \pi_3 w F). \end{aligned} \quad (17)$$

Using Pontryagin's maximum [26, 39], we can say the following theorem.

Theorem 4. Let I^*, S_p^*, S_t^* , and F^* be optimal state solutions with an associated optimal control (u^*, v^*, w^*) for the optimal control problem. Then there exist adjoint variables $\lambda_1, \lambda_2, \lambda_3$, and λ_4 satisfying

$$\begin{aligned} \lambda_1' &= - \left(-\lambda_1 \alpha_h S_p - \lambda_1 \alpha_e \frac{F}{\kappa + F} - \lambda_1 \mu - \lambda_1 \pi_1 u + \lambda_2 \theta \left(\alpha_h S_p + \alpha_e \frac{F}{\kappa + F} \right) + \lambda_3 (1 - \theta) \left(\alpha_h S_p I + \alpha_e I \frac{F}{\kappa + F} \right) + \lambda_3 \pi_1 u \right), \\ \lambda_2' &= - \left(1 - \lambda_1 \alpha_h I + \lambda_2 \theta \alpha_h I - \lambda_2 (\beta) - \lambda_2 (\gamma S_p + \lambda S_t) - \gamma \lambda_2 S_p - \pi_2 \lambda_2 v + \lambda_3 (1 - \theta) \alpha_h I + \lambda_3 (\gamma S_p + \lambda S_t) + \lambda_3 \gamma S_p + \lambda_4 (\varepsilon_2 + \delta_1) \right), \\ \lambda_3' &= - \left(-\lambda \lambda_2 S_p + \lambda_3 \lambda S_p - \mu \lambda_3 \right), \\ \lambda_4' &= - \left(-\lambda_1 \alpha_e I \frac{\kappa}{(\kappa + F)^2} + \lambda_2 \theta \alpha_e I \frac{\kappa}{(\kappa + F)^2} + \lambda_3 (1 - \theta) \alpha_e I \frac{\kappa}{(\kappa + F)^2} - \lambda_4 - \pi_3 \lambda_4 w \right), \end{aligned} \quad (18)$$

with transversality conditions at time T . One has

$$\begin{aligned}\lambda_1(T) &= 1, \\ \lambda_2(T) &= 0, \\ \lambda_3(T) &= 0, \\ \lambda_4(T) &= 0.\end{aligned}\tag{19}$$

Furthermore, $t \in [0, T]$ and for $\pi_1 = \pi_2 = \pi_3 = 1$, the optimal controls $u^*(t)$, $v^*(t)$, and $w^*(t)$ are given by

$$\begin{aligned}u^* &= \min \left\{ \max \left\{ \frac{\pi_1 I (\lambda_1 - \lambda_3)}{A}, u_{\min} \right\}, u_{\max} \right\}, \\ v^* &= \min \left\{ \max \left\{ \frac{\lambda_2 \pi S_p S_t}{B}, v_{\min} \right\}, v_{\max} \right\}, \\ w^* &= \min \left\{ \max \left\{ \frac{\lambda_4 \pi_3 F}{C}, w_{\min} \right\}, w_{\max} \right\}.\end{aligned}\tag{20}$$

Proof. For $t \in [0, T]$, the adjoint equations and transversality conditions can be obtained by using Pontryagin's maximum principle [26, 39] such that

$$\begin{aligned}\lambda_1' &= -\frac{\partial H}{\partial I} = -\left(-\lambda_1 \alpha_h S_p - \lambda_1 \alpha_e \frac{F}{\kappa + F} - \lambda_1 \mu - \lambda_1 \pi_1 u + \lambda_2 \theta \left(\alpha_h S_p + \alpha_e \frac{F}{\kappa + F} \right) + \lambda_3 (1 - \theta) \left(\alpha_h S_p I + \alpha_e I \frac{F}{\kappa + F} \right) + \lambda_3 \pi_1 u \right), \\ \lambda_2' &= -\frac{\partial H}{\partial S_p} = -\left(1 - \lambda_1 \alpha_h I + \lambda_2 \theta \alpha_h I - \lambda_2 (\beta) - \lambda_2 (\gamma S_p + \lambda S_t) - \gamma \lambda_2 S_p - \pi_2 \lambda_2 v + \lambda_3 (1 - \theta) \alpha_h I \right. \\ &\quad \left. + \lambda_3 (\gamma S_p + \lambda S_t) + \lambda_3 \gamma S_p + \lambda_4 (\varepsilon_2 + \delta_1) \right), \\ \lambda_3' &= -\frac{\partial H}{\partial S_t} = -\left(-\lambda \lambda_2 S_p + \lambda_3 \lambda S_p - \mu \lambda_3 \right), \\ \lambda_4' &= -\frac{\partial H}{\partial F} = -\left(-\lambda_1 \alpha_e I \frac{\kappa}{(\kappa + F)^2} + \lambda_2 \theta \alpha_e I \frac{\kappa}{(\kappa + F)^2} + \lambda_3 (1 - \theta) \alpha_e I \frac{\kappa}{(\kappa + F)^2} - \lambda_4 - \pi_3 \lambda_4 w \right).\end{aligned}\tag{21}$$

For $t \in [0, T]$, the optimal controls u^* , v^* , and w^* can be solved from the optimality condition:

$$\begin{aligned}\frac{\partial H}{\partial u} &= Au - \pi_1 \lambda_1 I + \lambda_3 \pi_1 I = 0 \iff u = \frac{\pi_1 I (\lambda_1 - \lambda_3)}{A}, \\ \frac{\partial H}{\partial v} &= Bv - \lambda_2 \pi v S_p S_t = 0 \iff v = \frac{\lambda_2 \pi S_p S_t}{B}, \\ \frac{\partial H}{\partial w} &= Cw - \lambda_4 \pi_3 F = 0 \iff w = \frac{\lambda_4 \pi_3 F}{C}.\end{aligned}\tag{22}$$

For the bounds in U_{ad} of the controls, it is easy to obtain u^* , v^* , and w^* given by

$$\begin{aligned}u^* &= \min \left(1, \max \left(0, \frac{\pi_1 I (\lambda_1 - \lambda_3)}{A} \right) \right), \\ v^* &= \min \left(1, \max \left(0, \frac{\lambda_2 \pi S_p S_t}{B} \right) \right), \\ w^* &= \min \left(1, \max \left(0, \frac{\lambda_4 \pi_3 F}{C} \right) \right).\end{aligned}$$

However, if $\pi_i = 0$ where $i = 1, 2, 3$, the controls attached to this case will be eliminated and removed.

3.2. Numerical Simulation

3.2.1. Algorithm. In this section, we present the results obtained by solving numerically the optimality system. This system consists of the state system, adjoint system, initial and final time conditions, and the control characterization. So, the optimality system is given by the following:

step 1. $I_0 = i_0$, $S_{p0} = s_{p0}$, $S_{t0} = s_{t0}$, $F_0 = f_0$,
 $\lambda_{2,N} = \lambda_{3,N} = \lambda_{4,N} = 0$, $\lambda_{1,N} = A_N$, and given $u_{k;0}^*$, $v_{k;0}^*$,
 $w_{k;0}^*$
 step 2. for $k = 0; 1; \dots; N - 1$ do:

$$\begin{aligned}
 I_{k+1} &= \mu N - \alpha_h S_{p,k} I_k - \alpha_e I_k \frac{F_k}{\kappa + F_k} - \mu_1 I_k, \\
 S_{p(k+1)} &= \theta \left(\alpha_h S_{p,k} I_k + \alpha_e I_k \frac{F_k}{\kappa + F_k} \right) - (\mu + \beta) S_{p,k} - \gamma S_{p,k} (S_{p,k} + S_{t,k}), \\
 S_{p(k+1)} &= (1 - \theta) \left(\alpha_h S_{p,k} I_k + \alpha_e I_k \frac{F_k}{\kappa + F_k} \right) + \gamma S_{t,k} (S_{p,k} + S_{t,k}) + \beta S_{p,k} - \mu S_{t,k}, \\
 F_{k+1} &= \varepsilon_1 N + \varepsilon_2 S_{p,k} - \mu_2 F_k, \\
 &\vdots \\
 &\vdots \\
 \lambda_{1,T-k} &= \lambda_{1,T-k+1} \left(1 - \alpha_h S_{p,k} - \alpha_e \frac{F_k}{\kappa + F_k} - \mu_1 \right) + \lambda_{2,T-k+1} \theta \left(\alpha_h S_{p,k} + \alpha_e \frac{F_k}{\kappa + F_k} \right) + \lambda_{3,T-k+1} (1 - \theta) \left(\alpha_h S_{p,k} + \alpha_e \frac{F_k}{\kappa + F_k} \right), \\
 \lambda_{2,T-k} &= 1 + \lambda_{1,T-k+1} (-\alpha_h I_k) + \lambda_{2,T-k+1} (1 + \theta \alpha_h I_k - (\mu + \beta) - 2\gamma) + \lambda_{3,T-k+1} [(1 - \theta)(\alpha_h S_{p,k}) + 2\gamma + \beta] + \lambda_{4,T-k+1} \varepsilon_2, \\
 \lambda_{3,T-k} &= \lambda_{2,T-k+1} [-\gamma S_{p,k} S_{p,k}] + \lambda_{3,T-k+1} [1 + \gamma S_{p,k} - \mu], \\
 \lambda_{4,T-k} &= \lambda_{1,T-k+1} \left[-\alpha_e I_k \frac{\kappa}{(\kappa + F_k)^2} \right] + \lambda_{2,T-k+1} \theta \left[\alpha_e I_k \frac{\kappa}{(\kappa + F_k)^2} \right] + \lambda_{3,T-k+1} (1 - \theta) \left[\alpha_e I_k \frac{\kappa}{(\kappa + F_k)^2} \right] + \lambda_{4,T-k+1} (1 - \mu_2), \\
 u_{k+1} &= \min \left[b, \max \left(a, \frac{1}{A_k} (\lambda_{1,T-k+1} I_k - \lambda_{3,T-k+1} \gamma S_{p,k} I_k) \right) \right], \\
 v_{k+1} &= \min \left[d, \max \left(c, \frac{1}{B_k} (-\lambda_{2,T-k+1} \gamma (S_{p,k})^2 S_{t,k}) \right) \right], \\
 w_{k+1} &= \min \left[f, \max \left(e, \frac{1}{C_k} (-\lambda_{4,T-k+1} F_k) \right) \right],
 \end{aligned} \tag{24}$$

end for

step 3. for $k = 0; 1; \dots; N$; write:

$$\begin{aligned}
 I_k^* &= I_k, \\
 S_{p,k}^* &= S_{p,k}, \\
 S_{t,k}^* &= S_{t,k}, \\
 F_k^* &= F_k, \\
 u_k^* &= u_k, \\
 v_k^* &= v_k, \\
 w_k^* &= w_k,
 \end{aligned} \tag{25}$$

end for.

In this formulation, there were initial conditions for the state variables and terminal conditions for the adjoints. That is, the optimality system is a two-point boundary value problem with separated boundary conditions at time steps $k = 0$ and $k = N$. We solve the optimality system by an iterative method with forward solving of the state system followed by backward solving of the adjoint system. We start with an initial guess for the controls at the first iteration, and then before the next iteration, we update the controls by using the characterization. We continue until convergence of successive iterates is achieved.

In this paragraph, we give numerical simulation to highlight the effectiveness of the strategy that we have developed in the framework of eliminating the rumor and limit its spread; the initial values are the same as in

TABLE 1: Rumor model parameters and values.

Parameter	Description	Value
α_h	The proportion of ignorants who become spreaders after discussing with a spreader	(0.05/day)
α_e	The proportion of ignorants who become spreaders after consulting a page of rumor	(0.07/day)
θ	The proportion of ignorants who become spreaders	(0.85/day)
$(1 - \theta)$	The proportion of ignorants who become stiflers	(0.15/day)
μ	New users and deactivated users	0.08
β	The proportion of spreaders who become stiflers	(0.2/day)
γ	The proportion of spreaders who become stiflers after contacting another spreader	(0.005/day)
ε_1	The rate of shared publications of rumor page by ignorants	(0.05/day)
ε_2	The rate of shared publications of rumor page by spreaders	0.1/day
δ_1	New rumor pages created by spreaders	0.4/day

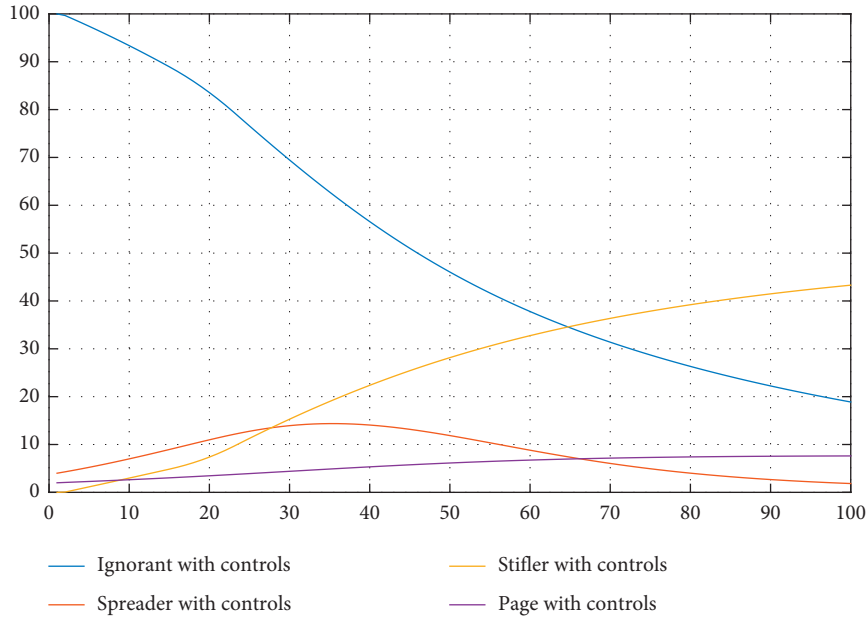
FIGURE 3: Dynamics with controls u , v , and w .

Table 1; with regard to other initial values, they proposed values after a statistical study.

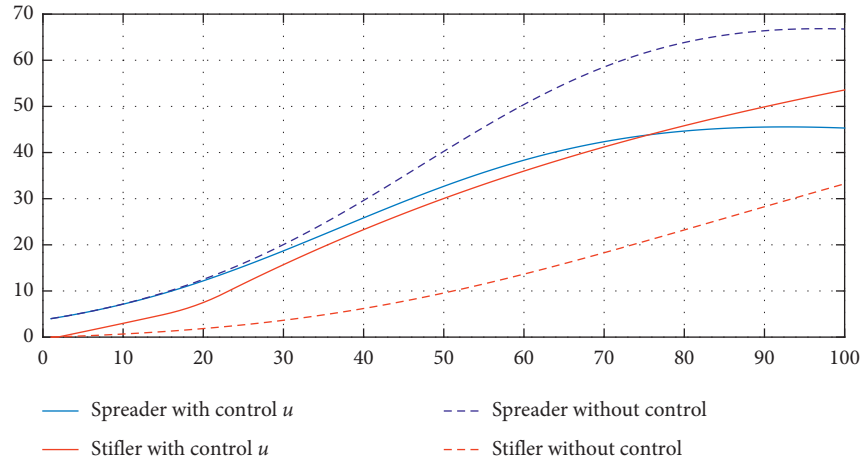
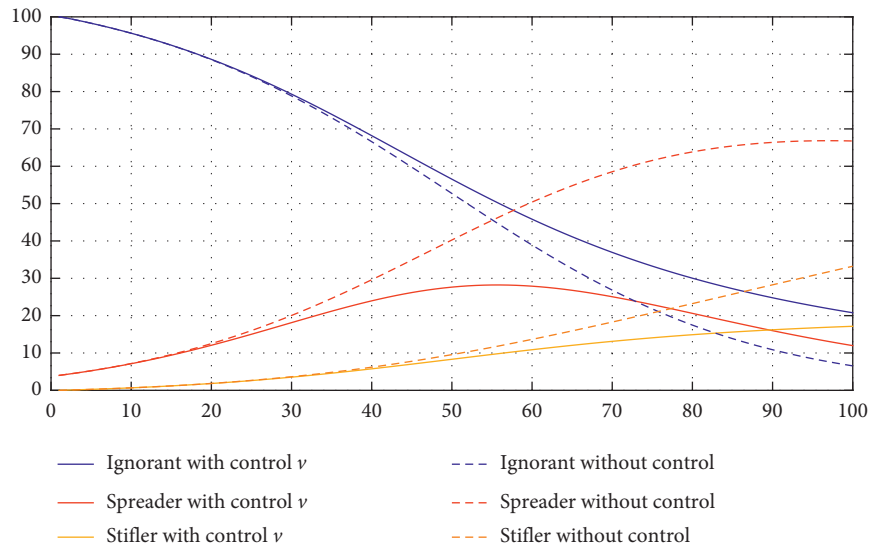
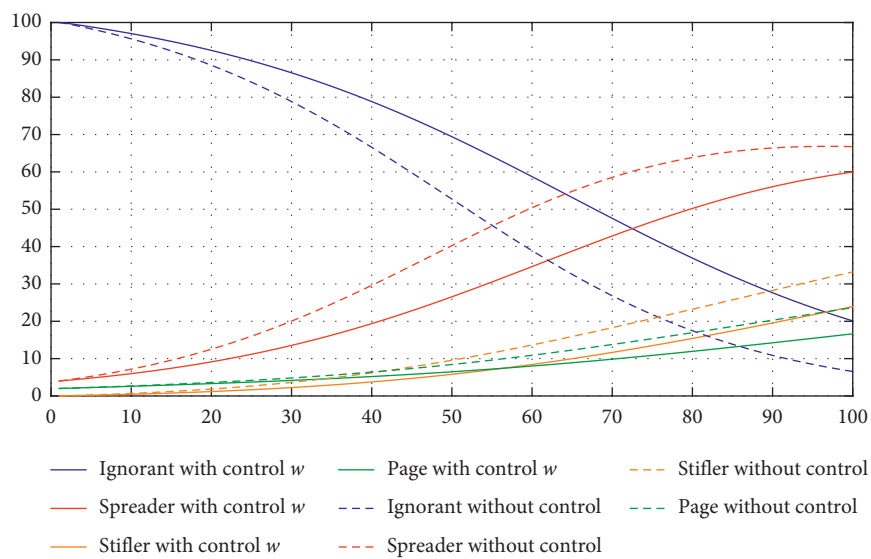
From Figure 3, we note that, after 30 days of the implementation of the preventive strategy, effect begins to appear where we can see again that the sharp decline in the number can be observed, but this time accompanied by a high number and a gradual decline for both S_p and F . This confirms that the proposed strategy in theory is paying off.

In this paragraph and with the aim of obtaining more accurate information about the impact of each control separately, we will develop a preventive strategy by applying each of them individually; numerical analysis will show us the effectiveness of each prevention strategy.

3.2.2. Case 1: Applying Only Control u . Since it will be applied to ignorant individuals, we will be limited to displaying and comparing the curves of S_p and S_t in both cases with and without control strategy. We observe from Figure 4 that, 30 days after the implementation of the strategy, the impact will start to appear as we note that the number will

gradually decrease until it stabilizes at 45. On the other hand, the number of S_t will suddenly start to rise from about the first day. This change is probably due to the fact that the control is aimed at telling the ignorant people to turn to stifler ones. In this way, we win a number of people in the fight against the spread of false news.

3.2.3. Case 2: Applying Only Control v . Here, we will implement only control v , noting through Figure 5 that the effect of the strategy will appear after 20 days on the number of S_p as the number will gradually decrease. This rapid change is attributed to the fact that control directly targets this group. The number of I and S_t change begins to appear after 40 to 50 days as the number of ignorant individuals is relatively high after the implementation of the strategy in parallel with the fact that there is a relatively high number of S_t people which is considered logical and simulates reality since the high number of S_t is the one that caused the number of I to be raised due to their transfer of the correct information to them.

FIGURE 4: Dynamics with controls u .FIGURE 5: Dynamics with controls v .FIGURE 6: Dynamics with controls w .

3.2.4. Case 3: Applying Only Control w . In the last case, we apply only control w . Note through Figure 6 that the effect begins immediately (after about 5 days); for the number of ignorants, we note that there is a gradual decline which is less than the number of ignorant in the absence of control; this is mainly due to low sources of rumors; the same observation is for spreader's number; it rises relatively weaker and is stabilizing at 60 thousand ones; the same thing gets with the number of stiflers where we observe that it rises up to the limits of 25 thousands; the number of pages further rises until the value reaches 15. These observations clearly illustrate the importance of this strategy in the fight against the spread of rumors, where we see the speed of its impact and also to reach the stage of stability after its application since it targets the sources of rumors directly.

4. Conclusion

In this paper, we give a new simple mathematical model which describes the dynamics of rumor propagation through social network. The model is based on two compartmental models by combining them in order to take into account more factors that are involved in the dynamic. Three control strategies were introduced, and referring to the introduction of three new variables π_i , $i = 1, 2, 3$, we could study and combine several scenarios in order to see the impact and the effect of each one of these controls on the reduction of the rumor spread. The goal is achieved and the numerical resolution of the system with difference equations as well as the numerical simulations enabled us to compare and see the difference between each scenario in a concrete way. The purpose of the work is achieved and we have proved the effectiveness of our strategy and its importance in fighting the spread of any rumor throughout any social network.

Data Availability

The disciplinary data used to support the findings of this study have been deposited in the Network Repository (<http://www.networkrepository.com>).

Conflicts of Interest

The authors declare that they have no conflicts of interest.

Acknowledgments

The research reported in this paper was supported by the Moroccan Systems Theory Network.

References

- [1] G. W. Allport and L. Postman, *The Psychology of Rumor*, Holt Rinehart & Winston, New York, NY, USA, 1947.
- [2] P. Bordia and N. Difonzo, "Psychological motivations in rumor spread," *Analysis of Commercial Rumors from the Perspective of Marketing Managers: Rumor Prevalence, Effects, and Control Tactics*, pp. 87–101, 2005.
- [3] R. Ghazali, A. E. A. Laaroussi, A. EL Bhih, and M. Rachik, "On the control of a reaction-diffusion system: a class of SIR distributed parameter systems," *International Journal of Dynamics and Control*, vol. 7, no. 3, pp. 1021–1034, 2019.
- [4] <https://zephoria.com/top-15-valuable-facebook-statistics/>.
- [5] L. J. Sabato, K. Kondik, and G. Skelley, *Republicans 2016: What to Do with the Donald?*, 2015, <http://centerforpolitics.org/crystalball/articles/republicans-2016-what-to-do-with-the-donald/>.
- [6] J. Fromm, S. Melzer, B. Ross, and S. Stieglitz, *Trump versus Clinton-Twitter Communication during the US Primaries*, Palgrave Macmillan, London, UK, 2016.
- [7] C. Lee and K. Quealy, *The 337 People, Places and Things Donald Trump Has Insulted on Twitter: A Complete List*, 2016, <https://www.nytimes.com/interactive/2016/01/28/upshot/donald-trump-twitter-insults.html>.
- [8] <https://www.reuters.com/article/us-russia-telegram-blocking/russia-starts-blocking-telegram-messenger-idUSKBN1HN13J>.
- [9] R. E. Bartholomew and P. Hassall, *A Colorful History of Popular Delusions*, Prometheus Books, Buffalo, NY, USA, 2015.
- [10] D. P. Maki and M. Thompson, *Mathematical Models and Applications*, Prentice-Hall, Englewood cliffs, NJ, USA, 1974.
- [11] A. Rapoport and L. I. Rebhun, "On the mathematical theory of rumor spread," *The Bulletin of Mathematical Biophysics*, vol. 14, no. 4, pp. 375–383, 1952.
- [12] M. H. Zheng, L. Y. Lv, and M. Zhao, "Spreading in online social networks: the role of social reinforcement," *Physical Review E*, vol. 88, no. 1, Article ID 012818, 2013.
- [13] L. Fan, W. Wu, X. Zhai, K. Xing, W. Lee, and D.-Z. Du, "Maximizing rumor containment in social networks with constrained time," *Social Network Analysis and Mining*, vol. 4, no. 1, 2014.
- [14] A. Jain, V. Borkar, and D. Garg, "Fast rumor source identification via random walks," *Social Network Analysis and Mining*, vol. 6, no. 1, p. 62, 2016.
- [15] S. Santhoshkumar and L. D. Dhinesh Babu, "Earlier detection of rumors in online social networks using certainty-factor-based convolutional neural networks," *Social Network Analysis and Mining*, vol. 10, no. 1, p. 20, 2020.
- [16] D. J. Daley and D. G. Kendall, "Epidemics and Rumours," *Nature*, vol. 204, p. 1118, 1964.
- [17] M. Z. Ndii, E. Carnia, and A. K. Supriatna, "Mathematical models for the spread of rumors: a review," in *Proceedings of the 6th International Congress on Interdisciplinary Behavior and Social Sciences (ICIBSoS 2017)*, Bali, Indonesia, July 2018.
- [18] W. O. Kermack and A. G. McKendrick, "A contribution to the mathematical theory of epidemics," *Proceedings of the Royal Society of London. Series A*, vol. 115, pp. 700–721, 1927.
- [19] W. Goffman and V. A. Newill, "Generalization of epidemic theory: an application to the transmission of ideas," *Nature*, vol. 204, no. 4955, pp. 225–228, 1964.
- [20] D. J. Daley and D. G. Kendall, "Statistics epidemics and rumours," *Nature*, vol. 204, p. 1964.
- [21] H. Laarabi, A. Abta, M. Rachik, and J. Bouyaghroumni, "Stability analysis of a delayed rumor propagation model," *Differential Equations and Dynamical Systems*, vol. 24, no. 4, pp. 407–415, 2016.
- [22] R. Zhang and D. Li, "Rumor propagation on networks with community structure," *Physica A: Statistical Mechanics and its Applications*, vol. 483, pp. 375–385, 2017.
- [23] J. Jia and W. Wu, "A rumor transmission model with incubation in social networks," *Physica A: Statistical Mechanics and its Applications*, vol. 491, pp. 453–462, 2018.
- [24] Y. Hu, Q. Pan, W. Hou, and M. He, "Rumor spreading model with the different attitudes towards rumors," *Physica A*:

- Statistical Mechanics and its Applications*, vol. 502, pp. 331–344, 2018.
- [25] A. G. Hakim, H. C. Favre¹, and D. A. Zighed, *Information Diffusion in Online Social Networks: A Survey SIGMOD Record*, vol. 42, no. 2, 2013.
 - [26] L. S. Pontryagin, V. G. Boltyanskii, R. V. Gamkrelidze, and E. Mishchenko, *The Mathematical Theory of Optimal Processes (International Series of Monographs in Pure and Applied Mathematics)*, Interscience, New York, NY, USA, 1962.
 - [27] A. El Bhiih, Y. Benfatah, S. Ben Rhila, M. Rachik, and A. El Alami Laaroussi, “A spatiotemporal prey-predator discrete model and optimal controls for environmental sustainability in the multifishing areas of Morocco,” *Discrete Dynamics in Nature and Society*, vol. 2020, pp. 1–18, 2020.
 - [28] B. Tian, X. Xiao, T. Xu et al., *Rumor Detection on Social Media with Bi-directional Graph Convolutional Networks*, <http://arxiv.org/abs/2001.06362>, 2020.
 - [29] J. Ma, W. Gao, Z. Wei, Y. Lu, and K.-F. Wong, “Detect rumors using time series of social context information on microblogging websites,” in *Proceedings of the 24th ACM International Conference on Information and Knowledge Management-CIKM’15*, Melbourne, Australia, 2015.
 - [30] G. Birkhoff and G. C. Rota, *Ordinary Differential Equations*, John Wiley & Sons, New York, NY, USA, 4th edition, 1989.
 - [31] H. Guo, J. Cao, Y. Zhang, J. Guo, and J. Li, “Rumor detection with hierarchical social attention network,” in *Proceedings of the 27th ACM International Conference on Information and Knowledge Management-CIKM’18*, Torino, Italy, October 2018.
 - [32] J. Li, T. Cai, K. Deng, X. Wang, T. Sellis, and F. Xia, “Community-diversified influence maximization in social networks,” *Information Systems*, vol. 92, p. 101522, 2020.
 - [33] J. Li, T. Sellis, J. S. Culpepper, Z. He, C. Liu, and J. Wang, “Geo-social influence spanning maximization,” *IEEE Transactions on Knowledge and Data Engineering*, vol. 29, no. 8, pp. 1653–1666, 2017.
 - [34] T. Cai, J. Li, A. S. Mian, R. Li, T. Sellis, and J. X. Yu, “Target-aware holistic influence maximization in spatial social networks,” *IEEE Transactions on Knowledge and Data Engineering*, p. 1, 2020.
 - [35] L. Zhao, H. Cui, X. Qiu, X. Wang, and J. Wang, “SIR rumor spreading model in the new media age,” *Physica A: Statistical Mechanics and its Applications*, vol. 392, no. 4, pp. 995–1003, 2013.
 - [36] J. Wang and C. Modnak, “Modeling cholera dynamics with controls canadian applied mathematics quarterly,” , vol. 19, no. 3, 2011.
 - [37] W. H. Fleming and R. W. Rishel, *Deterministic and Stochastic Optimal Control*, Springer, New York, NY, USA, 1975.
 - [38] W. E. Boyce and R. C. DiPrima, *Elementary Differential Equations and Boundary Value Problems*, John Wiley & Sons, New York, NY, USA, 2009.
 - [39] V. Guibout and A. M. Bloch, “A discrete maximum principle for solving optimal control problems,” in *Proceedings of the 2004 43rd IEEE Conference on Decision and Control (CDC)*, vol. 2, pp. 1806–1811, Atlantis, Bahamas, December 2004.

Research Article

C-SIW Rumor Propagation Model with Variable Propagation Rate and Perception Mechanism in Social Networks

Liqing Qiu  and Shuqi Liu 

Shandong Province Key Laboratory of Wisdom Mine Information Technology, College of Computer Science and Engineering, Shandong University of Science and Technology, Qingdao 266590, China

Correspondence should be addressed to Liqing Qiu; qiuliqing2019@163.com

Received 21 June 2020; Accepted 6 July 2020; Published 5 August 2020

Guest Editor: Jianxin Li

Copyright © 2020 Liqing Qiu and Shuqi Liu. This is an open access article distributed under the Creative Commons Attribution License, which permits unrestricted use, distribution, and reproduction in any medium, provided the original work is properly cited.

The propagation of rumor has become a common phenomenon in social networks. Studying the dynamic propagation of rumor can help locate the key points to control rumor propagation. To further research the internal motivation of state transition, a corrector-ignorant-spreader-weakened (C-SIW) model is proposed in this paper. When the individual changes state to transmit rumor, the neighbor may have a significant impact on rumor propagation. Considering the point, this paper constructs a function to describe the propagation rate, which relates to the state of neighbors and the reputation of the spreader. In addition, perception from life also can cause individual state changes. Based on the above fact, the links from the spreader and the weakener to the corrector are added to describe the perception mechanism. Then, combining the derived average field equations, the steady state of the model is analyzed and verified in experimental simulation. Moreover, the experimental results on different networks show that the perception mechanism reduces the rumor influence. Besides, the variable propagation rate can position the fast-growing stage of rumor propagation more accurately and facilitate the control of rumor propagation.

1. Introduction

Driven by the rapid development of the Internet and information technology, social networks [1, 2] have become an indispensable platform to meet people's information needs and daily communication. With the popularity of social platforms such as WeChat and Facebook, multichannel information enables people to know what is going on quickly and conveniently. However, it is inevitable that some information that is not based on facts, namely, rumors, also can spread rapidly. As a typical social phenomenon, the impact of rumors ranges from confusing the people's minds to endangering public order in various emergencies and crises, which is inestimable. For example, in November 2015, a large amount of information about the "terrorist attack in Baotou" appeared on such platforms as WeChat and Weibo, which has triggered public panic. In this case, it can help to stabilize people's mood that officials and the people on the scene clarify the cause and process of the incident in time.

Shortly afterward, it is verified that the two brothers smashed the passing vehicles in front of the farmer's market after getting drunk, which resulted in serious traffic jam rather than terrorist attack. Then the matter gradually subsides after people get to know the fact. Therefore, a thorough understanding of internal mechanisms and external factors is the most basic issue to help control the spread of rumors faster and more effectively.

With the rumor propagation gradually becoming a normal, the dynamic spread of rumors has become a hot research direction in the social network field. Considering that there are many similarities, the rumor models are mainly based on the epidemic spreading models. The first rumor model, Daley-Kendall (DK) model [3], divided the crowd into three types: one is the people who have not heard the rumor (ignorants), the second is the people who have heard the rumor and spread it (spreaders), and the third is the people who have heard the rumor but did not spread it (stiflers). The Maki-Thompson (MK) model [4], a variant of

the DK model, assumed that when two spreaders contact each other, the initial spreader will spread rumor no longer and become a stifler. Admittedly, the typical DK and MK rumor models established a solid foundation for future scholars' research. Sudbury [5] studied the influence of the network topology factor, which is not considered in the DK and MK models during propagation process. Afterward, Moreno et al. [6] combined the MK model with epidemics susceptible-infected-recovered (SIR) model and proposed a novel rumor model, in which S, I, and R represent spreaders, ignorants, and stiflers, respectively. Then, some rumor models explored the influence on the propagation process by considering various mechanisms such as forgetting [3, 4], stifling [7], trust [8], hesitating [9], and self-growth [10]. Nevertheless, these models did not consider that the experience from life may also promote individual state transition. Moreover, with the help of immune strategy [11, 12] to control epidemic infection, many researchers applied the idea of immunizing to prevent rumor propagation by spreading the truth. In addition, information diffusion [13] has been extensively studied from a different perspective. Researchers took different factors including geosocial data [14], community [15–17], location prediction [18], and topic search [19] into account, which evaluated the influence propagation in detail. By mapping the spread of rumors with the spread of wildfire in forest, Indu and Thampi [20] discussed an approach that calculated the probability of a node being affected by rumor and modeled the rumor propagation in a network. In the last few years, different from the previous studies, scholars have begun to focus on the perspective of individual. Afassinou [21] introduced the education rate of the population as a factor to examine the evolution of rumor, which proved that the improvement of individuals education rate can promote the termination of rumor propagation. Further, [22, 23] researched individual's awareness and debunking behavior, respectively, which advocated restraining rumor propagation by improving user awareness, imposing punishment on spreaders, and encouraging authoritative influencers to spread the truth. However, they ignored that neighbors have a certain impact on individuals. For example, a large number of stiflers in neighbors may reduce the probability of individual spreading rumor, and the spreader with big reputation may also have a greater impact on propagation.

Through the research studies of the above models considering various mechanisms and factors, more comprehensive understanding and cognition of the rumor propagation can be obtained. In reality, the propagation rate of rumors usually tends to increase with people's attention to it. However, few existing models exhibit this characteristic. They assume that the rumor propagation rate is a constant throughout the whole propagation process, which ignores the potential influence of ignorant's neighbors [24] on the ignorant when the ignorant turns into a spreader. There is also such a social phenomenon, that is, the attitude of individuals towards rumor would change due to the perception from life. Inspired by the above, starting with the individual's attitude to rumors, the stiflers are divided into weakeners and correctors based on the fundamental SIR

model. In this paper, a Corrector-Ignorant-Spreader-Weakener (C-SIW) rumor propagation model considering the variable propagation rate and perception mechanism is proposed. In particular, spreaders, weakeners, and correctors are defined as forwarding propagation, neutral propagation, and negative propagation state, respectively. In detail, the main research contributions of the paper can be reflected in the following aspects:

- (i) Considering the impact of social relations, the rumor propagation rate of C-SIW model depends on the comprehensive influence of neighbors and the reputation of the spreader when the ignorant is infected by a spreader.
- (ii) Considering the possible situations in life, the paper adds a link from the spreader and the weakener to the corrector triggered by perception mechanism, respectively. Besides, the perception mechanism from the weakener to the corrector breaks the dynamic balance between the two states.
- (iii) The C-SIW model is simulated on the generated BA and WS networks, and the experimental results are compared with those of the real social network Facebook.

The rest of the paper is organized as follows. The next section details the proposed C-SIW model and related mechanism. The third section carries on the steady state analysis to the model. The experimental simulation is generated in Section 4, and the results are explained systematically. Further, the last section covers the conclusions and future work.

2. C-SIW Rumor Propagation Model with Variable Propagation Rate and Perception Mechanism

In this section, the fundamental SIR model and the C-SIW model are presented in detail. Uniformly, the research environment social network of the model can be represented as an undirected graph $G(V, E)$ containing N individuals. All the individuals in social networks act as nodes set V , and different-connected edges set E contains the association between different individuals.

2.1. SIR Model. Up to now, the epidemics SIR model has made a great contribution to the development of rumor propagation. Before introducing the proposed C-SIW model, in this subsection, the basic SIR model is illustrated firstly.

In the SIR model, the individuals in the system can be divided into three categories: susceptible (the healthy individuals who may be infected, denoted as S), infected (the individuals who are in a diseased state and are contagious, denoted as I), and recovered (the individuals who recover and gain immunity or die after infection, denoted as R). The specific infection process is shown in Figure 1. The susceptible may contact an infected and then converts to an

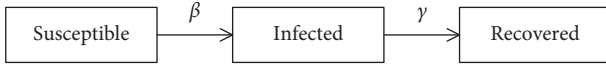


FIGURE 1: The infection process of the SIR model.

infected with the probability of β ; and the recovered comes from the infected people who recovered from disease or died with the probability of γ .

Then, to describe the above infection rules, the average field equations can be established as follows:

$$\begin{aligned}\frac{dS(t)}{dt} &= -\beta S(t)I(t), \\ \frac{dI(t)}{dt} &= \beta S(t)I(t) - \gamma I(t), \\ \frac{dR(t)}{dt} &= \gamma I(t).\end{aligned}\quad (1)$$

In equation (1), $S(t)$, $I(t)$, and $R(t)$ represent the density of the susceptible, the infected, and the recovered at time t , respectively; and, in the system, $S(t) + I(t) + R(t) = 1$ is maintained at any time.

2.2. Evolution Process of the C-SIW Rumor Propagation Model. To further study the intrinsic conversion motivation of promoting rumor propagation, the C-SIW model also follows the footsteps of predecessors and extends with the SIR as the fundamental model. In the C-SIW model, according to the different effects of each individual on rumor spreading, each individual in the system is in one of the following states at time t : the ignorant (who has not heard the rumor yet, similar to the susceptible), the spreader (who has heard the rumor and spread it, similar to the infected), and the stifler (similar to the recovered) that can be subdivided into the weakener (who has heard the rumor and no longer spread it because he/she is not interested or unsure about the truth of the rumor) and the corrector (who can distinguish the rumor and suppress the rumor spreading by disseminating the truth after he/she has heard the rumor). Different from the previous researches, in the process of rumor propagation, the state of the weakener may spontaneously transform into the corrector due to the effect of perception mechanism, rather than not into another state. The total propagation process is carried out through the link edges between the nodes. Specifically, the evolution process of the C-SIW rumor model is shown in Figure 2.

Combined with the state transition of the nodes in Figure 2, the rules for rumor propagation of the C-SIW model are as follows:

- (1) When the spreader in the system contacts an ignorant, there are three state transition options for the ignorant. One is that no matter the ignorant will believe or doubt the rumor spread by the spreader, he/she will spread the rumor with propagation rate β . The second is that the ignorant has rich

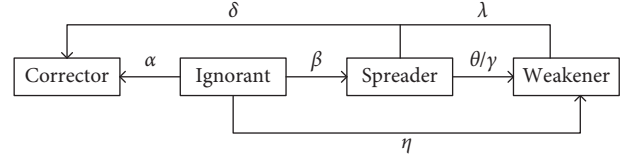


FIGURE 2: The evolution process of the C-SIW rumor propagation model.

knowledge to recognize the truth of the rumor and spread the truth with a containment rate of α to prevent the friends from being cheated, that is to say, converts to a corrector. The last possibility is that the ignorant is not interested in rumor or does not know whether the rumor is true or false, which shows a negative attitude and he/she turns into a weakener with the rate of η . Here, suppose that $\alpha + \beta + \eta = 1$.

- (2) With the contact between individuals, the spreader may convert to a weakener with the stifling rate γ ; or, after being influenced by the weakener and the corrector, the spreader doubts his cognition and converts to a weakener with the immune rate θ . Another situation is that the spreader himself/herself is conscious of the inaccuracy of the rumor by the perception of life and then converts to a corrector with a certain probability, called spontaneous control rate δ .
- (3) Similarly, due to the perception from life experience, the weakener may realize that the rumor is misleading. In this case, the weakener's attitude towards life, which is in the state of neutral propagation at this time, transforms into a positive way by spreading the fact with the probability of λ , named fact transmission rate.

2.3. Average Field Equations. Based on the propagation rules above, the average field equations of the C-SIW model are established to describe the propagation process. First, the proportions of ignorant, spreader, weakener, and corrector in the whole system at time t , that is, the density value, are marked as $I(t)$, $S(t)$, $W(t)$, and $C(t)$, respectively. The average degree of the network is expressed by k in this paper. Consistent with most of the former researches, the states in the system follow the following normalization conditions:

$$I(t) + S(t) + W(t) + C(t) = 1. \quad (2)$$

Then, the average field equations of C-SIW model are shown as the following equations:

$$\frac{dI(t)}{dt} = -k\beta S(t)I(t) - k\alpha S(t)I(t) - k\eta S(t)I(t), \quad (3)$$

$$\frac{dS(t)}{dt} = k\beta S(t)I(t) - \gamma S(t) - \delta S(t) - k\theta S(t)(W(t) + C(t)), \quad (4)$$

$$\frac{dW(t)}{dt} = k\eta S(t)I(t) + \gamma S(t) - \lambda W(t) + k\theta S(t)(W(t) + C(t)), \quad (5)$$

$$\frac{dC(t)}{dt} = k\alpha S(t)I(t) + \delta S(t) + \lambda W(t). \quad (6)$$

Here, in order to satisfy the generality, there is only one randomly selected individual spreading the rumor when $t = 0$. That is, the initial conditions for the evolution of the model are set as follows:

$$\begin{aligned} I(0) &= \frac{N-1}{N} \approx 1, \\ S(0) &= \frac{1}{N} \approx 0, \end{aligned} \quad (7)$$

$$W(0) = 0,$$

$$C(0) = 0.$$

2.4. Propagation Mechanisms. After understanding the propagation process of the model, the propagation mechanisms are introduced to explore the potential motives for influencing the rumor propagation. In the subsection, the variable propagation rate and perception mechanism are explained in detail.

2.4.1. Variable Propagation Rate. To more closely express that the propagation rate is not always constant, the paper introduces a function to describe this characteristic. As far as we know, the spread of rumors often depends on social relations, which are a strong feature performed by social networks. Therefore, particular research on the role of social relations in rumor propagation is conducted. As supposed in Section 1, both weakener and corrector are negative parties for rumor propagation. In such a situation, this paper considers that when an individual is infected to spread the rumor, social relationship is a comprehensive effect of potential contact between individual and neighbors. Meanwhile, the reputation of the spreader is also a critical factor contributing to propagation. The greater the reputation of the spreader is, the easier it is to gain individual trust in rumor. That is to say, the propagation probability of each individual is different by considering their situation. Therefore, for each individual i , such a function to describe the rumor propagation rate β concretely at time t can be defined as follows:

$$\beta_i(t) = \beta_0 e^{-(((C_i(t) + W_i(t) - S_i(t))/\text{tot}_i(t)) + (1-f))/2)}, \quad (8)$$

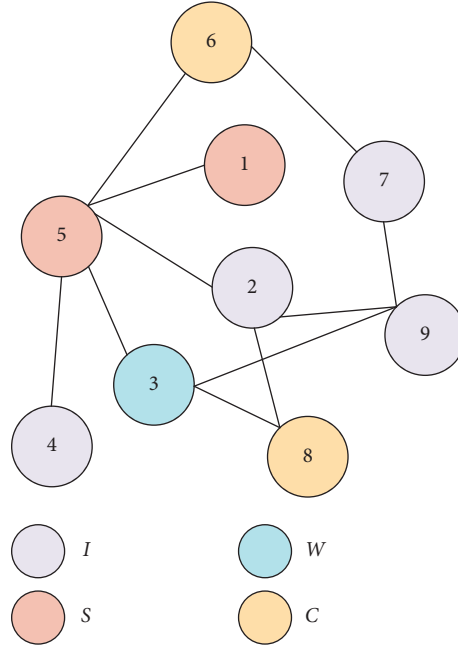
where β_0 represents the initial propagation rate; $((C_i(t) + W_i(t) - S_i(t))/\text{tot}_i(t))$ is assumed as the comprehensive influence of neighbors on individual i ; $C_i(t)$, $W_i(t)$, and $S_i(t)$ denote the number of correctors, weakeners, and spreaders in the total neighbors $\text{tot}_i(t)$ of individual i at time t , respectively; f reflects the reputation of the spreader; e means that the function is based on the irrational number of 2.7182818... For example, there is a social network G as shown in Figure 3. Assume that nodes 2, 4, 7, and 9 are ignorant, and nodes 1 and 5 are spreaders. Similarly, nodes 6 and 8 belong to the correctors, and node 3 is a weakener. For node 2, the neighbors' influence on it can be expressed as $((C_i(t) + W_i(t) - S_i(t))/\text{tot}_i(t)) = ((1 + 1 - 1)/4) = 0.25$. Therefore, assuming that $f = 0.6$ and $\beta_0 = 0.7$, $\beta_{\text{node } 2} = 0.7 * e^{-((0.25 + (1-0.6))/2)} \approx 0.5317$ when node 2 is infected by node 5 to spread rumor.

2.4.2. Perception Mechanism. In actual life, people are always impressed by the fact they have experienced, which makes it easy to get them against the rumor. To prevent more people from being deceived by rumor, they spread the fact with strong motivation. The above is the source of perception mechanism and the perception mechanism will take place on the spreader and weakener in the C-SIW rumor propagation system. This is reflected in the spontaneous control rate δ and fact transmission rate λ , respectively, when the spreader and weakener convert to the corrector as described in Section 2.2. To be specific, the parameters spontaneous control rate δ and fact transmission rate λ are both assumed to be an adjustable constant between 0 and 1 in this paper.

The above provides a general description of the proposed C-SIW model. Since the obtained average field equations (i.e., equations (3)–(6)) describe the propagation rules of the C-SIW model, the next work is to analyze systematically the dynamic propagation of rumor based on the average field equations.

3. Steady-State Analysis

As time goes on, the influence of rumor will have a range, which is the final size of the rumor. In a common way, the paper uses an indicator R to measure it, that is, $R = \lim_{t \rightarrow \infty} R(t) = R(\infty)$. There are $I = \lim_{t \rightarrow \infty} I(t) = I(\infty)$, $S = \lim_{t \rightarrow \infty} S(t) = S(\infty) = 0$, $W = \lim_{t \rightarrow \infty} W(t) = W(\infty)$, and $C = \lim_{t \rightarrow \infty} C(t) = C(\infty)$ when $t \rightarrow \infty$. In addition, it is pointed out that the weakeners and the correctors are the components of the stiflers in Section 1. Therefore, $R = R(\infty) = W(\infty) + C(\infty) = W + C = 1 - I - S = 1 - I$. Here, the final influence range R of rumor is researched by making use of the average field equations. First, dividing the sum of equations (5) and (6) by equation (3), there is

FIGURE 3: A social network G .

$$\begin{aligned}
 \frac{dR(t)}{dI(t)} &= \frac{d(W(t) + C(t))}{dI(t)} \\
 &= \frac{dW(t) + dC(t)}{dI(t)} \\
 &= \frac{k\eta S(t)I(t) + \gamma S(t) - \lambda W(t) + k\theta S(t)(W(t) + C(t)) + k\alpha S(t)I(t) + \delta S(t) + \lambda W(t)}{-k(\beta + \alpha + \eta)S(t)I(t)} \\
 &= \frac{k(\alpha + \eta)S(t)I(t) + (\gamma + \delta)S(t) + k\theta S(t)(W(t) + C(t))}{-kS(t)I(t)} \\
 &= -(\alpha + \eta) - \frac{\gamma + \delta}{kI(t)} - \frac{\theta R(t)}{I(t)}.
 \end{aligned} \tag{9}$$

Assuming that $R(t) = y$ and $I(t) = x$, $(dR(t)/dI(t)) = -(\alpha + \eta) - ((\gamma + \delta)/kI(t)) - (\theta R(t)/I(t))$ can be expressed as $(dy/dx) = -(\alpha + \eta) - ((\gamma + \delta)/kx) - (\theta y/x)$; i.e., $(dy/dx) + (\theta/x)y = -((\gamma + \delta)/kx) - (\alpha + \eta)$. According to the solution of the first-order linear nonhomogeneous equation, it can be obtained that

$$\begin{aligned}
 y &= e^{-\int (\theta/x) dx} \left[\int \left(-\frac{\gamma + \delta}{kx} - (\alpha + \eta) \right) e^{\int (\theta/x) dx} dx + C_1 \right] \\
 &= e^{-\theta \ln x} \left[\int \left(-\frac{\gamma + \delta}{kx} - (\alpha + \eta) \right) x^{\theta \ln x} dx + C_1 \right] \\
 &= x^{-\theta} \left[\int \left(-\frac{\gamma + \delta}{kx} - (\alpha + \eta) \right) x^{\theta} dx + C_1 \right] \\
 &= x^{-\theta} \left[-\frac{\gamma + \delta}{k\theta} x^{\theta} - \frac{\alpha + \eta}{\theta + 1} x^{\theta + 1} + C_1 \right]
 \end{aligned}$$

$$= -\frac{\gamma + \delta}{k\theta} - \frac{\alpha + \eta}{\theta + 1} x + C_1 x^{-\theta}. \tag{10}$$

Therefore,

$$R(t) = -\frac{\gamma + \delta}{k\theta} - \frac{\alpha + \eta}{\theta + 1} I(t) + C_1 I(t)^{-\theta}. \tag{11}$$

Theorem 1. *There exists propagation threshold $\beta_c = ((\gamma + \delta)/k)$ in the C-SIW model, and only when $\beta > \beta_c$ can the rumor be spread.*

Proof. Taking the initial condition equation (7) into equation (11), it can be obtained that $R(0) = -((\gamma + \delta)/k\theta) - ((\alpha + \eta)/(\theta + 1))I(0) + C_1 I(0)^{-\theta}$. After that, by solving the above equation, $C_1 = ((\gamma + \delta)/k\theta) + ((\alpha + \eta)/(\theta + 1))$. At this point, attention should be paid to the fact that all parameters are between 0 and 1 in the proposed model and it is easy to know that $C_1 > 0$. Further, by analyzing equation (11), we can get that when $t \rightarrow \infty$,

$$\begin{aligned}
R &= R(\infty) \\
&= \frac{\gamma + \delta}{k\theta} - \frac{\alpha + \eta}{\theta + 1} I(\infty) + C_1 I(\infty)^{-\theta} \\
&= \frac{\gamma + \delta}{k\theta} - \frac{\alpha + \eta}{\theta + 1} I + C_1 I^{-\theta}.
\end{aligned} \quad (12)$$

Taking $I = 1 - R$ from $R = 1 - I$ transformation into equation (12), we can get

$$R = \frac{\gamma + \delta}{k\theta} - \frac{\alpha + \eta}{\theta + 1} (1 - R) + C_1 (1 - R)^{-\theta}. \quad (13)$$

Arrange equation (13) and assume that

$$f(R) = \frac{\alpha + \eta}{\theta + 1} (1 - R) - R + C_1 (1 - R)^{-\theta} - \frac{\gamma + \delta}{k\theta}. \quad (14)$$

Then, the final size of rumor is analyzed by the properties of R in the domain interval $(0, 1)$. The derivation of function $f(R)$ on R is $f'(R) = ((\alpha + \eta)/(\theta + 1)) - 1 + C_1 \theta (1 - R)^{-\theta-1}$ and $f''(R) = C_1 \theta (\theta + 1) (1 - R)^{-\theta-2}$. Because of $C_1 > 0$, it is obvious that $f''(R) > 0$. Therefore, $f(R)$ is a concave function. Besides, according to equation (14), there are $f(0) = 0$ and $\lim_{R \rightarrow 1^-} f(R) = C_1 (1 - 1)^{-\theta} - ((\gamma + \delta)/k\theta) - 1 = \infty$. Under the circumstance, if $f(R)$ has another nonzero root R^* ($0 < R^* < 1$), it needs to satisfy that $f'(0) = ((\alpha + \eta)/(\theta + 1)) - 1 + C_1 \theta = ((\alpha + \eta)/(\theta + 1)) - 1 + (((\gamma + \delta)/k\theta) + ((\alpha + \eta)/(\theta + 1)))\theta < 0$; that is, $\beta > ((\gamma + \delta)/k)$. At the moment, there is a propagation threshold $\beta_c = ((\gamma + \delta)/k)$. It is necessary to notice the condition that the propagation probability $\beta > \beta_c$ must be met, so as to make the rumor spread.

Recently, the strategy has been introduced to inhibit the spread of rumors by immunizing some individuals. Here, at the beginning of spreading, the individuals with the proportion of p in the total individuals are randomly immunized, which means that these individuals will not spread rumor and will inhibit rumor spreading. In this case, the initial conditions for rumor propagation are

$$\begin{aligned}
I(0) &= 1 - p, \\
S(0) &= 0, \\
W(0) &= 0, \\
C(0) &= p.
\end{aligned} \quad (15)$$

Theorem 2. *Considering the implementation of immune strategy for the rumor model, the C-SIW model has an immune proportion threshold $p_c = ((k\beta - \gamma - \delta)/k(\theta + \beta))$. On the basis of satisfying $\beta > \beta_c$ (i.e., $\beta_c = ((\gamma + \delta)/k)$), only when $p < p_c$ can the rumor be spread.*

Proof. Bringing the initial conditions in equation (15) into equation (11), there is

$$\begin{aligned}
R(0) &= \frac{\gamma + \delta}{k\theta} - \frac{\alpha + \eta}{\theta + 1} I(0) + C_2 I(0)^{-\theta} \\
&= \frac{\gamma + \delta}{k\theta} - \frac{\alpha + \eta}{\theta + 1} (1 - p) + C_2 (1 - p)^{-\theta} \\
&= W(0) + C(0) \\
&= p.
\end{aligned} \quad (16)$$

From equation (16), $C_2 = p(1 - p)^{\theta} + ((\gamma + \delta)/k\theta)(1 - p)^{\theta} + ((\alpha + \eta)/(\theta + 1))(1 - p)^{\theta+1}$. It can be observed that $C_2 > 0$. Furthermore,

$$\begin{aligned}
R &= R(\infty) \\
&= \frac{\gamma + \delta}{k\theta} - \frac{\alpha + \eta}{\theta + 1} I(\infty) + C_2 I(\infty)^{-\theta} \\
&= \frac{\gamma + \delta}{k\theta} - \frac{\alpha + \eta}{\theta + 1} I + C_2 I^{-\theta} \\
&= \frac{\gamma + \delta}{k\theta} - \frac{\alpha + \eta}{\theta + 1} (1 - R) + C_2 (1 - R)^{-\theta}.
\end{aligned} \quad (17)$$

Assume that $g(R) = -((\alpha + \eta)/(\theta + 1))(1 - R) - R + C_1 (1 - R)^{-\theta} - ((\gamma + \delta)/k\theta)$. Similarly, by deriving $g(R)$, there are $g'(R) = ((\alpha + \eta)/(\theta + 1)) - 1 + C_2 \theta (1 - R)^{-\theta-1}$ and $g''(R) = C_2 \theta (\theta + 1) (1 - R)^{-\theta-2} > 0$. That is, $g(R)$ is a concave function. $g(p) = -((\alpha + \eta)/(\theta + 1))(1 - p) - p + C_2 (1 - p)^{-\theta} - ((\gamma + \delta)/k\theta) = 0$ and $\lim_{R \rightarrow 1^-} g(R) = C_2 (1 - 1)^{-\theta} - ((\gamma + \delta)/k\theta) - 1 = \infty$. Then, under the constraint of $g'(p) < 0$ (i.e., $p < ((k\beta - \gamma - \delta)/k(\theta + \beta))$), $g(R)$ will have two roots p and R^* ($p < R^* < 1$). As a result, it can be concluded that there exists an immune proportion threshold $p_c = ((k\beta - \gamma - \delta)/k(\theta + \beta))$ in the model, and the rumor can spread when immune proportion $p < p_c$.

4. Simulation Results and Analysis

In the section, utilizing the popular WS network [25] and BA network [26], the paper simulates and analyzes the steady state of the model. Furthermore, considering that the real social network has more complex topological structure and clustering characteristics than the generated network, the characteristics of the model in the real-world network are worth exploring. As a social platform, Facebook is closer to people's lives. Therefore, the paper investigates the dynamic spread of rumors and makes a concrete comparison with the results of the generated WS network and BA network through the experiment on the real social network Facebook. In detail, the employed Facebook network contains 4039 users and 88234 edges [27]. For the WS network and BA network, the number of individuals $N = 10^6$ is generated to avoid particularities. Besides, the random reconnection probability p' and average degree k of the BA network are 0.1 and 6, respectively, and the average degree k of the WS network is also set to 6. All the presented results are the average results of 70-time simulations by randomly selecting different initial spreader.

4.1. Verification of the Model's Steady State. First of all, experimental simulation is conducted to discuss the pre-conditions of rumor propagation. At the same time, the theorems outlined in Section 3 are verified through the analysis of system's steady state.

Figures 4(a) and 4(b) reflect the change of rumor final size R with β on WS network and BA network, respectively. Since the rumor propagation rate considered by this paper

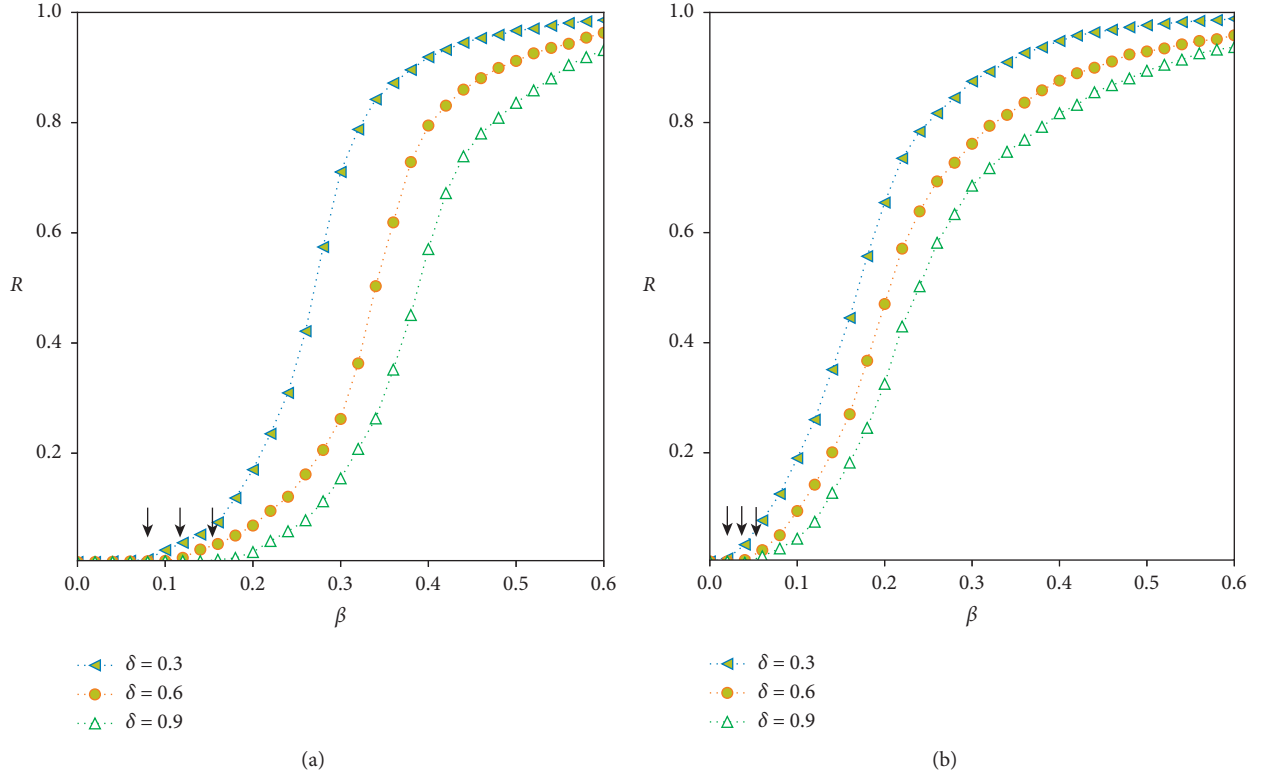


FIGURE 4: The relationship between the final size R and the propagation rate β under different δ on (a) WS network and (b) BA network. The parameters are $\theta = 0.1$, $\alpha = \eta$, $r = 0.1$, and $\lambda = 0.05$.

fluctuates slightly with time, the rumor propagation rate was taken as the average value of all values in the whole system here. From Figure 4(a), we can make out the different propagation threshold according to the different δ settings through the position indicated by arrows, which is close to β_c mentioned in Theorem 1. However, the obvious difference is that the propagation threshold in Figure 4(b) appears earlier, which is caused by the hub node in BA network promoting the spread of rumor. Besides, the reason leads to the increase of R being faster than that on WS network with the increase of β . Furthermore, in both BA network and WS network, the position of the propagation threshold shifts backward and R reduces with the increase of δ . It is caused by the perception mechanism introduced, which is explained further in the next section.

Figure 5 illustrates the trend of the final size R of rumor and its components C and W with different immune proportions p of nodes. Comparing Figures 5(a) and 5(b), it is clear that the immune proportion threshold appears earlier in the WS network than in the BA network. Increasing the number of immune nodes is more convenient to control the propagation of rumor in the WS network, which can be seen from the decline range of R in the same time interval. The main reason is that the degree of nodes in the WS network is more average, while most nodes in the BA network have smaller degree. From the perspective of C , it is worth noting that, in the WS network, the trend of C decreases slowly and then rapidly, indicating that the improvement of immune proportion can have an ideal effect. However, for the BA

network, the trend realizes that the rumor control reaches a transition from slow to fast as p increases, not as ideal as in the WS network. As the number of the correctors increases, the probability of the spreaders touching the correctors and then converting to the weakeners or correctors is increased, which achieves that individuals will remain uninfected when rumor disappears. In particular, after the immune proportion threshold, W researches zero while C maintains linear growth, which means that there are no weakeners in the system when the rumor disappears. In general, from the simulation on the BA network, Theorem 2 derived is also feasible. In order to prevent people from being hurt by the similar rumors that happened before, relevant staff can sort out relevant data and inform people in advance of what may happen when an event occurs, which can help achieve the effect of early immunization.

4.2. Simulation of Model-Related Mechanisms. Due to the gap between the generated network and the real social network, the differences in the results obtained in different networks cannot be ignored. From this point of departure, the dynamic propagation process of the proposed model on WS network, BA network, and Facebook social network is further discussed by adjusting parameters.

4.2.1. Influence of Variable Propagation Rate on Propagation Process. Figures 6(a)–6(d) demonstrate the effect of neighbors' influence and spreader's reputation on rumor

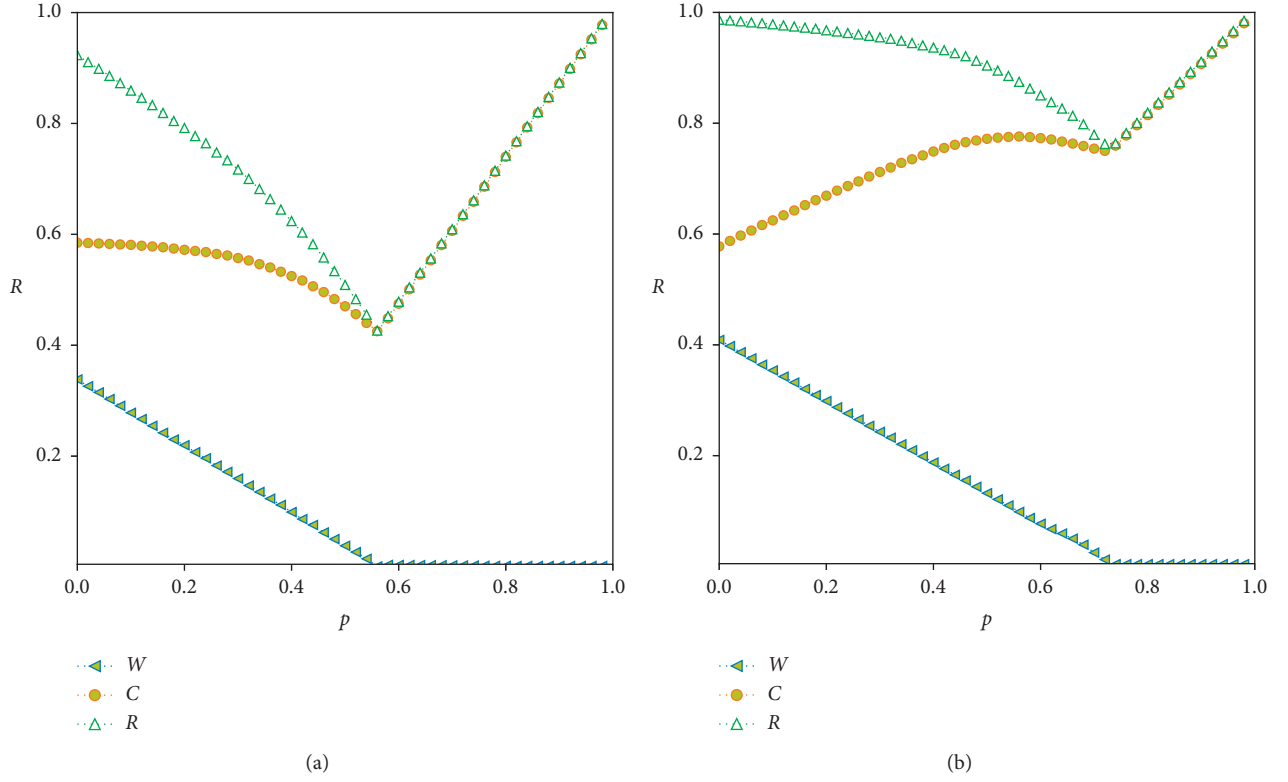


FIGURE 5: The relationship between the final size R and the immunization percentage p on (a) WS network and (b) BA network. The parameters are $\alpha = 0.2$, $\beta_0 = 0.6$, $f = 0.7$, $\eta = 1 - \beta - \alpha$, $\theta = 0.1$, $r = 0.1$, $\delta = 0.2$, and $\lambda = 0.05$.

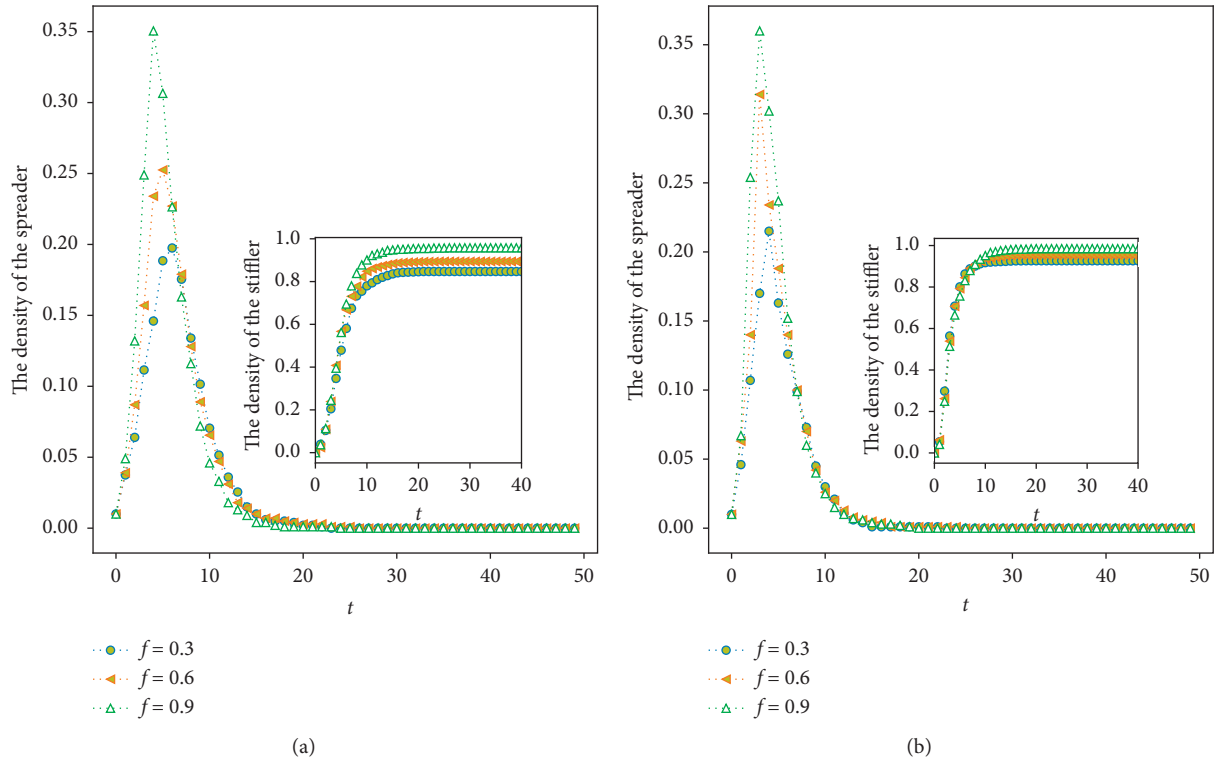


FIGURE 6: Continued.

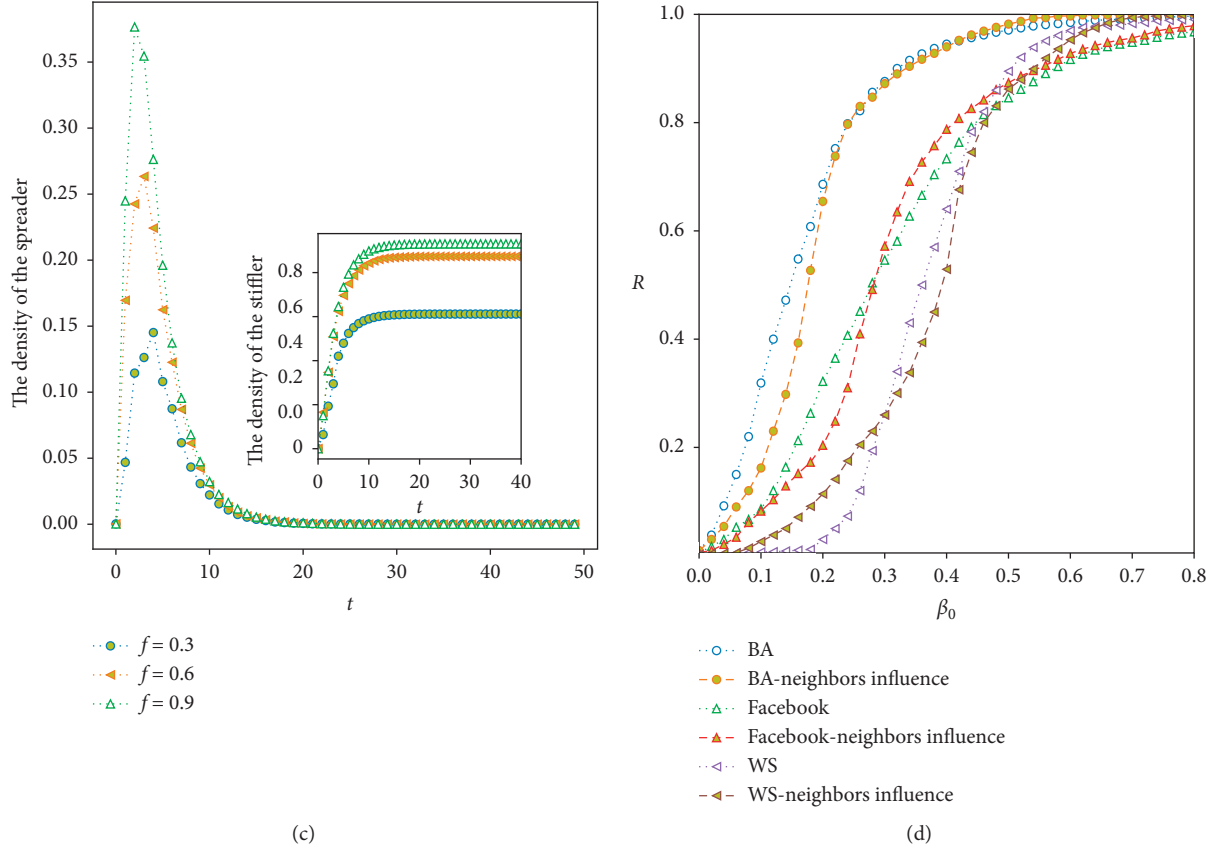


FIGURE 6: The density trend of state with different β . The density of spreader and stiffer with different f on (a) WS network, (b) BA network, and (c) Facebook. (d) The relationship between the final size R and the initial propagation rate β_0 with and without the comprehensive influence of neighbors on WS, BA, and Facebook networks.

propagation in the variable propagation rate function $\beta_i(t) = \beta_0 e^{-((C_i(t) + W_i(t) - S_i(t))/\text{tot}_i(t) + (1-f))/2)}$.

First of all, Figures 6(a)–6(c) describe, respectively, the role played by the different reputations of the spreader in WS, BA, and Facebook network, where the reputation of the spreader is assumed to be 0.3, 0.6, and 0.9 with the same interval. The parameters are $\alpha = 0.2$, $\beta_0 = 0.6$, $\eta = 1 - \beta - \alpha$, $\theta = 0.1$, $r = 0.1$, $\delta = 0.2$, and $\lambda = 0.05$. As shown in the figures, the peak density of the spreader increases with the increase of the reputation of the spreader, and the corresponding final rumor size also increases, which shows the famous celebrity effect [28]. The higher the reputation is, the more trust the spreader can gain by spreading rumor, thus promoting the spread of rumor. Inspired by the experiment, people with high reputation should improve their ability of discrimination and exert their influence in suppressing the spread of rumor.

Then, Figure 6(d) displays a comparison of neighbors comprehensive influence on the individual in each network with the change of initial propagation rate β_0 , in which the measure is the final rumor size R . The parameters are $f = 0.6$, $\alpha = \eta$, $\theta = 0.1$, $r = 0.1$, $\delta = 0.2$, and $\lambda = 0.05$. Independently, a common feature is that no matter whether the comprehensive influence of neighbors in network is considered or not, initially, with the increase of β_0 , the increased speed of R shows that BA is the largest, Facebook is the second, and

WS network is the last. However, the final rumor size R is $BA > WS > \text{Facebook}$ in the end. Besides, it is also crucial to understand how the final rumor size R changes when considering the comprehensive influence of neighbors. Different from the network without considering the comprehensive influence of neighbors, the growth trend of R in the network with considering the neighbors' influence presents an S-shaped curve when β_0 increases, which is described in a more detailed way rather than rapid rising and rapid falling. Undeniably, the stage when the final size R of the rumor grows rapidly is the entry point which can be easy to control. By analyzing the trend of R , the neighbors' influence proposed can provide government and relevant control personnel a better theoretical basis for locating the entry point to take rumor control measures.

4.2.2. Influence of Perception Mechanisms on Propagation Process. The perception mechanisms are mainly the state transition dominated by the individual's subjective psychological changes in the process of rumor propagation, which is reflected in the probability δ and λ of turning from the spreader and the weakener to the corrector.

As time goes by, the density of the spreader and the stiffer changes with the spontaneous control rate δ as shown in Figure 7. In general, the larger δ is, the smaller the density of

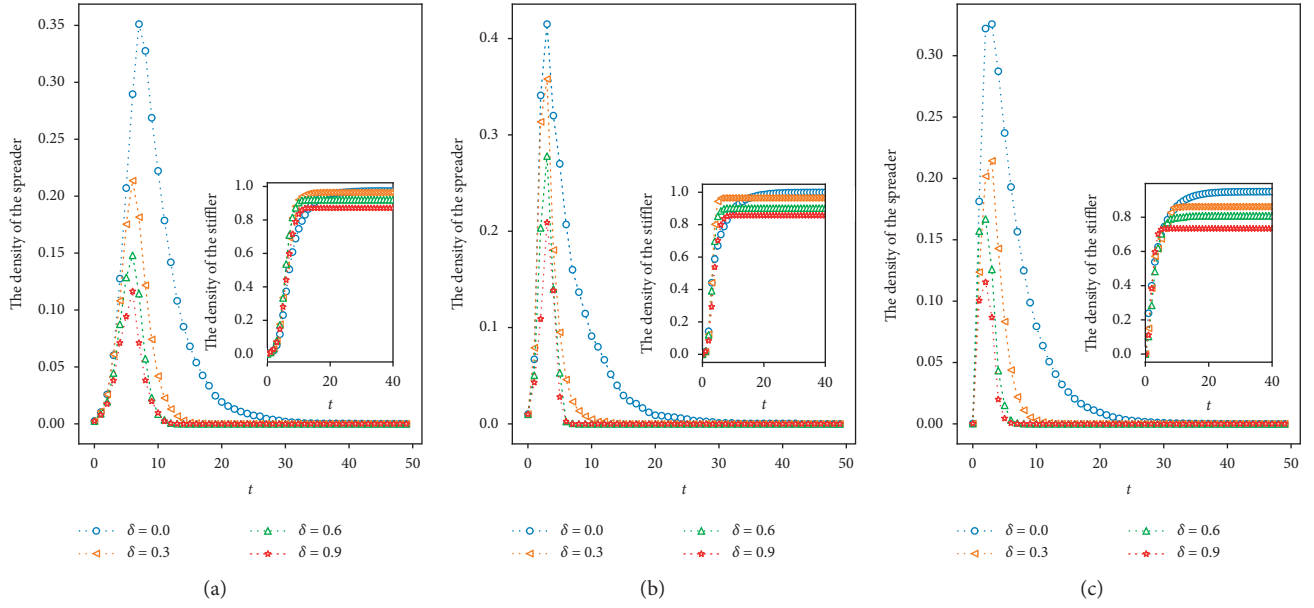


FIGURE 7: The density of the spreader with different δ on (a) WS network, (b) BA network, and (c) Facebook. The parameters are $\alpha = 0.2$, $\beta_0 = 0.6$, $f = 0.6$, $\eta = 1 - \beta - \alpha$, $\theta = 0.1$, $r = 0.1$, and $\lambda = 0.05$.

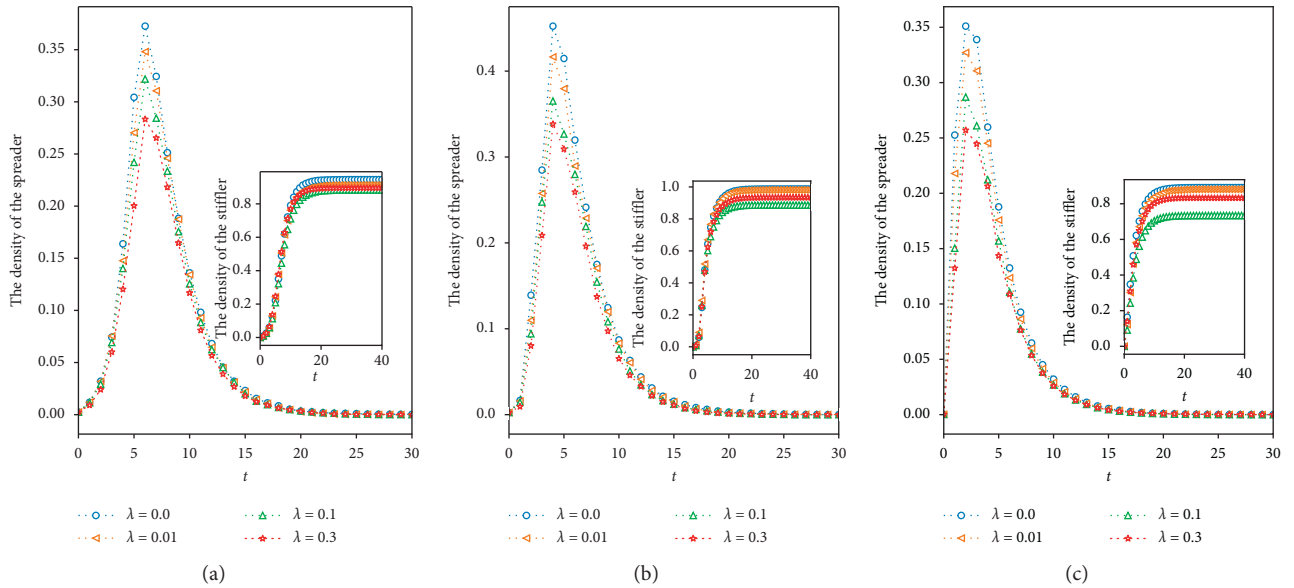


FIGURE 8: The density of spreader with different λ on (a) WS network, (b) BA network, and (c) Facebook. The parameters are $\alpha = 0.2$, $\beta_0 = 0.6$, $f = 0.6$, $\eta = 1 - \beta - \alpha$, $\theta = 0.1$, $r = 0.1$, and $\delta = 0.2$.

the spreader and the termination time of rumor are, which explains that the spreader's perception of life and the conversion to the corrector have a great influence on the individual's subjective choice in the face of rumor. Similarly, when comparing the final rumor size under different δ , that is, the density of the stifler when $t \rightarrow \infty$, the larger δ is, the smaller R is. Furthermore outstanding is that, in WS and BA networks, R has a similar interval change with the increase of δ , while Facebook network has a smaller R . Therefore, it is necessary to call on the corrector who is transferred from the

spreader for spreading his/her own perception experience actively to the friends around him/her, which is helpful for them to recognize the true face of the rumor.

Figure 8 shows the density trends of the spreader and the stifler with different λ over time. Compared with Figures 8(a)–8(c), it is obvious that the trends of density change are similar under different networks. From the figures, the density of the spreader decreases with the increase of λ . Correspondingly, because λ is the probability that the perception mechanism causes the weakener to be the corrector, there are more and

more correctors in the system with the increase of λ . When λ increases to a certain extent, the components of stiflers will be only correctors before the end of rumor propagation, and then more and more individuals in the system will be infected to correctors at the end of rumor propagation. Therefore, it explains that the density of the stifier in the figures shows an inverse growth trend with the increase of λ ; that is, the density of the stifier when $\lambda = 0.3$ is greater than that when $\lambda = 0.1$. In life, weakener is a negative role of life attitude, and the actual probability of the transformation from weakener to corrector is relatively low in general. Due to the fact that the perception mechanism reflects a kind of life phenomenon, it cannot be ignored. The existence of weakeners with high fact transmission rate λ in the system can effectively inhibit the spread of rumor.

5. Conclusions

In this paper, the C-SIW rumor propagation model with variable propagation rate and perception mechanism on social networks is proposed to explore the intrinsic motivation of state transformation. First of all, this paper employs a function to express the propagation rate, in which the spreader with high reputation can promote the spread of rumor. Besides, the variable propagation rate takes into account the comprehensive state of the neighbors contacted by individual, which further positions the stage of rapid growth of rumor propagation. In view of the possible influence of life on individuals, the paper also considers the perception mechanism. Experiments show that individuals with high perception probability including spontaneous control rate δ and fact transmission rate λ can facilitate the reduction of rumor influence.

The paper proposes a theoretical model and verifies it by experiments in WS network, BA network, and Facebook. In actual life, when another event like rumor occurs, it may cause a review of the previous event. At this point, the constant parameter value of perception mechanism is not applicable. Therefore, the future work will explore the impact of the subsequent event on propagation process, no matter whether the subsequent event occurs during or after rumor propagation.

Data Availability

The WS and BA data used to support the findings of this study are included within the article, and the Facebook data used to support the findings of this study are available in the Stanford large network data collection website (<http://snap.stanford.edu/data/ego-Facebook.html>).

Conflicts of Interest

The authors declare that there are no conflicts of interest regarding the publication of this paper.

Acknowledgments

This work was supported by the National Natural Science Foundation of China under Grant nos. 61502281 and 71772107.

References

- [1] C. Li, L. Zhao, Q. Zeng, H. Duan, and Z. Zhao, "Learner2Vec-based learner community evolution analysis—a case study involving student card data," *IEEE Access*, vol. 7, pp. 27416–27425, 2019.
- [2] S. Gao, M. Zhou, Y. Wang et al., "Dendritic neuron model with effective learning algorithms for classification, approximation, and prediction," *IEEE Transactions on Neural Networks & Learning Systems*, vol. 30, no. 2, pp. 601–614, 2018.
- [3] D. J. Daley and D. G. Kendall, "Stochastic rumours," *IMA Journal of Applied Mathematics*, vol. 1, no. 1, pp. 42–55, 1965.
- [4] D. P. Maki and M. Thompson, *Mathematical Models and Applications, with Emphasis on the Social, Life, and Management Sciences*, Prentice-Hall, Englewood Cliffs, NJ, USA, 1973.
- [5] A. Sudbury, "The proportion of the population never hearing a rumour," *Journal of Applied Probability*, vol. 22, no. 2, pp. 443–446, 1985.
- [6] Y. Moreno, M. Nekovee, and A. F. Pacheco, "Dynamics of rumor spreading in complex networks," *Physical Review E*, vol. 69, no. 6, Article ID 066130, 2004.
- [7] M. Nekovee, Y. Moreno, G. Bianconi, and M. Marsili, "Theory of rumour spreading in complex social networks," *Physica A: Statistical Mechanics and Its Applications*, vol. 374, no. 1, pp. 457–470, 2007.
- [8] Y.-Q. Wang, X.-Y. Yang, Y.-L. Han, and X.-A. Wang, "Rumor spreading model with trust mechanism in complex social networks," *Communications in Theoretical Physics*, vol. 59, no. 4, pp. 510–516, 2013.
- [9] L.-L. Xia, G.-P. Jiang, B. Song, and Y.-R. Song, "Rumor spreading model considering hesitating mechanism in complex social networks," *Physica A: Statistical Mechanics and Its Applications*, vol. 437, pp. 295–303, 2015.
- [10] L. A. Huo and Y. Y. Cheng, "Dynamical analysis of an IWSR rumor spreading model with considering the self-growth mechanism and indiscernible degree," *Physica A*, vol. 536, Article ID 120940, 2019.
- [11] L. J. Zhao, J. J. Wang, and R. B. Huang, "Immunization against the spread of rumors in homogenous networks," *PLoS One*, vol. 10, no. 5, Article ID e0124978, 2015.
- [12] J. Huang and X. Jin, "Preventing rumor spreading on small-world networks," *Journal of Systems Science and Complexity*, vol. 24, no. 3, pp. 449–456, 2011.
- [13] D. Kempe, J. M. Kleinberg, and E. Tardos, "Maximizing the spread of influence through a social network," in *Proceedings of the 2003 ACM SIGKDD International Conference on Knowledge Discovery and Data Mining*, pp. 137–146, Washington, DC, USA, 2003.
- [14] J. Li, T. Sellis, J. S. Culpepper, Z. He, C. Liu, and J. Wang, "Geo-social influence spanning maximization," *IEEE Transactions on Knowledge and Data Engineering*, vol. 29, no. 8, pp. 1653–1666, 2017.
- [15] J. Li, X. Wang, K. Deng et al., "Discovering influential community over large social networks," in *Proceedings of the 2017 IEEE International Conference on Data Engineering*, pp. 871–882, San Diego, CA, USA, April 2017.
- [16] J. Li, T. Cai, K. Deng et al., "Community-diversified influence maximization in social networks," *Information Systems*, vol. 92, pp. 1–12, 2020.
- [17] Z. Zhao, C. Li, X. Zhang, F. Chiclana, and E. H. Viedma, "An incremental method to detect communities in dynamic evolving social networks," *Knowledge-Based Systems*, vol. 163, pp. 404–415, 2019.

- [18] N. A. H. Haldar, J. Li, M. Reynolds et al., "Location prediction in large-scale social networks: an in-depth benchmarking study," *VLDB Journal*, vol. 28, no. 5, pp. 623–648, 2019.
- [19] J. Li, C. Liu, J. X. Yu, Y. Chen, T. Sellis, and J. S. Culpepper, "Personalized influential topic search via social network summarization," *IEEE Transactions on Knowledge and Data Engineering*, vol. 28, no. 7, pp. 1820–1834, 2016.
- [20] V. Indu and S. M. Thampi, "A nature-inspired approach based on forest fire model for modeling rumor propagation in social networks," *Journal of Network and Computer Applications*, vol. 125, pp. 28–41, 2019.
- [21] K. Afassinou, "Analysis of the impact of education rate on the rumor spreading mechanism," *Physica A: Statistical Mechanics and Its Applications*, vol. 414, pp. 43–52, 2014.
- [22] C. Y. Sang and S. G. Liao, "Modeling and simulation of information dissemination model considering user's awareness behavior in mobile social networks," *Physica A*, vol. 537, Article ID 122639, 2020.
- [23] Y. Tian and X. J. Ding, "Rumor spreading model with considering debunking behavior in emergencies," *Physica A*, vol. 363, Article ID 124599, 2019.
- [24] S. Ji, W. Yang, S. Guo, D. K. W. Chiu, C. Zhang, and X. Yuan, "Asymmetric response aggregation heuristics for rating prediction and recommendation," *Applied Intelligence*, vol. 50, no. 5, pp. 1416–1436, 2020.
- [25] D. J. Watts and S. H. Strogatz, "Collective dynamics of "small-world" networks," *Nature*, vol. 393, no. 6684, pp. 440–442, 1998.
- [26] A.-L. Barabási and R. Albert, "Emergence of scaling in random networks," *Science*, vol. 286, no. 5439, pp. 509–512, 1999.
- [27] J. McAuley and J. Leskovec, "Learning to discover social circles in ego networks," *Advances in Neural Information Processing Systems*, vol. 1, pp. 539–547, 2012.
- [28] H. Zhu, W. Hu, J. Ma et al., "Study on influence of community structure on opinion topic propagation of micro-blog," *Journal of System Simulation*, vol. 28, no. 7, 2016.

Research Article

Impact of Immunization Strategies on the Dynamics of Social Contagions

Hao Peng,^{1,2} Wangxin Peng,¹ Dandan Zhao ,¹ Zhaolong Hu,¹ Jianmin Han,¹ and Zhonglong Zheng¹

¹College of Mathematics and Computer Science, Zhejiang Normal University, Jinhua 321004, Zhejiang, China

²Shanghai Key Laboratory of Integrated Administration Technologies for Information Security, Shanghai 200240, China

Correspondence should be addressed to Dandan Zhao; ddzhao@zjnu.edu.cn

Received 29 May 2020; Accepted 22 June 2020; Published 1 August 2020

Guest Editor: Wei Wang

Copyright © 2020 Hao Peng et al. This is an open access article distributed under the Creative Commons Attribution License, which permits unrestricted use, distribution, and reproduction in any medium, provided the original work is properly cited.

Immunization strategies on complex networks are effective methods to control the spreading dynamics on complex networks, which change the topology and connectivity of the underlying network, thereby affecting the dynamics process of propagation. Here, we use a non-Markovian threshold model to study the impact of immunization strategies on social contagions, in which the immune index greater than (or equal to) 0 corresponds to targeted (random) immunization, and when the immune index is less than 0, the probability of an individual being immunized is inversely related to the degree of the individual. A generalized edge-based compartmental theory is developed to analyze the dynamics of social contagions under immunization, and theoretical predictions are very consistent with simulation results. We find that increasing the immune index or increasing the immune ratio will reduce the final adoption size and increase the outbreak threshold, in other words, make the residual network after immunization not conducive to social contagions. Interestingly, enhancing the network heterogeneity is proved to help improve the immune efficiency of targeted immunization. Besides, the dependence of the outbreak threshold on the network heterogeneity is correlated with the immune ratio and immune index.

1. Introduction

In many fields, such as sociology and biology, the diffusion mechanisms of some real spreading processes can be essentially described as the spreading dynamics on complex networks [1–6]. Unlike biological contagions, social contagions, such as rumor diffusion [7], behavior spreading [8, 9], information diffusion [10], the adoption of new product [11], the diffusion of microfinance [12], and innovation diffusion [13, 14], have a social reinforcement effect. The credibility of behavior or information usually needs to be confirmed multiple times to reduce risks. That is, the adoption probability of a certain contact depends on the amount of previous contacts. More specifically, for susceptible individuals, before the number of exposures to the same information reaches the adoption threshold, the more times the same information is received from different

neighbors, the greater the adoption possibility [15]. In the linear threshold model [16, 17], the dynamics of social contagions was regarded as a Markov process. In recent years, researchers found that the social reinforcement effect is based on the memory characteristic, and many distinct non-Markovian models [18–28] have been proposed. Wang et al. [18] proposed an edge-based compartmental (EBC) theory to qualitatively analyze the steady state of the dynamics of social contagions with nonredundant information memory characteristic and found that the change of some structural parameters (e.g., the heterogeneity of the network structure) or dynamic factors (e.g., the adoption threshold) will cause the crossover phenomenon of the system. Backlund et al. [19] found that sufficiently long time windows promote the global cascade of adoption on temporal networks. About the effects of community structure on social contagions on temporal networks, Liu et al. [20] found

that when the information transmission rate takes some appropriate values, increasing the community strength can promote the spreading of behavior in communities, and the optimal community strength can maximize the final adoption size. Besides, the heterogeneity of link weights [21], heterogeneous adoption threshold [22–24], and time delays [25] also affect the dynamics of social contagions.

In addition to proposing some more realistic propagation models, taking appropriate immunization strategies is also an effective way to forecast and control the spreading dynamics on complex networks. In the early years, researchers proposed three classic immunization strategies on complex networks, namely, random immunization [29], targeted immunization [29], and acquaintance immunization [30, 31]. From efficiency, acquaintance immunization is more efficient than random immunization and is slightly less efficient than targeted immunization. In another respect, targeted immunization needs to know the degree of each individual in the network, which is very difficult for a dynamically developing real network. However, acquaintance immunization is based on the local information of the network and does not need to identify hub individuals. Based on the three typical immunization strategies, some improving immunization strategies were proposed [32–35]. Considering that the underlying network plays an important role in the spreading dynamics on complex networks, some immunization strategies that take the role of the multiplex network [36, 37], community structure [38, 39], weighted network [40, 41] or time-varying network [42] into account have been proposed. The existing studies have found that immunizing important nodes in the network can effectively suppress or control the epidemic spreading.

However, there is still a lack of systematic theoretical and numerical simulations to address how immunization strategies affect the dynamics of social contagions. For this purpose, we use the non-Markovian susceptible-adopted-recovered (SAR) threshold model to study the effects of different immunization strategies on social contagions, in which we select different types of immunization strategies by adjusting the value of the immune index α . Then, we develop a generalized EBC theory to analyze the dynamics of social contagions under immunization. Through theoretical predictions and numerical simulations on scale-free (SF) networks, we found that (i) increasing the immune index will reduce the final adoption size and increase the outbreak threshold (threshold for short) when the immune ratio is the same; (ii) increasing the immune ratio will decrease the final adoption size and increase the threshold; (iii) when the immune ratio is small, the threshold decreases as the network heterogeneity increases (as γ_D decreases), but when the immune ratio is relatively large and under targeted immunization, the threshold increases as the network heterogeneity increases.

The remainder of the paper is organized as follows. In Section 2, we describe the dynamics of social contagions. Section 3 gives theoretical analysis through the EBC theory. Section 4 presents numerical simulations. Finally, the conclusions are presented in section 5.

2. Model Description

The non-Markovian SAR threshold model is a general model to describe the dynamics of social contagions with nonredundant information memory characteristic; thus, we adopt it to describe the dynamics of social contagions under immunization and study the effects of different immunization strategies on the final adoption size and outbreak threshold of social contagions. There are the following three states of the individual: susceptible state (S), adopted state (A), and recovered state (R). Susceptible individuals will not adopt the behavior unless the amount of nonredundant information received from neighbors is not less than the adoption threshold. Adopted individuals have adopted the behavior and can transmit the behavioral information to their susceptible neighbors with probability λ . If the adopted individual successfully recovers as the recovered individual with probability γ , then, in the subsequent social contagion process, the recovered individual will not share information with his/her neighbors and will always remain in the recovered state. Before the social contagion terminates, the state of individuals will change dynamically.

The immunization strategies in social networks refer to selecting some individuals in the network to be immune to social contagion. That is to say, these selected individuals and their links will be removed from the initial network; thus, they cannot participate in social contagion, which plays a significant role in the prevention and control of social contagions. In real-world networks, the probability of an individual being immune to social contagion is correlated with the number of his/her links (the degree), and each individual i with k_i links is assigned a value $M_\alpha(k_i)$, which denotes the probability of individual i being immunized. According to the family of functions [43–45], the expression of $M_\alpha(k_i)$ is

$$M_\alpha(k_i) = \frac{k_i^\alpha}{\sum_{i=1}^N k_i^\alpha}, \quad -\infty < \alpha < +\infty, \quad (1)$$

where the value of immune index α determines the correlation between an individual's degree and the probability of the individual being immune to social contagion. The case $\alpha > 0$ represents targeted immunization (TI), which means that individuals with higher degrees are more likely to be immunized. Case $\alpha = 1$, especially, corresponds to acquaintance immunization (AI), which is a localized immunization; that is, random neighbors of random individuals are chosen to be immunized. For $\alpha = 0$, all individuals have the same probability of being immunized (i.e., $M_0(k_i) = 1/N$), which represents random immunization (RI). Note that when $\alpha < 0$, individuals with lower degrees have a higher probability to be immunized, which is the opposite of when $\alpha > 0$.

In order to facilitate the analysis, the adoption threshold of all individuals is set to T . In the initial stage, a fraction $1 - q$ individuals are selected to be immunized first, which causes the topology of the underlying network to change. In other words, the residual network consists of the remaining q proportion individuals and their links, and these

individuals can participate in the subsequent social contagion. Specifically, we call the immunized individuals as invalid individuals, and the remaining unimmunized individuals are called valid individuals. Then, a proportion ρ_0 of valid individuals are selected randomly as the adopted individuals for triggering social contagion, and the remaining valid individuals are susceptible individuals and have not obtained any behavioral information. At each time step, in the residual network, each adopted individual j can transmit the behavioral information to its susceptible neighbors with probability λ in a nonredundant transmission way (i.e., a piece of information can only be passed once through an edge). Among valid individuals, if a random susceptible individual i receives the information from individual j , the amount m_i of nonredundant information received by individual i will increase by one. When $m_i \geq T$, individual i adopts the behavior; otherwise it is still in the susceptible state. Moreover, individuals in the adopted state try to recover with probability γ at each time step. If there are no adopted individuals in the residual network after immunization, the social contagion ends.

3. Theoretical Analysis

In this section, based on the non-Markovian SAR threshold model, a general EBC theory is developed to analyze the dynamics of social contagion under immunization. The three variables $S(t)$, $A(t)$, and $R(t)$, respectively, represent the proportion of individuals in the susceptible, adopted, and recovered states at time step t . If an immunization measure is implemented before social contagion occurs (i.e., the immune ratio $1 - \rho \neq 0$), these immunized individuals will be removed from the network; thus, $S(t) + A(t) + R(t) = q < 1$. When $t \rightarrow \infty$, the dynamic process of social contagion reaches the final state (i.e., the state of all individuals no longer changes), and $R(\infty)$ represents the percentage of individuals who have adopted the behavior (the final adoption size for short).

After the initial immunization, these immunized individuals and their links are removed from the initial network, which results in a change in the degree of the neighbors of these immunized individuals. Therefore, we first need to calculate the degree distribution $P_q(k)$ of the residual network after immunization, where q is the ratio of valid (unimmunized) individuals. According to the method in [45, 46], we let $G_q(k)$ denote the amount of valid individuals with degree k , and the degree distribution $P_q(k)$ of valid individuals is given as

$$P_q(k) = \frac{G_q(k)}{qN}. \quad (2)$$

When another individual is immunized and removed from the network, by using (1), the expression of $P_q(k)$ changes as

$$G_{(q-1/N)}(k) = G_q(k) - \frac{P_q(k)k^\alpha}{\langle k^\alpha(q) \rangle}, \quad (3)$$

where $\langle k^\alpha(q) \rangle = \sum_k P_q(k)k^\alpha$. In the limit of $N \rightarrow \infty$, (3) can be written as the derivative equation of $G_q(k)$,

$$\frac{dG_q(k)}{dq} = N \frac{P_q(k)k^\alpha}{\langle k^\alpha(q) \rangle}. \quad (4)$$

Taking the derivative of (2) with respect to q and combining (4), we have

$$-q \frac{dP_q(k)}{dq} = P_q(k) - \frac{P_q(k)k^\alpha}{\langle k^\alpha(q) \rangle}. \quad (5)$$

By direct differentiation and defining the function $F_\alpha(\psi) = \sum_k P(k)\psi^{k^\alpha}$ and variable $\psi = F_\alpha^{-1}(q)$ [46], we can get the expressions of $P_q(k)$ and $\langle k^\alpha(q) \rangle$ as

$$P_q(k) = \frac{1}{q} P(k)\psi^{k^\alpha}, \quad (6)$$

$$\langle k^\alpha(q) \rangle = \frac{\psi F'_\alpha(\psi)}{F_\alpha(\psi)}, \quad (7)$$

respectively.

After the immunization strategy is implemented, for a random individual i with degree k , the probability that it receives m pieces of nonredundant behavioral information by time t is

$$\pi(k, m, \tau(t)) = (1 - \rho_0) C_k^m \tau(t)^{k-m} [1 - \tau(t)]^m, \quad (8)$$

where $1 - \rho_0$ is the initial fraction of susceptible individuals after immunization and $\tau(t)$ represents the probability that by time t , a random edge of individual j has not transmitted the information to a susceptible neighbor i . According to the condition of a susceptible individual adopting behavior (i.e., $m \geq T$), the probability that individual i remains susceptible at time t is

$$s(k, t) = \sum_{m=0}^{T-1} \pi(k, m, \tau(t)). \quad (9)$$

Considering all possible values of the degree k of valid individuals, the fraction of susceptible individuals in the residual network at time t is

$$S(t) = \sum_k P_q(k) s(k, t). \quad (10)$$

It is worth noting that the neighbor of individual i may be in one of three states; therefore the expression of $\tau(t)$ is defined as

$$\tau(t) = \chi_S(t) + \chi_A(t) + \chi_R(t), \quad (11)$$

where $\chi_S(t)$, $\chi_A(t)$, and $\chi_R(t)$, respectively, represent the probabilities that a neighbor of individual i is in the susceptible, adopted, or recovered states and has not transmitted the information to its neighbors by time t .

Next, the evolution expression of $\tau(t)$ will be solved. Individual i is assumed to be in the cavity state [47, 48], i.e., it can only receive information from its neighbors but cannot transmit information to its neighbors. Therefore, the susceptible neighbor j with degree k' of individual i can only receive information from its $k' - 1$ neighbors except

neighbor i . Similarly, the probability that individual j acquires m pieces of information by time t is

$$\mu(k', m, \tau(t)) = C_{k'-1}^m \tau(t)^{k'-m-1} [1 - \tau(t)]^m. \quad (12)$$

Consequently, the probability that individual j remains in the susceptible state at time t is $\psi(k', t) = \sum_{m=0}^{T-1} \mu(k', m, \tau(t))$. The probability that individual i is connected to a neighbor with degree k' is $k' P_q(k') / \langle k \rangle$; thus, we have

$$\chi_S(t) = \frac{1 - \rho_0}{\langle k \rangle} \sum_{k'} k' P_q(k') \psi(k', t). \quad (13)$$

When the information fails to be transmitted through an edge with probability $1 - \lambda$ and the connected adopted individual recovers with probability γ , $\chi_R(t)$ increases. Thus, the evolution of $\chi_R(t)$ is obtained as

$$\frac{d\chi_R(t)}{dt} = \gamma(1 - \lambda)\chi_A(t). \quad (14)$$

At time t , the adopted individuals transmit information to their susceptible neighbors with probability λ ; thus, the evolution of $\tau(t)$ is

$$\frac{d\tau(t)}{dt} = -\lambda\chi_A(t). \quad (15)$$

Combining (14) and (15), we have $\chi_R(t) = \gamma(1 - \lambda)[1 - \tau(t)]/\lambda$. Then, by substituting the expressions of $\chi_R(t)$ and $\chi_S(t)$ into (11), we get the expression of $\chi_A(t)$. Thus, (15) is rewritten as

$$\begin{aligned} \frac{d\tau(t)}{dt} = & -\lambda \left[\tau(t) - \frac{1 - \rho_0}{\langle k \rangle} \sum_{k'} k' P_q(k') \psi(k', t) \right] \\ & + \gamma(1 - \lambda)[1 - \tau(t)]. \end{aligned} \quad (16)$$

As we know, susceptible individuals become adopted individuals once they adopt the behavior, and adopted individuals recover with probability γ ; thus, the time evolution of $A(t)$ and $R(t)$ is

$$\frac{dA(t)}{dt} = -\frac{dS(t)}{dt} - \gamma A(t), \quad (17)$$

$$\frac{dR(t)}{dt} = \gamma A(t), \quad (18)$$

respectively. By numerically integrating (10) and ((17)-(18)), the pattern of $R(t)$ versus t is given. When the process of social contagion reaches a final state (i.e., $t \rightarrow \infty$), $R(\infty)$ is the final adoption size.

4. Numerical Simulations and Analysis

In this section, we report the theoretical and numerical simulations on SF networks [49] with degree distribution $p(k) \sim k^{-\gamma_D}$, where γ_D denotes degree exponent, and the

structural heterogeneity of the network decreases as γ_D increases. Unless otherwise specified, the network size, maximum degree, average degree, initial seeds ratio, adoption threshold, and recovery probability are set to be $N = 10000$, $k_{\max} \sim \sqrt{N}$, $\langle k \rangle = 10$, $\rho_0 = 0.1$, $T = 3$, and $\gamma = 1.0$, respectively. The outbreak threshold λ_c indicates the critical value of information transmission probability. λ_c can be determined by calculating the relative variance of $R(\infty)$ [50], which is defined as

$$\Delta = \frac{\langle R(\infty) - \langle R(\infty) \rangle \rangle^2}{\langle R(\infty) \rangle^2}, \quad (19)$$

where $\langle \dots \rangle$ denotes ensemble averaging, and 10^3 independent simulations on a fixed network are performed to calculate the simulation value of the outbreak threshold. Δ reaches its peak at λ_c .

Figure 1 shows the dependence of the final adoption size $R(\infty)$ on the information transmission probability λ under different immune ratio $1 - q$, when the immune index $\alpha = 3$, 0 and -3 , respectively. The lines from the theory are very consistent with these symbols representing the simulation results. When $\alpha = 3$ (see Figure 1(a)), individuals with large degrees (hub individuals) in the network are given priority to be immunized, and a small immune ratio $1 - q$ can have a great impact on the network. Therefore, as $1 - q$ increases, $R(\infty)$ versus λ pattern is first continuous and then becomes discontinuous; finally, the social contagion ends.

Notably, under targeted immunization, a very small immune ratio (e.g., $1 - q = 0.14$) can effectively suppress social contagion. When $\alpha = 0$ (see Figure 1(b)), a number of individuals are randomly selected for immunization. In this case, with the increase of $1 - q$, $R(\infty)$ first continuously increases with λ , and a large immune ratio (e.g., $1 - q = 0.6$) can inhibit the outbreak of social contagion. When $\alpha = -3$ (see Figure 1(c)), individuals with small degrees are preferentially immunized. Immunizing some individuals with small degrees has less impact on network connectivity, so when the immune ratio is large (e.g., $1 - q = 0.8$), the connectivity of the residual network after immunization still supports the spread of information. By comparing Figures 1(a)–1(c), we note that targeted immunization has the strongest immune efficiency; that is, the increase of α will induce a better inhibitory effect on social contagions.

It can be seen from the above that the value of the immune index α has a significant impact on social contagions. We further investigate the effects of α on the final adoption size $R(\infty)$ and threshold λ_c in Figure 2. As shown in Figure 2(a), $R(\infty)$ shows a downward trend as α increases, while in Figure 2(b), λ_c increases as α increases, and $\lambda_c = 1$ means that social contagion cannot occur. In Figure 2(a), the theoretical results (lines) agree well with the simulated results (symbols). This phenomenon can be understood as, with the increase of α , a growing number of hub individuals are immunized, which is not conducive to social contagion.

More specifically, when the network heterogeneity is weak and a small number of individuals are immunized (i.e., $\gamma_D = 4$ and $1 - q = 0.05$), the increase of α has little impact

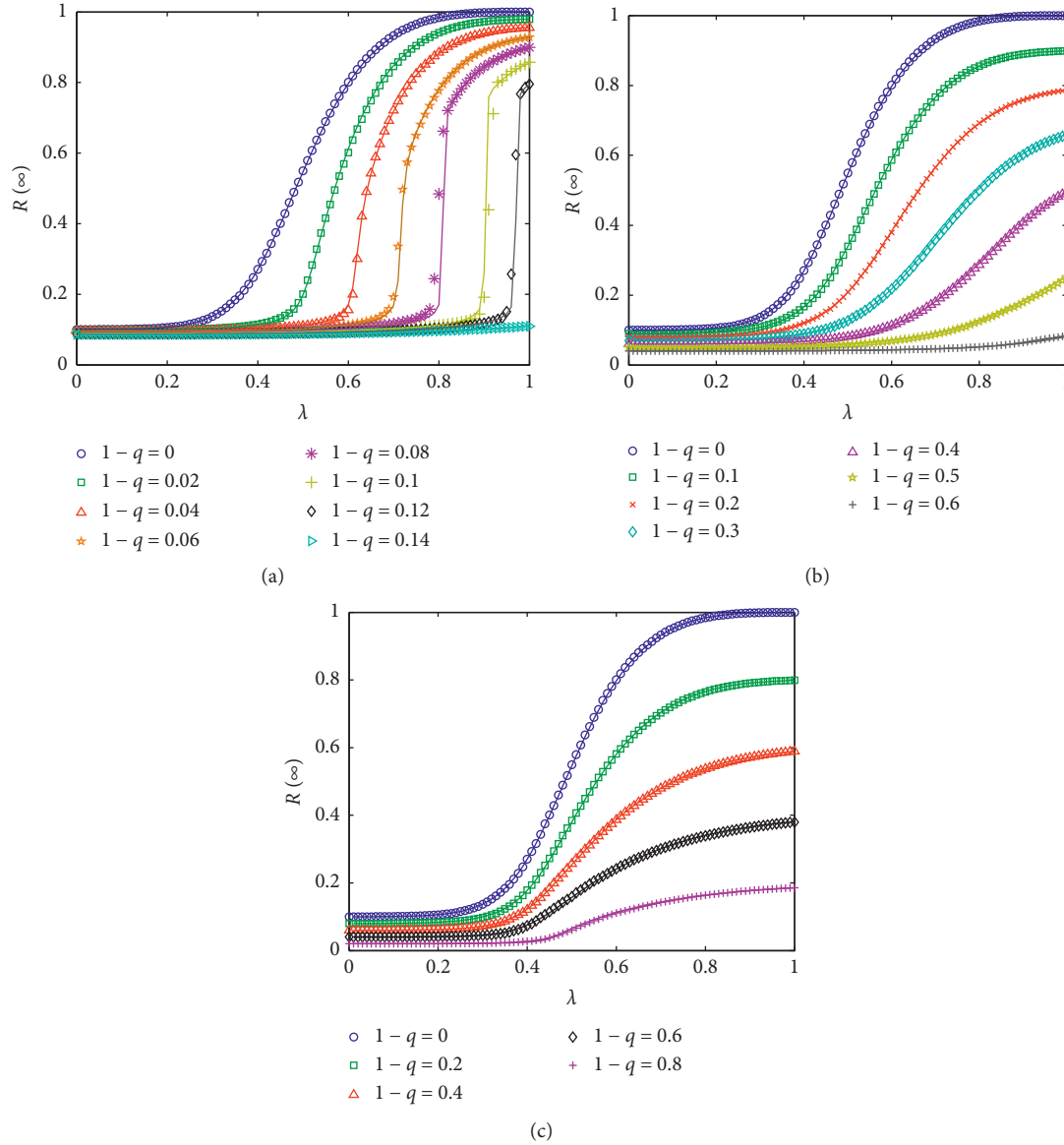


FIGURE 1: The final adoption size $R(\infty)$ versus the information transmission probability λ on SF network with degree exponent $\gamma_D = 3$ for (a) $\alpha = 3$, (b) $\alpha = 0$, and (c) $\alpha = -3$. Theoretical results (lines) agree well with simulated results (symbols).

on the network structure; thus, as α increases, $R(\infty)$ is basically unchanged and λ_c increases slowly (see the green line in Figure 2). However, when the network heterogeneity is strong ($\gamma_D = 2.2$), the increase of α has a great impact on network connectivity, and especially when $\alpha > 0$ and a relatively large number of individuals are immunized ($1 - q = 0.2$), $R(\infty)$ decreases sharply as α increases (see the red line in Figure 2(a)) and λ_c increases rapidly as α increases (see the red line in Figure 2(b)). In addition, we find from Figure 2(a) that network heterogeneity and immune ratio play a significant role in the effect of immunization strategies. Specifically, for the same immune ratio, the targeted immunization on the strong heterogeneous network has a better immune effect than the targeted immunization on the weak heterogeneous network, and the larger the immune ratio, the better the immune effect.

To study the effects of the immune ratio $1 - q$ on social contagion, we show the dependence of $R(\infty)$ and λ_c on $1 - q$ in Figure 3. In Figure 3(a), the lines from the theory are very consistent with these simulation results (symbols). Obviously, the increase of $1 - q$ causes $R(\infty)$ to decrease (see Figure 3(a)) and causes λ_c to increase (see Figure 3(b)). Since increasing $1 - q$ means that a growing number of individuals are immunized, it will greatly disrupt the connectivity of the network. Specifically, when $\alpha = 4$ (see the black and green lines in Figure 3), the hub individuals are immunized preferentially, as $1 - q$ increases, $R(\infty)$ decreases sharply and λ_c increases rapidly, and social contagion cannot break out when $1 - q$ is approximately 0.2. When $\alpha = 0$ (see the blue and red lines in Figure 3), the individuals in the network are randomly immunized, the connectivity of the network is not seriously damaged, that is, there are still

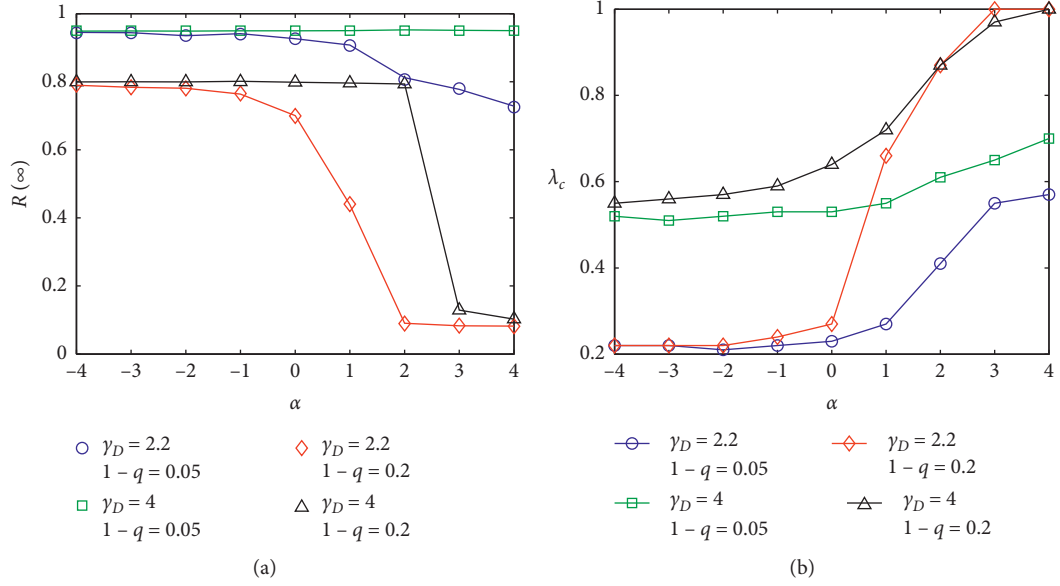


FIGURE 2: The effects of the immune index α on social contagions under different degree exponent γ_D and immune ratio $1 - q$: (a) the final adoption size $R(\infty)$ versus α when $\lambda = 1$ and (b) the threshold λ_c versus α .

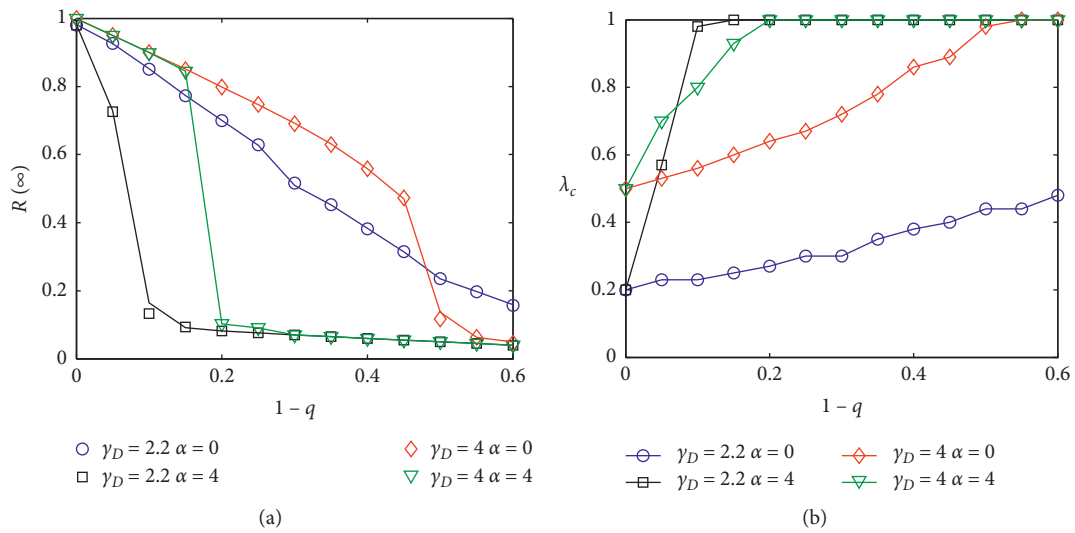


FIGURE 3: The effects of the immune ratio $1 - q$ on social contagions under different degree exponent γ_D and immune index α , (a) the final adoption size $R(\infty)$ versus $1 - q$ when $\lambda = 1$ and (b) the threshold λ_c versus $1 - q$.

some individuals with large degrees in the residual network after random immunization; thus, the behavior can be spread on the residual network. In addition, the stronger the heterogeneity of the degree distribution, the more the hub individuals in the residual network after random immunization. As a result, when $\gamma_D = 2.2$ and $\alpha = 0$ (see the blue lines in Figure 3), the increase of $1 - q$ has relatively minimal impact on the network structure; in other words, the system is more robust and stable.

The above studies have revealed that network heterogeneity has an important influence on the steady state of social contagion, for which the effects of the degree exponent γ_D and the information transmission probability λ on the

final adoption size $R(\infty)$ are studied in Figure 4. For $1 - q = 0.05$, Figures 4(a) and 4(c) show the theoretical results of $R(\infty)$ in the plane $\lambda - \gamma_D$ for $\alpha = 0$ and 4, respectively. For $1 - q = 0.1$, Figures 4(e) and 4(g) present the theoretical results of $R(\infty)$ for $\alpha = 0$ and 4, respectively. Figures 4(b), 4(d), 4(f), and 4(h) are the corresponding simulation results of Figures 4(a), 4(c), 4(e), and 4(g), respectively. The white circles in Figure 4 are simulated results of λ_c .

Overall, there is a remarkable agreement between theory and numerics in terms of the value of $R(\infty)$. For the case that $1 - q$ is small (e.g., $1 - q = 0.05$), because only a small proportion of individuals are immunized, no matter whether

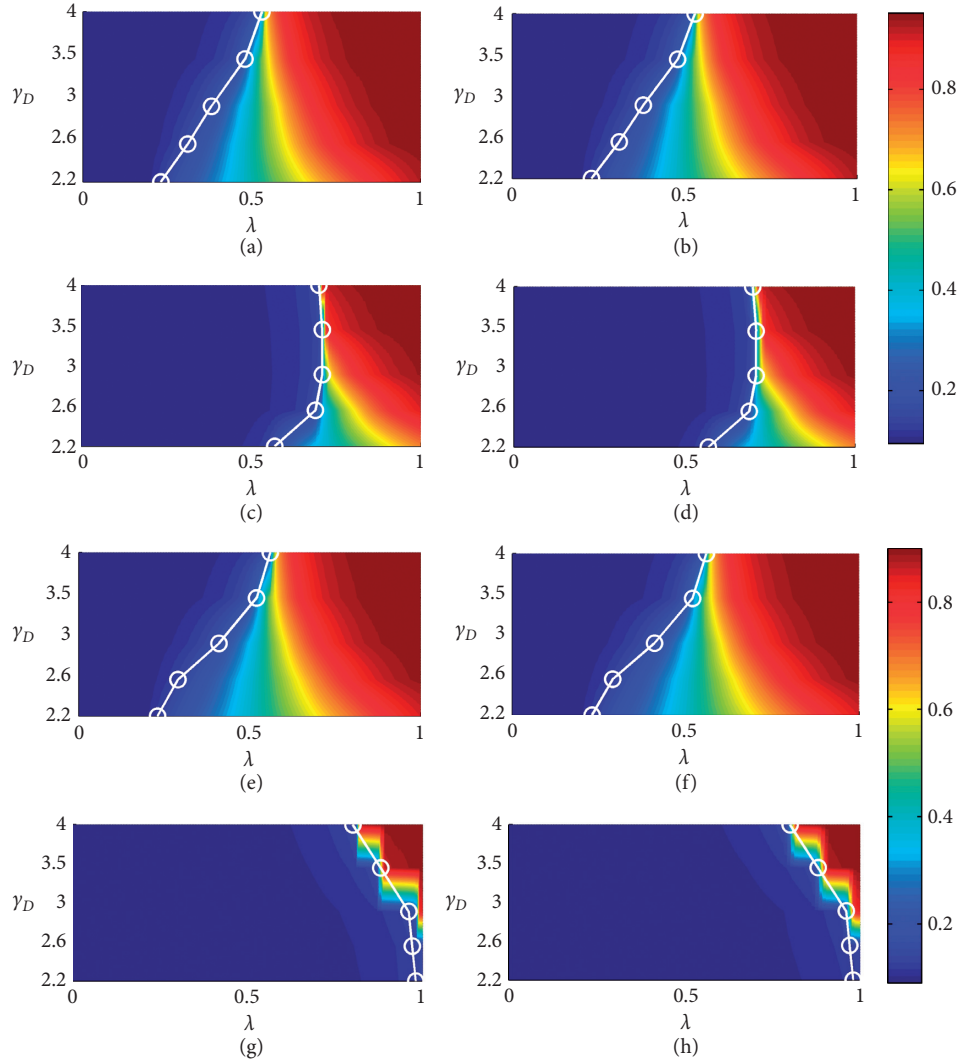


FIGURE 4: The final adoption size $R(\infty)$ versus information transmission probability λ and degree exponent γ_D on SF networks. The color-coded values of $R(\infty)$ from theoretical solutions in the plane $\lambda - \gamma_D$ for (a) $\alpha = 0, 1 - q = 0.05$, (c) $\alpha = 4, 1 - q = 0.05$, (e) $\alpha = 0, 1 - q = 0.1$, and (g) $\alpha = 4, 1 - q = 0.1$. The corresponding simulated results for (b) $\alpha = 0, 1 - q = 0.05$, (d) $\alpha = 4, 1 - q = 0.05$, (f) $\alpha = 0, 1 - q = 0.1$, and (h) $\alpha = 4, 1 - q = 0.1$. The white circles are the simulated results of λ_c .

$\alpha = 0$ (random immunization) or $\alpha = 4$ (targeted immunization), there are still a large number of hub individuals in the remanent network after immunization; that is, the structure of the network has not been greatly affected. Hub individuals are conducive to social contagion, and the smaller γ_D , the more the hub individuals in the network, so λ_c increases as γ_D increases (see Figures 4(a) and 4(c)). Nevertheless, as $1 - q$ increases to a relatively large value (e.g., $1 - q = 0.1$), the change trend of λ_c depends on the value of α . To be specific, when a random immunization strategy is adopted ($\alpha = 0$), after selecting some individuals for immunization with the same probability, there are still some hub individuals in the residual network, so λ_c increases as γ_D increases (see Figure 4(e)). Conversely, when a targeted immunization strategy is adopted ($\alpha = 4$), λ_c decreases as γ_D increases (see Figure 4(g)). In this case, when γ_D is relatively small, almost all hub individuals will be immunized, which will seriously change the topology structure of

the network, so it is not conducive to the spread of behavior, and even behavior cannot be spread (i.e., λ_c is approximately 1).

5. Conclusions

In summary, in this paper, we have systematically studied the effects of degree-based immunization strategies on the dynamics of social contagions. Using a non-Markovian SAR threshold model, we described the dynamics of social contagions under immunization, in which the adoption threshold of all individuals is the same, and the immune probability of each individual is related to its degree and the immune index. The type of immunization strategy depends on the size of the immune index. To give a dynamical analysis of social contagions under immunization, we developed a generalized edged-based compartmental theory. The predictions from theory are very consistent with these

simulation results on SF networks. Firstly, we found that targeted immunization can produce the best immune effect on social contagions. In addition, we found that increasing the immune index or immune ratio will decrease the final adoption size and increase the threshold. Furthermore, we noted that when the immune ratio is small, increasing the network heterogeneity will decrease the threshold. Conversely, when targeted immunization is adopted and the immunization ratio is relatively large, the threshold increases as the network heterogeneity increases. This work just provides a starting point to understand the effects of immunization strategies on social contagions, which can provide some implications for managing and controlling social contagions. A more in-depth understanding of the role of immunization strategies in social contagions still needs further efforts to discover.

Data Availability

No data were used to support this study.

Conflicts of Interest

The authors declare that they have no conflicts of interest.

Acknowledgments

This work was supported in part by the National Natural Science Foundation of China (Grant nos. 61902359, 61672467, and 61672468), Social Development Project of Zhejiang Provincial Public Technology Research (Grant no. 2016C33168), Zhejiang Provincial Natural Science Foundation of China (Grant no. LQ19F030010), and Opening Project of Shanghai Key Laboratory of Integrated Administration Technologies for Information Security (Grant no. AGK2018001).

References

- [1] P. S. Dodds and D. J. Watts, "Universal behavior in a generalized model of contagion," *Physical Review Letters*, vol. 92, no. 21, Article ID 218701, 2004.
- [2] N. A. Christakis and J. H. Fowler, "The spread of obesity in a large social network over 32 years," *New England Journal of Medicine*, vol. 357, no. 4, pp. 370–379, 2007.
- [3] S. Melnik, J. A. Ward, J. P. Gleeson, and M. A. Porter, "Multi-stage complex contagions," *Chaos: An Interdisciplinary Journal of Nonlinear Science*, vol. 23, no. 1, Article ID 013124, 2013.
- [4] M. Perc, "Diffusion dynamics and information spreading in multilayer networks: an overview," *The European Physical Journal Special Topics*, vol. 228, no. 11, pp. 2351–2355, 2019.
- [5] G. Cencetti and F. Battiston, "Diffusive behavior of multiplex networks," *New Journal of Physics*, vol. 21, no. 3, Article ID 035006, 2019.
- [6] R. Pastor-Satorras, C. Castellano, P. Van Mieghem, and A. Vespignani, "Epidemic processes in complex networks," *Reviews of Modern Physics*, vol. 87, no. 3, pp. 925–979, 2015.
- [7] J. Borge-Holthoefer and Y. Moreno, "Absence of influential spreaders in rumor dynamics," *Physical Review E*, vol. 85, Article ID 026116, 2012.
- [8] D. Centola, "The spread of behavior in an online social network experiment," *Science*, vol. 329, no. 5996, pp. 1194–1197, 2010.
- [9] D. Centola, "An experimental study of homophily in the adoption of health behavior," *Science*, vol. 334, no. 6060, pp. 1269–1272, 2011.
- [10] Z.-K. Zhang, C. Liu, X.-X. Zhan, X. Lu, C.-X. Zhang, and Y.-C. Zhang, "Dynamics of information diffusion and its applications on complex networks," *Physics Reports*, vol. 651, pp. 1–34, 2016.
- [11] R. Iyengar, C. Van den Bulte, and J. Y. Lee, "Social contagion in new product trial and repeat," *Marketing Science*, vol. 34, no. 3, pp. 408–429, 2015.
- [12] A. Banerjee, A. G. Chandrasekhar, E. Duflo, and M. O. Jackson, "The diffusion of microfinance," *Science*, vol. 341, no. 6144, Article ID 1236498, 2013.
- [13] X. Guardiola, A. Diaz-Guilera, C. J. Pérez, A. Arenas, and M. Llas, "Modeling diffusion of innovations in a social network," *Physical Review E*, vol. 66, no. 2, Article ID 026121, 2002.
- [14] A. Mellor, M. Mobilia, S. Redner, A. M. Rucklidge, and J. A. Ward, "Influence of luddism on innovation diffusion," *Physical Review E*, vol. 92, no. 1, Article ID 012806, 2015.
- [15] P. Bao, H.-W. Shen, W. Chen, and X.-Q. Cheng, "Cumulative effect in information diffusion: empirical study on a micro-blogging network," *PLoS One*, vol. 8, no. 10, Article ID e76027, 2013.
- [16] D. J. Watts, "A simple model of global cascades on random networks," *Proceedings of the National Academy of Sciences*, vol. 99, no. 9, pp. 5766–5771, 2002.
- [17] M. S. Granovetter, "The strength of weak ties," *American Journal of Sociology*, vol. 78, no. 6, pp. 1360–1380, 1973.
- [18] W. Wang, M. Tang, H.-F. Zhang, and Y.-C. Lai, "Dynamics of social contagions with memory of non-redundant information," *Physical Review E*, vol. 92, no. 1, Article ID 012820, 2015.
- [19] V.-P. Backlund, J. Saramäki, and R. K. Pan, "Effects of temporal correlations on cascades: threshold models on temporal networks," *Physical Review E*, vol. 89, no. 6, Article ID 062815, 2014.
- [20] M. X. Liu, W. Wang, Y. Liu, M. Tang, S.-M. Cai, and H.-F. Zhang, "Social contagions on time-varying community networks," *Physical Review E*, vol. 95, no. 5, Article ID 052306, 2017.
- [21] S. Unicom, G. Iniguez, and M. Karsai, "Threshold driven contagion on weighted networks," *Scientific Reports*, vol. 8, no. 1, 2018.
- [22] W. Wang, M. Tang, P. Shu, and Z. Wang, "Dynamics of social contagions with heterogeneous adoption thresholds: cross-over phenomena in phase transition," *New Journal of Physics*, vol. 18, no. 1, Article ID 013029, 2015.
- [23] X. Zhu, H. Tian, X. Chen, W. Wang, and S. Cai, "Heterogeneous behavioral adoption in multiplex networks," *New Journal of Physics*, vol. 20, no. 12, Article ID 125002, 2018.
- [24] H. Peng, W. Peng, D. Zhao, W. Wang, "Impact of the Heterogeneity of Adoption Thresholds on Behavior Spreading in Complex Networks (on publication), 2020.
- [25] W. Wang, H. E. Stanley, and L. A. Braunstein, "Effects of time-delays in the dynamics of social contagions," *New Journal of Physics*, vol. 20, no. 1, Article ID 013034, 2018.
- [26] A. Nematzadeh, E. Ferrara, A. Flammini, and Y.-Y. Ahn, "Optimal network modularity for information diffusion," *Physical Review Letters*, vol. 113, no. 25, Article ID 088701, 2014.
- [27] L. Han, Z. Lin, M. Tang, J. Zhou, Y. Zou, and S. Guan, "Impact of contact preference on social contagions on complex networks," *Physical Review E*, vol. 101, no. 4, 2020.

- [28] Z. Su, W. Wang, L. Li, H. E. Stanley, and L. A. Braunstein, "Optimal community structure for social contagions," *New Journal of Physics*, vol. 20, no. 5, Article ID 053053, 2018.
- [29] R. Pastor-Satorras and A. Vespignani, "Epidemic dynamics in finite size scale-free networks," *Physical Review E*, vol. 65, no. 3, Article ID 035108, 2002.
- [30] R. Cohen, S. Havlin, and D. ben Avraham, "Efficient immunization strategies for computer networks and populations," *Physical Review Letters*, vol. 91, no. 24, Article ID 247901, 2003.
- [31] N. Madar, T. Kalisky, R. Cohen, D. ben-Avraham, and S. Havlin, "Immunization and epidemic dynamics in complex networks," *The European Physical Journal B—Condensed Matter*, vol. 38, no. 2, pp. 269–276, 2004.
- [32] K. Hu and Y. Tang, "Immunization for scale-free networks by random walker," *Chinese Physics*, vol. 15, no. 12, pp. 2782–2787, 2006.
- [33] L. K. Gallos, F. Liljeros, P. Argyrakis, A. Bunde, and H. Shlomo, "Improving immunization strategies," *Physical Review E*, vol. 75, no. 4, Article ID 045104, 2007.
- [34] Z.-H. Liu, G.-L. Chen, N.-N. Wang, and B. Song, "Greedy immunization strategy in weighted scale-free networks," *Engineering Computations*, vol. 31, no. 8, pp. 1627–1634, 2014.
- [35] C. M. Schneider, T. Mihaljev, S. Havlin, and H. J. Herrmann, "Suppressing epidemics with a limited amount of immunization units," *Physical Review E*, vol. 84, no. 6, Article ID 061911, 2011.
- [36] C. Buono and L. A. Braunstein, "Immunization strategy for epidemic spreading on multilayer networks," *EPL (Europhysics Letters)*, vol. 109, no. 2, p. 26001, 2015.
- [37] D. Zhao, L. Wang, S. Li, Z. Wang, L. Wang, and B. Gao, "Immunization of epidemics in multiplex networks," *PLoS One*, vol. 9, no. 11, Article ID e112018, 2014.
- [38] S. Yan, S. Tang, W. Fang, S. Pei, and Z. Zheng, "Global and local targeted immunization in networks with community structure," *Journal of Statistical Mechanics: Theory and Experiment*, vol. 2015, no. 8, Article ID P08010, 2015.
- [39] P. Yuan and S. Tang, "Community-based immunization in opportunistic social networks," *Physica A: Statistical Mechanics and Its Applications*, vol. 420, pp. 85–97, 2015.
- [40] H.-J. Li, C. Zhang, and X.-S. Zhang, "A study of inflammation immunization strategy in weighted complex network," in *Proceedings of the 11th International Symposium on Operations Research and its Applications in Engineering, Technology and Management 2013 (ISORA 2013)*, pp. 1–7, Yellow Mountain, China, August 2013.
- [41] B. Lin, W. Guo, and G. Chen, "Edges immunization strategy based on discrete pso in weighted scale-free network," in *Proceedings of the 2012 Sixth International Conference on Innovative Mobile and Internet Services in Ubiquitous Computing*, pp. 384–389, Palermo, Italy, July 2012.
- [42] M. Starnini, A. Machens, C. Cattuto, A. Barrat, and R. Pastor-Satorras, "Immunization strategies for epidemic processes in time-varying contact networks," *Journal of Theoretical Biology*, vol. 337, pp. 89–100, 2013.
- [43] L. K. Gallos, R. Cohen, P. Argyrakis, A. Bunde, and S. Havlin, "Stability and topology of scale-free networks under attack and defense strategies," *Physical Review Letters*, vol. 94, no. 18, Article ID 188701, 2005.
- [44] X. Yuan, Y. Dai, H. E. Stanley, and S. Havlin, "k-core percolation on complex networks: comparing random, localized, and targeted attacks," *Physical Review E*, vol. 93, no. 6, Article ID 062302, 2016.
- [45] X. Huang, J. Gao, S. V. Buldyrev, S. Havlin, and H. E. Stanley, "Robustness of interdependent networks under targeted attack," *Physical Review E*, vol. 83, no. 6, Article ID 065101, 2011.
- [46] J. Shao, S. V. Buldyrev, L. A. Braunstein, S. Havlin, and H. E. Stanley, "Structure of shells in complex networks," *Physical Review E*, vol. 80, no. 3, Article ID 036105, 2009.
- [47] B. Karrer and M. E. J. Newman, "Message passing approach for general epidemic models," *Physical Review E*, vol. 82, no. 1, Article ID 016101, 2010.
- [48] B. Karrer, M. E. J. Newman, and L. Zdeborová, "Percolation on sparse networks," *Physical Review Letters*, vol. 113, no. 20, Article ID 208702, 2014.
- [49] M. Catanzaro, M. Boguñá, and R. Pastor-Satorras, "Generation of uncorrelated random scale-free networks," *Physical Review E*, vol. 71, no. 2, Article ID 027103, 2005.
- [50] M. Schroder, R. D'Souza, D. Sornette, and J. Nagler, "Microtransition cascades to percolation," *Physical Review Letters*, vol. 112, no. 15, Article ID 155701, 2014.

Research Article

Dynamical Modeling, Analysis, and Control of Information Diffusion over Social Networks: A Deep Learning-Based Recommendation Algorithm in Social Network

Kefei Cheng,¹ Xiaoyong Guo ,² Xiaotong Cui,¹ and Fengchi Shan ²

¹School of Cyber Security and Information Law, Chongqing University of Posts and Telecommunications, Chongqing 400065, China

²School of Computer Science and Technology, Chongqing University of Posts and Telecommunications, Chongqing 400065, China

Correspondence should be addressed to Xiaoyong Guo; 546740998@qq.com

Received 20 April 2020; Accepted 26 May 2020; Published 3 July 2020

Guest Editor: Wei Wang

Copyright © 2020 Kefei Cheng et al. This is an open access article distributed under the Creative Commons Attribution License, which permits unrestricted use, distribution, and reproduction in any medium, provided the original work is properly cited.

The recommendation algorithm can break the restriction of the topological structure of social networks, enhance the communication power of information (positive or negative) on social networks, and guide the information transmission way of the news in social networks to a certain extent. In order to solve the problem of data sparsity in news recommendation for social networks, this paper proposes a deep learning-based recommendation algorithm in social network (DLRASN). First, the algorithm is used to process behavioral data in a serializable way when users in the same social network browse information. Then, global variables are introduced to optimize the encoding way of the central sequence of Skip-gram, in which way online users' browsing behavior habits can be learned. Finally, the information that the target users' have interests in can be calculated by the similarity formula and the information is recommended in social networks. Experimental results show that the proposed algorithm can improve the recommendation accuracy.

1. Introduction

At present, the social network services composed of online information flow not only have a huge number of users but also accumulate a large amount of information data due to the active online behaviors of users. For example, the well-known domestic products, such as NetEase News, Tencent News, and Headlines Today, are counted in billions of monthly active users. Monthly active users of the well-known foreign online video company, YouTube, exceeded 2 billion in 2019, and the number of videos on the site reached millions. According to a report of 2012 by the International Data Group (IDG), by 2020, the total global data are expected to be 22 times those of 2011, reaching 35.2 ZB [1]. In these social networks composed of information flow services, information is usually disseminated probabilistically according to the topology structure of the social network. However, these huge information data make the spread of

information in the social network become congested, and a large amount of information cannot be browsed. The direct consequence to users is information overload. The recommendation algorithm can not only break the limitations of the traditional social network topology and enhance the spread of information in the social network but also improve the efficiency of obtaining information for multiple users and solve the problem of information overload. Therefore, personalized recommendation technology has become an important topic of common concern in academia and industry today.

The core part of the recommendation system is the recommendation algorithm. After years of research and development, recommendation algorithms are mainly divided into collaborative filtering algorithms and content-based algorithms. The collaborative filtering-based algorithm mainly does recommendation for users according to their past history and ratings, while the content-based

algorithm mainly depends on users' preferences and content information. There are some shortcomings in both algorithms. For example, when modeling users' behavior data, the real behavior data matrix tends to be very sparse, resulting in poor accuracy of prediction. In order to alleviate the sparsity of the behavior data matrix and improve the recommendation accuracy, the traditional method is used to improve the basic matrix decomposition. With the development of the research, the natural language processing model is used as a feature extraction method in the recommendation model. We have seen embeddings being leveraged for various types of recommendations on the Web [2–4], including item recommendation [5], advertising recommendation [6], movie recommendations [7, 8], and music recommendations [9]. Finally, similar extensions of embedding approaches have been proposed for social network analysis, where random walks on graphs can be used to learn embeddings of nodes in graph structure [10, 11].

In short, the users' browsing data used for online information flow recommendation often have a strong sparsity. Besides, most traditional models only focus on the learning of shallow features of the interaction data, ignoring the features of other browsing habits, which makes the ability to express features inadequate, resulting in poor recommendation results. In response to the above problems, it is very important to find a new method to model user interaction data for information recommendation in social network services. In this paper, the users' public data of news browsing in Caixin.com are taken as the research object. On the basis of the traditional content-based recommendation algorithm and the idea of word embedding, this paper proposes a deep learning-based recommendation algorithm in social network (DLRASN). First of all, the Skip-gram algorithm in Word2Vec is introduced into the information recommendation field in social networks. Each successive sequence of browsing information is treated as a sentence, and each browsing action is treated as a word in the sentence. Secondly, embedding operation is taken for the serialized user browsing data. While the intermediate sequence predicts the context sequence, the project click feature is introduced as a global variable to form an impact factor for the final result. Finally, a Top-N data recommendation set is formed. The experimental results show that the proposed method optimizes the recommendation effect to a certain extent and expands the application areas of embedded model.

2. Related Research

2.1. Content-Based Recommendation Algorithm. The basic principle of content-based recommendation algorithm is to obtain user's interest preferences according to his historical behavior and then recommend similar items. The data to be studied include item information (such as text description, labels, user comments, and manually labeled information), user information (such as age, gender, preference, region, and income), and interaction behavior (such as commenting, collecting, giving a like, watching, browsing, clicking, adding to cart, and purchasing). These data will be used to

extract features thereafter by constructing user interest model, and thus it will be transformed into measurable attributes, such as text represented by vectors, text types, and release time. At last, some methods can be used to calculate the similarity for recommendation [12].

The content-based recommendation algorithm generally depends on the user's own behavior and the item's own attributes to provide recommendations and. It focuses on analyzing extracted features and does not pay attention to other users' behavior. Once features of two items are found similar, the algorithm will mark them as the same category. Thus, the algorithm has a good effect on the recommendation for similar items. For example, after a user saw the love movie "crazy call," the content-based recommendation algorithm may recommend the movie "love saint" for him because the two movies have the similar characteristics. Melucci [13] combined the vector space model (VSM) with TF-IDF algorithm and used the model to calculate the news text similarity. Blei et al. [14] used the correlation between corresponding topics in the context to establish the LDA model.

Though the content-based recommendation algorithm has obtained a good result, the sparsity existing in user behavior data will affect the accuracy of recommendation to a certain extent. In order to address this shortcoming, the concept of embedding is introduced in the field of Web Search, e-commerce, and marketplace. The researchers find that one can train word embeddings by treating a sequence of words in a sentence as context, and the same can be done for training embeddings of user actions, e.g., items that were clicked or purchased [5] and searches and rents that were clicked [15], by treating sequence of user actions as context. Ever since, embeddings have been applied to various types of recommendations on the Web, including music recommendations, house search, movie recommendations, etc. However, there are few research studies on news recommendation in social network.

2.2. Word Embedding Model. The embedded model is a concept of the natural language processing (NLP). In the traditional NLP, the classic bag-of-words model is the earliest embedded model. However, it only considers the word frequency in the article and ignores the word order information of the sentence. When the corpus is huge, the generated word vector is very sparse, which will affect the accuracy of the semantic representation. Hence, the neural network language model gradually replaces it [16]. But this model can only handle fixed-length sequences and the training speed will slow down when the vocabulary in the corpus becomes too large. In order to solve these problems, Mikolov et al. [17] proposed the Word2Vec model in 2013. The Word2Vec model first converts the words in the vocabulary to one-hot codes. Then, the codes will be mapped to low-latitude dense word vectors by using a classic three-layer neural network. Word2Vec is very suitable for solving sequence problems because there is a very strong correlation between the adjacent words and it can learn the hidden features in the entire sequence. A typical one is the text

sequence. The Word2Vec model mainly includes two models: Skip-gram and continuous bag of words (CBOW).

Skip-gram model uses the central sequence to predict its context sequence, as shown in Figure 1. $W(t)$ is defined as the central word, which can be represented by a V -dimensional vector and V is the length of the vocabulary. $W(t+1)$ and $W(t-1)$ are defined as the relevant forward looking and backward looking context (neighborhood) for the central word. For example, for a sentence “The quick brown fox jumps over lazy dog,” if we select “fox” as the central word to predict its two words nearby, the task of the model is to calculate the occurrence probability of “quick,” “brown,” “jumps,” and “over.”

The CBOW model shown in Figure 2 predicts the central sequence through the context sequence, $W(t+1)$ and $W(t-1)$ represent the context sequence as the input vector, and $W(t)$ represents the center sequence as the output vector, where the input vector is V -dimensional, and V is also the length of the vocabulary.

As shown in Figure 2, after the model is trained, each word will be used as the center word. So, the number of its prediction is equal to the size of the entire vocabulary, and the time complexity is $O(V)$. However, the number of predictions using the Skip-gram model is more than CBOW. This is because when a word is used as the central word, the model must predict the context once. Therefore, the number of every prediction is more than K times. K is the size of the context window, so the Skip-gram model's time complexity is $O(KV)$. Although the time complexity of Skip-gram is higher than that of CBOW, the result trained by the Skip-gram model will be more accurate. So, when the data are small or sparse, the Skip-gram model can learn more information and obtain more precise word vectors. This is the main reason of selecting the Skip-gram model in this paper.

3. The Proposed Approach

The flow of the proposed algorithm is shown in Figure 3. The main work is to improve the word embedding model by adding clicking list as global context and use the improved model as the feature extractor of the content-based recommendation algorithm. The details are introduced as follows.

3.1. The Optimization of Word Embedding Model. Suppose that the dataset S is composed of news browsing sets collected from N users and each $s = (l_1, \dots, l_m) \in S$ is defined as a continuous sequence of M news browsed by the user. As long as the time interval between two consecutive user browses is more than t days, a new browsing sequence is generated. The goal of constructing this dataset is to learn a d -dimensional representation for each browsing list l_i by using the word embedding model, that is, to learn the representations of browsing data using the Skip-gram model by maximizing the objective function L on the entire dataset S . The objective function is defined as follows:

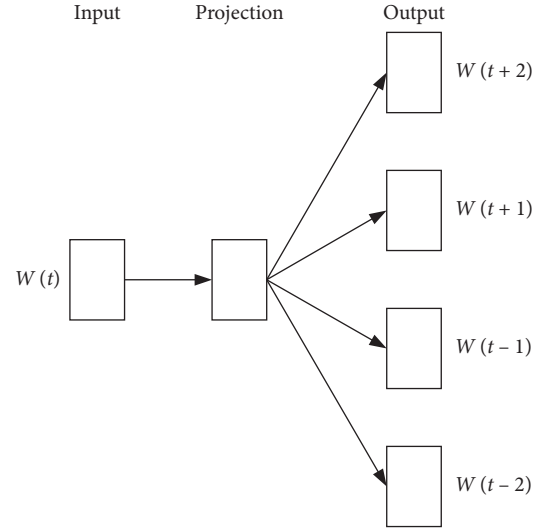


FIGURE 1: Schematic diagram of skip-gram model structure.

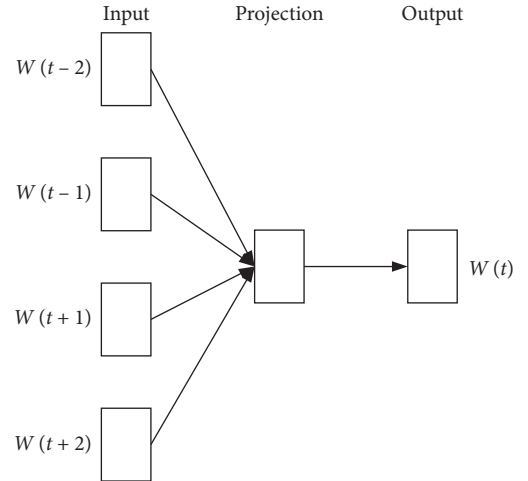


FIGURE 2: Schematic diagram of CBOW model structure.

$$L = \sum_{s \in S} \sum_{l_i \in s} \left(\sum_{-m \leq j \leq m, i \neq j} \log P(l_{i+j} | l_i) \right). \quad (1)$$

It needs to evaluate the probability $P(l_{i+j} | l_i)$ of a browsing list l_{i+j} which is represented as the contextual neighborhood of browsing list l_i . $P(l_{i+j} | l_i)$ is defined using the soft-max as follows:

$$P(l_{i+j} | l_i) = \frac{\exp(v_{l_i}^T v'_{l_{i+j}})}{\sum_{l' \in V} \exp(v_{l_i}^T v'_{l'})}, \quad (2)$$

where v_l and v'_l are input vector and output vector of browsing list l , the parameter m is defined as the length of the sliding window in the browsing list, and V is the ID set of all news. As we can see from (1) and (2), the context of user browsing sequences is modeled. The result is that browsing lists with similar contexts will have similar embedded representations.

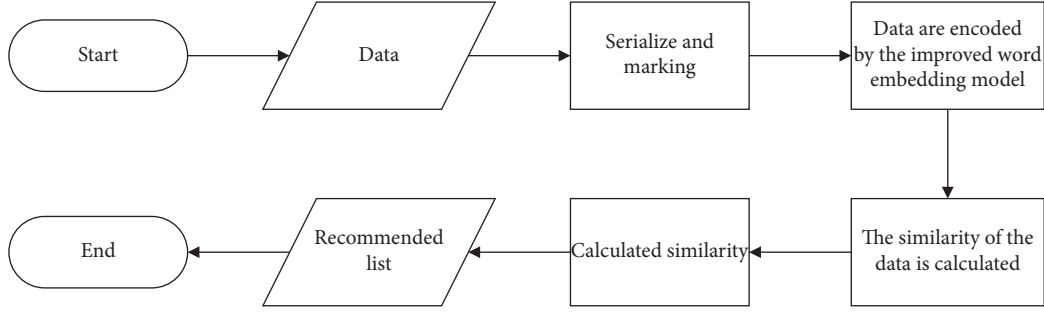


FIGURE 3: Flowchart of DLRASN.

The core principle of the objective function is to evaluate the probability of the contextual neighborhood appearance when the central sequence has existed, that is, to find the value of $P(l_0 | l_i) * \dots * P(l_{i+j} | l_i)$ and $P(l_0 | l_i) + \dots + P(l_{i+j} | l_i)$. It also follows the definition of the joint probability model. For example, a sentence “The [weather] is [nice] today” is given. If we select the target word as “weather,” the sliding results are “the [weather,” “is [weather,” “nice [weather,” and “today [weather.” Assume the contextual sliding window is one word, and then only “the [weather and is [weather” are the correct samples. For the original Skip-gram model, this is a 4-class classification problem. When we input “the [weather,” the probability of the four situations is $P(\text{the} | \text{weather})$, $P(\text{is} | \text{weather})$, $P(\text{nice} | \text{weather})$, and $P(\text{today} | \text{weather})$. The aim is to maximize the probability $P = P(\text{the} | \text{weather}) * P(\text{is} | \text{weather}) * P(\text{nice} | \text{weather}) * P(\text{today} | \text{weather})$. It can be seen that the probabilities of all the situations in the vocabulary need to be calculated at the same time. Furthermore, when the backpropagation optimization is conducted, all word vectors need to be updated. If the vocabulary is too large, the amount of calculation is very large. Assuming that the word vector is 100-dimensional, here it needs to update 500 parameters. Thus, a negative sampling method is proposed to optimize the calculation method [16]. Firstly, $P(l_{i+j} | l_i)$ will be replaced by using the sigmoid function:

$$P(l_{i+j} | l_i) = \text{sigmoid}(v_c * v_j) = \log \frac{1}{1 + e^{v_c v_j}} \quad (3)$$

Secondly, the browsing sequence of $D_p(l, c)$ is generated in the original dataset, which is the news data that the user browsed. And the browsing sequence of negative pair $D_n(l, c)$ is generated, which is the data randomly selected from the unbrowsed data of the user. In the above example, the word “weather” is entered, the probability of $P(\text{today} | \text{weather})$, $P(\text{very} | \text{weather})$, and $P(\text{nice} | \text{weather})$ is output, and the 400 parameters are updated and the computation is reduced. The objective function is changed into the following form:

$$\arg \max_{\theta} \sum_{(l,c) \in D_p} \log \frac{1}{1 + e^{-v'_c v_l}} + \sum_{(l,c) \in D_n} \log \frac{1}{1 + e^{v'_c v_l}}, \quad (4)$$

where parameters θ to be learned are v_l and v_c , $l, c \in V$. The optimization is done via stochastic gradient ascent.

3.1.1. Views Are Used as the Global Context. Multiple words are formed into sentence sequences in the NLP domain. However, the browsing sequence data in social networks are more complex than sentence sequences in NLP. Because first the user’s browsing behavior is generated, and then the news view data are also generated. Users’ overall behavior preferences are reflected not only by the number of news views but also by their browsing behavior. So, news views are used as an additional condition to influence the training process and to improve the model. In other words, when users’ browsing habits are trained by the Skip-gram model, the results are affected by the view data. For example, “news 1, news 2, news 3, news 4, news 5” is used as a user browsing sequence, and “view 1, view 2, view 3, view 4, view 5” is used as a view sequence. Firstly, “news 4” is taken as the input item, secondly, the context sliding window is 1, and the training process is optimized by negative sampling. Finally, the probability of $P(\text{News1} | \text{News4}) * P(\text{News3} | \text{News4}) * P(\text{News5} | \text{News4}) * P(\text{view4} | \text{News4})$ is calculated. The objective function is changed into the following form:

$$\arg \max_{\theta} \sum_{(l,c) \in D_p} \log \frac{1}{1 + e^{-v'_c v_l}} + \sum_{(l,c) \in D_n} \log \frac{1}{1 + e^{v'_c v_l}} + \log \frac{1}{1 + e^{-v'_b v_l}}, \quad (5)$$

where v'_b is the embedding of the page views l_b .

The improved Skip-gram model is shown in Figure 4. The model has a window of size $2n + 1$, and when the window is slid from left to right, the context sequence and views are predicted by the central sequence.

3.2. The Result of Item Similarity and List of Recommendations

3.2.1. The Similarity of the Target Items Is Calculated by the Model. First, the improved word embedding model is used as a feature extractor for content-based recommendation algorithms. Secondly, the user’s browsing behavior data are trained by the model, and the user’s implicit features are extracted. Assuming that there are m users and n texts, the user-browse feature matrix is constructed as follows: user u ’s behavior of browsing text i is represented by the characteristic result r_{ui} .

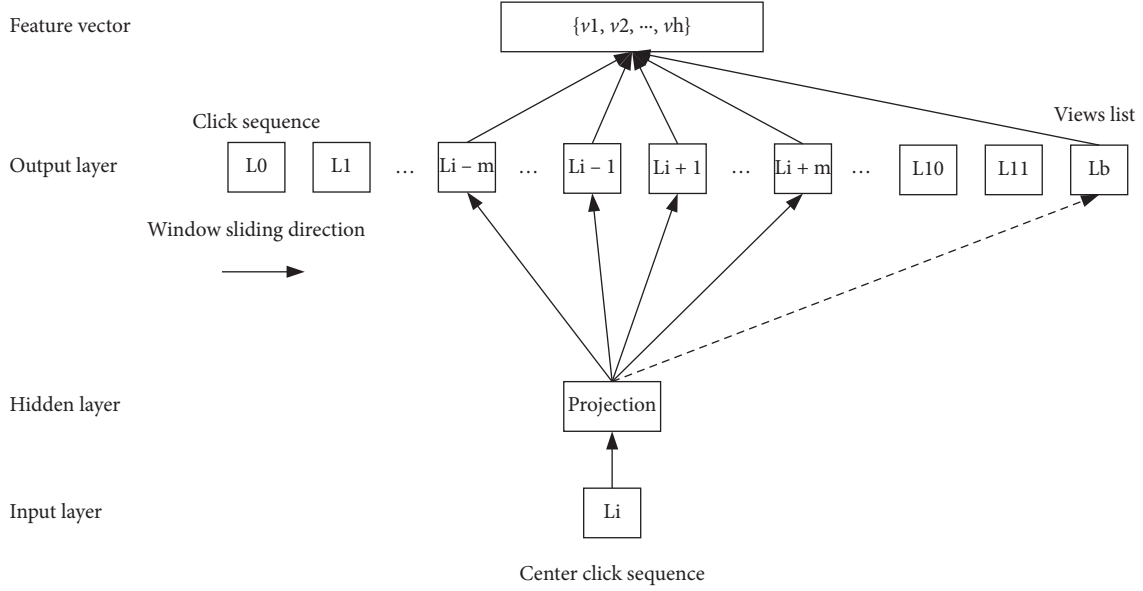


FIGURE 4: Schematic diagram of the model structure.

$$S = \begin{bmatrix} r_{11} & r_{12} & \cdots & r_{1n} \\ \vdots & \vdots & \cdots & \vdots \\ r_{m1} & r_{m2} & \cdots & r_{mn} \end{bmatrix}. \quad (6)$$

Secondly, the cosine similarity is calculated according to the user's current browsing behavior and the candidate vector in S , and the calculation formula is as follows:

$$\text{sim}(u, v) = \cos(u, v) = \frac{\vec{u} \cdot \vec{v}}{\|\vec{u}\| \times \|\vec{v}\|}. \quad (7)$$

Among them, the data of users u and v are represented by vectors \vec{u} and \vec{v} . It can be seen from $\text{sim}(u, v) \in [-1, 1]$ that the smaller the angle between the vectors, the higher the similarity.

3.2.2. A List of Recommendations Is Generated. Finally, the recommended K projects are calculated by the following equation (the maximum number of recommended projects is represented by K):

$$y = \max_{k < n} (\text{sim}(u, v)). \quad (8)$$

4. Experimental Results and Evaluation

4.1. Dataset. The data in this article were collected from Caixin.com; the data are a public dataset for users to browse news data. The data include 116,225 interaction data from 10,000 users during March 2014. Each record includes user ID, news ID, browsing time (counted in the form of time stamp), news content, and news release time.

This study made a preliminary analysis of user-news data and learned that the basic distribution of the dataset as shown in Table 1:

Table 1 shows that this dataset has a total of 10,000 user interaction data, and each user has viewed about 12 news

TABLE 1: User reading distribution statistics.

Statistical indicators	Quantity
Count	10000
Mean	12
Std	59
Min	5
25%	6
50%	7
75%	10
Max	5357

articles on average. Among all users, the least read users only browsed 5 news articles, 50% of users read more than 7 news articles, and nearly 74% of users read less than 10 news articles. The users who read the most news articles read a total of 5354 news articles.

According to the reading statistics of the news reading distribution in Table 2, there are 6183 news articles in this dataset, and each news article has been viewed by an average of 19 users. The minimum number of news articles browsed is 1, 50% of the news articles is only browsed by one or two people, 75% of the news articles is browsed by less than 8 people, and the most read news articles have 2000 records.

From the distribution statistics of the above browse data, we can see that the browse data are sparse. The sparsity is a mathematical index to calculate the sparsity of data, which can directly calculate the sparsity of a data. (9) is used to calculate the sparsity of user behavior data:

$$\text{sparsity} = 1 - \frac{\text{number of ratings}}{\text{number of users} \times \text{number of news articles}}. \quad (9)$$

The result is obtained according to the sparsity calculation formula (see Table 3).

TABLE 2: News reading distribution statistics.

Statistical indicators	c_t
Count	6183
Mean	19
Std	86
Min	5
25%	1
50%	1
75%	8
Max	2000

TABLE 3: Data sparse degree.

User	News	Numbers of ratings	Sparsity (%)
10000	6183	91049	99.85

According to the above analysis, it is found that news reading data are highly sparse, and users only browse few news articles, and a large amount of news articles is not used. For users who do not browse news, it does not mean that users are not interested in the news. If you use a recommendation system, it can allow users to find more useful information more effectively and can help users enhance their ability to perceive information. Even more useful unpopular information is found, which proves the importance of the recommendation system again from the data side. It can also be found from the sparseness data because the sparseness of the dataset is very high, which leads to the limitations of the traditional interest model.

4.2. Data Screening. The dataset in this paper does not directly represent users' preference for news. For this problem, this paper refers to the negative sampling technique in reference [15] to overcome this problem. The following rules are followed when processing data:

(1) For each user, the data in the negative sample are news data that the user has not read; (2) for each user, news with more than 20 views in the dataset shall be taken as negative sampling data, which shall account for 25% in the dataset; (3) for each user, news with 2 to 20 views in the dataset shall be taken as negative sample data, which shall account for 75% in the negative sample dataset; (4) for each user, each user contains the same amount of positive sample data and negative sample data.

In this paper, the experimental dataset is divided into training set and test set. First, the user data with 0 to 2 views in the dataset are eliminated. Second, each user's last browsing history is used as a test set. Finally, the dataset contains a total of 9,543 users and 5,768 news articles, and the data sparsity is 99.81%.

4.3. Experimental Evaluation Criteria. In this paper, $F1$ -Score and Map are selected as the indexes for experimental evaluation [18]. Among them, $F1$ -Score is the weighted

average of recall rate and accuracy, which is mainly used as the evaluation standard for the accuracy of the recommendation system. $F1_N$ represents the result of $F1$ -Score when N news articles are recommended. The calculation method of $F1$ -Score is as follows:

$$F1\text{-Score} = 2 \frac{\text{recall} \times \text{precision}}{\text{recall} + \text{precision}}, \quad (10)$$

where recall represents the proportion of the positive samples predicted by the algorithm in the original positive samples and precision represents the ratio of the number of correct recommendations to the total number of recommendations.

Map is the average of calculating the average accuracy. The high value of Map indicates that the recommendation algorithm has a better recommendation effect. Map_N represents the result of Map when the algorithm recommends N news articles. The calculation equation is as follows:

$$\text{Map} = \frac{1}{N} \sum_{i=1}^N AP_i, \quad (11)$$

where AP represents the average of accuracy.

4.4. Experimental Results and Analysis. We compare our proposed DLRSN with the following baselines:

- (i) Content-based recommendation (CR) has a good effect in recommending similar projects and is the most basic and classic recommendation algorithm.
- (ii) WMD [19] combines the advantages of singular value decomposition model and Word2Vec model. It has good abstraction ability to extract user characteristics.
- (iii) RPE [15] uses the word embedding model to directly analyze the interactive data of users to complete the recommendation work.
- (iv) RPEW uses Word2Vec to process text features based on RPE. The model combines the features of news text information to train the recommendation results.

The experimental results of $F1$ -Score are shown in Table 4 and Figure 5. The experimental results of Map are shown in Table 5 and Figure 6.

Experimental results show the following. (1) According to the experiments of CR, RPE, and DLRSN, we can see that Skip-gram is superior to traditional machine learning methods. (2) According to the experiments of CR, WMD, RPEW, and DLRSN, we can see that additional project features or user features can affect the recommendation accuracy of the recommendation model. (3) According to the experiments of RPE, RPEW and DLRSN, we can see that the recommendation algorithm containing click characteristics is superior to the recommendation algorithm containing text features.

TABLE 4: Experimental results of *F1*-Score.

	F1_10	F1_20	F1_30	F1_40	F1_50
CR	0.015764	0.014894	0.014732	0.013846	0.013564
WMD	0.055231	0.033629	0.024226	0.020231	0.018235
RPE	0.056902	0.036284	0.02695	0.021704	0.018233
RPEW	0.057455	0.035139	0.026968	0.021462	0.018
DLRASN	0.05965	0.036972	0.02815	0.021801	0.018624

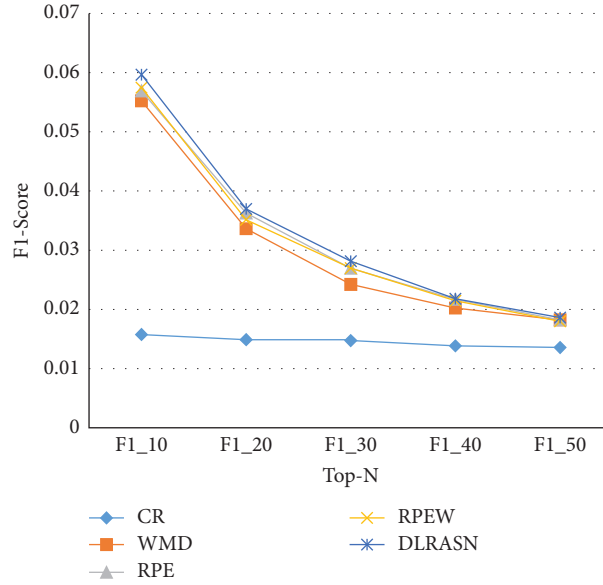
FIGURE 5: Comparison of *F1*-Score values of various models.

TABLE 5: Experimental results of Map.

	Map_10	Map_20	Map_30	Map_40	Map_50
CR	0.064215	0.065755	0.066313	0.066651	0.066844
WMD	0.17251	0.1759	0.1768	0.1789	0.1792
RPE	0.1915	0.195	0.1995	0.2	0.2007
RPEW	0.1918	0.2	0.2021	0.20311	0.198
DLRASN	0.1993	0.211	0.2061	0.20584	0.20645

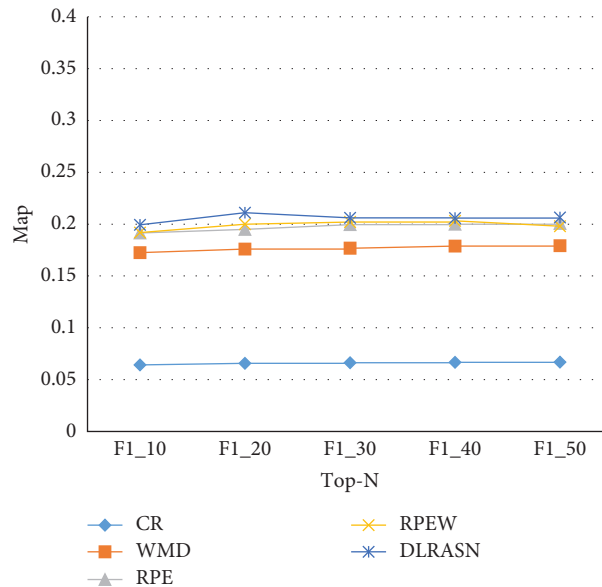


FIGURE 6: Comparison of Map values of various models.

5. Summary

This paper first introduces theories about Skip-gram and then proposes DLRASN. This model adopts improved Skip-gram to learn users' behavioral habits and holistically builds the recommendation model combined with ideas of the content-based recommendation algorithm. On the one hand, this algorithm copes with data sparsity faced with recommendation algorithms. On the other hand, the recommendation of users' information in social networks can be improved by learning features of users' preferences. Simulation experiments show that the proposed DLRASN is of higher accuracy and proved to be effective.

Despite the positive results that this model has achieved in information recommendation, the positive and negative information is not distinguished from each other. Hence, how to enhance the recommendation of positive information and reduce that of negative information will be our future work.

Data Availability

The data used to support the findings of this study are available from the corresponding author upon request.

Conflicts of Interest

The authors declare that they have no conflicts of interest.

References

- [1] J. Gantz and D. Reinsel, "The digital universe in 2020: big data, bigger digital shadows, and biggest growth in the far east," *IDC iView: IDC Analyzethe Future*, vol. 2007, pp. 1–16, 2012.
- [2] N. Djuric, V. Radosavljevic, M. Grbovic, and N. Bhamidipati, "Hidden conditional random fields with Deep user embeddings for ad targeting," in *Proceedings of the 2014 IEEE International Conference on Data Mining*, pp. 779–784, Shenzhen, China, December 2014.
- [3] M. Grbovic, V. Radosavljevic, N. Djuric et al., "E-commerce in your inbox: product recommendations at scale," in *Proceedings of the 21th ACM SIGKDD International Conference on Knowledge Discovery and Data Mining*, pp. 1809–1818, Sydney, NSW, Australia, August 2015.
- [4] Y. Tagami, H. Kobayashi, S. Ono, and A. Tajima, "Modeling user activities on the Web using paragraph vector," in *Proceedings of the 24th International Conference on World Wide Web*, pp. 125–126, ACM, Florence, Italy, May 2015.
- [5] T. Nedelec, E. Smirnova, and F. Vasile, "Specializing joint representations for the task of product recommendation," in *Proceedings of the 2nd Workshop on Deep Learning for Recommender Systems DLRs 2017*, pp. 10–18, Como, Italy, August 2017.
- [6] M. Grbovic, N. Djuric, V. Radosavljevic et al., "Scalable semantic matching of queries to ads in sponsored search advertising," in *Proceedings of the 39th International ACM SIGIR conference on Research and Development in Information Retrieval*, pp. 375–384, Pisa, Italy, July 2016.
- [7] O. Barkan and N. Koenigstein, "ITEM2VEC: neural item embedding for collaborative filtering," in *Proceedings of the 26th International Workshop on Machine Learning for Signal Processing (MLSP)*, pp. 1–6, IEEE, Vietri sul Mare, Italy, September 2016.
- [8] N. Djuric, H. Wu, V. Radosavljevic, M. Grbovic, and N. Bhamidipati, "Hierarchical neural language models for joint representation of streaming documents and their content," in *Proceedings of the 24th International Conference on World Wide Web*, pp. 248–255, International World Wide Web Conferences Steering Committee, Florence, Italy, May 2015.
- [9] D. Wang, S. Deng, X. Zhang, and G. Xu, "Learning music embedding with metadata for context aware recommendation," in *Proceedings of the 2016 ACM on International Conference on Multimedia Retrieval*, pp. 249–253, Xi'an City, China, August 2016.
- [10] A. Grover and J. Leskovec, "NODE2VEC: scalable feature learning for networks," in *Proceedings of the 22nd ACM SIGKDD International Conference On Knowledge Discovery and Data Mining*, pp. 855–864, ACM, San Francisco, CA, USA, August 2016.
- [11] B. Perozzi, R. Al-Rfou, and S. Skiena, "Deepwalk: Online learning of social representations," in *Proceedings of the 20th ACM SIGKDD International Conference On Knowledge Discovery and Data Mining*, pp. 701–710, ACM, Newyork, NY, USA, August 2014.
- [12] Y. Cai, H.-f. Leung, Q. Li, H. Min, J. Tang, and J. Li, "Typicality-based collaborative filtering recommendation," *IEEE Transactions on Knowledge and Data Engineering*, vol. 26, no. 3, pp. 766–779, 2014.
- [13] M. Melucci, "Vector-space model," *Encyclopedia of Database Systems*, pp. 3259–3263, Springer, Boston, MA, USA, 2009.
- [14] D. Blei, A. Ng, and M. Jordan, "Latent dirichlet allocation," *Journal of Machine Learning Research*, vol. 3, pp. 993–1022, 2003.
- [15] M. Grbovic and H. Cheng, "Real-time personalization using embeddings for search ranking at Airbnb," in *Proceedings of the 24th ACM SIGKDD International Conference on Knowledge Discovery & Data Mining*, pp. 19–23, London, UK, August 2018.
- [16] J. Weston, R. Weiss, and H. Yee, "Nonlinear latent factorization by embedding multiple user interests," in *Proceedings of the 7th ACM Conference on Recommender systems*, pp. 65–68, ACM, Hong Kong, October 2013.
- [17] T. Mikolov, I. Sutskever, K. Chen, G. Corrado, and J. Dean, "Distributed representations of words and phrases and their compositionality," *Advances in Neural Information Processing Systems*, vol. 2, pp. 3111–3119, 2013, <https://arxiv.org/abs/1310.4546>.
- [18] Xiang, *Practice of Recommendation System*, pp. 23–22, People's Posts and Telecommunications Press, Beijing, China, 2012.
- [19] Y. Wang and J. Tang, "Deep learning-based personalized paper recommender system," *Journal of Chinese Information Processing*, vol. 32, no. 4, pp. 114–119, 2018.

Research Article

Modeling and Analysis of Dynamic Social Ties in D2D Collaborative Video Transmission

Qi Zhang,^{1,2,3} Zufan Zhang^{1,2,3}, Tian Zeng,^{1,2,3} and Xiaoke Li^{1,2,3}

¹School of Communication and Information Engineering, Chongqing University of Posts and Telecommunications, Chongqing 400065, China

²Chongqing Key Laboratory of Mobile Communications Technology, Chongqing 400065, China

³Engineering Research Center of Mobile Communications, Ministry of Education, Chongqing 400065, China

Correspondence should be addressed to Zufan Zhang; zhangzf@cqupt.edu.cn

Received 11 May 2020; Accepted 8 June 2020; Published 23 June 2020

Guest Editor: Wei Wang

Copyright © 2020 Qi Zhang et al. This is an open access article distributed under the Creative Commons Attribution License, which permits unrestricted use, distribution, and reproduction in any medium, provided the original work is properly cited.

Social networks are one of the main carriers of information diffusion. Changes in social ties will affect the quality of Device-to-Device (D2D) communications especially the video transmission. For further improving the communication utility of users, it is of great significance to effectively integrate D2D communications and social networks. To this end, this paper utilizes a stochastic approach to modeling and analysis of dynamic social ties in D2D collaborative video transmission. Specifically, a stochastic mathematical model is established and analyzed, in which the combined effect of many factors such as interest, geographical position, career, social class, value system, and interaction is considered. Based on the Brownian motion theory, the strength of social ties among social individuals with time is studied. Next, the reliability function and adaptive parameter estimation are performed. Finally, some examples are conducted to illustrate the main results of this paper, from which one can see that the proposed model has a good predictive ability of the changing trend of social ties.

1. Introduction

With the development of mobile Internet and wireless communication technology, Device-to-Device (D2D) communications have become one of the key technologies of the future wireless communication and social networks have become one of the main carriers of information diffusion [1]. Through D2D communications and social networks, people can not only communicate with friends but also share pictures and videos faster and more conveniently. Since the communication equipment are usually carried by people, the dynamic social environment and a wide range of social applications require D2D communications, especially the D2D collaborative video transmission, to be more self-adapting and to meet more general communication needs. When users share videos locally through the wireless short-distance D2D communications, if users successfully establish a D2D link, the video streams will spread rapidly over social networks. However, there are users' mobility and the

occurrence of random events in social networks, and changes in users behavior will lead to dynamic interactions between users, which will affect the success rate of users to establish D2D links, thereby affecting the information diffusion [2]. Therefore, it is essential to study the D2D collaborative video transmission in conjunction with social networks.

In [3], a D2D communication-assisted caching framework for video multicast was proposed, which considers the social trust and social reciprocity to encourage effective collaboration between users. Wang et al. [4] studied an Expected Available Duration (EAD) indicator to measure the chance of D2D users' downloading video packets from neighbors. Zhang et al. [5] considered the D2D pairing for cooperative video transmission. The social tie in previous work was usually calculated according to the personal information of users and the interaction information among different users. However, the social communication is affected by many factors, including social topology, user

behavior, and inherent content characteristics, and the social ties are a dynamic process that changes with time.

The study of social ties is conducive to understanding human behavior, which can be applied in viral spread [6], information recommendation [7], traffic planning, and complex socioeconomic phenomena [8]. Granovetter [9] first defined the social ties that are a combination of time, emotional intensity, intimacy, and reciprocity, which provides a theoretical basis for many researchers to analyze the linear combination of the four elements of social ties.

With the development of social network, the research of modeling the structure of social ties has been paid attention increasingly. In [10], the authors pointed out that strangers established social ties based on shared interests, career, or activities. Xiang et al. [11] proposed an unsupervised model, in which the social ties between users were regarded as a latent variable that caused interactive behaviors. Based on this idea, Zhao et al. [12] presented a probabilistic generative model, which considers life activities and moving patterns. However, Xiang et al. and Zhao et al. [11, 12] neglect the assignment of activity topics. Meanwhile, Xiong et al. [13] proposed a general framework to measure social ties by similarities, interaction activities, and the co-occurrence of users' names. In [14], the authors calculated social ties based on users' profile information and interaction activities in different activity fields. In [15], a language model based on sentiment classification, similarity, and interactivity was applied to compute social ties before adopting K-means clustering method to cluster the users. It is noteworthy that Zhao et al. and Ju and Tao [14, 15] both assume that social ties are a static constant, resulting that the dynamic behavior of social network cannot be analyzed.

In addition to the above theoretical studies on social ties, there are also some application scenarios that describe social ties [16–19]. In traditional social networking websites, modeling the social ties has a wide spectrum of applications [16, 17]. In [18], a graphical probabilistic model and Topical Affinity Propagation (TAP) approach were applied to study social ties and social influence, respectively. In [19], the spatiotemporal patterns of social ties were represented by the factors of the tensors. Yi et al. [20] proposed a dynamic model with social ties and self-confirmation mechanism, and verified the key role of social connections in information diffusion.

Inspired by the abovementioned work and based on the fact that the real world is a dynamic environment and it is difficult to gather accurate real-time data to track the changes of social ties, this paper attempts to utilize stochastic processes to study social ties. A stochastic mathematical model, which incorporates the combined effect of many factors such as interest, geographical position, career, social class, value system, and interaction, is proposed and analyzed. Specifically, the reliability function and adaptive parameter estimation are conducted. To illustrate the main results, some numerical examples are given at the end of this paper.

The subsequent materials of this paper are organized as follows. Section 2 formulates the stochastic model. Section 3 makes a mathematical analysis of this model. Some

numerical examples are given in Section 4. Finally, Section 5 outlines this work.

2. Model Formulation

2.1. Scenario Description. Social tie is a key factor for the successful spread of video streaming among users in D2D communications. Since there are many influencing factors in social networks that affect the social tie between users, the social tie between users is dynamic, which will affect the success rate of D2D link establishment between users, thereby affecting communication performance. Based on the above description, the purpose of this paper is to build a dynamic model of social ties among social individuals for better understanding the D2D collaborative video transmission. As shown in Figure 1, considering a single-cell cellular network, there are D D2D users $D = \{D_1, D_2, \dots, D_D\}$ and M cellular users $C = \{C_1, C_2, \dots, C_M\}$ in the coverage area of the base station. At time $t = t_k$, users D_1 and D_2 establish a D2D communication link and reuse the spectrum resources of cellular user C_2 . Between time $t = t_k$ and $t = t_{k+1}$, if D_1 and D_2 have a negative interaction, resulting that the strength of the social ties decreases and is below the trust threshold of user D_1 . Then, at time $t = t_{k+1}$, users D_1 and D_2 cannot successfully communicate. Similarly, at time $t = t_k$, user D_4 needs to obtain the required video resources from D_3 , and user D_3 is willing to share the data packet with D_4 if the physical conditions are met, then a trust relationship is established between D_4 and D_3 at time $t = t_{k+1}$. Based on this background, starting from the social level of users, a model of dynamic social ties between users is established. The strength of the social ties between any two users i and j can be regarded as a set of random variables $\{S_{ij}(t), t \geq 0\}$ that related to the time t .

2.2. Model Assumption. At any time t , $S_{ij}(t)$ can be defined as a random representation of the strength of social ties between individuals, then $\{S_{ij}(t), t > 0\}$ can be understood as a random process of social ties strength between individuals. To modeling and analysis of dynamic social ties $\{S_{ij}(t), t \geq 0\}$ between users i and j at any given time t , the following assumptions are imposed:

- (A1) As the social ties between users i and j can be regarded as a random variable $S_{ij}(t)$, then for $\tau > 0$, let $\Delta S_{ij}(t) = S_{ij}(t + \tau) - S_{ij}(t)$ represent the change of $S_{ij}(t)$ during the interval $(t, t + \tau]$ and $S_{ij}(t) = \sum_{l=1}^t \Delta S_{ij}(l)$.
- (A2) The social ties are influenced by many random factors, such as interest, geographical position, career, social class, value system, and interaction. Let a set of random variables $\{\xi_m(t), m \in N^+\}$ represent these random factors.
- (A3) The random variables $\xi_1(t), \xi_2(t), \dots, \xi_m(t), m \in N^+$ are independent of each other. Let $\Delta \xi_m(t)$ represent the change of $\xi_m(t)$.

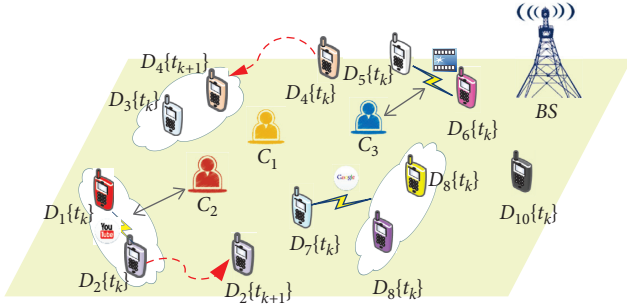


FIGURE 1: D2D collaborative video transmission scenario.

(A4) $\Delta\xi_1(t), \Delta\xi_2(t), \dots, \Delta\xi_m(t), m \in N^+$ obey the same distribution. Let $E[\Delta\xi_m(t)] = \mu, D[\Delta\xi_m(t)] = \sigma^2 > 0$ and $\Delta S_{ij}(t) = \sum_{k=1}^m \Delta\xi_k(t)$.

Lemma 1. $\{S_{ij}(t), t > 0\}$ is a Markov process.

Proof. Assume that $S_{ij}(t_k) = S_{t_k}$, for any time $t = t_k, k \in N^+$. Then,

$$\begin{aligned} & P\{S_{ij}(t_k) \leq S_{t_k} \mid S_{ij}(t_1) = S_{t_1}, \dots, S_{ij}(t_{k-1}) = S_{t_{k-1}}\} \\ &= P\{S_{ij}(t_k) - S_{ij}(t_{k-1}) \leq S_{t_k} - S_{t_{k-1}} \mid \Delta S_{ij}(t_1), \dots, \Delta S_{ij}(t_{k-1})\} \\ &= P\{S_{ij}(t_k) \leq S_{t_k} \mid S_{ij}(t_{k-1}) = S_{t_{k-1}}\}. \end{aligned} \quad (1)$$

According to the above formula, one can get that, given the present state of the process, the future state is independent of the past. From the definition of Markov process in [21], the random variable $S_{ij}(t)$ satisfies the Markov property, and $\{S_{ij}(t), t > 0\}$ is called the Markov process. Thus, the proof is complete. \square

Lemma 2. The random variable $\Delta S_{ij}(t)$ obeys the normal distribution.

Proof. From assumptions (A3) and (A4), the claimed result follows from the central limit theorem [22].

Collecting the foregoing assumptions and Lemmas 1 and 2, at time $t = t_k, k \in N^+$, the social ties $S_{ij}(t)$ can be modeled by the Wiener process with an adaptive drift, which can be expressed by the following stochastic system [23]:

$$\begin{aligned} & \{u(t_k) = u(t_{k-1}) + \eta W(t_k), \\ & S_{ij}(t_k) = S_{ij}(t_{k-1}) + u(t_{k-1})\Delta t_k + \alpha B(\Delta t_k), \end{aligned} \quad (2)$$

where $\Delta t_k = t_k - t_{k-1}$, $W(t_k)$ is a Brownian motion independent of $B(t_k)$ ($B(t_k)$ is the standard Brownian motion) and $W \sim N(0, Q)$, Q is a constant, $u(t_k)$ is the drift parameter at t_k , and η and α are diffusion coefficients of the adaptive drift and social ties, respectively. \square

3. Model Analysis

3.1. Reliability Function. This section considers a liner model of system (2) based on a Wiener process as follows:

$$S_{ij}(t) = S_{t_0} + ut + \alpha B_t, \quad (3)$$

where S_{t_0} is the observed social tie at $t = t_0$, u is the drift parameter and $u_{t_k} \sim N(u_k, \sigma_k)$ at $t = t_k, k \in N^+$, and B_t is the standard Brownian motion.

During the interaction, any two users i and j trust each other whether their relationship reaches to a given threshold S_{ij}^T or not, $T = \{t \mid S_{ij}(t) \geq S_{ij}^T\}$ is the time that users trust each other for the first time. It is well known that the Probability Density Function (PDF) of T follows inverse Gaussian distribution [24]. Then, it can be expressed as follows [25]:

$$F^T(t \mid u) = \frac{S_{ij}^T}{\sqrt{2\pi\alpha^2 t^3}} \exp\left(-\frac{(S_{ij}^T - ut)^2}{2\alpha^2 t}\right). \quad (4)$$

According to statistic characteristics and conditional distribution of the Wiener process, the cumulative distribution function (CDF) can be expressed as the following reliability function [24, 25]:

$$\begin{aligned} R^T(t \mid u) &= 1 - P(S_{ij}(t) \leq S_{ij}^T) \\ &= 1 - \Phi\left(\frac{S_{ij}^T - ut}{\alpha\sqrt{t}}\right) + \Phi\left(\frac{S_{ij}^T + ut}{\alpha\sqrt{t}}\right) \exp\left(-\frac{2uS_{ij}^T}{\alpha^2}\right), \end{aligned} \quad (5)$$

where $\Phi(\cdot)$ expresses the CDF of the standard normal random variable.

Combined the foregoing analysis, one of main results of this paper can be obtained as follows.

Theorem 1. For the social tie process $\{S_{ij}(t), t > 0\}$ given by system (3), the PDF and CDF can be expressed as equations (4) and (5), respectively.

3.2. Adaptive Parameter Estimation. In this section, the Kalman filtering [26] is applied to estimate the mean and variance of drift parameter u . On this basis, parameters α and Q are estimated by the expectation-maximization (EM) algorithm [27].

For a given observation sample $\mathbf{S} = \{S_{t_1}, S_{t_2}, \dots, S_{t_k}\}$, the observation equation of drift parameter u forms a Kalman filtering framework. Let u_{t_k} and σ_{t_k} stand for the updated drift parameter and variance, respectively. Let $u_{t_k|t_{k-1}}$ and $\sigma_{t_k|t_{k-1}}$ represent the estimated mean and variance based on the previous moment, respectively. Therefore, the mean and variance of drift parameter u can be derived from the following Kalman filtering equations for $k \in N^+$:

$$\begin{aligned} & u_{t_k|t_{k-1}} = u_{t_{k-1}}, \\ & \sigma_{t_k|t_{k-1}} = \sigma_{t_{k-1}} + \eta^2 Q, \\ & K_k = \sigma_{t_k|t_{k-1}} + (\sigma_{t_k|t_{k-1}} + \alpha^2)^{-1}, \\ & u_{t_k} = u_{t_{k-1}} + \sigma_{t_k|t_{k-1}} K_k (S_{t_k} - u_{t_k|t_{k-1}}), \\ & \sigma_{t_k} = (1 - K_k) \sigma_{t_k|t_{k-1}}. \end{aligned} \quad (6)$$

With initial conditions $u_{t_0} = u_0$ and $\sigma_{t_0} = \sigma_0$, K_k is the Kalman gain.

The EM algorithm includes E-step and M-step, and it is necessary to take the expectation of the complete log-likelihood function in the first step, and then maximize the expectation to obtain estimated parameters until a convergence is achieved.

Let $\Theta = (u_0, \sigma_0, \alpha, Q)$ and $\mathbf{u} = \{u_{t_0}, u_{t_1}, \dots, u_{t_{k-1}}\}$. Then, the complete log-likelihood function for n points can be expressed as follows [28]:

$$L(\Theta, \mathbf{S}; \mathbf{u}) = \log \left[P(u_{t_0}; \Theta) \prod_{k=1}^{n-1} P(u_{t_k} | u_{t_{k-1}}; \Theta) \prod_{k=1}^n P(S_{t_k} | u_{t_{k-1}}; \Theta) \right], \quad (7)$$

where

$$\begin{aligned} u_{t_0} &\sim N(u_0, \sigma_0), \\ u_{t_k} | u_{t_{k-1}} &\sim N(u_{t_{k-1}}, Q), \\ S_{t_k} | u_{t_{k-1}} &\sim N(S_{t_{k-1}} + u_{t_{k-1}}(t_k - t_{k-1}), \sigma^2(t_k - t_{k-1})). \end{aligned} \quad (8)$$

By ignoring constant terms, the function $L(\Theta, \mathbf{S}; \mathbf{u})$ can be rewritten as follows:

$$\begin{aligned} 2L(\Theta, \mathbf{S}; \mathbf{u}) &= -\log \sigma_0 - \frac{(u_{t_0} - u_0)^2}{\sigma_0} - \sum_{k=1}^{n-1} \left(\log Q - \frac{(u_{t_k} - u_{t_{k-1}})^2}{\sigma_0} \right) \\ &\quad - \sum_{k=1}^n \left(2 \log \alpha - \frac{(S_{t_k} - S_{t_{k-1}} - u_{t_{k-1}} \Delta t_k)^2}{\sigma^2 \Delta t_k} \right). \end{aligned} \quad (9)$$

Next, $E(u_{t_k}^2 | \mathbf{S}, \Theta)$ and $E(u_{t_k} u_{t_{k-1}} | \mathbf{S}, \Theta)$ are calculated by the Rauch–Tung–Striebel (RTS) smoothing algorithm [29]. The backward iteration rules are as follows:

$$\begin{aligned} D_{t_{k-1}} &= \sigma_{t_{k-1}} \sigma_{t_k}^{-1} |_{t_{k-1}}, \\ u_{t_{k|n}} &= u_{t_k} + D_{t_k} (u_{t_{k+1}|n} - u_{t_k}), \\ \sigma_{t_{k|n}} &= \sigma_{t_k} |_{t_k} + D_{t_k}^2 (\sigma_{t_{k+1}|n} - u_{t_{k+1}} | t_k), \end{aligned} \quad (10)$$

where $u_{t_{k|n}}$, $\sigma_{t_{k|n}}$, and $D_{t_{k-1}}$ are the RTS smoothing state estimation, variance, and gain function on the basis of the current estimated parameters, respectively. Then,

$$\begin{aligned} E(u_{t_k} | \mathbf{S}, \Theta) &= u_{t_{k|n}}, \\ E(u_{t_k}^2 | \mathbf{S}, \Theta) &= \sigma_{t_{k|n}} + u_{t_{k|n}}^2, \\ E(u_{t_k} u_{t_{k-1}} | \mathbf{S}, \Theta) &= D_{t_{k-1}} \sigma_{t_{k|n}} + u_{t_{k|n}} u_{t_{k-1}|n}. \end{aligned} \quad (11)$$

Let $E_u\{L(\Theta, \mathbf{S}; \mathbf{u})\}$ denote the conditional expectation of the complete log-likelihood function given u_{t_k} , $C_{t_k t_{k-1}|n} = E(u_{t_k} u_{t_{k-1}} | \mathbf{S}, \Theta)$, and $C_{t_k|n} = E(u_{t_k}^2 | \mathbf{S}, \Theta)$. Then,

$$\begin{aligned} E_u\{L(\Theta, \mathbf{S}; \mathbf{u})\} &= -\log \sigma_0 - \frac{C_{t_0|n} - 2u_0 u_{0|n} + u_0^2}{\sigma_0} \\ &\quad + \sum_{k=1}^{n-1} \left(\log \frac{1}{Q} - \frac{C_{t_k|n} + C_{t_{k-1}|n} - 2C_{t_k t_{k-1}|n}}{Q} \right) \\ &\quad - \sum_{k=1}^n \left(2 \log \alpha + \frac{(S_{t_k} - S_{t_{k-1}})^2 + (t_k - t_{k-1})^2 C_{t_k t_{k-1}|n}}{\alpha^2 (t_k - t_{k-1})} \right) \\ &\quad + \sum_{k=1}^n \frac{2(S_{t_k} - S_{t_{k-1}})(t_k - t_{k-1}) u_{t_{k-1}|n}}{\alpha^2 (t_k - t_{k-1})}. \end{aligned} \quad (12)$$

Finally, the estimation of parameters can be obtained by maximizing the complete log-likelihood function in (12).

4. Numerical Examples

Some numerical examples are given to illustrate the main results of this paper in this section.

Example 1. Consider system (2) with initial conditions $u_0 = 0.1$, $\sigma_0 = 0.1$, $n = 50$, and $S_{ij}^T = 0.7$. The social tie sample \mathbf{S} is randomly produced by obeying normal distribution. Figure 2 shows the estimated mean and variance of the drift parameter u and the square of diffusion coefficients α^2 and Q .

Example 2. Consider system (2) with initial conditions $u_0 = 0.1$, $\sigma_0 = 0.1$, $n = 3$, and $S_{ij}^T = 0.7$. The social tie sample \mathbf{S} is randomly produced by obeying normal distribution. Figure 3 displays the probability density function of achieving social trust for the first time.

Example 3. Consider system (2) with initial conditions $u_0 = 0.1$, $\sigma_0 = 0.1$, $n = 3$, and $S_{ij}^T = 0.7$. The social tie sample \mathbf{S} is randomly produced by obeying normal distribution. Figure 4 shows the reliability of social tie over time. As time increases, the reliability between users gradually increases with time. In addition, at the same time point, the greater the drift coefficient, the greater the reliability.

Example 4. Consider system (2) with initial conditions $u_0 = 0.1$, $\sigma_0 = 0.1$, and $n = 50$. The social tie sample \mathbf{S} is randomly produced by obeying normal distribution. Figure 5 reveals the variation curve of the estimated social tie strength under adaptive and fixed drift coefficient, respectively. The changes of social tie over time are not monotonous, and the interaction process is positive or negative. The estimated values obtained from the two methods have the same trend as the observed values, and the model has a good predictive ability. In addition, the predicted value

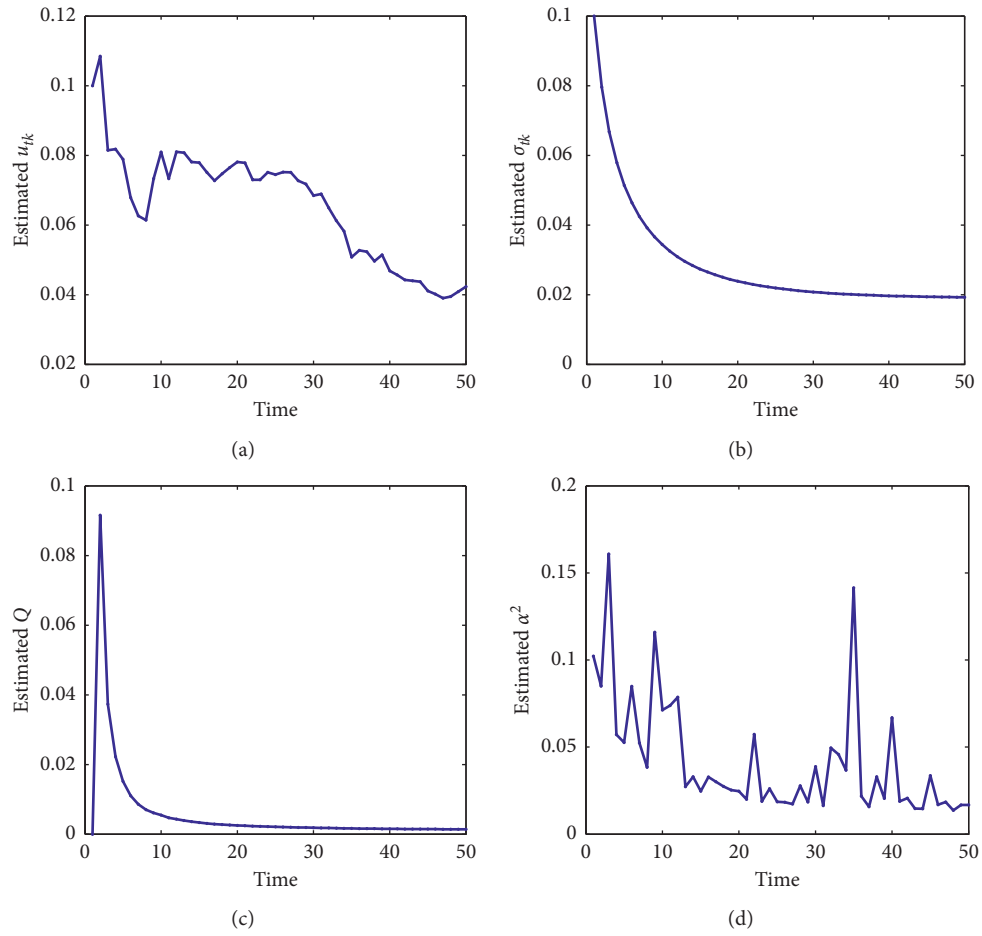


FIGURE 2: The estimated parameters for system (2) with initial conditions given in Example 1.

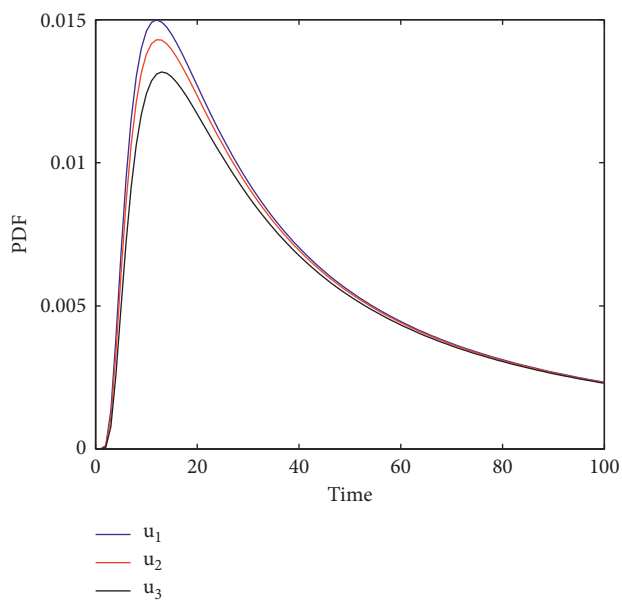


FIGURE 3: The PDF of achieving social trust for system (2) with initial conditions given in Example 2.

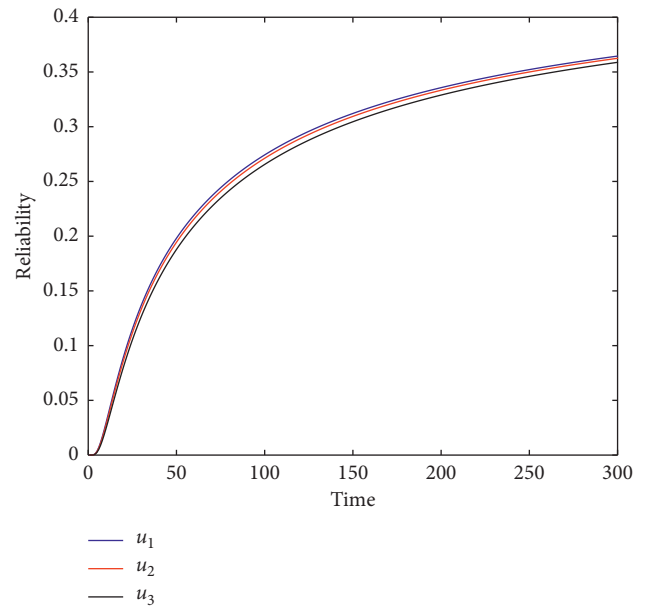


FIGURE 4: The reliability of social tie for system (2) with initial conditions given in Example 3.

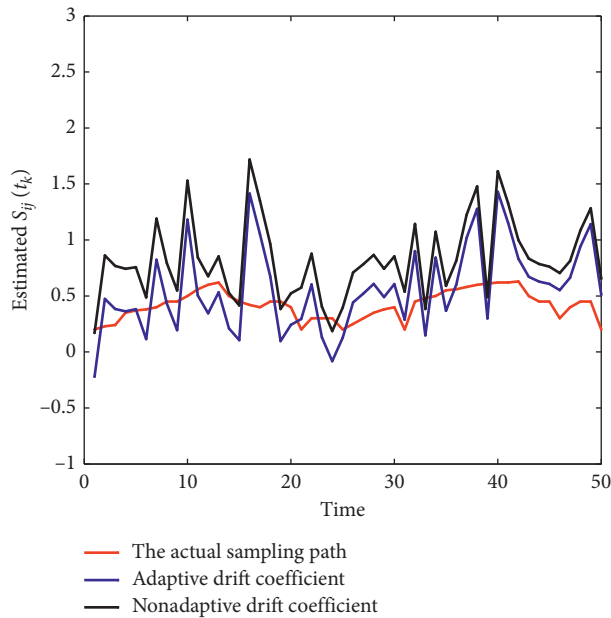


FIGURE 5: The estimated social tie for different drift parameters with initial conditions given in Example 4.

obtained by updating the drift parameter is closer to the real value than that of the fixed drift parameter.

5. Conclusions and Future Work

In this paper, a stochastic mathematical model describing the social ties, which incorporates the combined effect of many factors, such as interest, geographical position, career, social class, value system, and interaction, has been proposed and analyzed. The reliability function and adaptive parameter estimation have both been determined. To illustrate the main results, some numerical examples have been given at the end of this paper. This work contributes to the understanding of social phenomena.

As research based on the background of big data and artificial intelligence gradually enters people's vision [30, 31], our proposed model can also open up new research directions under this background. For example, using artificial intelligence methods to abstract and analyze multidimensional features such as network behavior, content attributes, positional relationships, structural features, and privacy protection policies. In addition, the data in the social network is dynamic and transmitted in the form of data streams. The linking and generation of relationships are constantly changing, and the popularity of the video will also change over time. For large-scale dynamic networks, it is of great significance to further study efficient dynamic models and algorithms for video transmission.

Data Availability

Data sharing is not applicable to this article as no datasets were generated.

Conflicts of Interest

The authors declare no conflicts of interest.

Authors' Contributions

The authors claim that the research was realized in collaboration with the same responsibility. All authors read and approved the last version of the manuscript.

Acknowledgments

This work was supported by the Natural Science Foundation of China (Grant nos. 61702066 and 11747125), Major Project of Science and Technology Research Program of Chongqing Education Commission of China (Grant no. KJZD-M201900601), Chongqing Research Program of Basic Research and Frontier Technology (Grant nos. cstc2017jcyjAX0256 and cstc2018jcyjAX0154), Project Supported by Chongqing Municipal Key Laboratory of Institutions of Higher Education (Grant no. cqjpt-mct-201901), Technology Foundation of Guizhou Province (QianKeHeJiChu [2020]1Y269), and New Academic Seedling Cultivation and Exploration Innovation Project (QianKeHe Platform Talents [2017]5789-21).

References

- [1] Y. Yi, Z. Zhang, L. Yang, C. Gan, X. Deng, and L. Yi, "Reemergence modeling of intelligent information diffusion in heterogeneous social networks: the dynamics perspective," *IEEE Transactions on Network Science and Engineering*, 2020.
- [2] C. Gan, X. Li, L. Wang, and Z. Zhang, "The impact of user behavior on information diffusion in D2D communications: a discrete dynamical model," *Discrete Dynamics in Nature and Society*, vol. 2018, Article ID 3745769, 9 pages, 2018.
- [3] Y. Cao, T. Jiang, X. Chen, and J. Zhang, "Social-aware video multicast based on device-to-device communications," *IEEE Transactions on Mobile Computing*, vol. 15, no. 6, pp. 1528–1539, 2016.
- [4] Z. Wang, H. Shah-Mansouri, and V. W. S. Wong, "How to download more data from neighbors? A metric for D2D data offloading opportunity," *IEEE Transactions on Mobile Computing*, vol. 16, no. 6, pp. 1658–1675, 2017.
- [5] Z. Zhang, T. Zeng, X. Yu, and S. Sun, "Social-aware D2D pairing for cooperative video transmission using matching theory," *Mobile Networks and Applications*, vol. 23, no. 3, pp. 639–649, 2018.
- [6] C. Gan, Q. Feng, Q. Zhu, Z. Zhang, Y. Zhang, and Y. Xiang, "Analysis of computer virus propagation behaviors over complex networks: a case study of Oregon routing network," *Nonlinear Dynamics*, vol. 100, no. 2, pp. 1725–1740, 2020.
- [7] Z. Zhao, H. Lu, D. Cai, X. He, and Y. Zhuang, "User preference learning for online social recommendation," *IEEE Transactions on Knowledge and Data Engineering*, vol. 28, no. 9, pp. 2522–2534, 2016.
- [8] X. Hu, T. H. S. Chu, V. C. M. Leung, E. C.-H. Ngai, P. Kruchten, and H. C. B. Chan, "A survey on mobile social networks: applications, platforms, system architectures, and future research directions," *IEEE Communications Surveys & Tutorials*, vol. 17, no. 3, pp. 1557–1581, 2015.
- [9] M. Granovetter, "The strength of weak ties: a network theory revisited," *Sociological Theory*, vol. 1, no. 6, pp. 201–233, 1983.
- [10] D. M. Boyd and N. Ellison, "Social network sites: definition, history, and scholarship," *IEEE Engineering Management Review*, vol. 38, no. 3, pp. 210–230, 2010.

- [11] R. Xiang, J. Neville, and M. Rogati, "Modeling relationship strength in online social networks," in *Proceedings of the ACM International Conference on World Wide Web*, pp. 981–990, ACM, Raleigh, NC, USA, April 2010.
- [12] W. X. Zhao, N. Zhou, W. Zhang, J.-R. Wen, S. Wang, and E. Y. Chang, "A probabilistic lifestyle-based trajectory model for social strength inference from human trajectory data," *ACM Transactions on Information Systems*, vol. 35, no. 1, pp. 1–28, 2016.
- [13] L. Xiong, Y. Lei, W. Huang, X. Huang, and M. Zhong, "An estimation model for social relationship strength based on users' profiles, co-occurrence and interaction activities," *Neurocomputing*, vol. 214, pp. 927–934, 2016.
- [14] X. Zhao, J. Yuan, G. Li, X. Chen, and Z. Li, "Relationship strength estimation for online social networks with the study on Facebook," *Neurocomputing*, vol. 95, pp. 89–97, 2012.
- [15] C. Ju and W. Tao, "A novel relationship strength model for online social networks," *Multimedia Tools and Applications*, vol. 76, no. 16, pp. 17577–17594, 2017.
- [16] J. Sang and C. Xu, "Right buddy makes the difference: an early exploration of social relation analysis in multimedia applications," in *Proceedings of the 20th ACM international conference on Multimedia-MM'12*, ACM, Nara Japan, pp. 19–28, 2012.
- [17] C. Huang, D. Wang, J. Tao, and B. Mann, "On physical-social-aware localness inference by exploring big data from location-based services," *IEEE Transactions on Big Data*, 2017.
- [18] J. Tang, J. Sun, C. Wang, and Z. Yang, "Social influence analysis in large-scale networks," in *Proceedings of the ACM Sigkdd International Conference on Knowledge Discovery and Data Mining*, ACM, Paris, France, pp. 807–816, 2009.
- [19] B. Yang, H. Pei, H. Chen, J. Liu, and S. Xia, "Characterizing and discovering spatiotemporal social contact patterns for healthcare," *IEEE Transactions on Pattern Analysis and Machine Intelligence*, vol. 39, no. 8, pp. 1532–1546, 2017.
- [20] Y. Yi, Z. Zhang, and C. Gan, "The effect of social tie on information diffusion in complex networks," *Physica A: Statistical Mechanics and Its Applications*, vol. 509, pp. 783–794, 2018.
- [21] O. Ibe, *Fundamentals of Applied Probability and Random Processes*, Academic Press, Cambridge, MA, USA, Second edition, 2014.
- [22] B. W. Gnedenko, "Limit distributions for sums of independent random variables," *Mathematical Gazette*, vol. 39, no. 330, pp. 264–343, 1953.
- [23] X.-S. Si, Z. X. Zhang, and C. H. Hu, "An adaptive prognostic approach via nonlinear degradation modeling: application to battery data," *IEEE Transactions on Industrial Electronics*, vol. 62, no. 8, pp. 5082–5096, 2015.
- [24] G. Jin, D. Matthews, Y. Fan, and Q. Liu, "Physics of failure-based degradation modeling and lifetime prediction of the momentum wheel in a dynamic covariate environment," *Engineering Failure Analysis*, vol. 28, pp. 222–240, 2013.
- [25] Y. S. Sherif and M. L. Smith, "First-passage time distribution of Brownian motion as a reliability model," *IEEE Transactions on Reliability*, vol. 29, no. 5, pp. 425–426, 1980.
- [26] A. Harvey, *Forecasting, Structural Time Series Models and the Kalman Filter*, Cambridge University Press, Cambridge, MA, USA, 1989.
- [27] A. P. Dempster, N. M. Laird, and D. B. Rubin, "Maximum likelihood from incomplete data via the EM algorithm," *Journal of the Royal Statistical Society: Series B (Methodological)*, vol. 39, no. 1, pp. 1–22, 1977.
- [28] H. Li, D. Pan, and C. L. P. Chen, "Reliability modeling and life estimation using an expectation maximization based wiener degradation model for momentum wheels," *IEEE Transactions on Cybernetics*, vol. 45, no. 5, pp. 969–977, 2015.
- [29] L. L. Cam, "Maximum likelihood: an introduction," *International Statistical Review/Revue Internationale de Statistique*, vol. 58, no. 2, pp. 153–171, 1990.
- [30] Z. Zhang, C. Wang, C. Gan, S. Sun, and M. Wang, "Automatic modulation classification using convolutional neural network with features fusion of SPWVD and BJD," *IEEE Transactions on Signal and Information Processing Over Networks*, vol. 5, no. 3, pp. 469–478, 2019.
- [31] C. Gan, L. Wang, Z. Zhang, and Z. Wang, "Sparse attention based separable dilated convolutional neural network for targeted sentiment analysis," *Knowledge-Based Systems*, vol. 188, pp. 1–10, 2020.